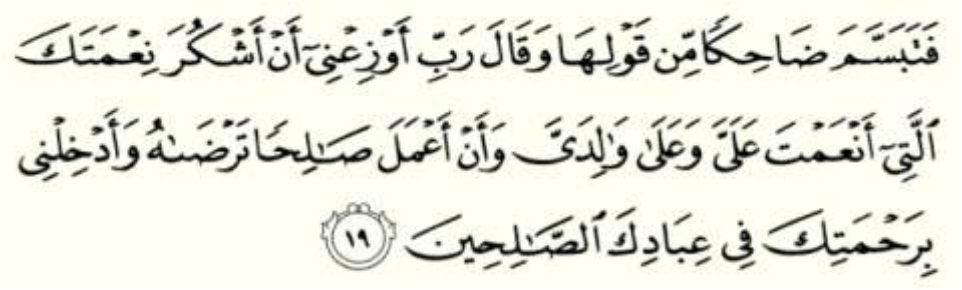
فَتَبَسَّمَ ضَاحِكًا مِّن قَوْلِهَا وَقَالَ رَبِّ أَوْزِعْنِيٓ أَنْ أَشْكُرَ نِعْمَتَكَ
ٱلَّتِيٓ أَنْعَمْتَ عَلَيَّ وَعَلَىٰ وَٰلِدَيَّ وَأَنْ أَعْمَلَ صَٰلِحًا تَرْضَىٰهُ وَأَدْخِلْنِي
بِرَحْمَتِكَ فِي عِبَادِكَ ٱلصَّٰلِحِينَ ١٩

So he [Solomon] smiled, amused at her speech and said, "My Lord, grant me the power and ability that I may be grateful for Your Favours which You have bestowed on me and on my parents, and that I may do righteous good deeds that will please You, and admit me by Your Mercy among Your righteous slaves".

Quran 27:19

University of Alberta

Geomechanical Assessment of Leakage through Oil Wellbores

By

Ahmad Nabih Abdel-Hady Alsayed

A thesis submitted to the Faculty of Graduate Studies and Research
in partial fulfillment of the requirements for the degree of

Doctor of Philosophy

in

Geotechnical Engineering

Department of Civil and Environmental Engineering

Spring 2014
Edmonton, Alberta

Dedication

To the memory of my mother,
To my dear respected father,
To my lovely wife,
and
To my precious brother,

I dedicate this work

Abstract

Carbon capture and storage (CCS) is an approach to reduce carbon dioxide (CO2) emissions. The approach involves three main steps; capturing, transporting, and storing of CO2. Storing is done by injecting CO2 directly into underground deep geological formations such as depleted oil and gas reservoirs, un-minable coal seams, saline formations, and declining oil and gas reservoirs.

Safe storage of CO2 into oil and gas reservoirs depends mainly on the caprock sealing that provide a physical natural barrier for leakage to the surface and/or a strata where other energy, mineral and/or groundwater resources are present. Storage integrity assurance is controlled by two mechanisms; geological leakage mechanism and wellbore leakage mechanism. In all problems, dealing with CCS, safety assessment of wellbore integrity is a major challenge.

Researchers' main objective is to gain more information and knowledge to understand wellbore behavior under different states and/or conditions.

However, all of these efforts are scattered and dispersed due to either the various approaches of the study and the multi-disciplinary nature of the problem. There is no unified and universally accepted procedure to investigate wellbore leakage mechanism.

There is a need for a methodology to standardize the assessment of wellbore integrity in a more regulatory manner. To be a standard code of practice, key elements of the methodology must be gathered, recognized, classified, and systematically ordered.

Such considerations necessitate an appropriate procedure that can be standardized and considered as a sound practical tool to check the safety evaluation of wellbores with respect to wellbore leakage mechanism.

Wellbore sealing efficiency index is introduced to assess wellbore leakage mechanism with engineering rigor. It can be used as a quantification index to assess wellbore leakage failure mechanism. The index is proposed to be a criterion to rank different wellbore elements in the same formation, to

compare with different elements within the same wellbore, and/or to check the safety condition of wellbore.

Two indices, storage index and permeability index, are found to govern wellbore leakage mechanism and facilitate the creation of wellbore performance charts that monitor and check wellbores' leakage mechanism and their lifecycle performance.

Acknowledgement

All praises and thanks are to Almighty, Allah, the Lord of the worlds, the Sustainer of the universe, and the Ruler of the day of resurrection. He bestowed upon me all means of support, guidance, patience and ability to complete this work.

I am very indebted with great favor to Dr. Rick Chalaturnyk for his support and encouragement. I am grateful to have the honorable opportunity to work under his wise and gentle supervision and be one of his Reservoir Geomechanics Research Group in University of Alberta, Canada.

I would like to acknowledge the support of the IEA-GHG Weyburn-Midale CO2-EOR Storage and Monitoring Project and the Helmholtz-Alberta Initiative for their financial support of this research.

I am very grateful to my lovely wife Aisha for her kindness, help, patience and prayers and to my beautiful daughters Asmaa, Zahraa, and Aminah for the warm feelings and flavor they added to my life.

I wish to express my sincere gratitude to my parents and my brother for their everlasting love, support and encouragement over the years.

I extend my appreciation to my colleagues and friends with whom I spent my time as a graduate student at University of Alberta for their moral support and sincere advice. Among all special thanks to Muhammad Saber, Ehab Hamza, Ahmad Ismail, Muhammad Hamoud, Nafisul-Islam, Mazda Irani, and Seungjoo Lee.

Table of Contents

List of Tables

List of Figures

Chapter 1: Introduction

1.1 Background

Climate is commonly defined as the average weather for a specific location, region or the entire globe over a period of time. The weather is described by temperature, humidity, cloudiness, perception, and wind speed and direction. This average day-to-day and/or long-term weather is considered as a result of interaction between climate system components and Earth's biosphere. Climate system components involves the earth's atmosphere, land surface and the ocean, along with the snow and ice that is so prominent in much of Canada (Moran, 2006).

The United Nations Framework Convention on Climate Change (UNFCCC) defines climate change as "*a change of climate that is attributed directly or indirectly to human activity and that is in addition to natural climate variability observed over comparable time periods*" (IPCC, 2004). However, Environment Canada defines climate change as "*a long-term shift in average weather conditions over time, including temperature, precipitation, winds, and other indicator which can be caused by both natural variability or as a result of human activity*" (Environment Canada, 2012; IPCC, 2004).

The UNFCCC definition distinguishes between climate change due to human activities, and climate variability attributable to natural causes (IPCC, 2004).

In 1935, the international Meteorological Conference at Warsaw, Poland standardized computations of climatic norms to be based on the averages compiled over a period of 30 years. The period is then adjusted every 10 years to add the latest decade and drop the earliest one Canada (Moran, 2006).

1.2 Global Warming

One of the aspects of climate change is global warming, which can be defined as the increase in the average temperature of the Earth's near-surface air and the oceans and its projected continuation. Figure 1.1 shows annual anomalies of global average land-surface air temperature, 1861 to 2000, relative to 1961 to 1990 values.

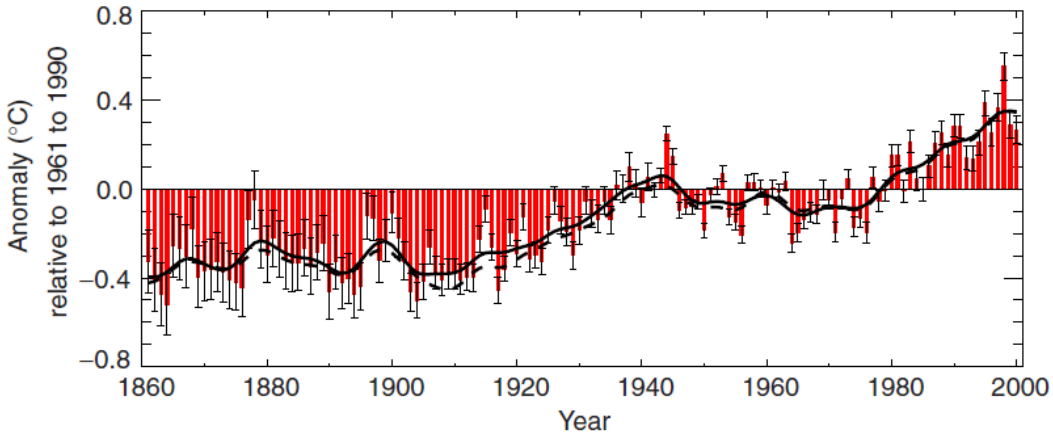

Figure 1.1: Variation of the Earth's surface temperature (after IPCC, 2001).

In 1988, the World Meteorological Organization (WMO) and the United Nations Environment Program (UNEP) founded the Intergovernmental Panel on Climate Change (IPCC). The IPCC has worked as a scientific intergovernmental body, (IPCC, 2004, 2012; Espie, 2005), to:

1) assess scientific, technical, socio-economic literature,
2) understand the risk of climate change,
3) predict future impacts, and
4) provide options for mitigations.

The assessment indicated that anthropogenic greenhouse gases (GHG) are responsible for most of the observed temperature increase since the middle of

the twentieth century (IPCC, 2013). GHG is defined as a gas that allows short-wave radiation (i.e. visible light) to pass through the atmosphere but absorbs long-wave radiation (i.e. thermal energy) (Humphries, 2008). Radiative forcing, Figure 1.2, is a measure of a factor influence in altering the balance of incoming and outgoing energy. Positive forcing tends to warm the surface while negative forcing tends to cool it (IPCC, 2013).

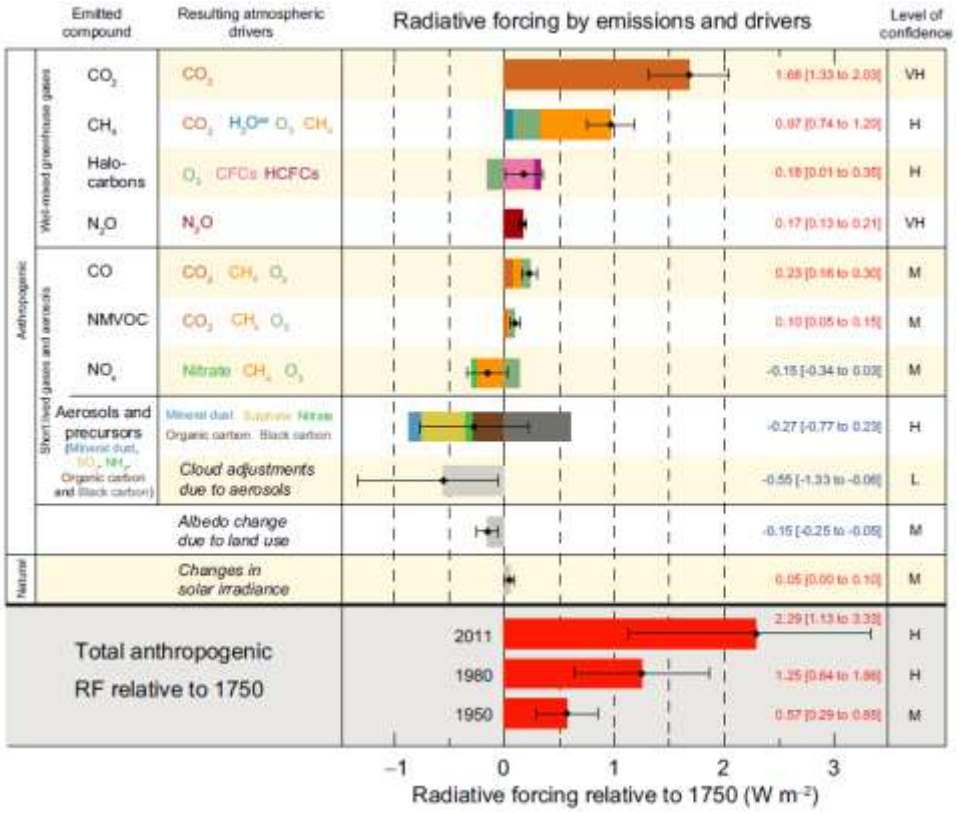

Figure 1.2: Average radiative forcing (after IPCC, 2013).

Common GHGs in the Earth's atmosphere include water vapor, carbon dioxide, methane, nitrous oxide, ozone, and chlorofluorocarbons. As shown in Figure 1.2, Carbon dioxide (CO2) is the most important anthropogenic

GHG that a has significant contribution to the climate change. Monthly average CO2 concentration measurements taken continuously from 1958 at several observatories around the globe are presented in Figure 1.3.

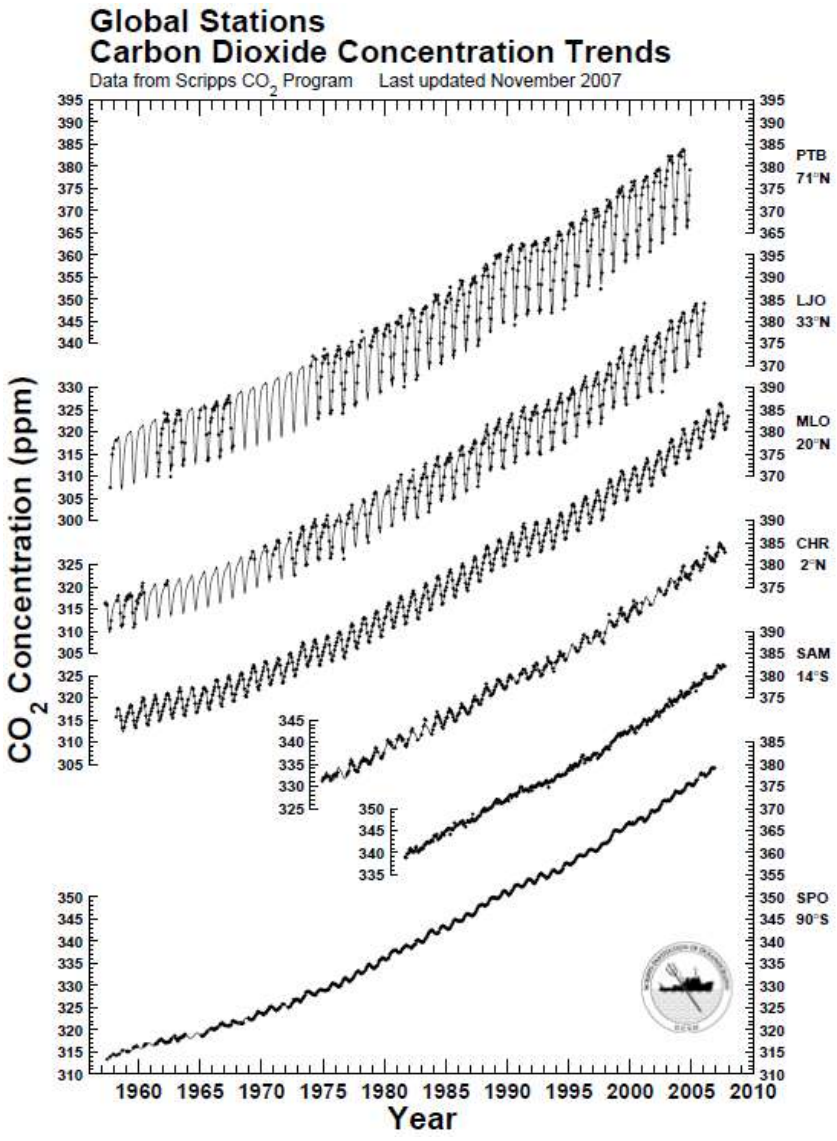

Monitoring sites are: South Pole (SPO), Samoa (SAM), Christmas Island (CHR), Mauna Loa, Hawaii (MLO), La Jolla, California (LJO), and Point Barrow, Alaska (PTB)

Figure 1.3: Average CO2 concentration measurements (after Humphries, 2008).

1.3 Carbon Dioxide Stabilization

There is variability in concentration growth rates of CO2 from year to year and an emission of 1 Gt C corresponds to 3.67 Gt CO2 (IPCC, 2007). In 2011, CO2 atmospheric concentration level exceeded the pre-industrial level by 40% and reached 391 ppm with average cumulative anthropogenic emissions of 555 GtC from 1750 to 2011. The IPCC indicated that the annual CO2 average emissions were 8.30 GtC/year from fossil fuel combustion and cement production while anthropogenic land use emissions were 0.90 GtC/year between 2002 and 2011 (IPCC, 2013).

Pacala and Socolow (2004), as part of the Carbon Mitigation Initiative (CMI) at Princeton University, introduced the concept of a "stabilization triangle". The stabilization triangle, Figure 1.4, was divided into seven wedges, each representing a reduction of 1 Gt C/year (corresponds to 3.67 Gt CO2/year) over a 50-year period.

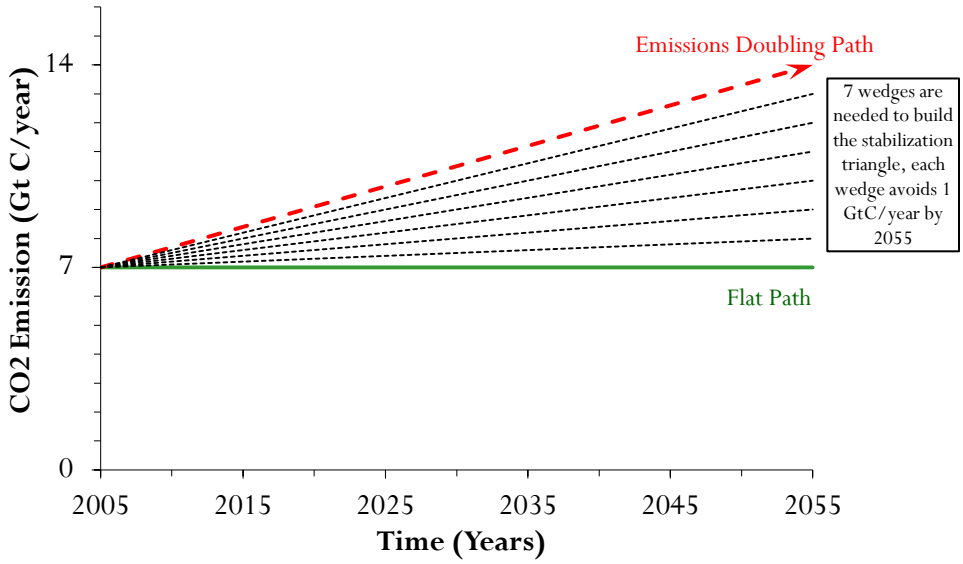

Figure 1.4: The stabilization triangle (after Pacala and Socolow , 2004).

The conclusions of this analysis were the following:

1) that at least 15 strategies are available to achieve CO2 emissions reduction,
2) that no single technology is likely to provide a magic solution to stabilization,
3) that the component technologies capable of delivering stabilization of CO2 concentrations in the atmosphere already exist or are under development; and
4) these technologies fall within the main categories of energy efficiency and conservation, energy de-carbonization, carbon capture and storage, and enhancing natural sinks.

A global reduction of approximately 7.0 Gt C/year (25.70 Gt CO2/year) is required in order to achieve stabilization in CO2 emissions (Pacala and Socolow, 2004). Stabilization of CO2 emissions is needed to avoid serious consequences of global warming. A 2 °C is considered as an upper limit for average global temperature rise (Espie, 2005).

1.4 Carbon Capture and Storage

Carbon capture and storage (CCS) is an approach to reduce CO2 emissions to global warming as concluded by Pacala and Socolow (2004). CCS involves three main stages of capturing CO2 from point sources then transporting CO2 to suitable geological storage sites, and finally injecting CO2 in supercritical form into deep geological formation for storage. The last process of storing CO2 is defined as geological CO2 sequestration or CO2 geo-sequestration. Geological formations suitable for CO2 sequestration depends on two factors; location of the storage site and storage integrity of this site.

Location of the storage site is normally controlled by the project economics, which is driven primarily by the first two stages of CCS. Location of the site depends on:

1) the distance between CO2 point sources in the first stage of CCS and the proposed storage sites, and
2) the available and/or required infrastructure to facilitate the second stage, which is CO2 transportation.

On the other hand, storage integrity is normally controlled by safety assurance of the stored CO2 in the underground geological formation. IPCC (2005) recognized that secure storage sites fall into four main target sites, as depicted in Figure 1.5. These target sites are; depleted oil and gas reservoirs, un-minable coal seams, saline formations, and declining oil and gas reservoirs.

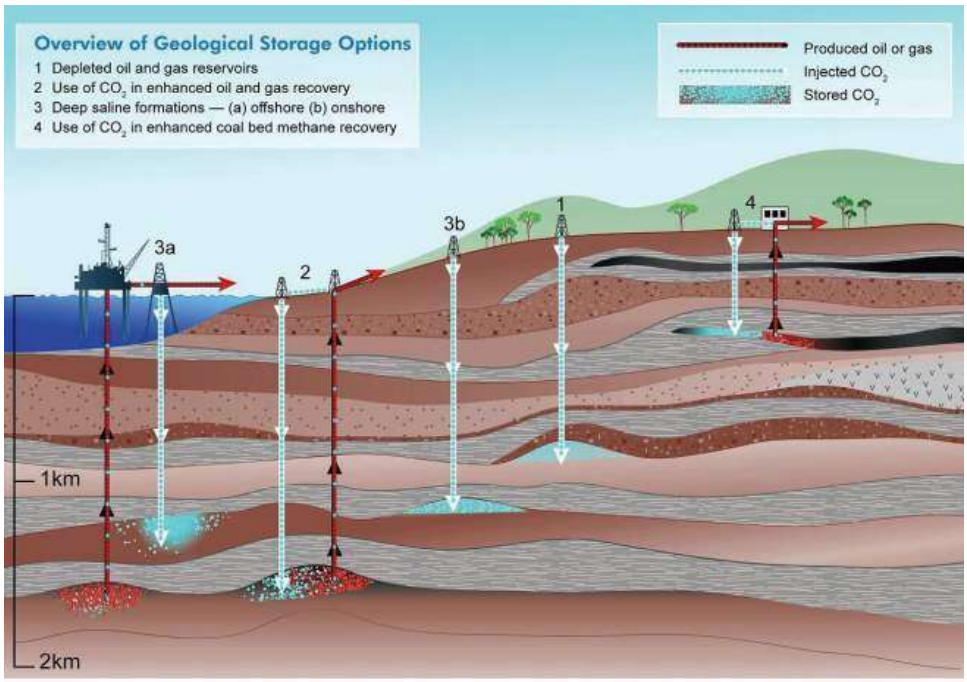

Figure 1.5: Geological CO2 sequestration options (after IPCC, 2005).

Generally, these sites enhance CO2 storage because CO2 will be a supercritical fluid and in addition to natural physical trapping, will posses other types of trapping, (Cantucci et al., 2009), such as:

1) hydrodynamic trapping by slow migration of CO2 fluid,
2) solubility trapping due to dissolved CO2 (aq) into groundwater, and
3) mineral trapping due to newly-formed carbonates.

Oil and gas reservoirs are suitable storage sites because they are characterized, Gasda (2008), by existence of:

1) storing medium provide sufficient pore volume to store CO2, and
2) physical trapping represented by a structural trap called caprock provide enough integrity to contain the stored CO2.

Furthermore, these reservoirs are well investigated and are historically documented. Injecting CO2 is common practice during enhanced oil recovery (EOR) process that adds an advantage by reducing the cost of the produced oil from depleted sites.

1.5 Storage Integrity Assurance

Leakage of stored CO2 from a storage formation may take place due a loss in the structural integrity of the caprock. This integrity is controlled by two mechanisms, which are geological leakage mechanism and wellbore leakage mechanism (Espie, 2005), as discussed below.

1.5.1 Geological Leakage Mechanism

Geological leakage mechanism represents failure in the performance of the physical trapping that provides a seal for the storage formation. Many features

lead to such failure either naturally and/or artificially. These features may include faults, fractures that, if connected, provide leakage paths to the surface and/or may contaminate specific strata where other energy, mineral and/or groundwater resources are present.

This mechanism is identified by investigating lateral continuity of the sealing formation across the storage site and the state of the sealing condition before injection.

1.5.2 Wellbore Leakage Mechanism

Wellbore leakage mechanism is due to the presence of wellbores in the storage site. Wellbores are artificially generated points of weakness within a seal formation and are considered as localized sources for CO2 leakage through a seal formation. These localized sources of potential flow have different characteristics relative to the sealing formation and relative to each other.

Wellbores can be classified into two categories, which are unidentified wellbores and abandoned wellbores. Unidentified wellbores are a potential issue if they penetrate deep formations but in general, most are shallow. Abandoned wellbores on the other hand are a concern because they may not provide a robust seal. In addition, the locations of some deep abandoned wellbores are unknown (Espie, 2005).

In general, leakage through wellbores is due to poor bonding that forms micro-annuli at the interfaces between the cement with either formation rock and/or the casing.

1.6 Problem Definition

Wellbores, which provide access to a reservoir, may serve as preferential flow paths allowing upward migration of injected CO2. Possible leakage through existing oil wellbores appears to be important in mature sedimentary basins that have been intensively explored and exploited for hydrocarbon production (Bachu and Haug, 2006).

Storage sites associated with depleted oil and gas reservoirs may contain many unidentified and thousands of abandoned wellbores. All of these wellbores have historically variable quality and quantity of cement that will have undergone ranging degrees of degradation.

Cement sheath performance in a single wellbore is believed dependent on the events (i.e. pressure and temperature changes) that occur within the life of the wellbore (Fourmaintraux et al., 2005; Gray et al., 2007). Therefore, wellbore integrity is a function of lifetime as a domain affected by the change of life events of this wellbore and/or the change of its material properties during same period.

There is significant uncertainty surrounding the integrity of existing wellbores. To get a better chance of success in practice, successful CCS will depend on solving the small-scale leakage problem associated with localized flow along wellbores. Our knowledge of oil wellbore performance under different life stages of a well is still weak. Consequently, each wellbore is unique and general conclusions about well integrity are difficult to ascertain from analyzing only a single well. Each wellbore is considered as a risk and robust tools are needed to allow for the assessment of the performance for wellbores and investigate wellbore leakage mechanism.

1.7 Objectives of the Study

It is postulated that the inclusion of all stages of a wells life (in a numerical modelling assessment framework) will lead to improved assessment of the long-term hydraulic integrity of a wellbore for CO2 geological storage projects. Modeling all phases in the history of a wellbore, from drilling to abandonment, will provide a basis for developing a monitoring program of status of a wellbore and provides quantitative estimates for performance of the well.

The objective of this research is to develop a framework that is capable of assessing the performance of wellbore for storage purposes. The framework is not developed for quantification of leakage rates but rather as a self-consistent model that could be applied to risk ranking of wellbore integrity based on the hydraulic integrity state of the wellbore.

Such consideration necessitates an appropriate procedure that can be standardized and considered as a sound and a practical tool to check the safety evaluation of wellbores with respect to wellbore leakage mechanism.

1.8 Research Methodology

The research methodology will include a logical workflow with the intent of evolving into a practical engineering tool for CO2 geological storage projects.

The methodology is to develop an approach to incorporate the evolution of cement properties during cement hydration process (Chapter 2). Cement properties will be used in a geomechanical modeling procedure to assess wellbore integrity to investigate and monitor debonding of the wellbore interfaces. The model is based on the available dataset for caprock formation

in Weyburn storage site (Chapter 3). To check the wellbore leakage mechanism for a wellbore element, new analytical modeling of wellbore element is suggested (Chapter 4). Output of the model described in Chapter 3 is then used to estimate wellbore effective permeability (Chapter 5). Implementation of the work discussed in Chapters 2, 3, 4, 5 is to assess the performance of wellbore and complete the framework to check wellbore leakage mechanism.

Finally, the developed analytical model in Chapter 4 to assess wellbore element mechanism is then extended and applied to the entire wellbore system (Chapter 6). The results are performance charts to check the safety of the storage condition for both wellbore element and wellbore system.

1.9 Structure of the Thesis

The thesis is composed of seven chapters and is organized as follows:

Chapter 1: Introduction,
Chapter 2: Cement Properties during Hydration,
Chapter 3: Assessment of Wellbore Integrity,
Chapter 4: Wellbore Element Modeling,
Chapter 5: Wellbore Bulk Permeability,
Chapter 6: Assessment of Wellbore Performance, and
Chapter 7: Conclusions and Recommendations.

1.10 References

Bachu, S., and Haug, K., (2006), Evaluation of the Potential for CO2 Leakage through Wells at Penn West's Pembina-Cardium CO2-Enhanced Oil Recovery Pilot Operation, Alberta Energy Research Institute, EUB/AGG Client Report, 50 p.

Cantucci, B., Montegrossi, G., Vaselli, O. Tassi, F. Quattrocchi, F. and Perkins, E.H. (2009), Geochemical Modeling of CO2 Storage in Deep Reservoirs: The Weyburn Project (Canada) Case Study, Chemical Geology 265, pp. 181-197.

Environment Canada, (2012), About Climate Change Web Page, http://www.ec.gc.ca/cc/default.asp?lang=En&n=9C2CF393-1, Last accessed on December 17th, 2012,

Espie, A.A., (2005), CO2 Capture and Storage: Contributing to Sustainable World Growth, International Petroleum Technology Conference, 21-23 November, Doha, Qatar, IPTC 10936, 7 p.

Fourmaintraux, D., Bois, A.P., Franco, C., Fraboulet B. and Brossollet, P., (2005), Efficient Wellbore Cement Sheath Design Using the SRC (System Response Curve) Method, SPE Europec/EAGE Annual Conference, 13-16 June, Madrid, Spain, SPE 94176, 10 p.

Gasda, S.A., (2008), Numerical Models for Evaluation CO2 Storage in Deep, Saline Aquifers: Leaky Wells and Large-Scale Geological Features, Ph.D. Thesis, Princeton University, USA, 188 p.

Gray, K.E., Podnos, E., and Becker, E., (2007), Finite Element Studies of Near-Wellbore Region during Cementing Operations; Part I, SPE Production and Operations Symposium, 31 March-3 April, Oklahoma City, Oklahoma, USA, SPE 106998, 15 p.

Humphries, S.D., (2008), Carbon Dioxide Sequestration Monitoring and Verification via Laser Based Detection System in the 2μm Band, Ph.D. Thesis, Montana State University, Montana, USA, 106 p.

IPCC, (2001), Climate Change 2001: The Scientific Basis, 3rd Assessment Report, WGI, Cambridge University Press, UK, 881 p.

IPCC, (2004), 16 Years of Scientific Assessment in Support of the Climate Convention, 19 p.

IPCC, (2005), Carbon Capture and Storage, Special Report, Cambridge Press, 431 p.

IPCC, (2007), Climate Change 2007: The Physical Science Basis, 4th Assessment Report, WGI, Cambridge University Press, UK, 996 p.

IPCC, (2012), IPCC Organization Web Page, Last accessed on December 17th, 2012, http://www.ipcc.ch/organization/organization.htm

IPCC, (2013), Climate Change 2013: The Physical Science Basis, 5th Assessment Report, WGI, Cambridge University Press, UK, 1536 p.

Moran, J.M., (2006), Weather Studies: Introduction to Atmospheric Science, 3rd edition, American Meteorological Society, 516 p.

Pacala, S. and Socolow, R., (2004), Stabilization Wedges: Solving the Climate Problem for the Next 50 Years with Current Technology, Science, Vol.305, pp. 968-972.

Chapter 2: Cement Properties during Hydration[1]

2.1 Introduction

Concrete is a compact whole of mineral fragments that is bonded by adhesive and/or cohesive material called cement. Concrete, derived from the Latin term concretus meaning "to grow together", may take different expressions in the field of civil engineering according to its components. Additives may be used in concrete to obtain specific desired properties. Table 2.1 illustrates these different definitions of concrete.

Table 2.1: Definitions for concrete (Mindess et al., 2003).

Concrete	**Filler**	**+**	**Binder**
Paste =	Cement	+	Water
Mortar =	Fine aggregate	+	Paste
Cement Concrete =	Fine & Coarse aggregate	+	Cement paste

In the oil and gas industry, a cement job is done by using paste as an equivalent term used by civil engineers where cement is added to water to form cement slurry.

Cementing job has a direct impact on any successful carbon capture and storage (CCS) process. Wellbores, which provide access to a reservoir, may serve as preferential flow paths allowing upward migration of injected CO2

[1] A version of this chapter has been submitted for publication in the Proceedings of 2014 OTC, Offshore Technology Conference, Houston, Texas, USA, 5-8 May 2014.
Nabih, A., and Chalaturnyk, R., (2014), Characterization of Wellbore Cement Properties by Means of Maturity Rule and Population Growth Models, OTC 25091.

(Espie, 2005). Thus, any numerical modeling of wellbores will have different outcomes according to the proposed cement properties.

Leakage through a well's cement sheath has been a concern under study since the 1960's (Fourmaintraux et al., 2005; Bois et al., 2009). However, it was not until 1990's that the work of Goodwin and Crook (1992) and Jackson and Murphey (1993) highlighted the possibility of the damage in cement sheath due to various events during life time frame of the wellbore (Bois et al., 2009).

Wellbore integrity modeling can focus either on either short-term or long-term behavior. Short-term modeling generally refers to primary cementing to setting of cement, while long-term modeling studies the behavior after setting of cement. Different approaches have mainly been used to evaluate wellbore cement sheath state of stresses for design applications. However, these models generally do not simulate the cement hydration process and its effect on the initial stress state in cement sheath (Saint-Marc et al., 2008).

For short-term modeling, Gray et al. (2007) included in their simulations the general concept of cement hydration but did not effectively evolve the cement mechanical properties during cement hydration process (Saint-Marc et al., 2008). Fourmaintraux et al. (2005) modeled cement properties evolution using a linearly incremented function.

Simulation of cement hydration is performed by Total in SealWell model. The simulation adopted the Arrhenius equation to describe the hydration process. The SealWell methodology includes two modules, which are TEXO and MEXO. TEXO module adopted the Arrhenius equation to specify degree of

hydration, which is subsequently used in the MEXO model to estimate displacements and stresses in the cement sheath (Saint-Marc et al. 2008).

Performance of cement sheath in a single wellbore is believed to be dependent on each stage in the life of a well (Fourmaintraux et al., 2005; Gray et al., 2007). Nabih and Chalaturnyk (2013a, 2013b) proposed an assessment of the state of wellbore performance against wellbore leakage mechanism for CO2 storage sites. The assessment requires the wellbore permeability in order to check the performance of wellbore system.

Wellbores have high variability in both quality and quantity of cement used in their original construction process. As such, a significant uncertainty surrounding the hydraulic integrity of existing wellbores exists due to lack of data. Moreover, cement has different physical states throughout hydration, (fluid state, gel-state, and solid state), and each physical state over this time duration has its own physical properties. During the hydration period, the cement materials are subjected to a certain conditions such as temperature and pressure (i.e. wellbore conditions). These changing conditions, (model conditions parameters), during the hydration process will result in changes in cements' physical and mechanical properties and thus affecting the initial state of the cement.

Successful carbon capture and storage (CCS) depends on solving the small-scale leakage problem associated with localized flow along these wellbores. Wellbore integrity is a function of lifetime as a domain affected by the change of life events (i.e. pressure and temperature) and/or change of material properties.

To complete the proposed framework for wellbore assessment, cement properties during the hydration stage is needed as input data to perform the numerical detailed near-wellbore modeling. Detailed staged near-wellbore modeling requires a methodology to estimate cement properties during hydration, which will affect the initial stress state in cement sheath.

This chapter illustrates different key elements of the cement hydration and relates these basics elements within a proposed methodology to predict the evolution of the wellbore cement properties during the hydration process. The relevance of the methodology as a tool that can be used in numerical wellbore modeling is also discussed.

2.2 Cement Hydration Process

Hydration is a chemical reaction in which water is added to a mineral to form a new mineral called hydrate (hydration product). Hydration, as all chemical reactions, can be described by rates of reaction and heats of reaction. Chemical reactions may be heterogeneous because reactants are in two or more phases and exothermic due to releasing of heat during hydration.

The hydration of cement is a sequence of overlapping chemical reactions leading to continuous cement-slurry thickening and hardening. Cement hydration process involves both heterogeneous reactions and exothermic reactions.

Cement, as bonding material, is a heterogeneous mixture and its hydration is a heterogeneous exothermic reaction. By means of the heat released, Figure 2.1, it is possible to determine the degree of hydration relative to hydration duration according to the equation:

$$\alpha_{(t)} = \frac{Q_{(t)}}{Q_{\infty}} \qquad (2.1)$$

where ,

$Q_{(t)}$: accumulated hydration heat at time t, and

Q_{∞}: ultimate (max.) hydration heat until completion.

For pure minerals, $\alpha_{(t)}$ is the mineral reaction degree, while for cement it is consequence of the combined effect of heat released by all constitutes present.

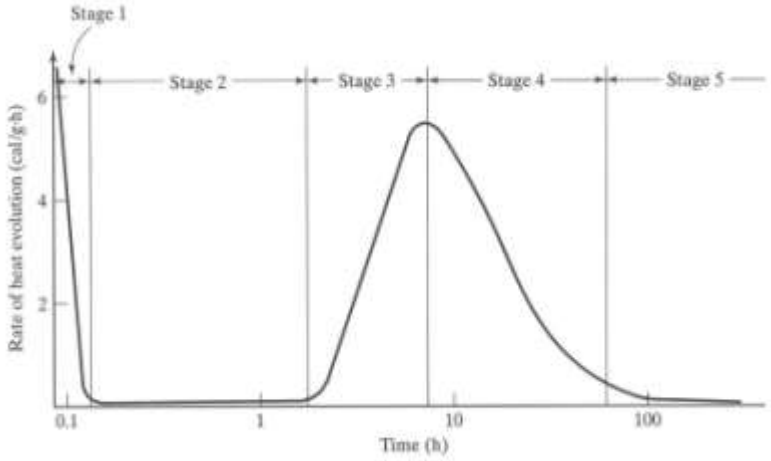

Figure 2.1: Rate of heat evolution during hydration (after Mindess et al., 2003).

Although the cement hydration process is a sequence of overlapping chemical reactions between different components, cement hydration process can be described by the stages, (Muller et al., 1996; Mindess et al., 2003; Nelson and Guillot, 2006), shown in Figure 2.1. These stages are:

- Stage 1 represents a rapid evolution period of heat which ceases within about 15-20 minutes.

- Stage 2 shows an inactive period called the induction period. This period ends when initial set occurs in 2 to 4 hours.
- Stage 3 is known as the accelerated period, which begins at the end of the induction period and terminates in 4 to 8 hours when reaching a maximum rate of heat evolution. Final set of cement has passed and early hardening has begun (solid phase).
- Stage 4 indicates the slowing down of the rate of reaction, and
- Stage 5 corresponds to a steady state within 18 to 36 hours.

Table 2.2: Kinetic model processes (Krstulovic and Dabic, 2000).

Process	**Mathematical Model**
Nucleation and crystal growth (NG)	$\left(-\ln(1-\alpha_{(t)})\right)^{\frac{1}{3}} = K_{NG}t$
Interactions at phase boundaries (I)	$1-\left(1-\alpha_{(t)}\right)^{\frac{1}{3}} = K_{I}t$
Diffusion (D)	$\left(1-\left(1-\alpha_{(t)}\right)^{\frac{1}{3}}\right)^{2} = K_{D}t$

During cement hydration, kinetic models assume three basic processes are taking place. These processes are nucleation and crystal growth, interactions, and diffusion. Each of these processes, Table 2.2, has a different rate constant, K_i, for each process.

These three reaction stages cover stages 3, 4 and 5 shown in Figure 2.1. All these three processes are assumed to occur simultaneously but the slowest one controls the hydration processes as a whole (Tomosawa, 1997; Krstulovic and Dabic, 2000; Dabic et al., 2000; Park et al., 2004).

2.3 Methods of Interpretation of Test Data

Wellbore performance will need a methodology to expect physical and mechanical properties of cement during hydration. These properties can be estimated from data measurements that may be from the laboratory and/or in-situ. Different criteria for interpreting the results of a test could be classified into one or more of the following three recommended categories (Hirany and Kulhawy, 1989a, 1989b):

1) Limitation,
2) Graphical Construction, and
3) Mathematical Modeling.

Hirany and Kulhawy (1989a) and (1989b) indicated that limitation methods are generally independent of individual judgment and scale of the data plotting. However, these methods are not satisfactory for adequate interpretation because of the lack of universal agreement. On the other hand, graphical methods are influenced by individual judgment and scale.

Mathematical modeling will be the best choice because of being independent of the scale relations and the opinions of the individual interpreter. Mathematical modeling is very instructive to justify the assumption of certain parameter or property by means of a function or an equation to describe real-world phenomena.

The evolution of a cement property, P during the hydration process approaches rapidly to an asymptotic value (ultimate P value) according to the rate of hydration (rate constant). A mathematical model is considered as an idealization of the phenomena and hence interpretation of the measured data leads normally to an investigation of a response not a mechanism.

2.4 Maturity Method

The maturity method is considered as a simple tool for approximating complex effects of time and temperature on strength development of concrete. The method is suitable during the hydration process period and is not applicable beyond this period (Neville, 1981; Ansari et al., 1999; Malhotra and Carino, 2004). The method describes the thermo-chemical coupling condition and the influence of temperature on the early age behavior of cement (Viviani et al., 2005; Pertué et al., 2008).

Although McIntoch (1949) was the first to introduce the same concept by an index called "Basic age", but it is Saul (1951) who was the first to recognize and formulate the rule. Saul (1951) established the "maturity rule", schematically illustrated in Figure 2.2, and stated as follows: "*Concrete of the same mix at the same maturity has approximately the same strength whatever combination of temperature and time go to make up that maturity*".

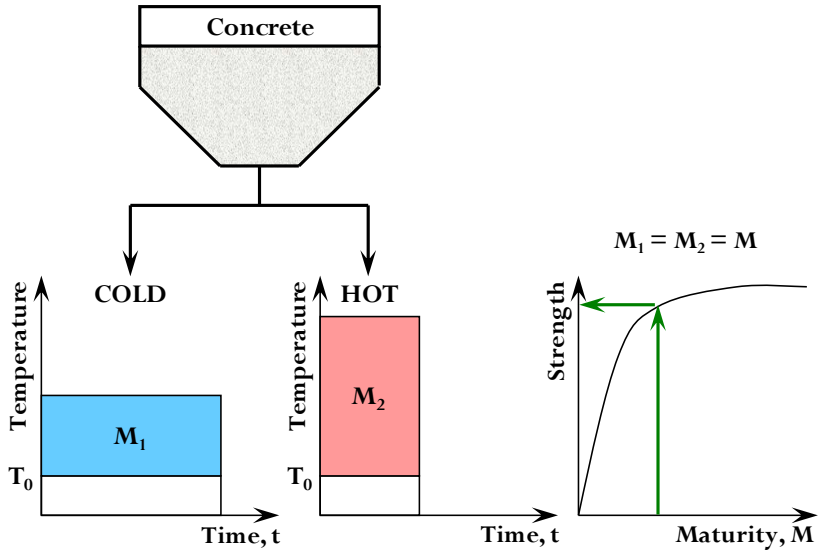

Figure 2.2: Saul's maturity rule (after Garcia-Monzon, 2006).

Maturity is defined as the product of temperature function and time. Maturity in its general form is based on the summation of the temperature histories and can be written as follows;

$$M = \sum_{0}^{t} k_T \,.\, \Delta t \tag{2.2}$$

and hence may be expressed by the following equation;

$$M = \int_{0}^{t} k_T \,.\, dt \tag{2.3}$$

where,

M: maturity at time "age" t,

k_T: rate constant influenced by curing temperature T, and

Δt: time interval between temperature reading.

Bernhardt (1956) was the first to describe the compressive strength, σ_c, development of concrete by a mathematical expression by assuming that the increase in compressive strength will depend on:

1) The degree of previous hardening, and
2) The hardening conditions at the given moment.

He related the strength gain rate with time as follows:

$$\frac{d\sigma_c}{dt} = \phi(T) \,.\, g(\sigma_c) \tag{2.4}$$

where,

$\phi(T)$: a function of temperature, and

$g(\sigma_c)$: a function of strength.

He described the function of temperature, $\phi(T)$, with a constant A and thus the equation that describes his work is:

$$\frac{d\sigma_c}{dt} = A\, f(T).\sigma_\infty \left(1 - \frac{\sigma_c}{\sigma_\infty}\right)^2 \tag{2.5}$$

Assuming that hardening begins after cement placement (i.e. $t_0 = 0$), then the strength prediction equation can be obtained by integrating Equation (2.5):

$$\begin{aligned} \sigma_c &= \sigma_\infty \frac{A\, f(T).t}{1 + A\, f(T).t} \\ &= \sigma_\infty \frac{k_T.t}{1 + k_T.t} \\ &= \sigma_\infty \frac{M}{1 + M} \end{aligned} \tag{2.6}$$

Carino (1984) modified Bernhardt's equation by assuming that the hardening starts not at placement time but at time t_0 and hence:

$$\begin{aligned} \sigma_c &= \sigma_\infty \frac{k_T.(t - t_0)}{1 + k_T.(t - t_0)} \\ &= \sigma_\infty \frac{(M - M_0)}{1 + (M - M_0)} \end{aligned} \tag{2.7}$$

Compressive strength is normally considered as an indicator of cement integrity. Therefore, the maturity rule was the motivation for many researchers to relate compressive strength with the maturity index (Bergström, 1953; Rastrup, 1954, 1956; Nykänen, 1956; Plowman, 1956; Bernhardt, 1956; Goral, 1956; Chin, 1971, 1975; Lew and Reichard, 1978; Carino, 1984; Hansen and Pedersen, 1985; Yi et al., 2005).

Table 2.3 chronologically summarizes other strength relationships. Note that these relationships have either logarithmic or exponential forms.

Table 2.3: Strength maturity relationships (Malhotra and Carino, 2004).

Author	Strength
Nykänen (1956)	$\sigma_c = \sigma_\infty \left(1 - e^{-aM}\right)$
Plowman (1956)	$\sigma_c = a + b \,.\, \log(M)$
Bernhardt (1956), Goral (1956) and Chin (1971)	$\sigma_c = \sigma_\infty \frac{M}{1+M}$
Lew and Reichard (1978)	$\sigma_c = \frac{\sigma_\infty}{1 + D \,.\, \log(M - 16.70)^b}$
Carino (1984)	$\sigma_c = \sigma_\infty \frac{(M - M_0)}{1 + (M - M_0)}$
Hansen and Pedersen (1985)	$\sigma_c = \sigma_\infty e^{-\left(\frac{\tau}{M}\right)^a}$

2.5 Hydration Rate Constant

McIntosh (1949, 1956) and Saul (1951) defined a datum temperature, T_d, to determine the maturity of concrete. The datum temperature is the lowest curing temperature at which strength gain is observed (i.e. k_T=0). The rate constant proposed was:

$$k_T = T - T_d \tag{2.8}$$

Rastrup (1956) was the first to consider the change of reaction rate with respect to temperature. He proposed a method based on the well-known axiom from physical chemistry, which states: "*the reaction velocity is doubled if the temperature is increased by 10 °C*". Thus, he proposed that the rate constant can be expressed by:

$$k_T = 2^{\left(\frac{T}{10}\right)} \tag{2.9}$$

Hansen and Pedersen (1977) introduced the application of the scientific Arrhenius equation (Garcia-Monzon, 2006). The Arrhenius rate constant equation is:

$$k_T = Ae^{\left(-\frac{E_A}{RT}\right)} \tag{2.10}$$

where,

A: pre-exponential factor,

E_A: apparent activation energy,

= 33500 J/mol if $T \geq 293$ °K

= 33500 + 1470 (293-T) J/mol if $T < 293$ °K

R: universal gas constant (8.314 J/K.mol), and

T: given absolute temperature, °K.

2.6 Mathematical Models for Population Growth

Bernhardt (1956) was the first to describe the compressive strength, σ_c, development of concrete by a mathematical expression. He assumed the increase in compressive strength depends on the degree of previous hardening (strength) and the hardening conditions (rate constant).

In fact, the two assumptions of Bernhardt's are the same basic assumptions of mathematical models used in studying of population dynamics. In these models, the competition for available resources tends to limit the population growth to a saturation level. The population often increases rapidly in its early stages and reaches an asymptotic value represents its carrying capacity because of limited resources. The rate of reproduction depends on:

1) the existing population, and
2) the proportional amount of available resources.

Population dynamics is the branch of mathematical biology to monitor the change of age and/or size of populations in certain locality. The exponential increase law of Malthus, after Robert Thomas Malthus, is the first principle to study population dynamics. The Malthusian growth model considers that the rate of population growth is directly proportional to its current size.

$$\frac{dp}{dt} = r.P \tag{2.11}$$

The solution of Equation (2.11) is given by:

$$P = P_0.e^{rt} \tag{2.12}$$

where,

P: population size at time t,

P_0: initial population at time t_0, and

r: intrinsic "basic" growth rate.

After Malthus's work, two pioneers models, (Benjamin Gompertz, 1825; Pierre Francois Verhulst, 1838), were developed to model the rapid increase of population that will reach an asymptotic threshold. Winsor (1932) summarized, Table 2.4, the mathematical properties of the Gompertz curve and the Verhulst "logistic" curve where K is the carrying capacity, steady state, or saturation level.

Consequently, the cement properties modeling approach assumes that cement strength gain as a property is analogous to the maximum population of a locality under the resources available. In case of cement, water is considered the main resource for any hydration process. The rate hydration process may change according to wellbore conditions and mainly the borehole temperature.

Table 2.4: Properties of Gompertz and Verhulst models (Winsor, 1932).

Property	Gompertz	Verhulst "Logistic"
Equation	$P = K.e^{-e^{(a-rt)}}$	$P = \frac{K}{1+e^{(a-rt)}}$
Number of constants	3	3
Asymptotes	Lower Asymptote = 0 Upper Asymptote = K	Lower Asymptote = 0 Upper Asymptote = K
Inflection point	$\left(\frac{a}{r}, \frac{K}{e}\right)$	$\left(\frac{a}{r}, \frac{K}{2}\right)$
Straight line form of equation	$\ln\left(\ln\frac{K}{P}\right) = a - rt$	$\ln\left(\frac{K-P}{P}\right) = a - rt$
symmetry	Asymmetrical	Symmetrical
Growth rate	$\frac{dp}{dt} = rP\ln\left(\frac{K}{P}\right)$	$\frac{dp}{dt} = rP\left(1-\frac{P}{K}\right)$
Maximum growth rate	$\frac{rK}{e}$	$\frac{rK}{4}$

2.7 Maturity vs Population Growth

Carino and Lew (2001) pointed out that there are different capabilities of the various strength-age "maturity" functions. They indicated that the exponential model (i.e. Hansen and Pedersen model) is capable of modeling strength gain over the full spectrum of hydration ages. Originally, Hansen and Pedersen (1985) showed that the relationship between heat of hydration and maturity. They proposed the following heat-maturity relationship:

$$Q_{(M)} = Q_{\infty}.e^{-\left(\frac{\tau}{M}\right)^{\alpha}} \qquad (2.13)$$

where,

$Q_{(M)}$: heat developed at maturity M,

Q_∞: total heat development for M_∞,

M: maturity index,

τ: characteristic time constant, and

α: curve "shape" parameter.

They suggested that the strength-maturity relationship should be similar to the relationship between heat of hydration and maturity. Therefore, strength-maturity relationship is:

$$\sigma_c = \sigma_\infty . e^{-\left(\frac{\tau}{M}\right)^\alpha} \tag{2.14}$$

As a general form for the Hansen and Pedersen equation with the property value and its interpreted limiting value denoted as P and K respectively, then Equation (2.14) can be written as:

$$\begin{aligned} P &= K . e^{-\left(\frac{\tau}{M}\right)^\alpha} \\ &= K . e^{-\left(e^{\ln\left(\frac{\tau}{M}\right)^\alpha}\right)} \\ &= K . e^{-e^{\alpha(\ln\tau - \ln M)}} \\ &= K . e^{-e^{a - r\ln M}} \end{aligned} \tag{2.15}$$

Equation (2.15) shows that the Hansen and Pedersen equation follows Gompertz's model for population growth. The equation can be rewritten in the following form:

$$\sigma_c = \sigma_\infty . e^{-e^{a - r\ln M}} \tag{2.16}$$

For isothermal condition when the curing temperature (here borehole temperature) is constant, the rate constant function k_T has a constant value and hence Equation (2.16) becomes:

$$\begin{aligned}\sigma_c &= \sigma_\infty \cdot e^{-e^{a-r\ln M}} \\ &= \sigma_\infty \cdot e^{-e^{a-r\ln(k_T \cdot t)}} \\ &= \sigma_\infty \cdot e^{-e^{a_0-r\ln t}}\end{aligned} \tag{2.17}$$

Following the same procedure, we will assume that property value, P can be modeled by a population growth model and has the following general formula as:

$$P = P_\infty \cdot e^{-e^{a_0-r\ln t}} \tag{2.18}$$

where,

P_∞: ultimate value for this property.

2.8 Cement Experimental Data

Cement samples are normally cured either under wellbore conditions (i.e. temperature and pressure) or under laboratory conditions (i.e. atmospheric pressure). However, in almost all cases, samples are allowed to equilibrate to ambient (i.e. lab) conditions before testing. Therefore, the engineering analysis based on these measured cement properties is not representative due to depressurization and cooling to ambient conditions. The predicted cement performance under different wellbore conditions may not be correct (Reddy et al., 2005).

Non-destructive tests by the means of ultrasound pulse velocity tests and volume change are usually used to determine the integrity of wellbore cement (Keating et al., 1989; Muller et al., 1996; Lacy and Rickards, 1996; Reddy et al., 2005; Van Den Abeele et al., 2009).

Keating et al. (1989) investigated the correlation between cube strength, ultrasonic pulse velocity, and volume change for oil wellbore cement slurries. Muller et al. (1996) have studied the characterization of the initial, transitional and set properties of oil wellbore cement. Van Den Abeele et al. (2009) clearly indicated that the inflection point for the cement property during the hydration process represents the point at which peak temperature during the hydration process has been reached.

All of these studies are based on graphical data interpretation. Any change in cement response (i.e. measurements) is considered as an indirect reflection of different stages occurring during the process of hydration. A summary of the properties of the cement slurries used in Keating et al. (1989) and Muller et al. (1996) is given in Table 2.5.

Table 2.5: Summary of the cement slurries data.

Reference:	**Keating et al. (1989)**		**Mueller et al. (1996)**		
Reference Slurry:	Mix A	Mix C	H	G	FA:H
Cement Type:	Accelerated Class G	Neat Class G	Class H	Class G	Fly Ash : H Blend
No. of Samples:	5	4	1	1	1
Slurry Density (ppg):	16.27	16.36	16.48	15.80	14.40
Temperature (^{o}C):	20	50	77	77	77
Pressure ($p_f$si):	N/A	N/A	2000	2000	2000
w/c Ratio (%):	44.00	44.00	38.00	44.00	53.76
Sample Length (inch):	N/A	N/A	1.504	1.551	1.504

The measurements of cement properties were based on the change of the response of plunger movement, ΔL and transit time, t_t. Figures 2.3, 2.4, and 2.5 summarize the well-documented tests results for class G cement obtained by Keating et al. (1989) and Muller et al. (1996).

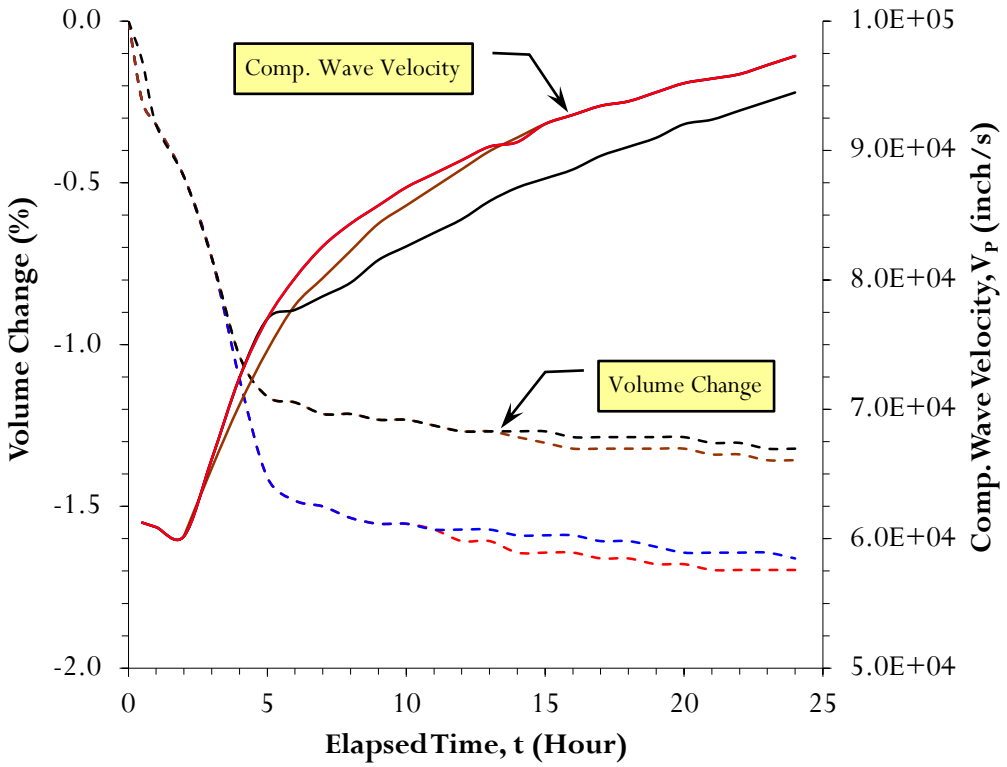

Figure 2.3: Cement data for mix A (after Keating et al., 1989).

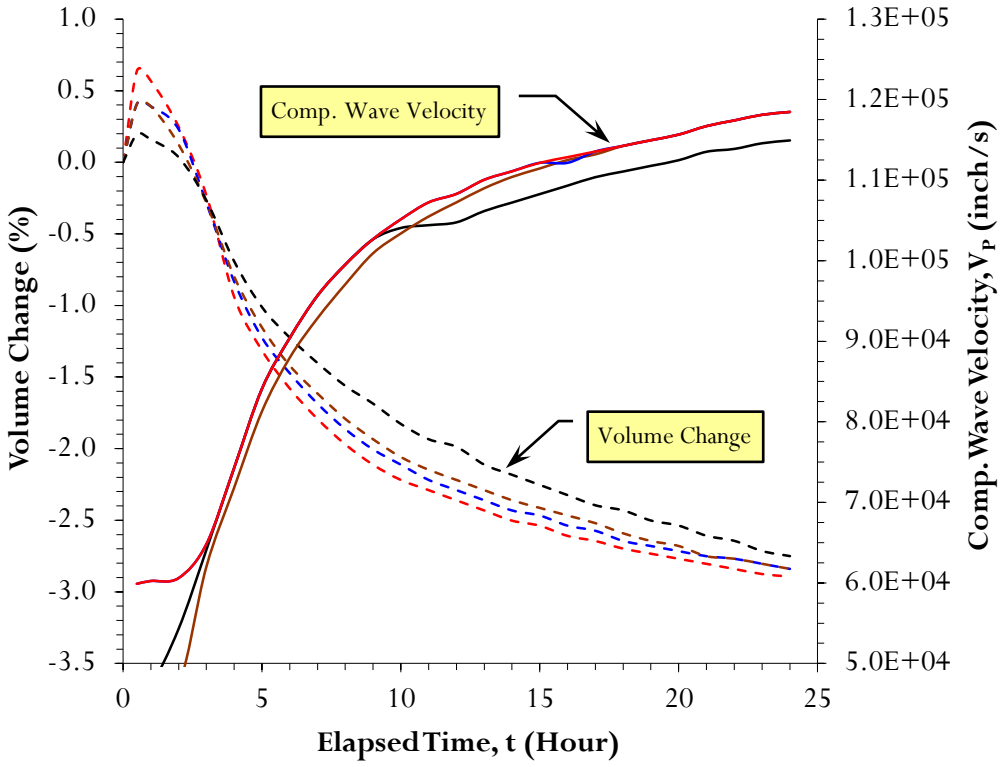

Figure 2.4: Cement data for mix C (after Keating et al., 1989).

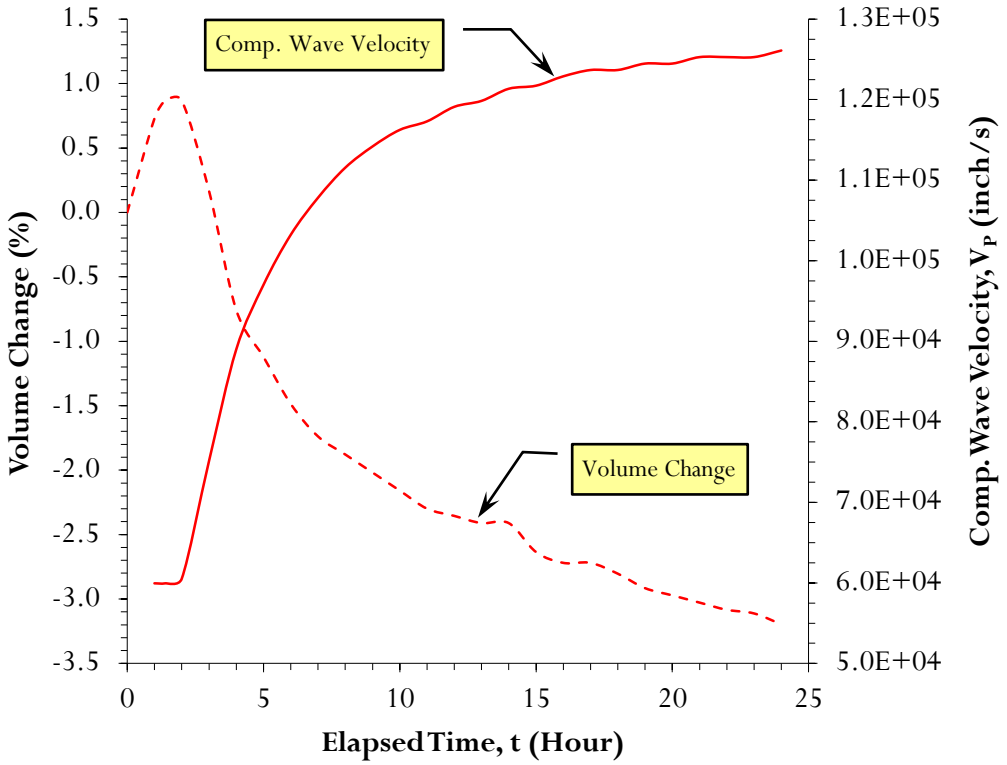

Figure 2.5: Cement data for class G (after Muller et al., 1996).

Lacy and Rickards (1996) relate the changes in sample density, $\Delta\rho$ with changes in sample length, ΔL such that:

$$\frac{\Delta\rho}{\rho_0} = -\frac{\Delta L}{L_0} \tag{2.19}$$

where ,

ρ_0: initial cement slurry density, and

L_0: initial sample length.

Conclusion of Equation (2.19) shows that a slight modification should be considered as follows:

$$\rho_0 V_0 = \rho_t V_t \tag{2.20}$$

and hence,

$$\rho_0 V_0 = (\rho_0 + \Delta\rho_t) V_t \tag{2.21}$$

Equation (2.21) can be rearranged to be:

$$\frac{\Delta\rho_t}{\rho_0} = \frac{V_0}{V_t} - 1 = \frac{V_0 - (V_0 + \Delta V_t)}{V_t} \tag{2.22}$$

Therefore,

$$\begin{aligned} \frac{\Delta\rho_t}{\rho_0} &= -\frac{\Delta V_t}{V_t} \\ &= -\frac{\Delta(AL_t)}{(AL_t)} \end{aligned} \tag{2.23}$$

For constant area, Equation (2.23) leads to:

$$\frac{\Delta\rho_t}{\rho_0} = -\frac{\Delta L_t}{L_t} \tag{2.24}$$

where ,

L_t: sample length at time t.

The elastic dynamic modulus, E_d can be determined from compression wave velocity, V_p by:

$$E_d = \rho V_p^2 \frac{(1+\nu_d)(1-2\nu_d)}{(1-\nu_d)} \tag{2.25}$$

where ,

ν_d : dynamic Poisson's ratio.

Compression wave velocity is the reciprocal of the transit time, t_t (Turchaninov et al., 1979; Neville, 1981; Lacy and Rickards, 1996; Reddy et al., 2005). Lacy and Rickards (1996) used C_0 and n as proprietary values to relate compressive strength, σ_c, with the dynamic modulus, E_d, as follows:

$$\sigma_c = C_0(E_d)^n \tag{2.26}$$

where,

$C_0 = 2x10^{-14}$ while n = 2.71.

2.9 Cement Hydration Model

The population dynamics modeling concept and the maturity rule will be combined to form the framework to verify the approach and to propose a methodology for predicting the change of cement properties during the cement hydration process.

The properties measured were compression wave velocity, V_P, and the density, ρ, based on the measured plunger movement in case of Muller et al. (1996) and volume change in case of Keating et al. (1989).

Recalling Equation (2.18), the general form of the mathematical model for a cement property can be described by:

$$P = P_\infty . e^{-e^{a_0 - r \ln t}} \tag{2.27}$$

where,

P_∞: ultimate value for this property,

r: apparent intrinsic rate constant, and

a_0: apparent induction period constant.

The concept of population growth model has been applied to the measured data. Verification of the approach has been based on the comparison of the measured data values with the predicted values according to the chosen mathematical model. In this study, verification results for Mix C compared with that of Keating et al. (1989) are shown in Figure 2.6 and Figure 2.7 respectively. Colored points indicate the corresponding test shown in Figure 2.4.

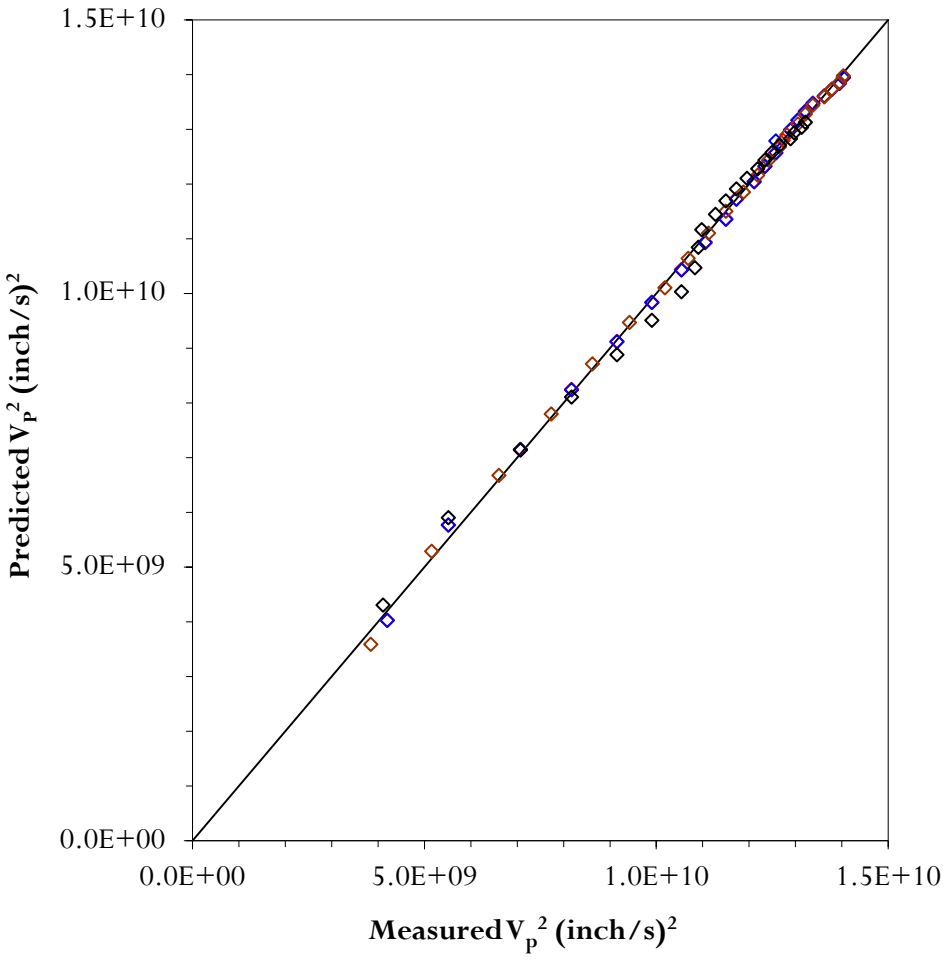

Figure 2.6: Compression velocity verification for mix C.

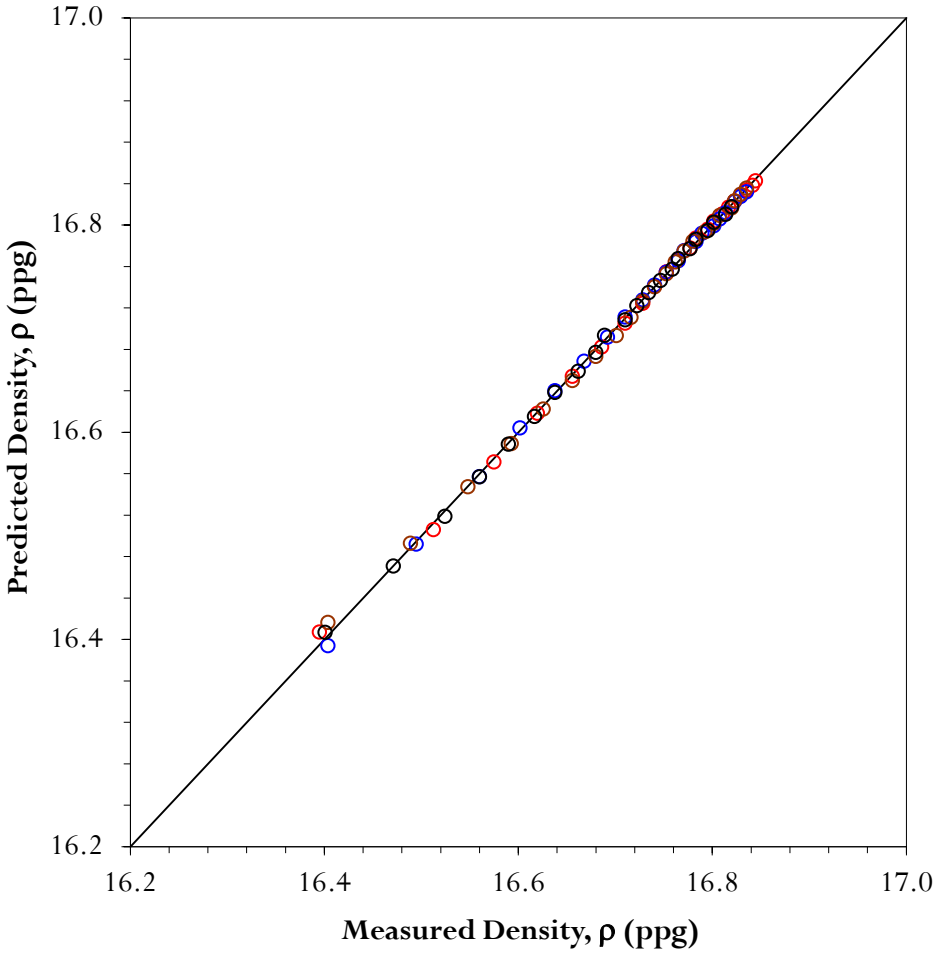

Figure 2.7: Density verification for mix C.

Table 2.6 through Table 2.8 represent the results of the proposed mathematical model predictions of cement properties during hydration.

Table 2.6: Summary of cement density modelling results.

Reference	Density, ρ (ppg)		Model Regression Parameters			Predicted		Correlation Coefficient
			a_ρ	r_ρ	R^2	Max. Value	Induction Period	
Keating et al. (1989)	Mix A	A01	3.39061	1.25252	0.975	16.565	2.556	0.980
		A02	3.59395	1.24409	0.941	16.555	2.292	0.964
		A03	4.22194	0.89896	0.958	16.510	2.251	0.961
		A04	4.31740	1.00644	0.940	16.499	2.071	0.949
		A05	4.44081	0.94643	0.952	16.457	2.248	0.963
		Avg.	**3.99294**	**1.06969**		**16.517**	**2.284**	
	Mix C	C01	2.63025	0.64493	0.999	17.00	2.903	0.999
		C02	2.63088	0.62403	0.999	17.00	3.077	0.999
		C03	2.62940	0.34237	0.999	17.25	2.863	0.999
		C04	2.21479	0.14932	0.999	18.00	2.917	0.999
		Avg.	**2.52633**	**0.44016**		**17.31**	**2.940**	
Muller et al. (1996)	H	-----	2.68726	1.02539	0.911	16.85	2.138	0.950
	G	-----	2.44434	0.37346	0.992	16.75	2.678	0.996
	FA:H	-----	1.74917	0.83011	0.989	15.10	3.522	0.986

Table 2.7: Summary of cement compression wave velocity modelling results.

Reference	Comp. Velocity, V_P^2 $(inch/s)^2$		Model Regression Parameters			Predicted		Correlation Coefficient
			a_{V_P}	r_{V_P}	R^2	Max. Value	Induction Period	
Keating et al. (1989)	Mix A	A01	-0.68724	0.56775	0.998	1.30e10	2.887	0.999
		A02	-0.68724	0.56775	0.998	1.30e10	2.887	0.999
		A03	-0.77052	0.48507	0.999	1.50e10	3.073	0.999
		A04	-0.62282	0.38797	0.984	1.50e10	2.907	0.992
		A05	-0.69409	0.36146	0.998	1.50e10	2.829	0.999
		Avg.	**-0.69238**	**0.47400**		**1.42e10**	**2.917**	
	Mix C	C01	-1.46910	1.02414	0.998	1.65e10	3.089	0.999
		C02	-1.46637	1.02216	0.998	1.65e10	3.087	0.999
		C03	-1.53668	0.99689	0.999	1.70e10	3.137	0.999
		C04	-1.32706	0.98288	0.991	1.55e10	2.890	0.996
		Avg.	**-1.44980**	**1.00652**		**1.64e10**	**3.051**	
Muller et al. (1996)	H	-----	-1.80684	1.40420	0.995	1.57e10	2.766	0.997
	G	-----	-1.62241	1.34392	0.998	1.70e10	3.107	0.999
	FA:H	-----	-1.65971	1.21015	0.994	1.25e10	3.290	0.996

Table 2.8: Summary of cement compression strength modelling results.

Reference	Comp. Strength, σ_c ($p_f$si)		Model Regression Parameters			Predicted		Correlation Coefficient
			a_σ	r_σ	R^2	Max. Value	Induction Period	
Keating et al. (1989)	Mix A	A01	-1.69927	0.58081	0.998	2000	2.889	0.999
		A02	-1.69759	0.57982	0.998	2000	2.886	0.999
		A03	-1.77294	0.48605	0.999	3000	3.064	0.999
		A04	-1.62488	0.38878	0.984	3000	2.894	0.992
		A05	-1.67332	0.43521	0.998	2000	2.918	0.999
		Avg.	**-1.69360**	**0.49413**		**2400**	**2.930**	
	Mix C	C01	-2.53066	1.05742	0.998	4000	3.130	0.999
		C02	-2.52632	1.05379	0.997	4000	3.130	0.999
		C03	-2.46484	0.91611	0.999	5000	3.061	0.999
		C04	-2.34673	0.97719	0.992	3500	2.907	0.995
		Avg.	**-2.46714**	**1.00113**		**4125**	**3.057**	
Muller et al. (1996)	H	-----	-2.89795	1.45525	0.993	3500	2.818	0.998
	G	-----	-2.54653	1.26152	0.999	4250	3.051	0.999
	FA:H	-----	-2.71862	1.21797	0.994	1400	3.322	0.998

Figures 2.8, 2.9, and 2.10 represent the calculated cement properties and the predicted values during the hydration process. Figures indicate very good agreements and show that cement properties follow the proposed mathematical model of population growth.

The proposed mathematical model shows that irrespective of the type of cement, property changes follow the same trend and the difference is only in the coefficients controlling the model.

Figures 2.11 and 2.12 depict the effect of temperature on the mathematical model coefficients. There are two coefficients for each property, the apparent rate constant, r_P and the induction period constant, a_P where the subscript P stands for property under investigation. The approach is used to predict cement compressive strength and to illustrate how the model coefficients change for strength predictions, as shown in Figure 2.13.

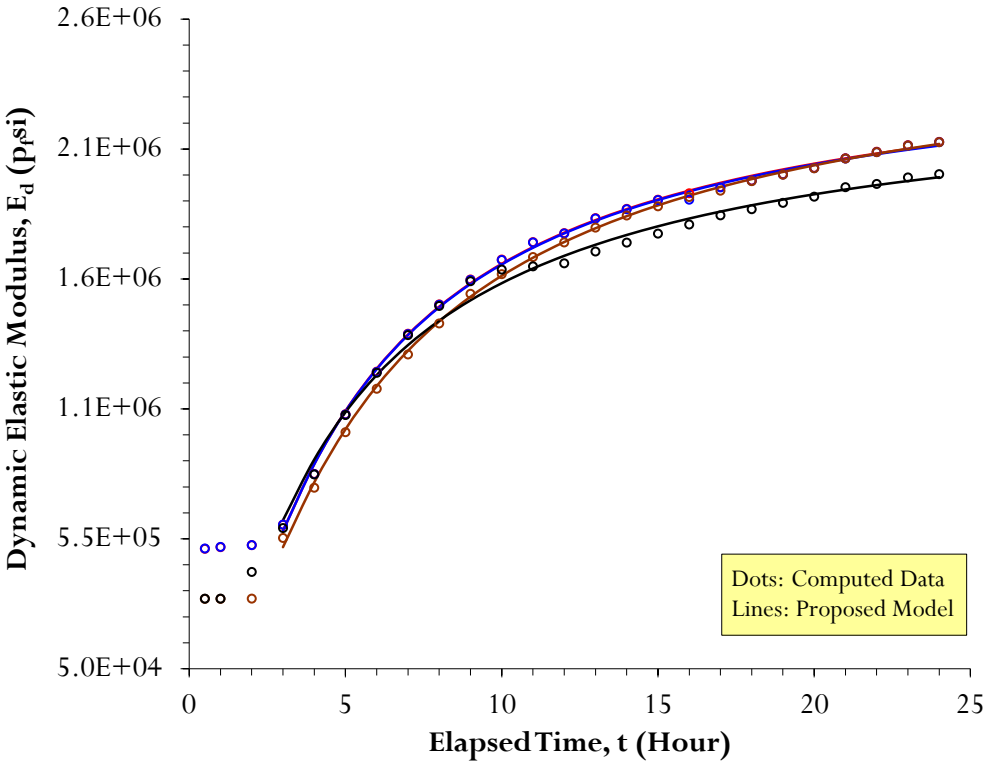

Figure 2.8: Cement dynamic elastic modulus prediction for mix C.

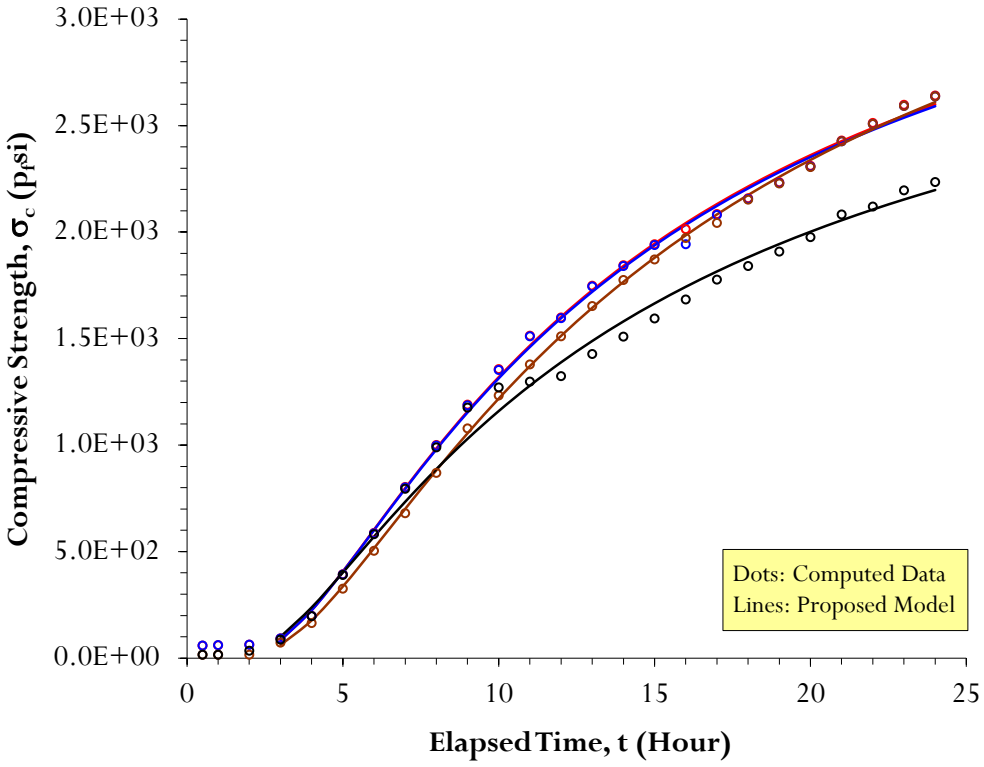

Figure 2.9: Cement compressive strength prediction for mix C.

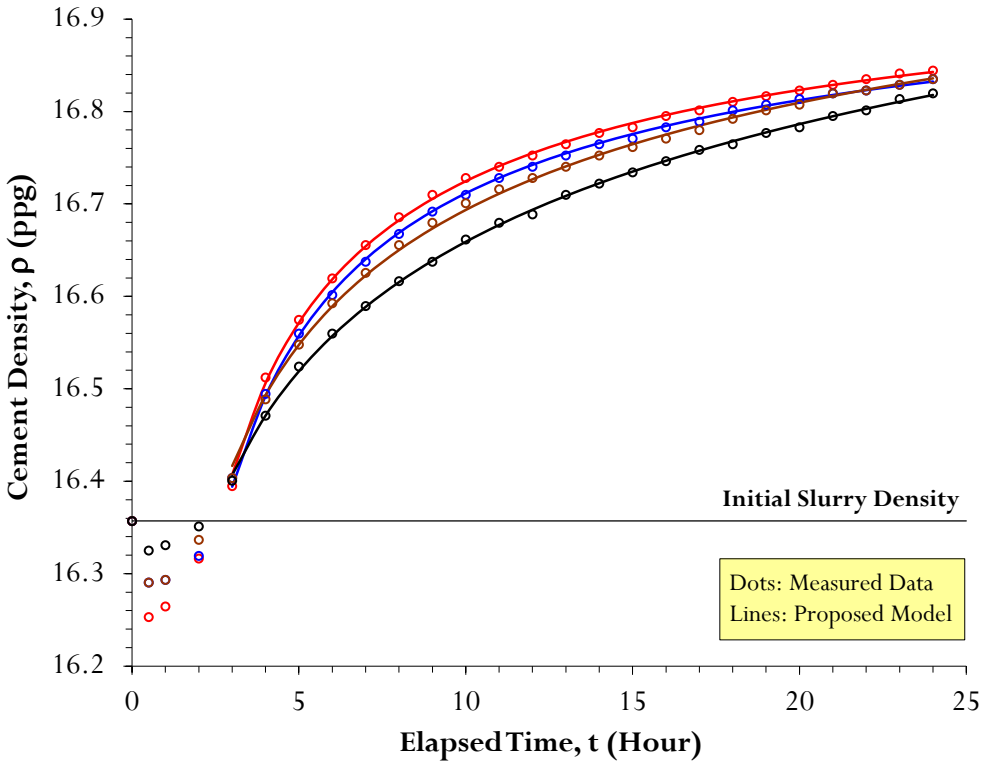

Figure 2.10: Cement density prediction for mix C.

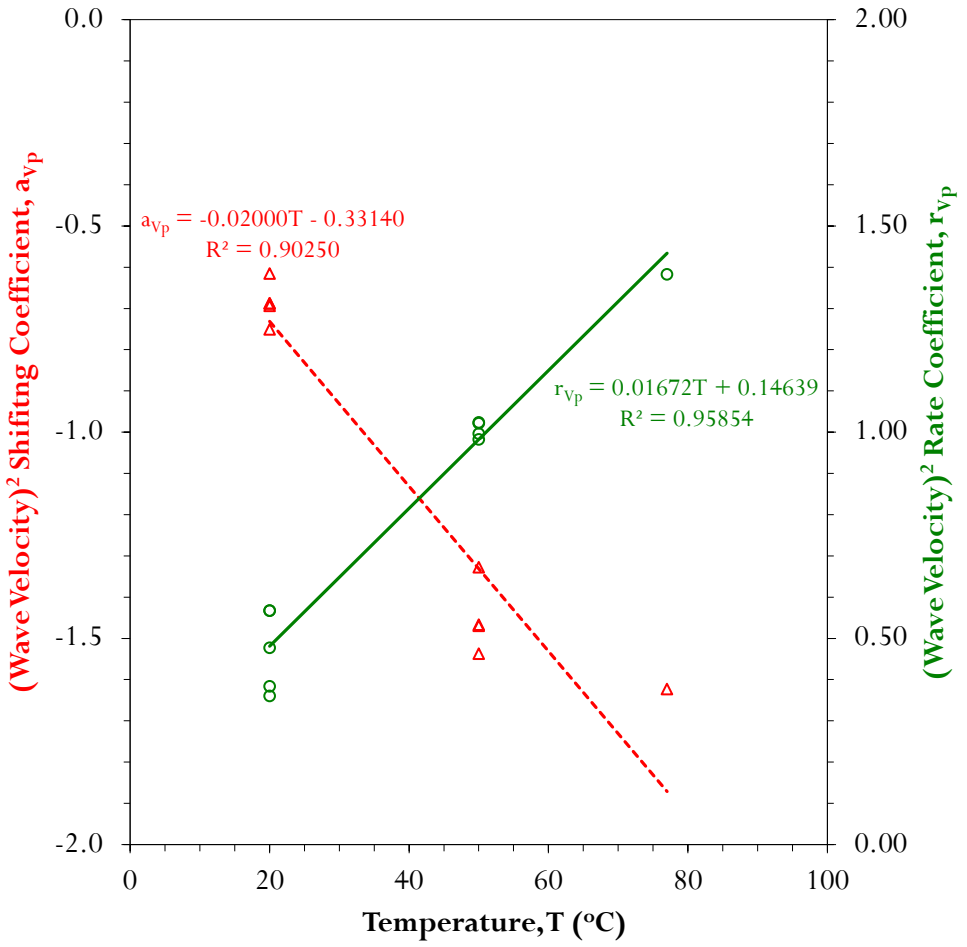

Figure 2.11: Mathematical model coefficients for wave velocity calculations.

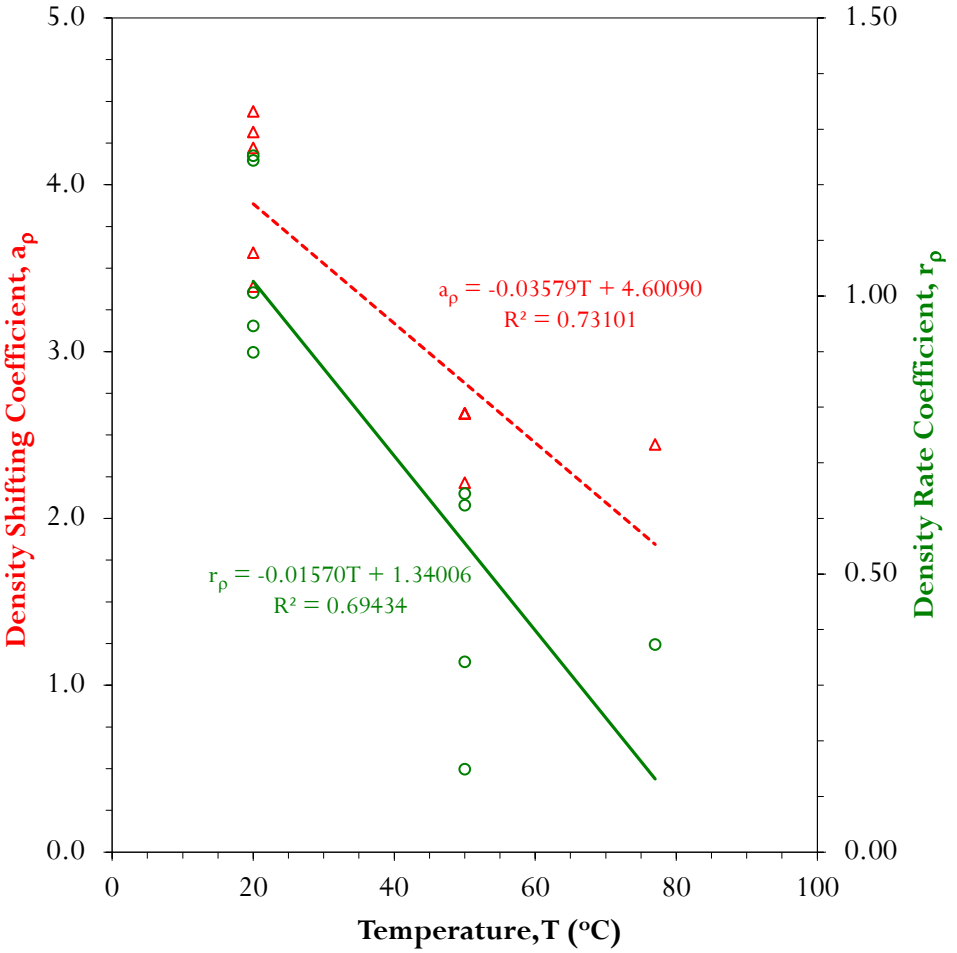

Figure 2.12: Mathematical model coefficients for density calculations.

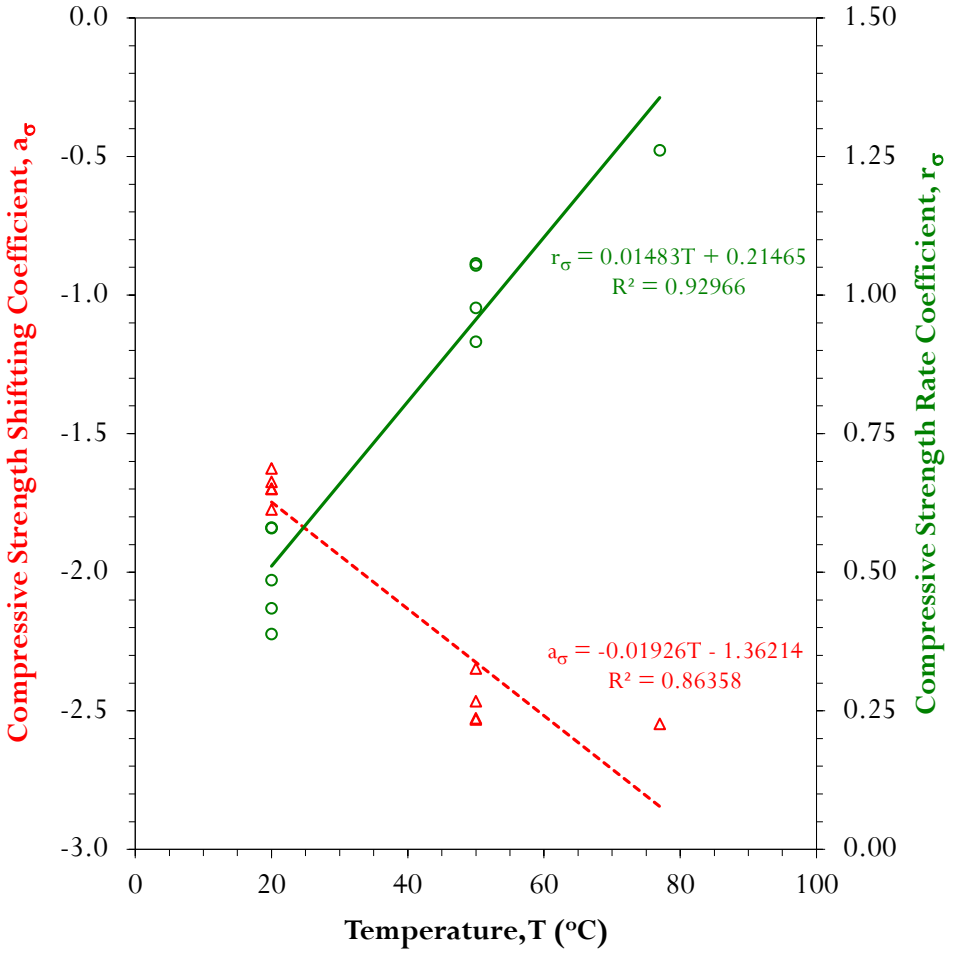

Figure 2.13: Mathematical model coefficients for strength calculations.

2.10 Summary

Wellbore cement properties during the hydration stage are important in detailed near-wellbore modeling. There is a need to improve our understanding about the initial state of a wellbore even when the objective is understanding the long-term behavior. The maturity rule is used in Civil Engineering and has been used to check the integrity of concrete job. Population dynamics monitors the change of age and/or size of populations. Both concepts have been integrated to formulate a methodology to model the evolution of cement properties during the hydration process.

Utilizing the basics of the maturity rule and population growth models, a mathematical model for predicting cement properties changes has been proposed. The model has been verified to predict the measurements of test data of well-documented test results available in the literature.

The mathematical model shows that despite the type of cement, cement property changes follow the same trend and the difference in behavior is reflected in the coefficients controlling the model. The model can be considered as a sound tool for predicting cement properties during hydration in any numerical model. The proposed methodology has an advantage of being based on a minimum number of coefficients that can be characterized under wellbore conditions. These coefficients are the apparent rate constant, r_P and the induction period constant, a_P where the subscript P stands for property under investigation.

The model proposed indicates clearly that its coefficients are function of borehole condition (i.e. temperature dependant). The coefficients can be used to check beforehand the effect of borehole condition on the performance of cement during hydration and will enhance the design of any cement mix.

2.11 References

Ansari, F., Luke, A., Dong, Y., and Maher, A., (1999), Development of Maturity Protocol for Construction of NJDOT Concrete Structures, Final Report, Center for Advanced Infrastructure & Transportation (CAIT), The State University, NJ, USA, 34 p.

Bergström, S.G., (1953), Curing Temperature, Age and Strength of Concrete, Magazine of Concrete Research (London), December 1953, Vol. 5, No. 14, pp. 61-66.

Bernhardt, C.J., (1956), Hardening of Concrete at Different Temperature, Proceeding of RILEM Symposium on Winter Concreting, Copenhagen, Danish National Institute for Building Research, Section BII, 19 p.

Bois, A-P., Garnier, A., Rodot, F., Saint-Mark, J., and Aimard, N., (2009), How to Prevent Loss of Zonal Isolation through a Comprehensive Analysis of Microannulus Formation, SPE Annual Technical Conference and Exhibition, 4-7 October, New Orleans, Louisiana, USA, SPE 124719, 20 p.

Carino, N.J., (1984), The Maturity Method: Theory and Application, ASTM J. Cem. Conct. Aggregates, Vol. 6, Issue 2, pp. 61-73.

Carino, N.J., and Lew, H.S., (2001), The Maturity Method: From Theory to Application, Proceeding of the 2001 Structures Congress & Exposition, May 21-23, Washington, D.C., American Society of Civil Engineers, 19 p.

Chin, F.K., (1971), Relation between Strength and Maturity of Concrete, Journal of American Concrete Institute, Vol. 68, Issue 3, pp. 196-203.

Dabic, P., and Krstulovic, R., and Rušic, D., (2000), A New Approach in Mathematical Modeling of Cement Hydration Development, Cement and Concrete Research, 30, pp. 1017-1021.

Espie, A.A., (2005), CO2 Capture and Storage: Contributing to Sustainable World Growth, International Petroleum Technology Conference, 21-23 November, Doha, Qatar, IPTC 10936, 7 p.

Fourmaintraux, D., Bois, A.P., Franco, C., Fraboulet B. and Brossollet, P., (2005), Efficient Wellbore Cement Sheath Design Using the SRC (System Response

Curve) Method, SPE Europec/EAGE Annual Conference, 13-16 June, Madrid, Spain, SPE 94176, 10 p.

Garcia-Monzon, H., (2006), Strength Durability Index (SDI) for Improved Concrete Strength and Durability Assessment, Ph.D. Thesis, Texas Tech University, USA, 186 p.

Goodwin, K.J., and Crook, R.J., (1992), Cement Sheath Stress Failure, Journal of SPE Drilling Engineering, Vol. 7, Issue 04, SPE 20453, pp. 291-296.

Goral, M.L., (1956), Empirical Time-Strength Relations of Concrete, Journal of American Concrete Institute, Vol. 53, Issue 2, pp. 215-224.

Gray, K.E., Podnos, E., and Becker, E., (2007), Finite Element Studies of Near-Wellbore Region during Cementing Operations; Part I, SPE Production and Operations Symposium, 31 March-3 April, Oklahoma City, Oklahoma, USA, SPE 106998, 15 p.

Hansen, P.F., and Pedersen, E.J., (1985), Curing of Concrete Structures, Danish Concrete and Structural Research Institute, Report, 39 p.

Hirany, A., and Kulhawy, F.H., (1989a), Interpretation of Load Tests on Drilled Shafts Part 1: Axial Compression, Foundation Engineering; Current Principles & Practices (GSP 22), ASCE, pp. 1132-1149.

Hirany, A., and Kulhawy, F.H., (1989b), Interpretation of Load Tests on Drilled Shafts Part 2: Axial Tension, Foundation Engineering; Current Principles & Practices (GSP 22), ASCE, pp. 1150-1159.

Jackson, P.B., and Murphy, C.E., (1993), Effect of Casing Pressure on Gas Flow through a Sheath of Set Cement, SPE/IADC Drilling Conference, 22-25 February, Amsterdam, Netherlands, SPE 25698, 10 p.

Keating, J., Hannat, D.J., and Hibbert, A.P., (1989), Correlation between Cube Strength, Ultrasonic Pulse Velocity and Volume Change for Oil Well Cement Slurries, Cement and Concrete Research, Vol. 19, pp. 715-726.

Kim, T, (2004), Concrete Maturity: A Quantitative Understanding of How Early-Age Temperature Affects the Maturity Concept, Ph.D. Thesis, University of Colorado, USA, 174 p.

Krstulovic, R., and Dabic, P., (2000), A Conceptual Model of the Cement Hydration Process, Cement and Concrete Research, 30, pp. 693-698.

Lacy, L.L., and Rickard, A., (1996), Analyzing Cements and Completion Gels using Dynamic Modulus, SPE Annual Technical Conference and Exhibition, 6-9 October, Denver, Colorado, USA, SPE 36476, 12 p.

Lew, H.S., and Reichard, T.W., (1978), Mechanical Properties of Concrete at Early Ages, Journal of American Concrete Institute, Vol. 75, issue 10, pp. 533-542.

Malhotra, V.M., and Carino, N.J., (2004), Handbook of Non Destructive Testing of Concrete, 2nd edition, CRC Press.

McIntoch, J.D., (1949), Electrical Curing of Concrete, Magazine of Concrete Research (London), January 1949, Vol. 1, No. 1, pp. 21-28.

McIntoch, J.D., (1956), The Effect of Low Temperature Curing on the Compressive Strength of Concrete, Proceeding of RILEM Symposium on Winter Concreting, Copenhagen, Danish National Institute for Building Research, Section BII, 17 p.

Mindess, S., Young, J.F., and Darwin, D., (2003), Concrete, 2nd edition, Prentice-Hall Inc., 644 p.

Mueller, D.T., Lacy, L.L., and GoBoncan, V., (1996), Characterization of the Initial Transitional and Set Properties of Oilwell Cement, SPE 36475, pp. 613-623.

Nabih, A, and Chalaturnyk, R, (2013a), Wellbore Efficiency Model for CO2 Geological Storage Part I: Theory and Wellbore Element, SPE Heavy Oil Conference, June 11-13, Calgary, Canada, SPE 165411, 14 p.

Nabih, A, and Chalaturnyk, R, (2013b), Wellbore Efficiency Model for CO2 Geological Storage Part II: Wellbore System, SPE Unconventional Resources Conference, November 5-7, Calgary, Canada, SPE 167149, 14 p.

Nelson, E.B. and Guillot, D., (2006), "Well Cementing", 2nd edition, Schlumberger, 773 p.

Neville, A.M., (1981), Properties of Concrete, 3rd edition, Pitman Publishing Ltd., 779 p.

Newman, J., and Choo, B.S., (2003), Advanced Concrete Technology: Concrete Properties, 1st edition, Elsevier Ltd., 321 p.

Nykänen, A., (1956), Hardening of Concrete at Different Temperatures Especially below the Freezing Point, Proceeding of RILEM Symposium on Winter Concreting, Copenhagen, Danish National Institute for Building Research, Section BII, 20 p.

Park, K., Noguchi, T., and Plawsky, J., (2004), Modeling of hydration Reactions Using Neural Networks to Predict the Average Properties of Cement Paste, Cement and Concrete Research, 34, pp. 1676-1684.

Pertué, A., Mounanga, P., and Khelidj, (2008), Application of the Maturity Concept for the Prediction of Restrained Autogenous Shrinkage of Cement Pastes, Proceeding of 3rd International Symposium GEOProc'2008, ISTE Ltd., J. Wiley, London, pp. 231-238.

Plowman, J.M., (1956), Maturity and the Strength of Concrete, Magazine of Concrete Research (London), March 1956, Vol. 8, No. 22, pp. 13-22.

Rastrup, E., (1954), Heat of Hydration in Concrete, Magazine of Concrete Research (London), September 1954, Vol. 6, No. 17, pp. 79-92.

Rastrup, E., (1956), The temperature function for Heat of Hydration in Concrete, Proceeding of RILEM Symposium on Winter Concreting, Copenhagen, Danish National Institute for Building Research, Section BII, 22 p.

Reddy, B.R., Santra, A., McMechan, D., Gray, D., Brennis, C., and Dunn, R., (2005), Cement Mechanical Property Measurements under Wellbore Conditions, SPE Annual Technical Conference and Exhibition, 9-12 October, Dallas, Texas, USA, SPE 95921, 8 p.

Saint-Marc, J., Garnier, A., Bois, A, (2008), Initial State of Stress: The key to Achieving Long-Term Cement-Sheath Integrity, SPE Annual Technical Conference and Exhibition, 21-24 September, Denver, Colorado, USA, SPE 116651, 15 p.

Saul, A.G.A., (1951), Principles Underlying the Steam Curing of Concrete at Atmospheric Pressure, Magazine of Concrete Research (London), March 1951, Vol. 2, No. 6, pp. 127-140.

Tomosawa, F., (1997), Development of a Kinetic Model for Hydration of Cement, Proceeding of the 10th Int. Cong. Chemistry of Cement, Vol.II, 8 p.

Turchaninov, I.A., Iofis, M.A., Kasparyan, E.V., (1979), Principles of Rock Mechanics, Translated version, 1st edition, Terraspace Inc., 493 p.

Van Den Abeele, K., Desadeleer, W., De Schutter, G., and Wevers, M., (2009), Active and Passive Monitoring of the Early Hydration Process in Concrete Using Linear and Nonlinear Acoustics, Cement and Concrete Research, 39, pp. 426-432.

Viviani, M., Glisic, B., and Smith, I.F.C., (2005), Three-Day Prediction of Concrete Compressive Strength Evolution, American Cement Institute Materials, Vol. 102, No. 4, pp. 231-236.

White, G.R., (1991), Concrete Technology, 3rd edition, Delmar Publishers Inc., 144 p.

Winsor, C.P., (1932), The Gompertz Curve as a Growth Curve, Proceeding of the National Academy of Sciences, Vol. 18, No. 1, pp.1-8.

Yi, S., Moon, Y., and Kim, J., (2005), Long-term Strength Prediction of Concrete with Curing Temperature, Cement and Concrete Research, Vol. 35, pp. 1961-1969.

Chapter 3: Assessment of Wellbore Integrity [2]

3.1 Introduction

Storing carbon dioxide (CO2) in deep geological formations is one part of the carbon capture and storage (CCS) process that is defined as geological CO2 sequestration or CO2 geo-sequestration. Injecting CO2 into a reservoir does not guarantee safe storage because CO2 could leak back to the surface and/or may contaminate specific strata where other energy, mineral and/or groundwater resources are present. Two mechanisms control assurance of storage integrity; geological leakage mechanism and wellbore leakage mechanism (Espie, 2005).

Leakage through cement sheath has been under study since the 1960's (Fourmaintraux et al., 2005; Bois et al., 2009). However, it was not until the 1990's that the work of Goodwin and Crook (1992) and Jackson and Murphy (1993) highlighted the possibility of damage in a cement sheath due to various events over the lifetime of the wellbore (Bois et al., 2009).

Norsk Sokkels Konkuranseposisjon (NORSOK), standards developed by the Norwegian Technology Centre, defines wellbore integrity as the "*application of technical, operational and organizational solutions to reduce risk of uncontrolled release of formation fluids throughout the life cycle of the wellbore*".

---

[2] A version of this chapter has been submitted for publication in the Proceedings of SPE Heavy Oil Conference Canada held in Calgary, Alberta, Canada, 10-12 June 2014.
Nabih, A., and Chalaturnyk, R., (2014), Stochastic Life Cycle Approach to Assess Wellbore Integrity for CO2 Geological Storage, SPE 170183.

NORSOK's definition is robust and practical because it includes the objective of reducing the risk of leakage, gathering the aspects of the procedure to achieve the objective, and defining the time frame of investigation to be the full lifecycle of the wellbore (Anders et al. 2006).

Researchers adopted the concept of the wellbore lifecycle and recognized its importance in simulating different stages that the wellbore has gone through. Two approaches were adopted that are either a geomechanical modeling approach (Bosma et al., 1999; Philippacopoulos and Berndt, 2002; Fourmaintraux et al., 2005; Gray et al., 2007; Takase et al., 2010; Nygaard and Salehi, 2011; Jandhyala et al., 2013) or managerial scope for decision-making (Moreno et al., 2004; Anders et al., 2006; Bachu and Haug, 2006; Watson and Bachu, 2007).

Geomechanical modeling for wellbore integrity has focused either on short-term scenarios from primary cementing until setting of cement or on long-term scenarios after setting of cement. However, different geomechanical approaches used either numerical modeling such as finite element analysis (FEA) method or system response curve (SRC) method to evaluate wellbore cement sheath state of stresses and enhance design (Saint-Marc et al., 2008).

Bosma et al. (1999) used the FEA method as an approach to investigate cement sheath design as a sealing material. Philippacopoulos and Berndt (2002); Pershikova et al. (2010); Takase et al. (2010); Guen et al. (2012); Jandhyala et al. (2013) also used the FEA method to perform thermal cement sheath integrity analysis and to investigate stresses due to thermo-elastic response of various cements. However, these studies did not include simulation of the cement hydration process and its effect on the initial stress state in cement sheath.

Gray et al. (2007) described in more detail different stages covering the life cycle of wellbore. However, they simulated cement hydration in a general sense and did not evolve the cement mechanical properties according to a sound function during cement hydration process (Saint-Marc et al., 2008). They neglected any initial state of stress in both casing and cement.

Fourmaintraux et al. (2005) used the SRC method to investigate efficient wellbore cement sheath designs. Using SRC was due to absence of clear understating of the fundamentals and difficulty to include all phenomena in one global model. However, their approach focused only on the mechanical simulation of the cement sheath in the solid state and neglected any initial state of stress due to cement hydration.

Saint-Marc et al. (2008) indicated that the SRC method does not include interface elements to simulate debonding at cement-casing and cement-formations interface. Debonding is not quantified but is observed when mismatch between the response curves exist. Various damage indices, defined by state of the stresses, characterized cement sheath integrity.

Nabih and Chalaturnyk (2013a) proposed a new analytical modeling of wellbore element as a basic unit for developing a model of an entire wellbore system. An "element" in this context refers to a control volume of a wellbore slice with any arbitrary thickness but coincident with the thickness of an adjacent formation. Nabih and Chalaturnyk (2013b) then used this basic model to analytically model the whole wellbore system. The approach will be discussed in more detail in Chapter 4 and Chapter 6.

The approach discussed above involves specifying a wellbore bulk "effective" permeability, which is likely best treated as an indicator of wellbore integrity.

This is a problematic property as there have been no direct measurements of the bulk permeability along well segments (Nordbotten et al., 2009; Celia et al., 2011). Researchers deal with wellbore element bulk permeability by assuming either a deterministic value (Nordbotten et al., 2004, 2005, 2009; Gasda, 2008; Janzen, 2010; Celia et al., 2011; Nogues et al., 2011) or random variable value picked from an assumed probability distribution (Celia et al., 2009, 2011; Court, 2011; Dobossy et al., 2011; Nogues et al., 2012; Nicot et al., 2013).

For CO2 storage, the ultimate goal for well-leakage models is to serve as inputs for a certification framework and risk analysis (Gasda and Celia, 2005; Watson and Bachu, 2008; Celia and Nordbotten, 2009; Celia et al., 2009; Oldenburg et al., 2009; Dobossy et al., 2011; Humez et al., 2011; LeNeveu, 2012). In order to achieve this goal, there is a need for further study to investigate a more realistic representation of wellbore element bulk permeability that can differ from element to element within a wellbore system.

No well-defined and accepted universal procedure has been adopted for detailed near-wellbore modeling due to insufficient knowledge and interaction between different parameters affecting the wellbore element. There is a need to develop a unified method and a conceptual model, which can be used as a practical engineering platform to assess wellbore integrity (Fourmaintraux et al., 2005). As well, assessing wellbore integrity is a challenging task because it needs a multi-faceted discipline management system. This management system is immature due to evolving of standards, regulatory requirements and guidelines (Anders et al. 2006).

In this chapter, a full lifecycle methodology is proposed to estimate the wellbore permeability as a measure of the risk of leakage and a tool to assess wellbore integrity. The methodology identifies the key elements to model the wellbore element. It incorporates the use of a statistical approach to better understand the uncertainty in the risk estimation and interaction between various parameters controlling the model.

3.2 Wellbore Modeling Approach

It is a fact that in petroleum geomechanics, uncertainty is embedded in all elements of wellbore integrity. Sheng et al. (2006) indicated that dealing with uncertainty may include passive solutions (i.e. ignoring or neglecting), being conservative, observational method, and recently to quantify the uncertainty.

Uncertainty is a part of the profession and has significant influence of the expected behavior of any system. Any time staged professional job will include different aspects where each has its own characteristics such as site characterization, analysis, design, decision-making, and construction (El-Ramly, 2001). For wellbore integrity, these aspects must definitely add operational and abandonment activities.

Holling (1978) introduced a classification system to model problems in ecology illustrated in Figure 3.1. The horizontal axis is a measure of understanding of the problem need to be solved, while the vertical axis is a measure of either quality and/or quantity of information and available data (Starfield and Cundall, 1988).

Starfield and Cundall (1988) summarized Hollings' categorization for modeling a problem into four distinctive regions as:

1) Region 1; available data with less understanding of the phenomena is present and where statistics is the appropriate modeling tool,
2) Region 2; both data and understanding exist and hence models can be validated,
3) Region 3; the problem has a limited data with some understanding and knowledge of the key factors governs the model proposed, and
4) Region 4; the critical region where the problem has limited data either by unavailability or by easiness to obtain with low knowledge and understanding of the proposed model.

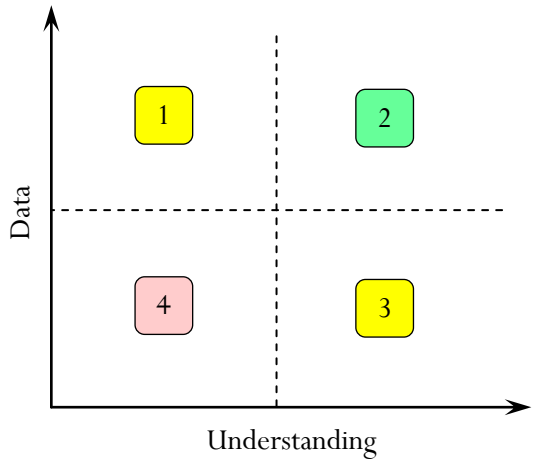

Figure 3.1: Modeling problems classification (after Starfield and Cundall, 1988).

One may argue that understating exist due to many efforts to define the basic pieces and concepts of understanding of leakage problem and hence classify wellbore modeling to be located in Region 2 which make the problem more predictive. While a basic understanding of wellbore modeling does exist, data

limitation remains a source of deficiency and models based on FEA method fall in this region or at least in region 3.

From Holling's classification, assessing wellbore leakage likely falls in Region 3 and Region 4 where data are insufficient. In wellbore modeling, insufficient data is one part of the problem. Assessing wellbore integrity is a challenging task because of insufficient knowledge (Fourmaintraux et al., 2005) and being a multi-faceted system (Anders et al., 2006) that would move wellbore modeling problem toward Region 4 where the response of the modeled system is the major objective.

3.3 Statistical Models

Probabilistic models have the advantage to include the full range of the possible outcomes where the spread in these models outcomes quantifies the uncertainty in the predicted behavior of the system (El-Ramly, 2001).

Probabilistic approach can be utilized to treat uncertainty in the wellbore performance assessment. In this approach, uncertainties in model inputs (parameters) are propagated using statistical methods to produce corresponding uncertainties in model output (predictions). Uncertain parameters can be described in a probabilistic framework in which multiple realizations of model inputs are sampled, and the model outputs are computed.

Statistical continuous distributions are applicable whenever the random variable may take any value within some range. The most two common continuous statistical distributions models are uniform and normal distributions. In the following sub-sections, for any random variable, x, then

f(x) denotes the probability density function (PDF), F(x) denotes cumulative density function (CDF), μ denotes the mean and σ denotes the standard deviation.

3.3.1 Uniform Distribution Model

Uniform distribution is the simplest type of continuous distributions that gives equal likelihoods to any possible values within the specified maximum and minimum values of a random variable, x.

$$\text{PDF:} \qquad f(x) = \frac{1}{b-a} \qquad ; \ a \le x \le b \tag{3.1}$$

where b and a are maximum and minimum variable respectively.

$$\text{CDF:} \qquad F(x) = \frac{x-a}{b-a} \qquad ; \ a \le x \le b \tag{3.2}$$

and,

$$\text{Moments:} \quad \mu = \frac{a+b}{2} \quad ; \text{ and } \quad \sigma^2 = \frac{(b-a)^2}{12} \tag{3.3}$$

For a uniform distributed variables, a linear transformation model can be used, (Ayyub and McCuen, 2003; Fenton and Griffiths, 2008), as:

$$x = x_{min.} + U(x_{max.} - x_{min.}) \tag{3.4}$$

where,

$x_{min.}$: minimum value of the random variable,

$x_{min.}$: maximum value of the random variable, and

U: generated random value from uniform distribution [0,1].

It is a rough model for representing low states of knowledge when only the upper and lower bounds are known and prior reasoning or available information does not indicate otherwise. In general, uniform distribution is

appropriate to represent a random variable range that is based on physical arguments, expert knowledge or historical data but not much else is known about the relative likelihood of values within this range (Mishra, 2002; Fenton and Griffiths, 2008).

3.3.2 Normal Distribution Model

Normal distribution is useful to model natural processes and physical phenomena. Central limit theory is the reason to assume that the variable is normally distributed. The normal distribution is an unbounded statistical distribution. Sampling of a random variable should avoid resulting in negative (non-physical) sampled values at the lower tail (Mishra, 2002; Ayyub and McCuen, 2003).

PDF: $$f(x) = \frac{1}{\sqrt{2\pi\sigma^2}} \exp\left(-\frac{1}{2}\left(\frac{x-\mu}{\sigma} \right)^2 \right) \quad ; -\infty < x < \infty \qquad (3.5)$$

where,

μ: mean, and

σ: standard deviation.

CDF: F(x) has no closed form solution, but it can be expressed in terms of the standard normal CDF, G(.),

and,

Moments: Same as parameters of the distribution.

The central limit theorem states that the sum of independent observations asymptotically approaches a normal distribution regardless of the shape of the underlying distribution(s). The central limit theory is the rationale to assume that a random variable follows a normal distribution model.

3.3.3 Generating Normal Numbers

It is important to generate random numbers that follow any arbitrary PDF. The task can be performed by uniform random number. The generation of normal random numbers do not have an explicit form. A common method is to generate two independent uniform random numbers U_1 and U_2. Based on these uniform numbers, another two independent standard normal numbers Z_1 and Z_2 can be generated, (Baecher and Christian, 2003; Fenton and Griffiths, 2008), as follows:

$$Z_1 = \cos(2\pi U_2).\sqrt{-2\ln(U_1)} \tag{3.6}$$

and,

$$Z_2 = \sin(2\pi U_2).\sqrt{-2\ln(U_1)} \tag{3.7}$$

3.3.4 Number of Simulations

Large sample size is required to perform a Monte Carlo analysis in order to approximate the original distribution. Consequently, the computational cost may become a critical concern. An important aspect is to find the necessary number of simulation runs to evaluate a probability of failure, P_f, of required accuracy. Without prior knowledge of P_f, the maximum possible value 0.25 can be used (Hughes and Grawoig, 1971; Milton and Tsokos, 1983; Hohnson and Bhattacharyya, 1996; Baecher and Christan, 2003).

Figure 3.2 shows the appropriate sample size for estimating a proportion. The estimation is determined in much the same way as is the sample required for estimating the mean. In order to determine how large a sample is needed for estimating a population mean, we must specify the desired error margin, d and the probability associated with that error margin, $(1-\alpha)$.

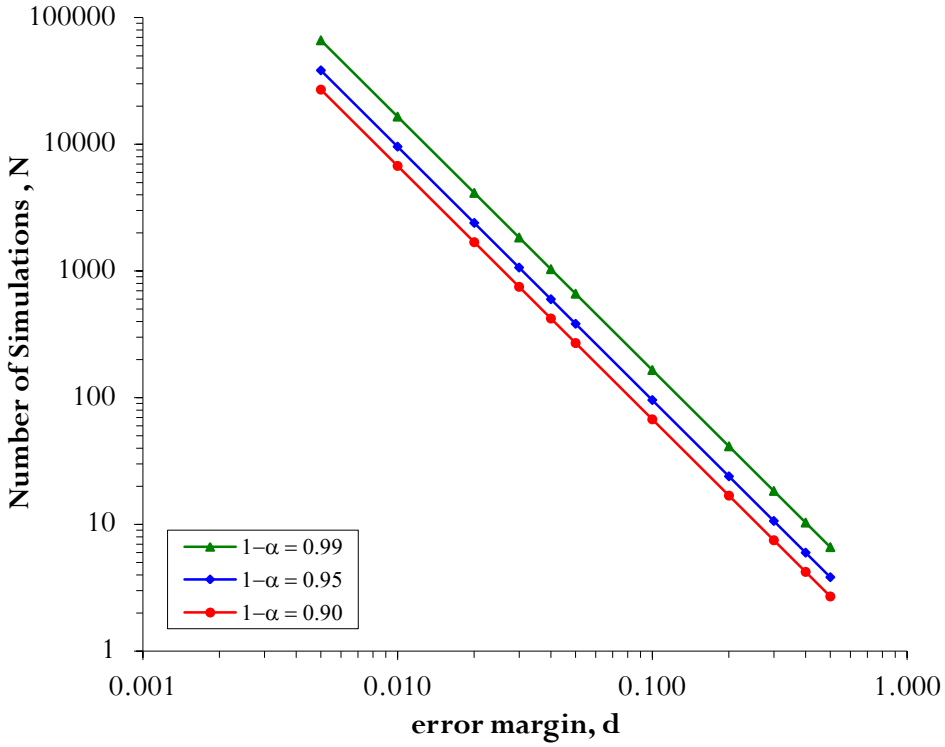

Figure 3.2: Required number of Simulation (after Baecher and Christan, 2003).

The number of simulations, N, is:

$$N = \frac{1}{4}\left(\frac{Z_{\alpha/2}}{d}\right)^2 \tag{3.8}$$

where the value of $Z_{\alpha/2}$ can be obtained from the statistical tables and few of these values appear in Table 3.1 for reference.

Table 3.1: Values of $Z_{\alpha/2}$

1 - α	0.80	0.85	0.90	0.95	0.99
$Z_{\alpha/2}$	1.280	1.440	1.645	1.960	2.580

In practice, usually a sample size of 1000 is sufficient to provide an acceptable uncertainty and the 95th percentile value would fall within $\pm$3.7% of a reported value (Milton and Tsokos, 1983; Sheng et al., 2006; Nogues et al. 2012).

Melchers (1999) cited that Broding et al. (1964) suggested number of simulation runs, N to be:

$$N > \frac{-\ln(1-\alpha)}{P_f} \tag{3.9}$$

where,

α: confidence level for obtaining a probability of failure P_f.

Simulation runs N is about 300 for α =0.95 and P_f = 0.01. The number of variables should be multiplied by this number of simulation (Honjo, 2008).

3.3.5 Statistical Data Representation

Histogram is the graphical representation of the distribution of statistical data. Horizontal axis of the histogram gives the range of values "random variable". The range is usually divided into equal intervals (bins) which are called classes or cells. Although there is no optimum number of cells, care should be exercised in choosing the number of cells, n_c. Few numbers of cells will omit important features of data, while many will lead to fluctuations that will not give a clear picture about the distribution (Kottegoda and Rosso, 1997).

Table 3.2 summarizes in chronological order different attempts to determine the optimum number of cells, n_c, compiled by Kottegoda and Rosso (1997). A rule of thumb is the square root choice and to let $n_c = \sqrt{N}$ but not less than

5 and not more than 25. This means that minimum number of data required for a histogram is 25 (Kottegoda and Rosso, 1997).

Table 3.2: Estimation of number of cells (Kottegoda and Rosso, 1997).

Author(s)	Year	Number of Classes, n_c	Note(s)
Sturges	1926	$1+3.3\log(N)$	Assume normal distribution
Scott	1979	$\frac{r(N)^{\frac{1}{3}}}{3.5\sigma}$	r: range = $x_{max.}$-$x_{min.}$, and σ: sample std. deviation
Freedman and Diaconis	1981	$\frac{r(N)^{\frac{1}{3}}}{2\,IQR}$	IQR: interquartile range $IQR = Q_3 - Q_1$
Kottegoda and Rosso	1997	$\sqrt{N}$	Rule of Thumb

3.4 Wellbore Interfaces

There are several instances in geomechanics when it is desirable to represent planes on which sliding or separation can occur. The following sections discuss the interface modeling approach adopted in this research.

3.4.1 Types of Interfaces

Interfaces can be classified into either perfect interfaces and imperfect interfaces. The perfect "classical" interface is the interface where the displacement vector and stress vector are continuous. Continuity in the former is based on the hypothesis of perfect bonding while in the latter is based on local equilibrium. Imperfect interface is the interface when any of these conditions are violated (Hashin, 2002).

Hashin (2002) investigated the problem in two ways. The first approach is the exact "detailed" three-phase elastic problem where the phases are cylindrical (e.g. casing), concentric coating (e.g. cement) and a surrounding medium (e.g. formation). The second approaches adopted a two-phase problem cylinder surrounding a medium separated by an imperfect interface conditions. The two approaches are numerically indistinguishable except for extremely high values of the ratio between shear modulus of the interface and surrounding cylinder (e.g. G_{cem}/G_{form}). The two solutions begin to diverge when this ratio having the order 10^8. Such stiffness ratio does not exist in nature except perhaps in the case of a soft rubbery matrix (Hashin, 2002).

3.4.2 Interface Modeling

Depending on the level of accuracy or desired outcome from simulations, modeling of the interface can be further categorized into (Lourenço, 1994, 1996; Lourenço et al., 1995):

1) detailed micro-modeling; where units (e.g. casing and formation) and cement are represented by continuum elements whereas the unit-cement interface is represented by discontinuous elements,
2) simplified micro-modeling; where units are represented by continuum elements whereas the behavior of the cement unit-cement interface is lumped in discontinuous elements, and
3) macro-modeling; where units cement and unit-cement interface are smeared out in the continuum.

For leakage study purposes, wellbore permeability depends on the gap width that may exist between cement-formation and cement-casing interfaces, which suggests adopting the detailed micro-modeling approach.

3.4.3 Modeling Interfaces in FLAC

Numerical methods have a high degree of accuracy with lower number of assumptions. There are many examples for successful modeling of geomechanical problems but in a deterministic way (Sheng et al., 2006). FLAC software will be used model the wellbore element. FLAC has a built-in programing language that is called FISH, which will control and modify the wellbore simulation modeling process.

In FLAC environment, the interface is characterised by two opposite surfaces where each is divided into contiguous segments. As indicated in Figure 3.3, each side of the interface is composed of grid-points. The code keeps a list of the grid-points (i,j) that lie on each side of any particular surface.

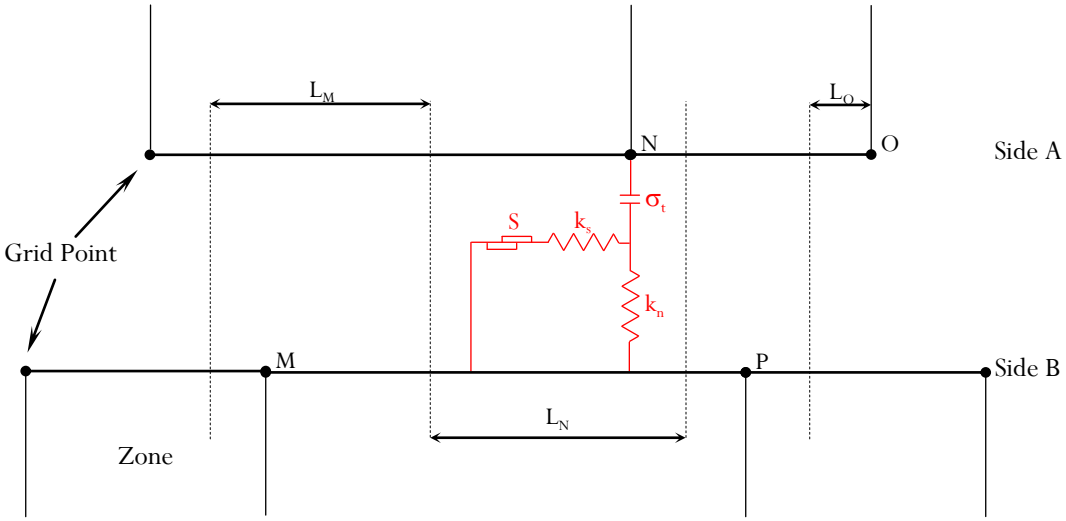

S: slider; σ_t: tensile strength; k_n: normal stiffness; k_s: shear stiffness;
L_M, L_N, L_O: length associated with grid point M, N and O respectively and
----- denotes limits for joint segment (placed halfway between adjacent grid points)

Figure 3.3: Interface modeling in FLAC (after Itasca, 2008).

The co-ordinates of these grid-points can be obtained at any stage of the simulation process by a coded sub-routine for any given range of the grid points. The produced co-ordinates are then coded to calculate the radial distance of each grid-point and the relative displacement of each interface side. This relative displacement will be used to calculate the gap width for cement-formation interface and cement-casing interface.

Any interface option requires defining shear stiffness, k_s, and normal stiffness, k_n. FLAC recommends that k_n and k_s be set to ten times the equivalent stiffness of the stiffest neighboring zone. Stiffness values have the units of stress/displacement as:

$$k_n, k_s = \left(\frac{K + \frac{4}{3}G}{\Delta z_{min.}} \right)_{max.} \times F_{int} \qquad (3.10)$$

where,

K, G: bulk and shear moduli,

$\Delta z_{min.}$: smallest width of an adjoining zone in the normal direction, and

F_{int}: interface factor taken as 10.

The interface factor, F_{int}, is applied to prevent movement on the interface. A value of 10 is typically chosen to avoid very slow solution convergence due to very high value. An interface is either used as an artificial tool to connect sub-grids or as a real interface that influence a behavior of a system. If there are two materials on each side of an interface, then Equation (3.10) should be applied to the softer side where the deformability of the whole system is dominated by the soft side (Itasca, 2008).

The interface factor is used because the stiffness values obtained from these formulae do not correspond to a penalty approach, which means that overlap

of neighboring units subjected to compression will become visible. Wellbore interface is a real interface problem where there is a need to use real physical values for its behavior and wellbore permeability depends on gaps developed at cement-formation and cement-casing interfaces.

3.5 Modeling Wellbore Uncertainties

Normally, deterministic approaches have used the averaged values for input parameters to numerical simulations. This may lead to conclusions that differ from the true behaviour of a system and provide no information regarding the uncertainty of numerical prediction. On the other hand, application of probabilistic approaches in wellbore modeling is relatively new (Mishra, 2002). Presence of uncertainties in all geomechanical problems results in uncertainty in the output of any analysis (El-Ramly, 2001). Probabilistic approaches can be utilized to quantify the effects of the uncertainties on wellbore problems. Investigation of wellbore response under the impact of different uncertainties expected to result in better design making around well design.

Morgenstern (1995) divided geotechnical uncertainty into three distinctive categories, which are human uncertainty, model uncertainty, and parameters uncertainty (El-Ramly, 2001). The following sub-sections are concerned with the reduction of uncertainty in the wellbore global modeling.

3.5.1 Human Uncertainty Reduction

Human uncertainty that is related to human errors and mistakes which may be reflected in determination of parameters or in-situ as-built model due to construction activity shown in Figure 3.4.

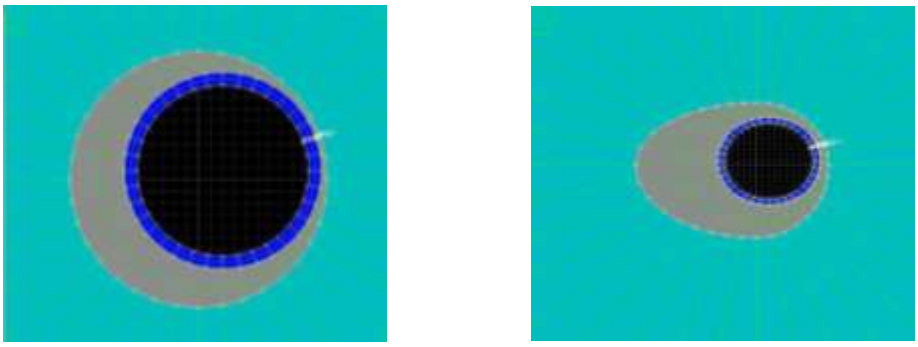

(a) Casing eccentricity (b) Non circular wellbore

Figure 3.4: Reduction of human uncertainties due to actual field problem.

To minimize the human uncertainty, the model should be representative and accurate. The wellbore global model should:

1) quantify spatial space of the problem; this include a model domain which will extend to a radial distance to minimize the boundary conditions to be 10 times of theoretical diameter of the well (i.e. 10 x bit diameter) and range varies along the height of a formation layer.
2) represent the in-situ geometrical conditions like eccentricity and non-circular well geometry, as illustrated in Figure 3.4.
3) follow mathematical approach and logic sequence as possible to minimize the personal judgments and interpretations.
4) be flexible to minimize the number of elements in the wellbore vicinity without affecting solution and running time.
5) reduce personal judgement and therefore the concept of the maturity method to justify the mechanical parameters evolution during cement hydration, as described in Chapter 2.

3.5.2 Model Uncertainty Reduction

Model uncertainty is due to the limitation of the theories and models used in performance prediction. It includes both the stress-strain condition and failure criteria used in wellbore modeling. For stress-strain condition, a plane-strain condition is chosen as a result of the leakage modeling through wellbore element (Nabih and Chalturnyk, 2013a).

Different failure criteria were used to justify rock shear failure. The Mohr-Coulomb criterion was chosen for this study because it is one of the most conservative criterion and a "two-principal-stress" criterion is adequate for the purposes of wellbore stability (Chen, 2001). Therefore, Mohr-Coulomb criterion will be used as it gives a higher factor of safety against leakage.

3.5.3 Parameter Uncertainty Reduction

Parameter uncertainty represents uncertainty in the data inputs of the analysis. Any parameter will take either a deterministic value, DV or a random value, RV. Model simulation parameters cover all aspects of the numerical model. Parameters can be classified to four main categories, which are:

1) Model State Parameters,
2) Model Geometrical Parameters,
3) Model Materials Parameters, and
4) Model Conditions Parameters.

These parameters are represented in details in Tables 3.3, 3.4, and 3.5. Model state parameters, Table 3.3, includes typical geomechanical parameters of a storage site that influence the initial state of a wellbore.

Table 3.3: Model state parameters

Sub-Category	Properties	Parameters	DV	RV
Initial State	Location	Depth, D		√
	Mechanical	Vertical stress gradient, σ_{zz}	√	
		Min. horizontal stress gradient, $\sigma_h = \sigma_{xx}$	√	
	Thermal	Average surface temperature, T_0	√	
		Geo-Thermal gradient	√	
	Hydraulic	Pore-Pressure gradient	√	
		Normal Pore-pressure Condition	√	

Table 3.4 represents model geometrical parameters that affect the configuration of wellbore element that will be modeled. It contains theoretical parameters and field parameters.

Table 3.4: Model geometrical parameters

Sub-Category	Properties	Parameters	DV	RV
Theoretical	Dimensions	Bit "well" diameter, d_{wo}	√	
		Outer casing diameter, d_{co}	√	
		Casing thickness, t_c	√	
	Accuracy	Angle Step,	√	
		Model Extent Factor, MXF	√	
In-Situ	Dimensions	Field Well Boundaries		√
		Eccentricity, e%		√
		Eccentricity azimuth angle, α	√	

Angle step parameter is the angle used to control how much dense the elements in the circumference direction and hence control the overall number of the element in the model. The model extent factor is the factor by which the model extends out to its external boundary. Eccentricity azimuth angle defines direction of eccentricity from north.

Model material parameters, as shown in Table 3.5, include the properties of the materials in wellbore modeling. The interaction between these materials under the effect of the state parameter, Table 3.3, and the conditions parameters will give the true response of a given wellbore element represented by the geometrical parameters.

Table 3.5: Model material parameters.

Sub-Category	Properties	Parameters	DV	RV
Casing	Mechanical	Surface force	√	
		Density, ρ_c	√	
		Modulus of Elasticity, E_c	√	
		Poisson's Ratio, ν_c	√	
	Thermal	Thermal Conductivity, $K_{th\,c}$	√	
		Specific Heat capacity, H_c	√	
		Linear thermal Expansion, α_c	√	
Formation	Mechanical	Density, ρ		√
&		Modulus of Elasticity, E		√
Hardened		Poisson's Ratio, ν		√
Cement		Cohesion, c		√
		Internal Angle of Friction, ϕ		√
		Dilation Angle, φ		√
		Tension, σ_t		√
	Thermal	Thermal Conductivity, $K_{th.}$		√
		Specific Heat capacity, H		√
		Linear thermal Expansion, α		√
	Hydraulic	Initial Porosity, n		√
		Initial permeability, $k_{hd.}$		√
		Fluid Density, $\rho_{f.}$		√
Fluids	Mechanical	Applied Pressure at G.S.	√	
		Density, ρ		√
	Thermal	Temperature, T		√

Model condition parameters are the borehole conditions at a given depth (i.e. pressure and/or temperature) affecting the inner face of the casing. These

conditions depend on the existence of wellbore records and define the history of the wellbore during drilling, cement job and hydration, operation, and any artificial activity and events.

These input parameters are classified in order to define the wellbore global simulation framework for each wellbore element. Each element locally is considered as sub-system, which has its own efficiency factor related to leakage potential as shown in Chapter 4. These sub-systems are connected in a serial manner as will be shown in Chapter 6 to predict the whole wellbore system. The global model will be organized sequentially to mimic the lifecycle stages of the wellbore.

3.6 Wellbore Simulation Process

For storage sites associated with depleted oil and gas reservoirs, many wellbores will have been drilled and abandoned over a range of time periods and the cement used in the construction of these different wellbores would have different quality and quantity. A very important element of successful CCS project depends on mitigating the risk of small-scale leakage associated with localized flow along wells.

The simulation process will involve two key features that relate to the conceptual procedure based on Holling's model. The process can be described as a sequential stochastic simulation of detailed near-wellbore modeling. The model used sequential simulation to model different stages during the wellbore time life, while using stochastic simulation to reduce risk of geomechanical uncertainties in input data.

3.6.1 Wellbore Sequential Simulation

Performance of a cement sheath in a single wellbore as a source of CO2 leakage is believed to dependent on events over the lifetime of the well (Fourmaintraux et al., 2005; Gray et al., 2007). Therefore, wellbore integrity is a function of lifetime where the domain is affected by the change of material properties with the change of wellbore events over the lifetime of this wellbore.

Table 3.6: Wellbore simulation sequence life span and coding.

Main Stage	Engineering Phase	Notes	Time, t	Coding
Initial	Planning	Formation only	$t = 0$	0000
Drilling	Construction	Mud	$\leq t_{\text{primary cementing}}$	0110
		Pre-flush		0120
Cementing		Cement Slurry	$\leq t_{\text{Induction Period}}$	0210
				0220
Cement Hydration		Day One	$\leq t_{\text{24 hrs Hydration}}$	0300
	Operation	Month One	$\leq t_{\text{30 days}}$	0400
Hardened Cement		Months	$\leq t_{\text{Deterioration}}$	0500
Deteriorated Cement	Aging	Years	$\leq t_{\text{Target}}$	0600

Stage coding in the staged simulation process, illustrated in Table 3.6, considers the following:

1) The oil well may be regarded as an object having its own time frame,
2) According to this time frame, the wellbore has the following main stages where each one defines an engineering phase and is represented by the first two numbers of stage coding; initial, drilling, cementing, operation and abandoned, aging stage.
3) These main stages can be subdivided into additional stages to provide additional simulation detail for assessing overall well performance.

This subdivision is represented by the last two number of any stage coding.

4) These two numbers facilitates programming counting for different time accuracy within a certain stage and/or different wellbore events.

Figure 3.5 shows the key features of these simulation stages. Initial "virgin" stage, Stage_0000, of the wellbore represents the state of formation before any activity controlled by model state parameters. Drilling stage, Stage_0100, represents phase of the wellbore construction when the formation is removed and is replaced by drilling mud defined by the coding Stage_0110. The stage may contain pre-flushing activity, coded as Stage_0120, since wellbore fluids affect the response of the wellbore.

Cementing Stage is also part of the construction activities of the wellbore. This stage is characterized by two different main stages, which are stage_0200 and stage_0300. Stage_0200 is similar to Stage_0100 by the existence of wellbore fluids (i.e. cement slurry). The sub-coding is to mimic the change of cement slurries properties when placing the cement slurry (Stage_0210) and the properties at maximum hydration and end of the induction period (Stage_0220).

Stage_0300 of cementing is to represent the cement hydration process in the first day where a timeframe can be presented in hours. The stage is to follow the procedure described in Chapter 2 to allow the change of cement properties. In addition, it allows simulating the waiting of cement (WOC) time before well completion operations continue.

Stage_0400 and Stage_0500 can be considered as transitional periods that have time frame defined in days and months respectively. First stage,

Stage_0400, is defined in days to allow the continuation of the hydration process until cement if fully set at one-month period and gained its hardening properties as a fully solid material. However, Stage_0500 is to allow representing the timeframe in months before transfer to an annual representation of the lifecycle of a wellbore. This stage is characterized by fully hydrated cement properties. The counting for any sub-stages will end at 99 month if required.

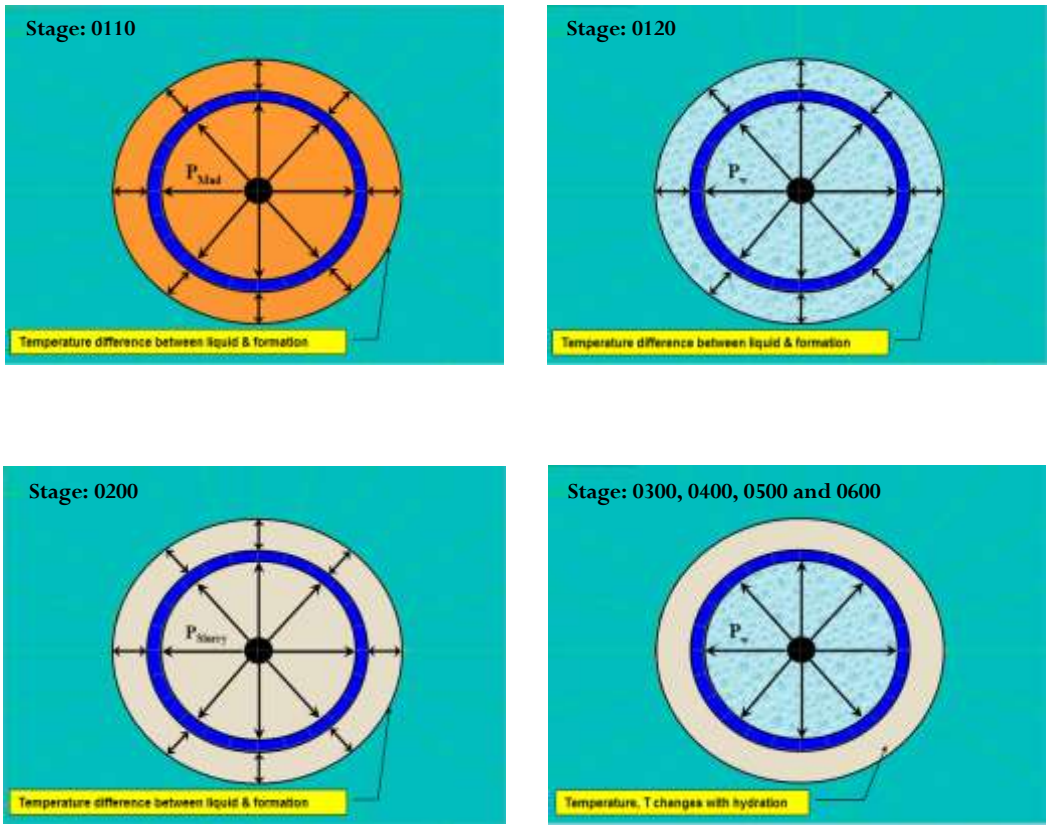

Figure 3.5: Schematic representation of wellbore sequential modeling.

Ageing phase, Stage_0600, begins when there is a need to simulate the deterioration of the cement properties according to a given mathematical

model (i.e. linear, power, exponential and hyperbolic) or any developed model either experimentally or theoretically. Stage_0600 is dominated by the wellbore events that may affect the behavior and the response of wellbore cement sheath. Wellbore condition parameters define wellbore events that also exist in the same time of the change cement properties.

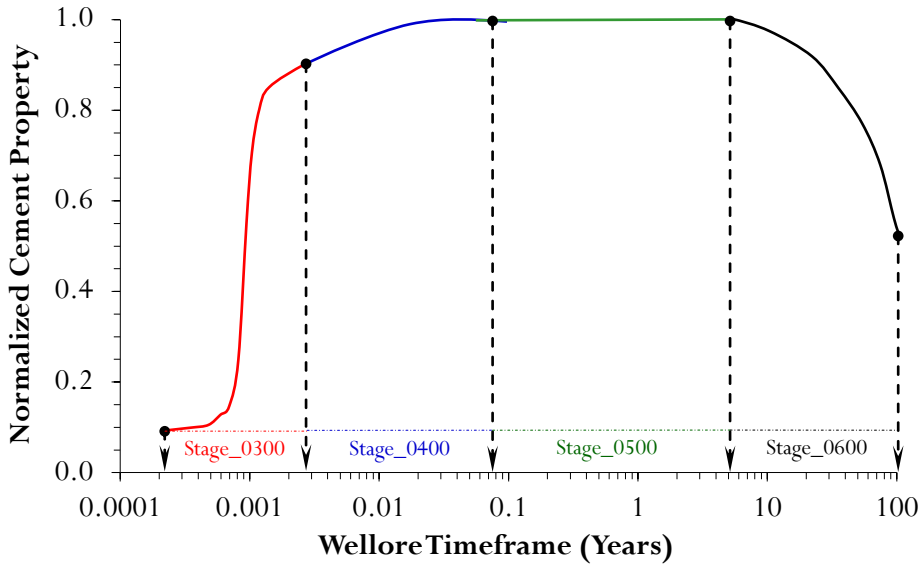

Figure 3.6: A schematic diagram of cement properties changes in modeling.

A schematic diagram, Figure 3.6, shows generic cement properties changes that should be considered in sequential modeling that illustrated in Table 3.6.

3.6.2 Wellbore Stochastic Simulation

Normally, deterministic approaches use the averaged values for the input parameters. This may lead to conclusions that differ from the true behaviour of a system. Probabilistic approaches can be utilized to quantify the effects of the uncertainties on wellbore problems (Mishra, 2002).

Stochastic simulation in a wellbore is done by picking a random value of each input data from a pre-specified probability distribution. These random variables will give, at the end of each sequential simulation (i.e. trial), a single and/or multi output data. Repeating this procedure will generate a range of all possible results, which provides an opportunity to assess uncertainty. Therefore, any output variable can be represented by a fitted nearest probability distribution that can be described by the mean and standard deviation. Thus, a risk based reliability analysis can be preformed.

3.7 Model Input Data

Whittaker et al. (2004) provided a detailed geological stratigraphy, Appendix A, of Weyburn storage site. Thickness of the caprock in Weyburn ranges from one meter to 10 m (Whittaker, 2005). Walton et al. (2004) gave a detailed description for the depth and thickness of different formations within the Weyburn storage site, as indicated in Appendix A.

The Weyburn storage reservoir is sealed by an anhydrite formation called Midale Evaporite. Assessment for the integrity of this caprock has indicated it remained intact throughout the history of the storage site prior to injection (Chalaturnyk et al., 2004). Depth was taken as a uniform random variables as shown in Appendix B.

For caprock formation deformability properties, Appendix B, Young's modulus, E_{form}, is linearly related to the unconfined compressive strength, whereas its Poisson's ratio, ν_{form}, is almost constant and independent of both Young's modulus and unconfined compressive (Gomez 2006). Modulus of elasticity can be expressed as:

$$E_{form} = 10^9 + 625\,\sigma_{c\,form} \qquad \text{(Pa)} \tag{3.11}$$

where $\sigma_{c\,form}$ is the unconfined compression strength for the formation while Poissons's ratio range is:

$$\nu_{form} = 0.20 - 0.40 \tag{3.12}$$

For strength properties, Appendix B, angle of internal friction, ϕ_{form}, was between 30° and 45° while cohesion, c_{form}, was between 13 and 20 MPa for most of the samples (Gomez 2006). Both strength properties have been assigned to be normally distributed between their given ranges. To overcome the unbounded nature of the normal distribution, a code was written depending on the Equations (3.6) and (3.7). This allowed the model to assign normally distributed variables within a specific range, as shown in Appendix B. Caprock formation is assumed to follow Mohr-Coulomb failure criterion which is expressed as:

$$\sigma_1' = 2c\frac{\cos\phi}{1-\sin\phi} + \frac{1+\sin\phi}{1-\sin\phi}\sigma_3' \tag{3.13}$$

where σ_1' and σ_3' are maximum and minimum principal effective stresses respectively. Thus, unconfined compressive strength can be estimated as:

$$\sigma_{c\,form} = 2c\frac{\cos\phi}{1-\sin\phi} \tag{3.14}$$

Normally tensile strength, $\sigma_{t\ form}$, if considered is estimated as ratio of unconfined compressive strength, Fjær et al. (2008), as:

$$\sigma_{t\,form} = \left(\frac{1}{8} - \frac{1}{12}\right)\sigma_{c\,form} \tag{3.15}$$

Data provided in Chapter 2 is considered as the base for the modeling of cement material during hydration. Weyburn geothermal gradient is 0.035 °C/m and temperature at the top of the reservoir is 63 °C (Walton et al., 2004). Temperature at any given depth can be estimated and is utilized to predict cement model evolution coefficients. These coefficients are then used to construct each property at each time step during hydration. This procedure is not only used to predict the cement properties but also is vital for assuring that there is reasonable development of the initial state of stress in each material.

For constructing cement deformability properties, each model coefficient is used to predict the dynamic properties. Reddy et al. (2005) indicated that the relation for the dynamic modulus of elasticity of cement is related to the static modulus of elasticity by:

$$E_{cem\ static} = \left(0.3543\, E_{cem\ dynamic} - 136269\right) \times 6894.757 \quad \text{(Pa)} \qquad (3.16)$$

Minimum reported cement Poisson's ratio is 0.15 (Gray et al., 2007). Cement Poisson's ratio is reported to be constant and has an average value of 0.20 (Muller et al., 1996; Lacy and Rickards, 1996; Philippacopoulos and Berndt, 2002; Reddy et al., 2005). The range for static cement Poisson's ratio is taken to be:

$$\nu_{cem\ static} = 0.15\text{-}0.25 \qquad (3.17)$$

Coefficients used to predict the cement unconfined compressive strength is used to predict the strength parameters of the cement. Average cement internal angle of friction is 17.1° while average cement cohesion is 21.6 MPa (Bosma et al., 1999; Gray et al., 2007).

3.7.1 Model Sensitive Parameters

In order to determine the number of the simulations to fulfill the statistical approach, it is required to know the number of the parameters that will affect the response of the wellbore. A sensitivity analysis is performed to monitor the wellbore response subjected to different wellbore model state parameters as shown in Table 3.3 and model material parameters as listed in Table 3.5.

Model state parameters, Figure 3.7, shows how the area of cement is decreased with the increase of in-situ horizontal stresses while the change of vertical stress does not affect the wellbore response. In the simulation input data, all of these stresses are function of a single variable, which is the depth, d that takes a random variable along the wellbore slice representing wellbore element.

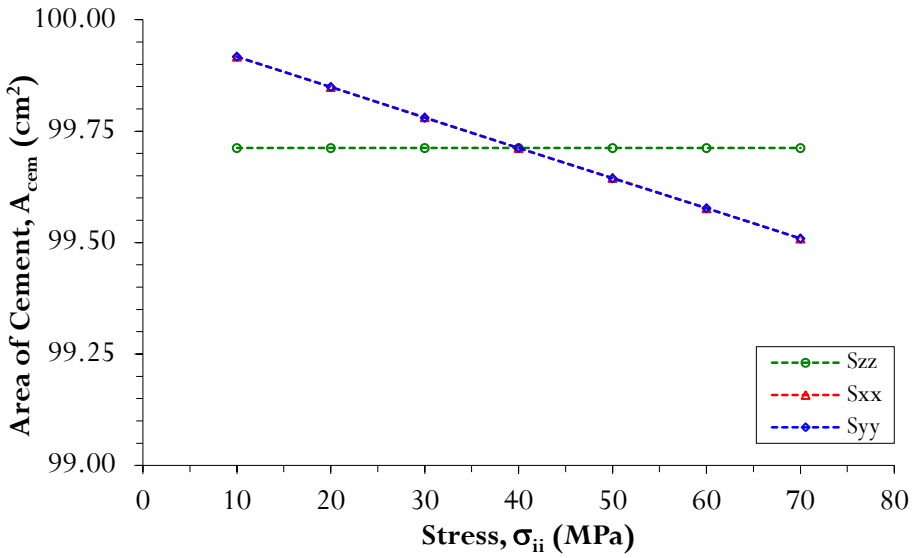

Figure 3.7: Effect of stress on area of cement.

Figure 3.8 shows the effect of changing the density of the materials forming the wellbore element. Density of the formation does not affect area of cement as it does not affect the state of stress. However, wellbore fluids lead to a different horizontal stress state in the wellbore, which in turn affects the wellbore deformation and hence area of cement sheath.

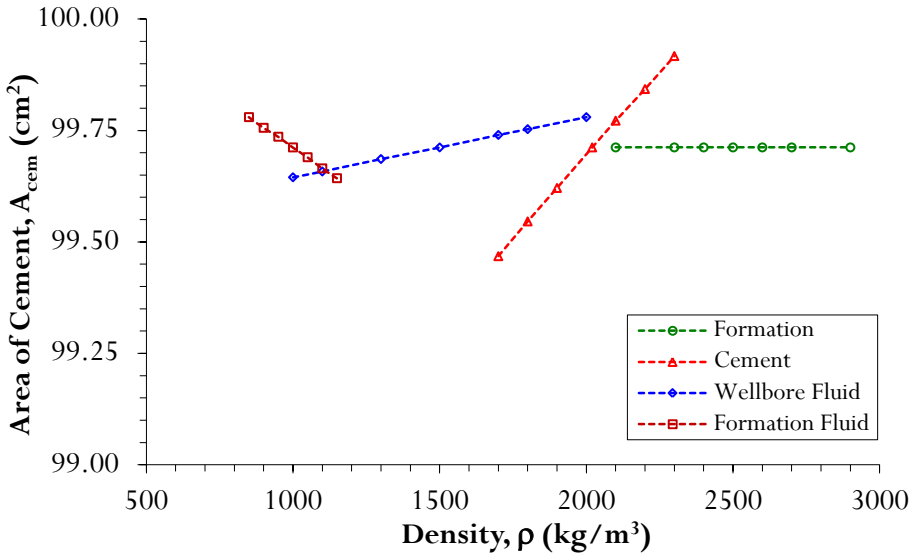

Figure 3.8: Effect of materials' density on area of cement.

Figure 3.9 represents the effect of the change of the deformability properties in the wellbore model. The properties are modulus of elasticity, E, and Poisson's ratio, ν. As expected, E has a major influence on the response of the wellbore while ν has a less effect.

Formation modulus of elasticity, E_{form}, will differ in response from cement modulus of elasticity, E_{cem}. The higher E_{form} the stiffer the formation leading to

less deformation of the borehole wall and hence gives more room for cement to be placed between the casing and the formation face.

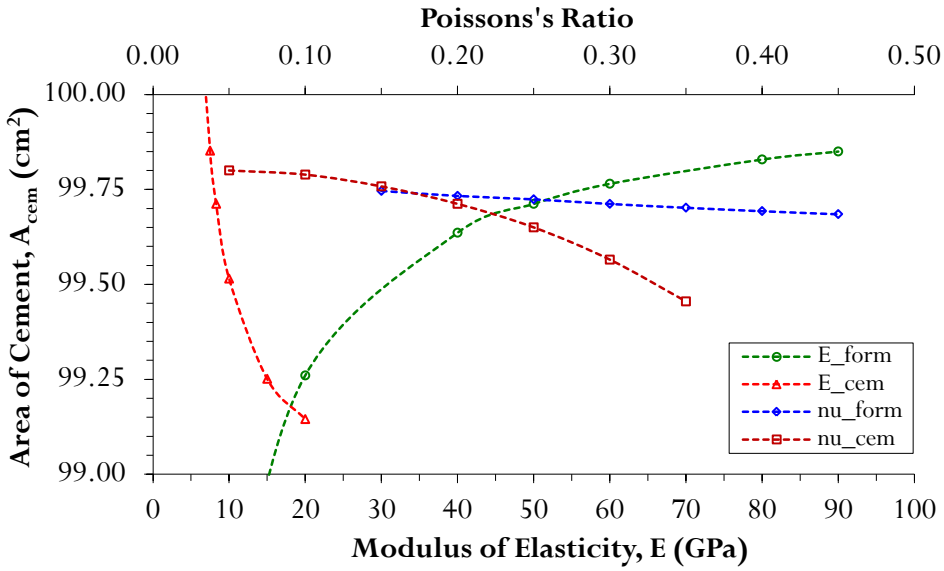

Figure 3.9: Effect of mechanical properties on area of cement.

However, state of loading inside the casing has the direct impact on area of the cement. The lower E_{cem} is the less cement sheath area at the same loading conditions. E_{cem} has more influence than E_{form}.

Poisson's ratio is another stress dependent and deformability property that is indirectly affected by modulus of elasticity. The higher Poisson's ratio is the lower the shear modulus, G that will result in higher radial displacement that causes decreasing area of cement.

Figure 3.10 indicates that there is no effect of strength parameters on cement sheath area. Strength parameters are material cohesion, c and internal friction angle, ϕ.

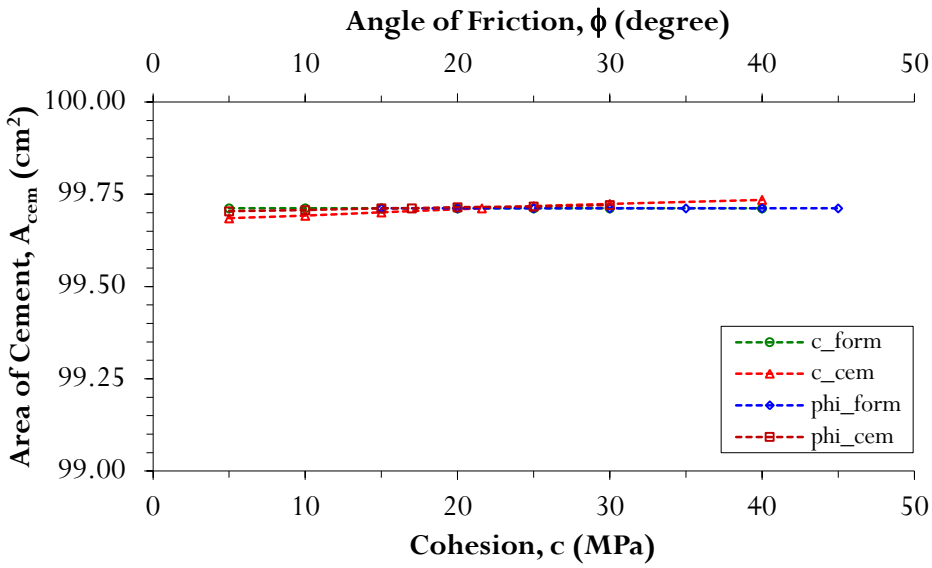

Figure 3.10: Effect of strength properties on area of cement.

For a stable wellbore, three scenarios exist which are net shrinkage cement, no (zero) shrinkage/expansion cement, and net expansion cement. For cement modulus of elasticity less than the formation modulus, a shear failure mode may be expected but this mode may not affect the cement sheath integrity (Bosma et al, 1999; Bois et al., 2009).

In the SRC method, radial displacement is the dependent variable which is a function of in-situ stress, wellbore fluids, and loading conditions without including material properties as independent variables.

From the above, variables that have an impact on wellbore model are the depth (reflected in in-situ stresses, pressures) and the material deformability parameters.

The system variables are the collection of all information needed to define what is happening within a system to a sufficient level in order to investigate a desired output and may be at a given point in time (Banks, 1998). The system variables were indicated to include model geometrical, state, material, and conditions parameters. Table 3.7 summarizes model geometrical parameters that may affect the response of the wellbore. The parameters were taken as deterministic variables.

3.7.2 Model State Parameters

Model state parameters are mainly the geomechanical parameters that are dependent on the storage site. In fact, these parameters, summarized in Table 3.8, categorize the parameters that will affect the wellbore by the same manner as long as it has the same depth.

Any simulation considering these parameters can represent all the wellbores in the storage site and output results will be site dependent.

3.7.3 Model Material Parameters

Model material parameters are parameters that describe different components of the wellbore in an engineering manner. In contrast to the state parameters, these parameters are highly dependent on the procedure and/or standards regulating the construction of the wellbore. Therefore, these parameters can be categorized as localized parameters that represent a specific wellbore at certain depth.

Table 3.9 summarizes these material parameters with their input data values, while the details of the generated variables are shown in Appendix B.

A summary of these model input parameters is presented in Table 3.7, Table 3.8, and Table 3.9.

Table 3.7: Model geometrical parameters.

Category	Parameters	Min. Value	Max. Value	DV	RV	Distribution
Theoretical	Bit "well" diameter (m)	0.20	0.20	√		Constant
	Outer casing diameter (m)	0.165	0.165	√		Constant
	Casing thickness (m)	0.005	0.005	√		Constant
	Eccentricity Angle (degree)	0.00	0.00	√		Constant
	Eccentricity (%)	0.00	0.00	√		Constant
	Model extent factor	21	21	√		Constant

* Casing data values is from Gabolde and Nguyen (1999).

Table 3.8: Model state parameters.

Category	Parameters	Min. Value	Max. Value	DV	RV	Distribution
Initial State	Depth (m)	1440	1447		√	Uniform
	Stress Gradient					
	Vertical (MPa/m)	0.024	0.024	√		Constant
	Min. horizontal (MPa/m)	0.018	0.018	√		Constant
	Max. horizontal (MPa/m)	0.028	0.028	√		Constant
	Geo-Thermal (°C/m)	0.035	0.035	√		Constant
	Pore-Pressure (MPa/m)	0.001	0.001	√		Constant
	Pore-pressure Condition	Normal		√		Constant

* Stress gradients values are from Gomez (2006).

Table 3.9: Model material parameters.

Category	Parameters	Min. Value	Max. Value	DV	RV	Distribution
Casing	Surface Force (N)	0.00	0.00	√		Constant
	Density (kg/m^3)	7850	7850	√		Constant
	Modulus of elasticity (Pa)	200e9	200e9	√		Constant
	Poisson's ratio (---)	0.33	0.33	√		Constant
Formation	Density (kg/m^3)	2600	2900		√	Uniform
	Modulus of elasticity (Pa)	Eq. (6.11)			√	
	Poisson's ratio (---)	0.20	0.40		√	Uniform
	Cohesion (Pa)	13e6	20e6		√	Normal
	Angle of friction (degree)	30	45		√	Normal
	Dilation (degree)	0	0	√		Constant
	Tension (Pa)	Eq. (6.15)			√	
Fluids	Surface Pressure (Pa)	0.00	0.00	√		Constant
	Fluid Densities					
	Mud (kg/m^3)	1000	1200		√	Uniform
	Water (kg/m^3)	1000	1000	√		Constant
	Cement (kg/m^3)	1700	2000		√	Uniform
	Completion fluid (kg/m^3)	1000	1000	√		Constant
Cement	Density (kg/m^3)	Slurry	2300		√	Uniform
	Modulus of elasticity (Pa)	6.6e6	10e6			
	Poisson's ratio (---)	0.15	0.25		√	Uniform
	Cohesion (Pa)	15e6	28e6		√	Normal
	Angle of friction (degree)	14	20		√	Normal
	Dilation (degree)	0	0	√		Constant
	Tension (Pa)	0.00	0.00	√		Constant

3.7.4 Model Condition Parameters

These parameters commonly differ from site to site and from well to well within the same site. Pressure inside the casing would be considered as a model condition parameters.

Researchers normally apply only one event to investigate wellbore integrity. The event may be either a temperature event (Philippacopoulos and Berndt,

2002; Bois et al., 2009; Takase et al., 2010; Guen et al., 2012) or a pressure event (Fourmaintraux et al., 2005; Gray et al., 2007; Saint-Mark et al., 2008; Bois et al., 2009, 2013; Takase et al., 2010; Nygaard and Salehi, 2011; Guen et al., 2012; Jandhyala et al., 2013).

Gomez (2006) provided a history of average reservoir pressure in the Weyburn field from 1957 until 2000. Figure 3.11 presents the minimum, average, and maximum pressure of the wellbores in the site.

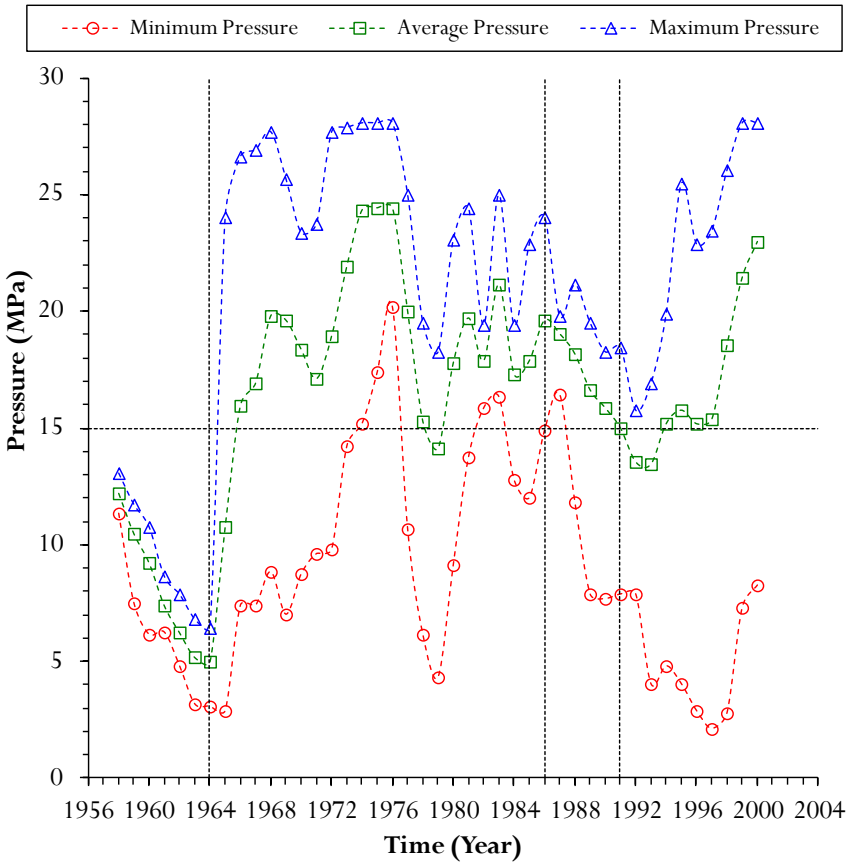

Figure 3.11: Reservoir pressure history (after Gomez, 2006).

For the modeling approach, there is a need to make a continuous tracing of wellbore events through its lifecycle. This continuous loading and unloading condition will provide a better representation of the different event activities within the well. However, the pressure used in the model is the one represented by the minimum pressure values, Figure 3.12, as a worst-case scenario for debonding to occur.

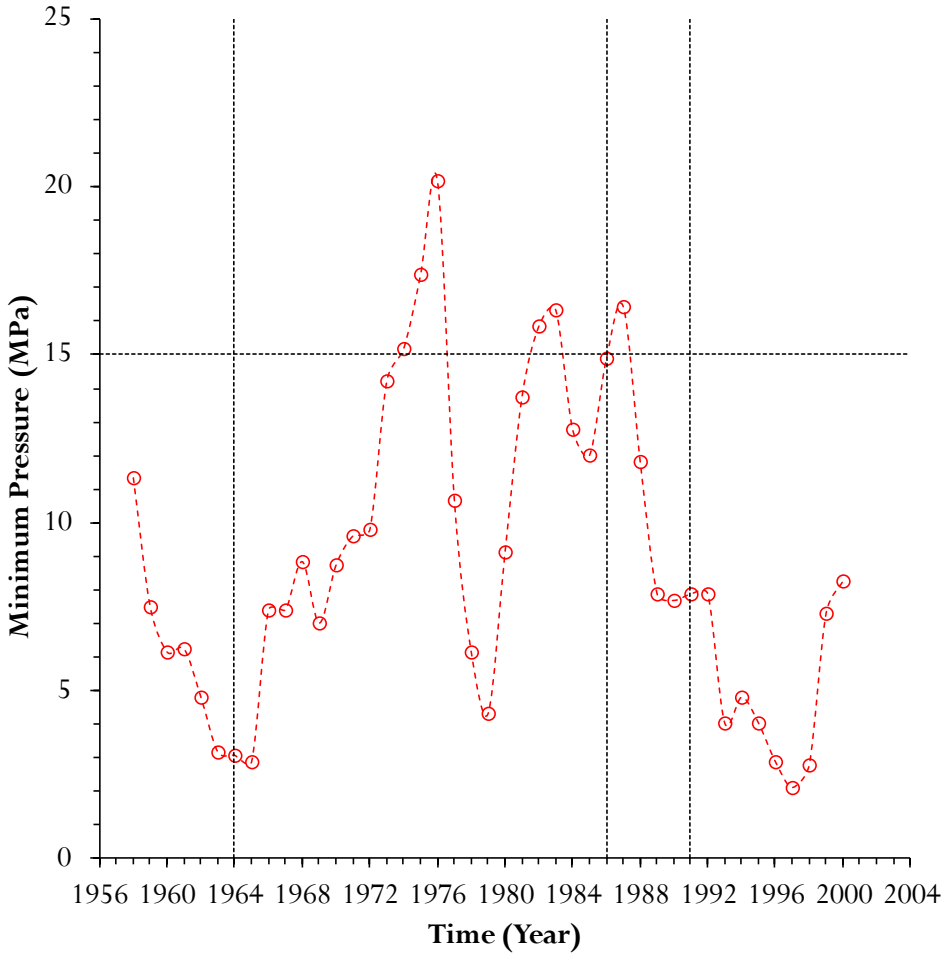

Figure 3.12: Minimum reservoir pressure history (after Gomez, 2006).

This continuous condition from year 1957 to 2000 is divided to sub intervals and minimum pressure data has been fitted, Figure 3.13, to a mathematical model. The curve fits range from linear, power, exponential, and hyperbolic functions, as shown in Figure 3.13.

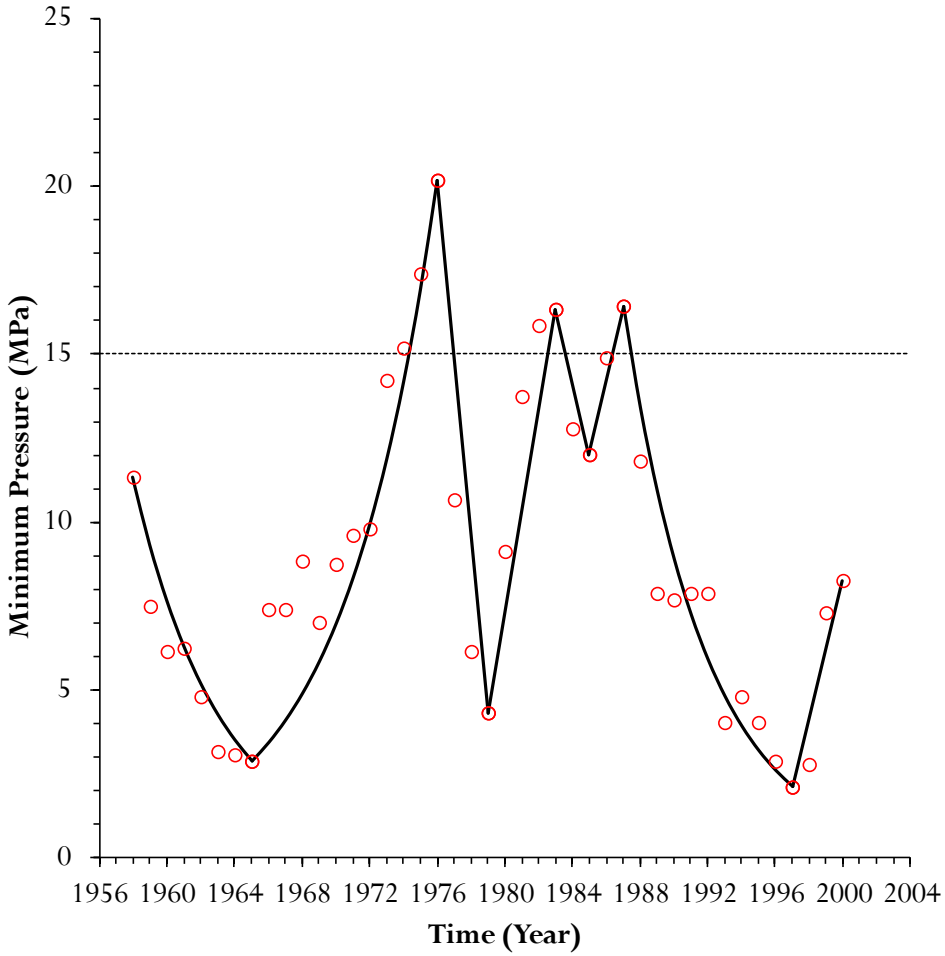

Figure 3.13: Fitted model condition parameters used in simulation.

3.7.5 Model Parameters Summary

Wellbore simulation input data is generated randomly according to their predefined statistical distribution. The simulated input data used in investigating wellbore integrity is detailed in Appendix B. Two types of representation that are used are graphical histogram and box and whiskers plots. Histograms are used to depict the distribution of generated input data, whereas box and whiskers plots are used to assess different quartiles for the same input data.

Independent variables are called natural variables as they are represented in their natural units such as Pa, m, or degree. Natural variables can be presented in a more convenient dimensionless variable ranging between -1 and +1. These dimensionless variables are known by the coded variables in any system response investigation (Myers et al., 2009).

The coded variable, x_c for a random variable x is:

$$x_c = \frac{x - \left(\frac{x_{max.} + x_{min.}}{2} \right)}{\left(\frac{x_{max.} - x_{min.}}{2} \right)} \tag{3.18}$$

Figure 3.14 illustrates different coded variables used in the wellbore simulation. Gathering the input coded variable data on the same plot has a benefit to summarize the statistical capability of the wellbore model.

Coded variables with smaller interquartile range, IQR, comparing to others variables indicate that their distributions are normally distributed. On the other side, coded variables with larger IQR and almost equal ranges for the quartiles show that their distributions are uniformly distributed.

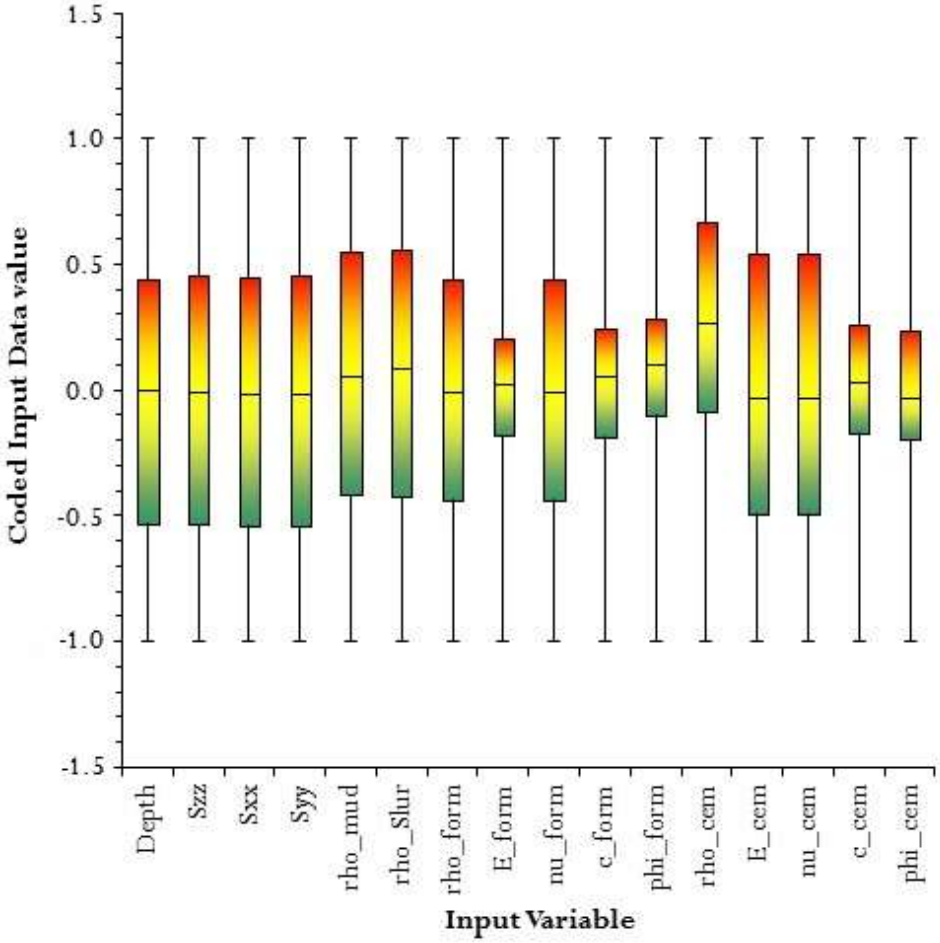

Figure 3.14: Box and Whiskers plot for generated coded input variables.

Variables with similar ranges identify either the variables are related by a specific variable (e.g. stresses depend on depth), or the same random number is used to generate the random variable as density and deformability properties. Deviation of the cement density is due to its generation from two random processes. The first one is generating the cement slurry density in Stage_0220, which will be the lower limit for the generation of the cement density used during Stage_0300 and Stage_0400.

3.8 Wellbore Integrity

The caprock in Weyburn field is highly suitable for geological storage of CO2. Primary seals that including the overlying Midale Evaporite are observed to be highly competent (Chalaturnyk et al., 2004).

Reduction of the leakage risk is the one of the main objectives of wellbore integrity according to NORSOK definition. The model variables are the input variables, which are called independent variables. The desired output as a performance measure is a dependent variable or a response for the model "system" variables. The dependent variable is the interface gap width. Estimating of the wellbore permeability depends mainly on the interface gap generated under different events during wellbore lifecycle. Chapter 5 will describe how the interface permeability is computed.

The model is numerically and sequentially processed. In the same time while processing, input data is randomly generated from predefined statistically distributions. The aim is to perform a sufficient number of simulations to generate a statistical distribution of an output "dependent" variable to create its own PDF.

A computer coded numerical model is implemented to assess and monitor wellbore integrity in a wellbore element over the wellbore lifecycle. The coded model of the wellbore includes main simulation modeling project and auxiliary secondary projects. The objective of the main project is to perform both sequential and stochastic simulation, while secondary projects aim to make automatic input files for the main project.

Firstly, secondary projects are categorized into three projects that were coded to:

1) generate automatic inputs files for downhole conditions for all stages of the main project,
2) generate the dependent variables (i.e. both grid points and zones) required for permeability calculations, and
3) generate a coded file to perform automatic multi-runs of the main project that controlling number of simulation and characterize output files at every desired event.

Main simulation Project is organized to include and to have the ability to:

1) represent the wellbore geometric configuration, Table 3.7,
2) calling wellbore conditions (i.e. temperature and pressure) overtime and over sub-periods of time according to proposed mathematical model, Figure 3.13,
3) model evolution of cement properties over time during cement hydration process, Stage_0300, according to the proposed hydration model proposed in Chapter 2,
4) apply a change of cement materials in deterioration stage over time according to assumed mathematical model,
5) calculate the variables required for wellbore permeability calculation inside FLAC environment, and
6) summarize both input data and output data for a given run in Microsoft Excel files.

The main output data extracted from FLAC environment is the co-ordinates of the grid points (i,j) on each side of an interface described in section 3.4.3. The Excel files is then organized to be gathered and merged in one Excel file where a desired variable "interface gap width" is calculated at both cement-formation interface and cement-casing interface.

Figures 3.15 and 3.16 show box-and-whiskers plots of the generated distribution of the formation-cement interface gap and casing-cement interface gap at selected years during wellbore lifecycle resulting from the change in pressure shown in Figure 3.13. These PDFs corresponding to these distributions are illustrated in Appendix C.

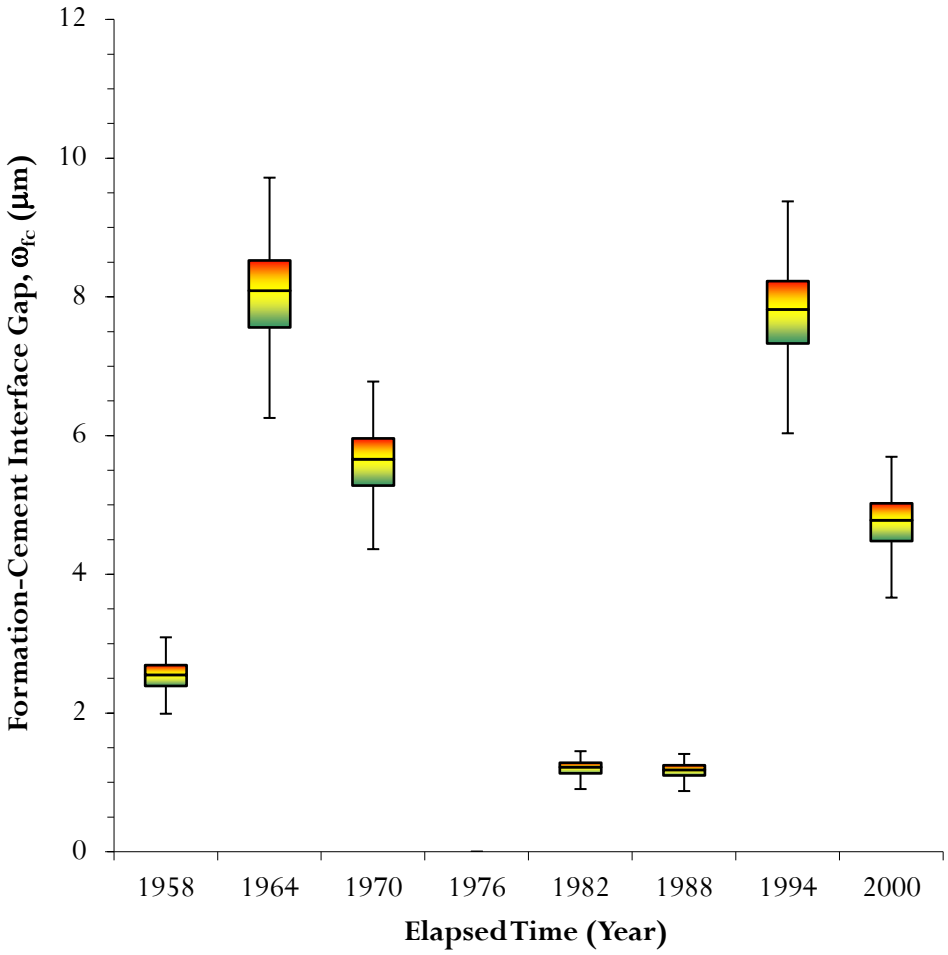

Figure 3.15: Expected cement-formation interface gap width.

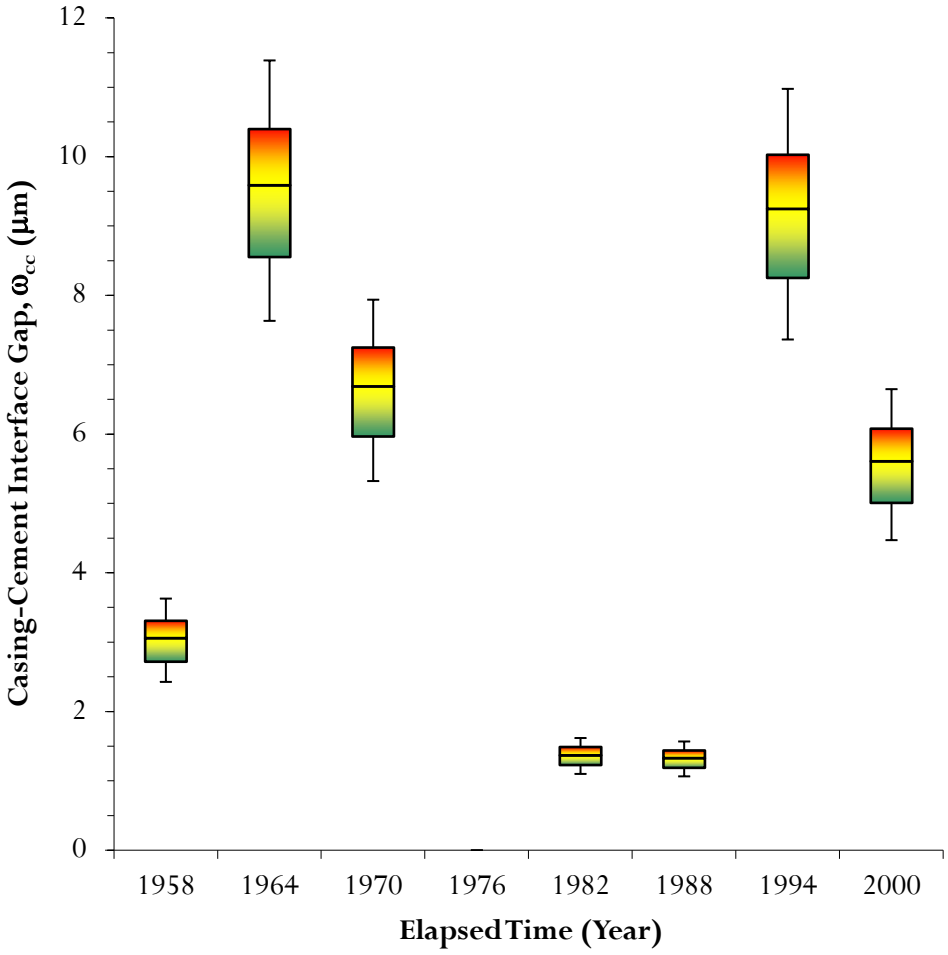

Figure 3.16: Expected cement-casing interface gap width.

3.9 Summary

The problem of wellbore integrity needs a selection procedure that requires a more sophistication rather than simple one (Philippacopoulos and Berndt, 2002). Detailed near-wellbore modeling is a very complex process. This process involves not only the geomechanical parameters that can give us an idea about the cement sheath performance but also geometrical and conditional parameters that affect the performance during the lifecycle of the wellbore. The model must include conceptual, generic, and organized procedures and details to optimize any desired output.

In facts, model inputs parameters can be obtained from an exploration program or well-documented literature. To reduce much idealization, as many models suggests, the approach has to perform a simulation process that is characterized by both sequential and stochastic procedures. The benefit is to generate a range of all possible results and hence reduce the risk if dealing with deterministic and/or averages variables.

Assessment of wellbore integrity depends on zonal isolation provided by a cement sheath. An interface gap may develop between different components of the wellbore and is considered as a preferential path for leakage.

The creation of the gaps is a response of the wellbore under the effect of conditions parameters and controlled by different state parameters (i.e. input data). The generated wellbore gap widths can be monitored at every wellbore event. Consequently, the estimation of wellbore permeability can be attained. The estimated wellbore interface permeability can be considered as a quantified indicator of wellbore integrity. The framework can be used to assess and monitor the full lifecycle wellbore integrity.

The use of such methodology will have two advantages. The first is to predict a range for any desired output variable instead of obtaining a single value (i.e. inequality approach). The second is the use of statistical distributions of input parameters to generate statistical distributions of output parameters, which can be used for risk-based reliability analysis and optimization of the wellbore system response for both wellbore integrity and CO2 Storage sites.

A case study of the main caprock in the Weyburn field illustrated that it is highly suitable for geological storage of CO2. It agrees with the results of Chalaturnyk et al. (2005) that primary seals that including Midale Evaporite formation is observed to be highly competent and shows quantitatively that the wellbore-caprock interaction in Weyburn field is highly suitable for geological storage of CO2.

3.10 References

Anders, J., Rossberg, S., Dube, A., Engel, H., and Andrews, D., (2006), Well Integrity Operations at Prudhoe Bay Alaska, SPE Annual Technical Conference and Exhibition, 24-27 September, San Antonio, Texas, USA, SPE 102524, 9 p.

Ayyub, B.M. and McCuen, R.H., 2003, Probability, Statistics, and Reliability for Engineers and Scientists, CHAPMAN & HALL/CRC, 2nd Edition, 640 p.

Bachu, S., and Haug, K., (2006), Evaluation of the Potential for CO2 Leakage through Wells at Penn West's Pembina-Cardium CO2-Enhanced Oil Recovery Pilot Operation, Alberta Energy Research Institute, EUB/AGG Client Report, 50 P.

Baecher, G.B., and Christian, J.T., (2003), Reliability and Statistics in Geotechnical Engineering, 1st edition, John Wiley & Sons Ltd., 591 p.

Banks, J., (1998), Handbook of Simulation Principles, Methodology, Advances, Applications, and Practices, 1st edition, John Wiley & Sons Inc., 870 p.

Bois, A-P., Garnier, A., Rodot, F., Saint-Mark, J., and Aimard, N., (2009), How to Prevent Loss of Zonal Isolation through a Comprehensive Analysis of Microannulus Formation, SPE Annual Technical Conference and Exhibition, 4-7 October, New Orleans, Louisiana, USA, SPE 124719, 20 p.

Bois, A-P., Vu, M., Ghabezloo, S., Sulem, J., Garnier, A., and Laudet, J-B., (2013), Cement Sheath Integrity for CO2 Stoarge - An Integrated Perspective, Energy Procedia, Vol. 37, pp. 5628 – 5641.

Bosma, M., Ravi, K., van Driel, W., and Schreppers, G.J., (1999), Design Approach to Sealant Selection for the Life of the Well, SPE Annual Technical Conference and Exhibition, 3-6 October, Houston, Texas USA, SPE 56536, 14 p.

Broding, W.C., Diederich, F.W. and Parker, P.S., 1960, "Structural Optimization and Design Based on a reliability Design Criterion", Journal of Spacecraft, Vol. 1, No. 1, pp 56-61.

Celia, M.A., and Nordbotten, J.M, (2009), Practical Modeling Approaches for Geological Storage of Carbon Dioxide, Ground Water, Vol. 47, No. 5, pp. 627-638.

Celia, M.A., Nordbotten, J.M., Bachu, S., Dobossy, M. and Court, B., (2009), Risk of Leakage versus Depth of Injection in Geological Storage, Energy Procedia, 1, pp. 2573-2580.

Celia, M.A., Nordbotten, J.M., Court, B., Dobossy, M., and Bachu, S., (2011), Field-Scale Application of a Semi-Analytical Model for Estimation of CO2 and Brine Leakage along old Wells, International Journal of Greenhouse Gas Control, Vol. 5, pp. 257-269.

Chalaturnyk, R., Zhou, W., Stenhouse, M., Sheppard, M., and Walton, F., (2004), Theme 4: Long-Term Risk Assessment of the Storage Site, IEA-GHG Weyburn CO2 Monitoring and Storage Project Summary Report 2000-2004, 7th International Conference on Greenhouse Gas Control technologies, 5-9 September 2004, Vancouver, Canada, Vol. III, pp. 211-268,.

Chen, G., (2001), A Study of Wellbore Stability in Shales including Poroelastic, Chemical, and Thermal Effects, Ph.D. Thesis, University of Texas at Austin, Texas, USA, 166 p.

Court, B., (2011), Safety and Water Challenges in CCS: Modeling Studies to Quantify CO2 and Brine Leakage Risk and Evaluate Promising Synergies for Active and Integrated Water Management, Ph.D. Thesis, Princeton University, USA, 244 p.

Dobossy, M.E., Celia, M.A., and Nordbotten, J.M., (2011), An Efficient Framework for performing Industrial Risk Assessment of Leakage for Geological Storage of CO2, Energy Procedia, 4, pp. 4207-4214.

El-Ramly, H, (2001), Probabilistic Analysis of Landslide Hazards & Risks: Bridging Theory and Practice, Ph.D. Thesis, University of Alberta, Alberta, Canada, 391 p.

Espie, A.A., (2005), CO2 Capture and Storage: Contributing to Sustainable World Growth, International Petroleum Technology Conference, 21-23 November, Doha, Qatar, IPTC 10936, 7 p.

Fjær, E., Holt, R.M., Horsrud, P., Raaen, A.M., and Risnes, (2008), Petroleum Realted Rock Mechanics, 2nd edition, Elsevier, 482 p.

Fenton, G.A, and Griffiths, D.V., (2008), Risk Assessment in Geotechnical Engineering, 1st edition, John Wiley & Sons Inc., 164 p.

Fourmaintraux, D., Bois, A.P., Franco, C., Fraboulet B. and Brossollet, P., (2005), Efficient Wellbore Cement Sheath Design Using the SRC (System Response Curve) Method, SPE Europec/EAGE Annual Conference, 13-16 June, Madrid, Spain, SPE 94176, 10 p.

Freedman, D., and Diaconis, P., (1981), On the Histogram as a Density Estimator: L_2 Theory, Zeitschrift für Wahrscheinlichkeitstheorie und verwandte Gebiete, Vol. 57, pp. 453-476.

Gabolde, G.J., and Nguyen, J., (1999), Drilling Data Handbook, 7th edition, Institut Français du Pétrole Publications.

Gasda, S.A., (2008), Numerical Models for Evalaution CO2 Storgae in Deep, Slaine Aquifers: Leaky Wells and Larga-Scale Geological Features, Ph.D. Thesis, Princeton University, USA, 188 p.

Gasda, S.E., and Celia, M.A., (2005), Upscaling Relative Permeabilities in a Structured Porous Medium, Advances in Water Resources, Vol. 28, pp. 493-506.

Gomez, J.A.J., (2006), Geomechanical Performance Assessment of CO2-EOR Geological Storage Projects, Ph.D. Thesis, University of Alberta, Alberta, Canada, 295 p.

Goodwin, K.J., and Crook, R.J., (1992), Cement Sheath Stress Failure, Journal of SPE Drilling Engineering, SPE 20453, Vol. 7, Issue 4, pp. 291-296.

Gray, K.E., Podnos, E., and Becker, E., (2007), Finite Element Studies of Near-Wellbore Region during Cementing Operations; Part I, Production and Operations Symposium, 31 March-3 April, Oklahoma City, Oklahoma, USA, SPE 106998, 15 p.

Guen, Y.L., Asamoto, S., Houdu, E., and Poupard, O., (2012), Well Integrity: Modeling of Thermo-Mechanical Behavior and Gas Migration along Wells - Application to Ketzin Injection Well, Energy Procedia, 23, pp. 462 – 471.

Hashin, Z., (2002), Thin Interface/Imperfect Interface in Elasticity with Application to Coated Fiber Composites, Journal of the Mechanics and Physics of Solids, Vol. 50, pp. 2509-2537.

Hohnson, R.A, and Bhattacharyya, (1996), Statistics Principles and Methods, 2nd edition, John Wiley & Sons Inc., 720 p.

Holling, C. S., (1978), Adaptive Environmental Assessment and Management, Wiley, Chichester.

Honjo, Y., (2008), Monte Carlo Simulation in Reliability Analysis, Chapter 4, in Reliability-Based Design in Geotechnical Engineering: Computations and Applications, editor Phoon, K., 1st edition, Taylor & Francis Group, 530 p.

Hughes, A., and Grawoig, D., (1971), Statistics: A foundation for Analysis, 1st edition, Addison-Wesley Publishing Company, 525 p.

Humez, P., Audigane, P., Lions, J., Chiaberge, C., and Bellenfant, G., (2011), Modeling of CO2 Leakage Up Through an Abandoned Well from Deep Saline Aquifer to Shallow Fresh Groundwaters, Transport in Porous Media, Vol. 90, Issue 1, pp. 153-181.

Itasca Consulting Group Inc., (2008), FLAC Manual: Theory and Background, Version 6.

Jackson, P.B., and Murphy, C.E., (1993), Effect of Casing Pressure on Gas Flow through a Sheath of Set Cement, SPE/IADC Drilling Conference, 22-25 February, Amsterdam, Netherlands, SPE 25698, 10 p.

Jaeger, J.C., and Cook, N.G.W., (1979), Fundamentals of Rock Mechanics, 3rd edition, Chapman and Hall, London.

Jandhyala, S., Barhate, Y.R., Anjos, J., Fonseca, C.E., and Ravi, K., (2013), Cement Sheath Integrity in Fast Creeping Salts, SPE Offshore Europe Oil and Gas Conference and Exhibition, 3-6 September, Aberdeen, UK , SPE 166622, 10 p.

Janzen, A.K., (2010), Development and Application of a Multi-Scale, Multi-Layer Numerical Model for CO2 Injection, M.Sc. Thesis, Princeton University, USA, 105 p.

Kottegoda, N.T., and Rosso, R., (1997), Statistics, Probability, and Reliability for Civil and Environmental Engineers, 1st edition, McGraw-Hill Inc., 735 p.

Kutasov, I.M., (1999), Applied Geothermics for Petroleum Engineers, 1st edition, Elsevier, 339 p.

Lacy, L.L., and Rickard, A., (1996), Analyzing Cements and Completion Gels using Dynamic Modulus, SPE 36476, pp. 625-635.

LeNeveu, D.M., (2012), Potential for Environmental Impact due to Acid Gas Leakage from Welbores at EOR Injection Sites Near Zama Lake, Alberta, Greenhouse Gases: Science & Technology, Vol. 2, Issue 2, pp. 99-114.

Lourenço, P.B., (1994), Analysis of Masonry Structures with Interface Elemenst: Theory and Applications, Report no. 03-21-22-0-01, Delft University of Technology, Netherland, 34 p.

Lourenço, P.B., (1996), Computational Strategies for Masonry Structures, Report no. 03-21-22-0-01, Delft University of Technology, Netherland, 207 p.

Lourenço, P.B., Rots, J.G., and Blaauwendraad, J., (1995), Two Approaches for the Analysis of Masonary Structures: Micro and Macro-Modeling, HERON, Vol. 40, No.4, pp. 313-340.

Melchers, R.E., 1999, Structural Reliability and Prediction, 2nd Edition, John Wiley & Sons Ltd., England.

Milton, J.S, and Tsokos, J.O, (1983), Statistical Methods in the Biological and Health Sciences, 1st edition, McGraw-Hill, 500 p.

Mishra, S., (2002), Assigning Probability Distributions to Input Parameters of Performance Assessment Models, INTERA Inc., USA, 49 p.

Moreno, F.J., Chalaturnyk, R., and Jimenez Jaime, (2004), Methodology for Assessing Integrity of Bounding Seals (Wells and Caprock) for Geological Storage of CO2, ELSEVIER Publications, Proceedings of the 7th International Conference on Greenhouse Gas Control Technology, Vol. I, 5-9 September 2004, Vancouver, Canada.

Mueller, D.T., Lacy, L.L., and GoBoncan, V., (1996), Characterization of the Initial Transitional and Set Properties of Oilwell Cement, SPE Annual

Technical Conference and Exhibition, 6-9 October, Denver, Colorado, USA, SPE 36475, 11 p.

Myers, R.H., Montgomery, D.C., and Anderson-Cook, C.M., (2009), Response Surface Methodoolgy: Process and Product Optimization Using Designed Experiments, 3rd edition, John Wiley & Sons Inc., 680 p.

Nabih, A., and Chalaturnyk, R., (2013a), Wellbore Efficiency Model for CO2 Geological Storage Part I: Theory and Wellbore Element, SPE Heavy Oil Conference-Canada, 11-13 June, Calgary, Alberta, Canada, SPE 165411, 14 p.

Nabih, A., and Chalaturnyk, R., (2013b), Wellbore Efficiency Model for CO2 Geological Storage Part II: Wellbore System, SPE Unconventional Resources Conference Canada, 5-7 November, Calgary, Alberta, Canada, SPE 167149, 14 p.

Nicot, J-P., Oldenburg, C.M., Houseworth, J.E., and Choi, J-W., (2013), Analysis of Potential Leakage Pathways at the Cranfield, MS, USA, CO2 Sequestration Site, International Journal of Greenhouse Gas Control, Vol. 18, pp. 388-400.

Nogues, J.P., Nordbotten, J.M., and Cleia, M.A., (2011), Detecting Leakage of Brine or CO2 through abandoned Wells in a Geological Sequestration Operation using Pressure Monitoring Wells, Energy Procedia, 4, pp. 3620-3627.

Nogues, J.P., Court, B., Dobossy, M., Nordbotten, J.M., and Cleia, M.A., (2012), A Methodology to estimate Maximum Probable Leakage along Old Wells in a Geological Sequestration Operation, International Journal of Greenhouse Gas Control, Vol. 7, pp. 39-47.

Nordbotten, J.M., Celia, M.A., and Bachu, S., (2004), Analytical solutions for leakage rates through abandoned wells, Water Resources Research, Vol. 40, Issue 4, W04204, doi:10.1029/2003WR002997.

Nordbotten, J.M., Celia, M.A., Bachu, S., and Dahle, H.K., (2005), Semianalytical Solution for CO2 Leakage through an Abandoned Well, Environmental Science & Technology, Vol. 39, No. 2, pp. 602-611.

Nordbotten, J.M., Kavettski, D., Celia, M.A., and Bachu, S., (2009), Model for CO2 Leakage Including Multiple Geological Layers and Multiple Leaky Wells, Environmental Science & Technology, Vol. 43, No. 3, pp. 743-749.

Nygaard, R., and Salehi, S., (2011), Effect of Dynamic Loading on Wellbore Leakage for the Wabamun Area CO2 Sequestration Project, Canadian Unconventional Resources Conference, 15-17 November, Alberta, Canada, SPE 146640, 19 p.

Oldenburg, C.M., Bryant, S.L., and Nicot, JP, (2009), Certification Framework based on Effective Trapping for Geologic Carbon Sequestration, International Journal of Greenhouse Gas Control, Vol. 3, pp. 444-457.

Pershikova, E.M., Chougnet-Sirapian, A., Loiseau, A., Khater, W, and Garnier, A., (2010), Evaluation of Specialized Cement System for Long-Term Steam Injection Well Integrity, Canadian Unconventional Resources and International Petroleum Conference, 19-21 October, Calgary, Alberta, Canada, SPE 137710, 12 p.

Philippacopoulos, A.J., and Berndt, M.L., (2002), Mechanical Response and Characterization of Well Cements, SPE Annual Technical Conference and Exhibition, 29 September-2 October, San Antonio, Texas, USA, SPE 77755, 8 p.

Reddy, B.R., Santra, A., McMechan, D., Gray, D., Brennis, C., and Dunn, R., (2005), Cement Mechanical Property Measurements under Wellbore Conditions, SPE Annual Technical Conference and Exhibition, 9-12 October, Dallas, Texas, USA, SPE 95921, 8 p.

Saint-Marc, J., Garnier, A., Bois, A, (2008), Initial State of Stress: The key to Achieving Long-Term Cement-Sheath Integrity, SPE Annual Technical Conference and Exhibition, 21-24 September, Denver, Colorado, USA, SPE 116651, 15 p.

Scott, D.W., (1979), On Optimal and Data-Based Histograms, Biometrika, Vol. 66, pp. 605-610.

Sheng, Y., Reddish, D. and Lu, Z., (2006), Assessment of Uncertainties in Wellbore Stability Analysis, in Modern Trends in Geomechanics, Springer Publications, pp. 541-557.

Starfield, A.M., and Cundall, P.A., (1988), Towards a Methodology for Rock Mechanics Modeling, Int. J. Rock Mech. Sci. & Geomech. Abstr., Vol. 25, No. 3, pp. 99-106.

Sturges, H.A., (1926), The choice of a Class Interval, J. Am. Statist. Assoc., Vol. 21, pp. 65-66.

Takase, K., Barhate, Y., and Hashimoto, H., and Lunkad, S.F., (2010), Cement-Sheath Wellbore Integrity for CO2 Injection and Storage Wells, SPE Oil and Gas India Conference and Exhibition, 20-22 January, Mumbai, India, SPE 127422, 11 p.

Walton, F,B., Sheppard, M.I., LeNeveu, D.M., Tait, J.C., and Goodwin, B.W., (2004), Probabilistic Risk Assessment of the IEA Weyburn CO2 Monitoring and Storage Project, Final Report, ECOMatters, 54 p.

Watson, T.L., and Bachu, S., (2007), Evaluation of the Potential for Gas and CO2 Leakage along Wellbores, E&P Environmental and Safety Conference, 5-7 March, Galveston, Texas, USA, SPE 106817, 16 p.

Watson, T.L., and Bachu, S., (2008), Identification of Wells with High CO2-Leakage Potential in Mature Oil Fields Developed for CO2-Enhanced Oil Recovery, SPE Symposium on Improved Oil Recovery, 20-23 April, Tulsa, Oklahoma, USA, SPE 112924, 10 p.

Whittaker, S.G., Rostron, B., Khan, D., Hajnal, Z., Qing, H., Penner, L., Maathuis, H., and Goussev, A., (2004), Theme 1: Geological Characterization, 7th International Conference on Greenhouse Gas Control technologies, Vol. III, IEA-GHG Weyburn CO2 Monitoring and Storage Project Summary Report 2000-2004, pp. 15-69, 5-9 September 2004, Vancouver, Canada.

Whittaker, S.G., (2005), Geological Characterization of the Weyburn Filed for Geological Storage of CO2: Summary of Phase I Results of the IEA GHG Weyburn CO2 Monitoring and Storage Project; in Summary of Investigation.

Chapter 4: Wellbore Element Modeling[3]

4.1 Introduction

Study of leakage of hazardous wastes by vertical communication between aquifers through wellbores into shallow groundwater aquifers began more than two decades ago. Several analytical and semi-analytical models have been developed on leakage detection and quantification (Nordbotten et al., 2004; Zeidouni, 2011; Zeidouni et al., 2011).

All of the analytical and semi-analytical methods, (Shakya and Singh, 1986; Shakya et al., 1986; Javandel et al., 1988; Silliman and Higgins, 1990; Avci, 1992, 1994; Brikowski, 1993; Lacombe et al., 1995; Nordbotten et al., 2004, 2005b; Chesnaux et al., 2006; Chesnaux, and Chapuis, 2007; Ebigbo et al. 2007; Gasda, 2008; Ellison, 2011; Humez et al., 2011; Zaidouni, 2011, Zaidouni et al. 2011; Hu et al. 2012), considered only two horizontal aquifers connected by a single vertical wellbore element bounded by a very low permeability zone called an aquitard. Figure 4.1 shows the basic components of this wellbore system. Thus, the wellbore system can be considered as a three (3) layer system which has an idealized arrangement of aquifer-aquitard-aquifer system that is bounded by two impermeable layers at the bottom and at the top of the system.

Models normally assume that formations are isotropic and homogenous with constant thickness within the radius of influence and infinitely extend in the

---

[3] A version of this chapter has been published in the Proceedings of SPE Heavy Oil Conference Canada held in Calgary, Alberta, Canada, 11-13 June 2013.
Nabih, A., and Chalaturnyk, R., (2013), Wellbore Efficiency Model for CO2 Geological Storage Part I: Theory and Wellbore Element, SPE 165411.

radial direction. The intervening aquitard between the two aquifers is impermeable and its effect is ignored.

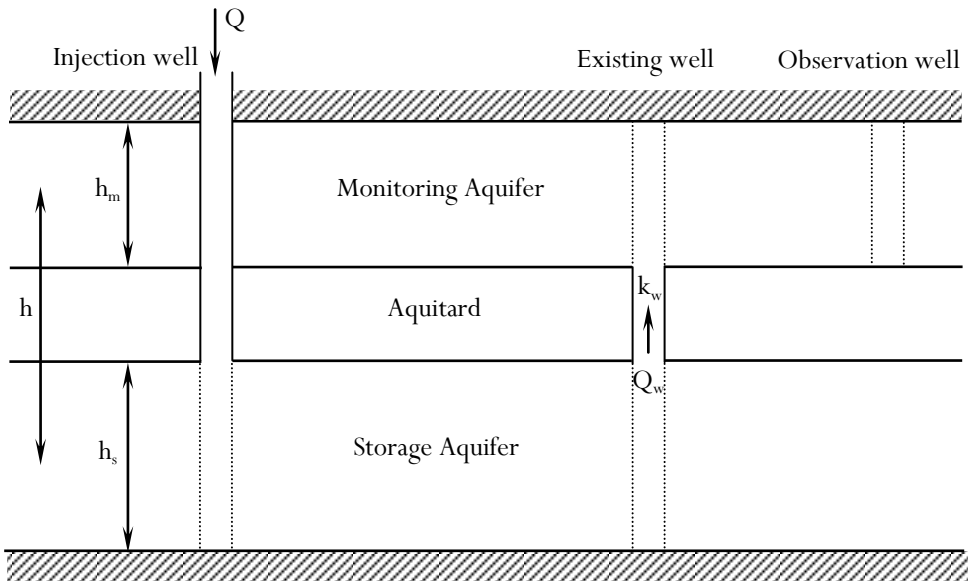

s: storage, and m: monitoring

Figure 4.1: Basic wellbore system used by different researchers.

Flow in the aquifers is radial such that no vertical variations in hydraulic head exist within aquifers. It is assumed that leaking fluids flow through small fractures or connected pathways so that the total flow along a leaky well element can be modeled using Darcy's Law (Nordbotten et al., 2004, 2005b). Flow within the aquifers was either modeled as steady state for fully penetrating wells (Shakya and Singh, 1986; Shakya et al., 1986; Silliman and Higgins, 1990; Brikowski, 1993) and for partially penetrating wells (Avci, 1992; Mishra et al., 2012) or was modeled as transient flow condition for fully penetrating wells (Javandel et al., 1988; Avci, 1994; Nordbotten et al., 2004, 2005b).

Norbotten et al. (2004) indicated that the hydraulic head, either naturally or by constant injection rate, is the cause of the leakage between the two aquifers and the leakage in the wellbore is controlled by a constant resistance to flow (Silliman and Higgins, 1990; Brikowski, 1993; Nordbotten et al., 2004, 2005b). In 2011, Zeidouni indicated that the Avci (1994) solution may not be applicable when the leak is considerably large and developed analytical models suitable for leakage from local weaknesses in the caprock that can provide large leakage pathways (Zeidouni, 2011).

For CO2 storage, the ultimate goal for well-leakage models is to serve as inputs for quantitative risk analysis (Gasda and Celia, 2005; Watson and Bachu, 2008; Celia and Nordbotten, 2009; Celia et al., 2009; Oldenburg et al., 2009; Dobossy et al., 2011; Humez et al., 2011; LeNeveu, 2012).

4.2 Possible Wellbore Leakage Paths

There are several possible pathways for CO2 leakage through a wellbore. These pathways, discussed by Gasda et al. (2004), produce seven potential leakage scenarios, as illustrated in Figure 4.2.

Due to poor cement bonding will allow leakage. Poor bonding is associated with the interface of the cement with either formation rock or the casing. Micro-annuli can develop during the production phase of the wellbore due to the variation of borehole conditions (i.e. pressure and temperature). Furthermore, micro-annuli can be formed if the integrity of the cement sheath is compromised and cement properties have been deteriorated due to interaction with rock formation fluid over time even beyond abandonment. This deterioration results in increasing of cement permeability and allows flow through cement sheath itself (Gasda, 2008).

Rigorous modeling of all possible leakage pathways would be far too complex to simulate. Humez et al. (2011) considered a 1D porous column and simulated leakage at the rock-cement interface. This interface was chosen as a possible pathway due to deterioration when the well is being drilled and affected by borehole conditions during production phase.

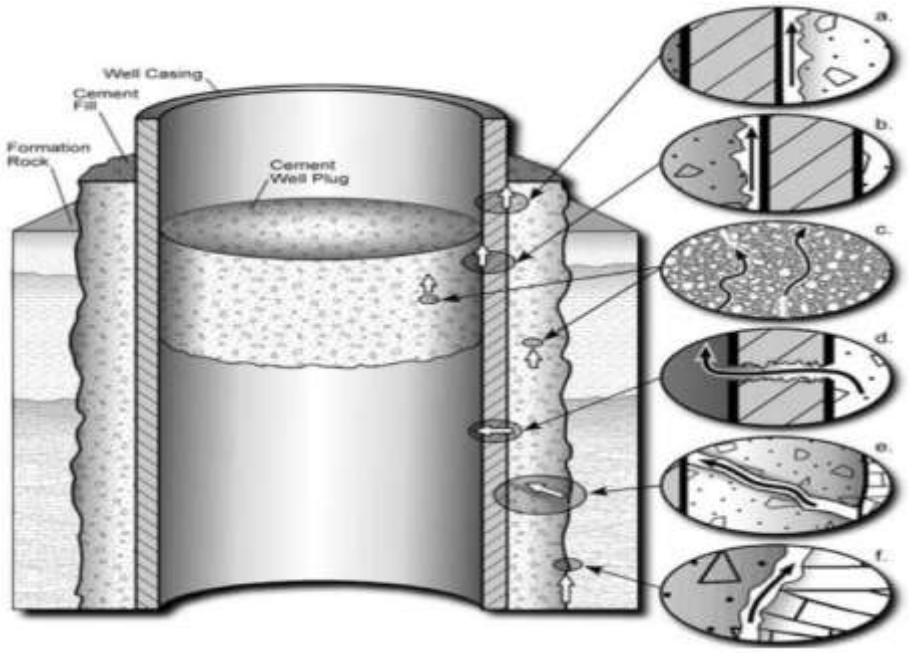

a) Between casing & cement; b) between cement plug & casing; c) through the cement pore space; d) through casing; e) through fractures in cement; and f) between cement & rock.

Figure 4.2: Possible leakage paths around a wellbore (after Gasda et al. 2004).

In Alberta, the Alberta Energy Regulator (AER) accepts three methods for abandonment of cased wellbores. The methods, shown in Figure 4.3, are: a) a cement plug that extends above and below the perforated interval for ≥ 15

meters, b) a cement squeeze through the perforations and, c) a mechanical bridge plug capped with 8 meters which is the most commonly used method (Watson and Bachu, 2008).

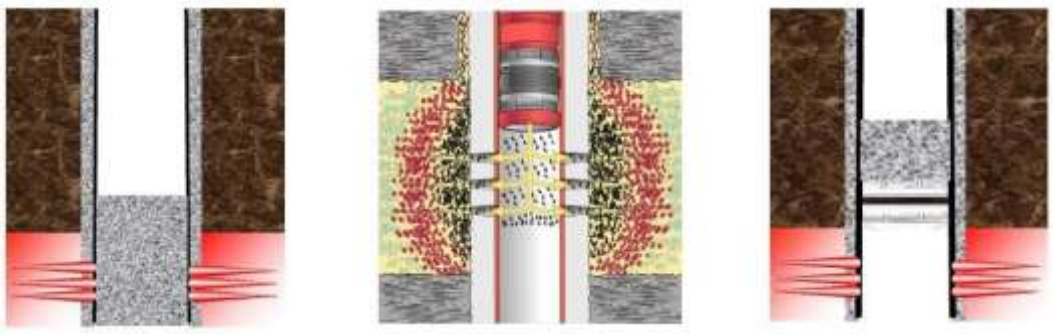

(a) (b) (c)

Figure 4.3: Abandonment methods in Alberta (after Watson and Bachu, 2008).

In the following sections, a one dimensional analytical leakage flow transfer model is developed. The analytical solution obtained for a wellbore element will be used for modeling leakage through the whole wellbore system (discussed in Chapter 6).

4.3 Concepts of Modeling Approach

As discussed previously, many approaches are possible to fulfill the target of assessing leakage through a wellbore. The approach that will be developed in this chapter starts with modeling the wellbore element and then extending this to the whole wellbore system. An "element" in this context refers to a control volume of a wellbore slice with any arbitrary thickness but coincident with the thickness of an adjacent formation. The approach adopted for modeling the wellbore element will adopt three concepts:

1) sequence scenarios of possible leakage paths,
2) wellbore efficiency for storage purposes, and
3) reference state.

Each of these concepts are dicussed in the following sections.

4.3.1 Concept of Sequence Scenarios

The sequence scenario concept adopts possible leakage paths indicated by Gasda et al. (2004), Gasda and Celia (2005), Nordbotten et al. (2005), (2009), Gasda (2008), and Celia and Nordbotten (2009) in addition to the confirmation that these paths are considered as events scenarios. The event scenarios must follow a logical order of sequence with the method of abandonment, as shown in Figure 4.3. For example, if it is assumed that wells are abondened in accordance with Figure 4.3 (c), Figure 4.4 illustrates the logical order sequences for all possible pathways.

The sequence scenario concept postulates that cases (e) and (d) in Figure 4.4 are actually the events that must occur first to allow the rest of the scenarios to occur. If they happen alone, it does not mean there is a leakage through the wellbore. Cases (f) and (e) are totally independent to each other. However, the rest of scenarios are absolutely dependent on case (e). In addition, occurrence of case (e) does not necessarily mean the leakage through these scenarios and resulting that case (f) is a standalone leakage scenario.

Different scenarios may not be independent, but assuming their likelihood is equal indicates that the cement part is the governing component that appears in all of them. The interface between the cement sheath and the formation represents 50% of the probable leakage paths. Both interfaces between cement and casing represents (inner and outer) 25%, while the remaining

25% represents flow through cement material itself through cement plug and cement sheath. In reality, the likelihood for each scenario will not be equal.

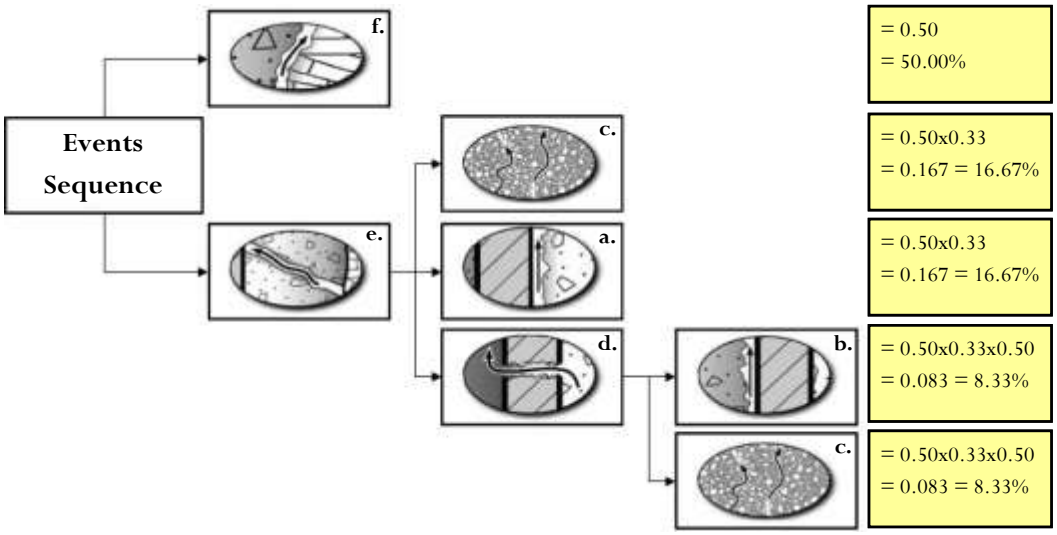

Figure 4.4: Sequence scenarios of possible leakage paths around a wellbore.

For all components of these scenarios, cement in the annulus zone of the wellbore is the most significant. It includes; interface between cement sheath and casing (50%), outer interface between cement sheath and casing (16.67%), and flow through cement sheath (16.67%).

Consequently, it seems reasonable to assume that the highest possible occurrence of leakage is the flow through cement sheath and the interface of this cement with the formation and/or the casing. This approach supported by the concept of the scenarios events illustrated in Figure 4.4, captures 83.34% of the probable paths for leakage.

4.3.2 Concept of Wellbore Efficiency

In order to develop a parameter that will serve as a proxy or indicator of well performance from a leakage potential perspective, we have chosen to develop and adopt the concept of wellbore efficiency. Wellbore efficiency is formulated using the thermodynamics similarity between heat engine efficiency and leakage through a wellbore element. The operation and efficiency of heat engines is normally studied in thermodynamics. A diagram shown in Figure 4.5 represents the system of a heat engine during operation. The system may extend to describe a gasoline engine, a jet engine, a steam engine, or even the human body (Young and Freedman, 2004).

In a heat engine, three processes occur during the operation. A heat input, Q_{in}, is supplied to the engine at a high temperature, T_{in}. Mechanical work, W_{out}, is done by using a portion of the heat input. An output heat, Q_{out}, is released at a lower temperature, T_{out}.

The thermal efficiency of a heat engine, η_{th}, is defined as the ratio of the work done by the engine to the heat supplied to the engine, and it is usually expressed as a percentage.

$$\eta_{th} = \frac{Q_{in} - Q_{out}}{Q_{in}} \tag{4.1}$$

Theoretically, Equation (4.1) shows that if a heat engine is perfect ($\eta = 1$), the engine would expel all the input energy by work. Real engine (system) efficiencies are less than 100%.

This fact is summarized in the Kelvin-Planck form of the second law of thermodynamics states the following: "*It is impossible to construct a heat engine*

that, operating in a cycle, produces no effect other than the input of energy by heat from a reservoir and the performance of an equal amount of work".

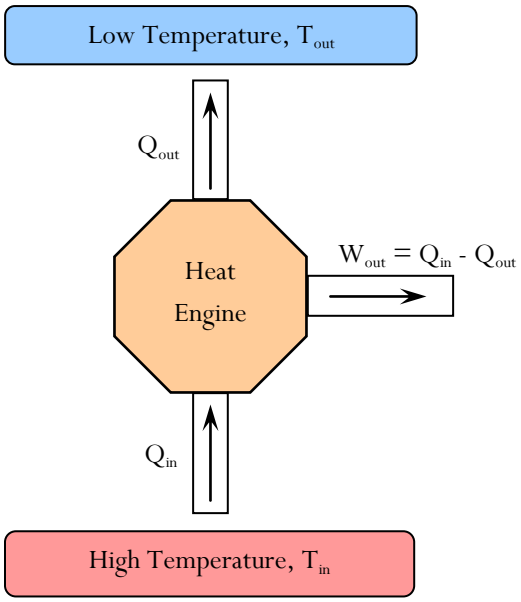

Figure 4.5: A schematic representation (diagram) for a heat engine.

By analogy, we assume the performance of a wellbore element for storage purposes has the same formulation as a heat engine. Mass enters the element, M, and leaves it with axially, M_a, and radially, M_r. For incompressible fluid, flow enters the element, Q, and leaves it with axial flow, Q_a, and radial flow, Q_r. A wellbore element, as illustrated in Figure 4.6, is part of the overall wellbore system and can be considered as a local sub-system.

The outcome target is to maximize storage flow, represented by radial flow, and to minimize the tendency for leakage, represented by axial flow, to any specific formation and/or the biosphere.

By analogy then, the wellbore element sealing efficiency, η, is defined as:

$$\eta = \frac{Q - Q_a}{Q} = \frac{Q_r}{Q} \tag{4.2}$$

To simplify the conclusion of the wellbore system in Chapter 6, a leakage factor for a wellbore element, λ, Equation (4.3), can be defined as the ratio between axial leakage to the flow enters the wellbore element and hence;

$$\lambda = \frac{Q_a}{Q} \tag{4.3}$$

Therefore, from Equation (4.2) and Equation (4.3):

$$\eta = 1 - \lambda \tag{4.4}$$

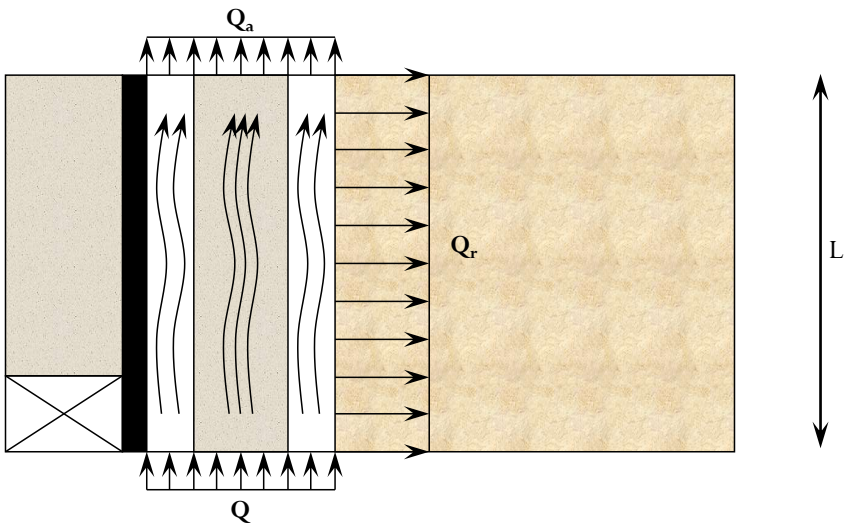

Figure 4.6: A schematic representation of wellbore element model.

The wellbore sealing efficiency parameter, η, will be used as an indicator of wellbore performance. The higher the efficiency, the better sealing condition is at a given strata and tendency for storage to be maintained at a given depth.

4.3.3 Concept of Reference State

The concept of reference state is introduced to define the state of the wellbore relative to the state of the geological formations through which the wellbore passes. By neglecting the presence of the wellbore, the vertical flow through the geological formations alone provides a reference state against which to compare the leakage prediction through the wellbore element and also for the wellbore system. This imaginary reference state is indeed a representation of the resistance of leakage by any geological strata in the vicinity of the wellbore and/or before drilling.

Comparing the leakage through a wellbore element and leakage through this reference state (virgin geological strata) provides a relative measure of the condition of the wellbore. If the ratio between the two leakages is ≥ 1.0, then the wellbore does represent a potential leakage path in comparison to the geologic strata itself. If the ratio is < 1.0, then the wellbore performance can fall below that of the geologic strata and may be a concern.

4.4 Basic Components of Wellbore Element

A wellbore element, as a control volume, is made up of a porous medium which may contain one or more fluid phases. The analytical model was not developed for quantification of leakage rates but rather as a self-consistent model that could be applied to risk ranking of wellbore integrity based on the hydraulic integrity state of the wellbore. The analytical model considers single-phase flow through the formation layers and the leakage pathway.

Complexities of compositional flow can be neglected and single-phase approach is sufficient and provides slightly conservative response during injection time and past injection time (Nicot et al., 2011).

The porous medium is treated as a continuum whose physical properties at any point are those of a representative element of the medium. The control volume, whose shape depends on the coordinate system used in the model, is chosen and a material balance equation is written for this control volume. The general material balance equation for any component, c, in the element may be expressed by:

$$Q_{in} + Q_{gen} = Q_{acc} + Q_{out} \tag{4.5}$$

where ,

Q_{in}: flow rate entering the control volume,

Q_{gen}: flow rate generated within the control volume (sink/source),

Q_{acc}: flow rate accumulated in the control volume (stored/depleted), and

Q_{out}: flow rate leaving the control volume.

The basic components to model a wellbore element are the flow rate component and the head loss component along that element. Each component can be further divided into sub-components. For this study, it is assumed that the accumulated flow rates inside the control volume are negligible. Therefore, the flow rate components, illustrated in Figure 4.5 and Figure 4.6, can be expressed mathematically by:

$$Q_{in} = Q_{out} \tag{4.6}$$

Therefore,

$$Q = Q_a + Q_r \tag{4.7}$$

where,

Q: axial flow rate entering the control volume,

Q_a: axial flow rate leaving the control volume, and

Q_r: radial flow rate leaving the control volume by radial flow flux q_r.

Head loss components, shown in Figure 4.7, along a wellbore element represents an axial head loss, h, along the wellbore element and a radial head loss, h_r. Radial head loss extends to a distance R symmetrical around the wellbore element. Total heads are presented by uppercase letter H and lowercase h represents the head losses responsible for the flow from the wellbore element.

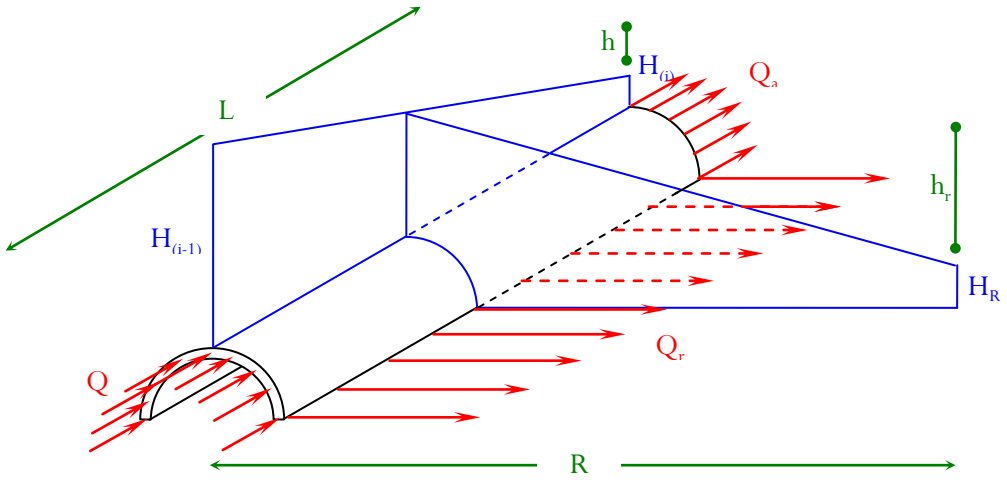

Figure 4.7: A schematic representation for head losses components.

A superposition model for the wellbore element, Figure 4.8, is proposed to connect between basic components (i.e. the flow rates and head losses) that govern the leakage through the wellbore element. The model will be used to derive the relation between wellbore element basic components.

Figure 4.8 illustrates the assumption of dividing the axial head loss into two head losses according to the flow subdivision. Axial head loss, h_{ar}, indicates

the fact that any leakage before leaving the element in the radial direction, will flow vertically for a certain distance (height) z along the element. Radial flow will be represented by a radial flux having an idealized distribution pattern that reflects this assumption. Head losses can be mathematically expressed by:

$$h = h_a + h_{ar} \tag{4.8}$$

where,

h: total axial head loss along the wellbore element,

h_a: axial head loss drives Q_a through wellbore element, and

h_{ar}: axial head loss associated with Q_r.

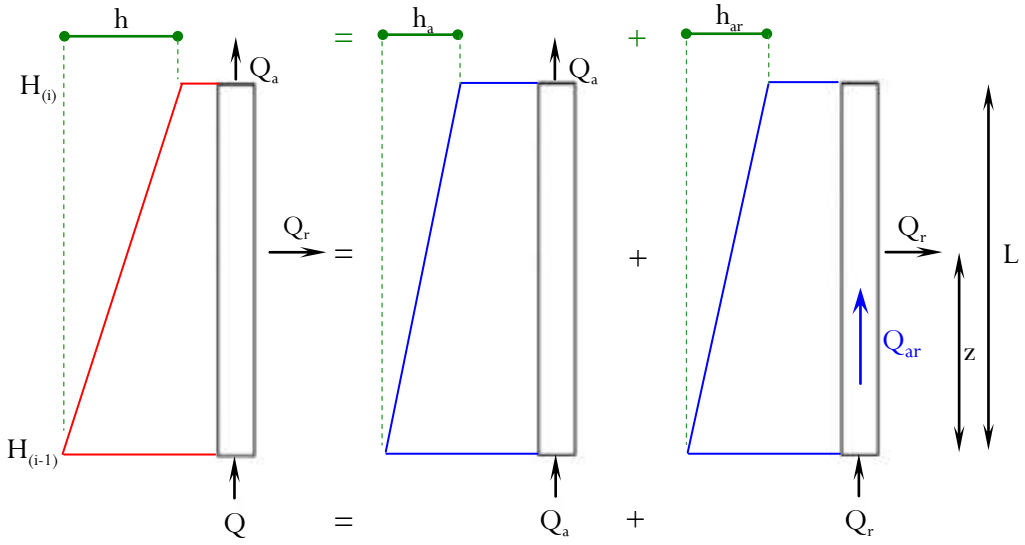

Figure 4.8: Superposition model for wellbore element leakage.

4.5 Leakage Flow Rates Modeling

As shown in Figure 4.8, the flow rate components, which leak through a specific length, L, of a wellbore element, are divided into two components. These two components are; leakage along well axis "through the well", Q_a, and leakage perpendicular to the well axis "radial direction", Q_r.

4.5.1 Leakage in Axial Direction

Leakage in the axial direction represents flow through wellbore at the cement-formation interface, outer cement-casing interface and the cement in the wellbore annulus. It covers the event scenarios (f), (c), and (a) depicted in Figure 4.4.

According to the superposition model in Figure 4.8, this leakage is characterized by the head loss h_a which is a part of the total head loss h affecting the whole model element. Axial leakage rate, Q_a, for an element is;

$$Q_a = \frac{KA}{L} h_a \tag{4.9}$$

where,

K: axial bulk wellbore hydraulic conductivity (i.e. vertical direction),

A: cross sectional area of the wellbore element, and

L: length of the wellbore element.

Axial bulk wellbore hydraulic conductivity, K, represents a "smeared" conductivity considering the effect of cement-formation interface, cement-casing interface and the cement sheath in the wellbore annulus characteristics. Comuting the bulk or "smeared" hydraulic conductivity is challenging and Chapter 5 describes the methodology adopted for determining K.

4.5.2 Leakage in Radial Direction

Leakage in the radial direction represents flow through the wellbore at the cement-formation interface that may leave the control volume and enters the adjacent formation. Radial leakage is driven by the existence of radial head loss h_r. Radial leakage does not leave the control volume at one location but it takes a distribution along wellbore surface area represented by a pattern of radial flux, q_r. Radial flow rate is;

$$Q_r = \frac{2\pi L K_r}{\ln\left(\frac{R}{r}\right)} h_r \tag{4.10}$$

where,

K_r: radial hydraulic conductivity,

h_r: radial head loss causing flow of Q_r,

R: radius of influence of the wellbore (i.e. well reach), and

r: radius of the wellbore.

Radius of influence of the well, R, is the distance at which the drawdown is negligible or unobservable. Equation (4.10) can be rewritten as:

$$\begin{aligned} Q_r &= \frac{K}{K} \times \frac{LA}{LA} \times \frac{2\pi L K_r}{\ln\left(\frac{R}{r}\right)} h_r \\ &= \frac{K_r}{K} \times \frac{2\pi L^2}{A \ln\left(\frac{R}{r}\right)} \times \frac{KA}{L} h_r \end{aligned} \tag{4.11}$$

Introducing radial leakage conductivity factor, Ω_r, defined as:

$$\Omega_r = \frac{K_r}{K} \times \left(\frac{L}{r}\right)^2 \times \frac{2}{\ln\left(\frac{R}{r}\right)} \tag{4.12}$$

then Equation (4.11) can be written as;

$$Q_r = \frac{KA}{L}\Omega_r h_r \qquad (4.13)$$

4.5.3 Leakage for Reference State

Leakage through the reference state represents the vertical leakage in the geological strata subjected to the same total head loss, h. By definition, it is the state at which $\eta = 0.00$ and hence it is the minimum geological formation resistance to leakage.

The equivalent geological element is the element with the same geometrical configuration as the wellbore element subjected to the same hydraulic gradient. Reference leakage rate, Q_R, for geological element equivalent to wellbore element is;

$$Q_R = \frac{K_F A}{L} h \qquad (4.14)$$

where,

K_F: axial formation hydraulic conductivity (i.e. vertical direction).

4.6 Leakage Head Losses Modeling

The head losses controlling the leakage through the element can be categorized as two head losses. The first is the total axial head loss, h, and the second is radial head loss, h_r.

According to the superposition model in Figure 4.8, total axial head h can be further divided into two axial head losses which are; axial head loss, h_a, and axial head loss associated with the existence of radial leakage flow along the

element, h_{ar}, as long as there is radial head loss, h_r, causing a radial leakage flow rate, Q_r.

4.6.1 Axial Head Loss

Axial head loss, h_a, is causing an axial leakage flow rate, Q_a, out of the wellbore element. From Equation (4.9), head loss causing axial flow is:

$$h_a = \frac{L}{KA} Q_a \tag{4.15}$$

4.6.2 Radial Head Loss

Radial head loss, h_r, is causing a radial leakage flow rate, Q_r, out of the wellbore element. From Equation (4.13), head loss causing radial flow is:

$$h_r = \frac{L}{KA} \frac{1}{\Omega_r} Q_r \tag{4.16}$$

4.6.3 Axial Head Loss associated with Radial leakage

Axial head loss associated with radial leakage, h_{ar}, is the head loss responsible for causing axial movement of the flow to a height z before it leaves the element in the radial direction. Radial distribution of leakage flux, q_r, can be idealized to take any of the illustrated idealized distributions patterns in Figure 4.9.

Martinez-Landa et al. (2013) investigated the same three different shapes (idealized patterns distribution) as assumed dimensional (absolute) values rather than patterns factors as proposed by this study.

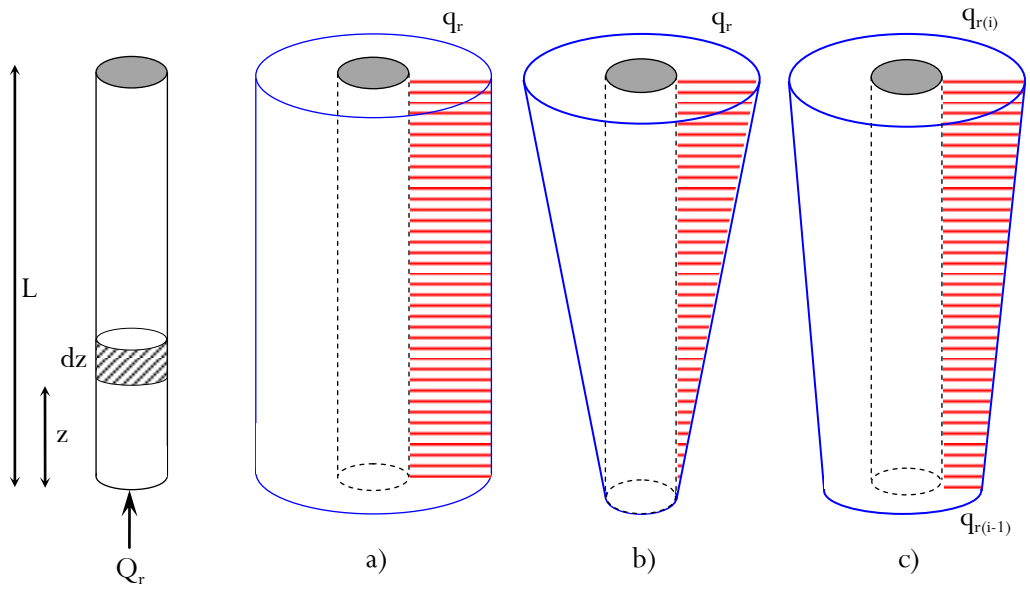

a) Cylindrical; b) Inversed Conical; c) Inversed Conical Frustum

Figure 4.9: Various radial flux distributions along a wellbore element.

The idealization is considered as a representation of different possibilities for the typical profile of the plume front in any storing aquifer, Figure 4.10, given by Nordbotten et al. (2005a, 2005b), Nordbotten and Celia (2006), Celia and Nordbotten (2009), Janzen (2010), Celia et al. (2011), Court (2011).

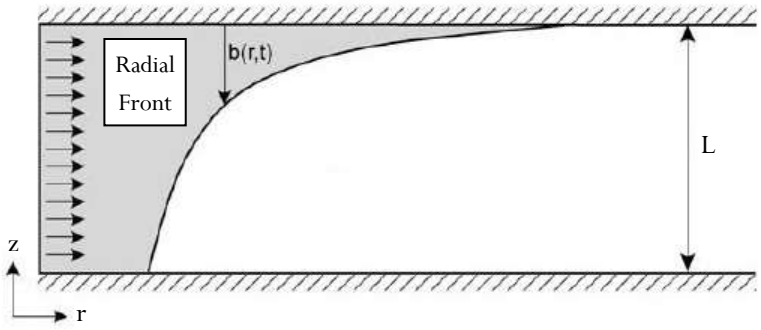

Figure 4.10: Typical profile of leakage plume (after Nordbotten et al., 2005).

In this section, a relation between both head losses, h_r and h_{ar}, will be developed to define the leakage superposition model components. As expected, the relation depends on the assumed associated radial distribution pattern. These assumed distributions reflect the fact that patterns may vary according to adjacent formation properties, which may be altered during wellbore life, and according to formation non-homogeneity. Figure 4.9 illustrated the idealization of these distributions to cylindrical, inversed conical and inversed conical frustum (inversed truncated cone) distribution.

The determination of axial head loss that causes radial leakage, h_{ar}, is not that straightforward through different cases. According to the radial distribution pattern that the radial flux, q_r, may take a corresponding axial flow rate, Q_{ar}, flows axially through the wellbore element before it dissipate completely at the end of the element.

The axial head loss increment for a segment dz at height z from the base of an element is:

$$\Delta h_{ar} = \frac{Q_{ar}}{KA} dz \tag{4.17}$$

Integrating Equation (4.17) defines the total h_{ar} along well axis such that:

$$\begin{aligned} h_{ar} &= \int_0^L \frac{Q_{ar}}{KA} dz \\ &= \frac{1}{KA} \int_0^L Q_{ar}\, dz \end{aligned} \tag{4.18}$$

The subsequent illustrates how h_{ar} varies for the radial flux distributions shown in Figure 4.10.

Case (a): Cylindrical Distribution

Cylindrical radial leakage distribution is formed due to the rotation of a plane with a finite uniform front around wellbore axis (axis of rotation). Thus, the h_{ar} can be determined as follows:

$$\begin{aligned} Q_{ar} &= Q_r - q_r Pz \\ &= q_r PL - q_r Pz \\ &= q_r P(L - z) \end{aligned} \tag{4.19}$$

where P is the wellbore perimeter. Then,

$$\begin{aligned} h_{ar} &= \frac{1}{KA}\int_0^L Q_{ar}\, dz \\ &= \frac{q_r P}{KA}\int_0^L (L - z)\, dz \end{aligned} \tag{4.20}$$

Integrating Equation (4.20), then

$$h_{ar} = \frac{PL^2}{KA}\frac{q_r}{2} \tag{4.21}$$

The radial head loss, h_r, associated with cylindrical distribution is;

$$\begin{aligned} h_r &= \frac{L}{KA}\frac{1}{\Omega_r} Q_r \\ &= \frac{L}{KA}\frac{1}{\Omega_r} PLq_r \\ &= \frac{PL^2}{KA}\frac{q_r}{\Omega_r} \end{aligned} \tag{4.22}$$

Case (b): Inversed Conical Distribution

Inversed conical radial leakage distribution is formed due to the rotation of a plane with a finite linearly increasing triangular front around wellbore axis (axis of rotation). Thus, h_{ar} can be determined as follows:

$$
\begin{aligned}
Q_{ar} &= Q_r - \left(q_r \frac{z}{L}\right)\frac{Pz}{2} \\
&= q_r \frac{PL}{2} - q_r \frac{Pz^2}{2L} \\
&= \frac{q_r P}{2L}(L^2 - z^2)
\end{aligned}
\tag{4.23}
$$

Then,

$$
\begin{aligned}
h_{ar} &= \frac{1}{KA}\int_0^L Q_{ar}\, dz \\
&= \frac{q_r P}{KA}\int_0^L (L^2 - z^2)\, dz
\end{aligned}
\tag{4.24}
$$

Integrating Equation (4.24), then

$$
h_{ar} = \frac{PL^2}{KA}\frac{q_r}{3} \tag{4.25}
$$

The radial head loss, h_r, associated with inversed conical distribution is;

$$
\begin{aligned}
h_r &= \frac{L}{KA}\frac{1}{\Omega_r} Q_r \\
&= \frac{L}{KA}\frac{1}{\Omega_r}\frac{PLq_r}{2} \\
&= \frac{PL^2}{KA}\frac{q_r}{2\Omega_r}
\end{aligned}
\tag{4.26}
$$

Case (c): Inversed Conical Frustum Distribution

Inversed conical frustum (truncated cone) radial leakage distribution is formed due to the rotation of a plane with finite linearly increasing trapezoidal front around wellbore axis (axis of rotation). Thus, h_{ar} determination is carried out for two different values of leakage fluxes; $q_{r(i-1)}$ at the bottom and $q_{r(i)}$ at the

top of the wellbore segment. This distribution is considered as a combination of the previous two distributions and leakage can be expressed as;

$$\begin{aligned} Q_{ar} &= Q_r - q_{r(i-1)}Pz - \left(\left(q_{r(i)} - q_{r(i-1)}\right)\frac{z}{L}\right)\frac{Pz}{2} \\ &= \left(\frac{q_{r(i-1)} + q_{r(i)}}{2}\right)PL - q_{r(i-1)}Pz - \left(q_{r(i)} + q_{r(i-1)}\right)\frac{Pz^2}{2L} \\ &= P\left(\left(q_{r(i-1)} + q_{r(i)}\right)\frac{L}{2} - \left(q_{r(i-1)}\right)z - \left(q_{r(i-1)} - q_{r(i)}\right)\frac{z^2}{2L}\right) \end{aligned} \tag{4.27}$$

Then,

$$\begin{aligned} h_{ar} &= \frac{1}{KA}\int_0^L Q_{ar}\, dz \\ &= \frac{P}{KA}\int_0^L \left(\left(q_{r(i-1)} + q_{r(i)}\right)\frac{L}{2} - \left(q_{r(i-1)}\right)z - \left(q_{r(i-1)} - q_{r(i)}\right)\frac{z^2}{2L}\right) dz \end{aligned} \tag{4.28}$$

Integrating Equation (4.28), then

$$h_{ar} = \frac{PL^2}{KA}\left(\frac{q_{r(i-1)} + 2q_{r(i)}}{6}\right) \tag{4.29}$$

However, Equation (4.29) is the summation of the cylindrical and the inversed conical distribution cases. Therefore, for inversed conical frustum distribution, the Equation (4.29) can be rewritten in the form such that;

$$h_{ar} = \frac{PL^2}{KA}\left(\frac{q_{r(i-1)}}{2} + \frac{q_{r(i)} - q_{r(i-1)}}{3}\right) \tag{4.30}$$

The radial head loss, h_r, associated with inversed conical frustum distribution is;

$$h_r = \frac{L}{KA}\frac{1}{\Omega_r}Q_r$$
$$= \frac{L}{KA}\frac{1}{\Omega_r}\left(\frac{q_{r(i-1)} + q_{r(i)}}{2}\right)PL \qquad (4.31)$$
$$= \frac{PL^2}{KA}\left(\frac{q_{r(i-1)} + q_{r(i)}}{2\Omega_r}\right)$$

4.7 Radial Leakage Distribution Factor

The value of h_{ar} will change with radial distribution pattern. The ratio between both head losses h_{ar} and h_r can be considered as a function of Ω_r with a factor varies with the pattern of radial flow flux distribution. This factor will be defined as radial distribution factor, f_d. As a summary to explain this relation, Table 4.1 presents a summary of the equations to estimate h_{ar}, h_r and f_d for different radial pattern distributions.

Table 4.1: Radial distribution factor for various distributions.

Distribution	Cylindrical	Conical	Conical Frustum
h_{ar}	$\frac{PL^2}{KA}\frac{q_r}{2}$	$\frac{PL^2}{KA}\frac{q_r}{3}$	$\frac{PL^2}{KA}\left(\frac{q_{r(i-1)} + 2q_{r(i)}}{6}\right)$
h_r	$\frac{PL^2}{KA}\frac{q_r}{\Omega_r}$	$\frac{PL^2}{KA}\frac{q_r}{2\Omega_r}$	$\frac{PL^2}{KA}\left(\frac{q_{r(i-1)} + q_{r(i)}}{2\Omega_r}\right)$
$\frac{h_{ar}}{h_r}$	$\frac{1}{2}\Omega_r$	$\frac{2}{3}\Omega_r$	$\frac{1}{3}\left(\frac{q_{r(i-1)} + 2q_{r(i)}}{q_{r(i-1)} + q_{r(i)}}\right)\Omega_r$
f_d	$\frac{1}{2}$	$\frac{2}{3}$	$\frac{1}{3}\left(\frac{q_{r(i-1)} + 2q_{r(i)}}{q_{r(i-1)} + q_{r(i)}}\right)$

The relation can be expressed mathematically the following equation, which is:

$$\frac{h_{ar}}{h_r} = f_d \, \Omega_r \tag{4.32}$$

And hence,

$$h_{ar} = f_d \, \Omega_r h_r \tag{4.33}$$

Figure 4.11 depicts the change of f_d with different cases of radial flux distribution.

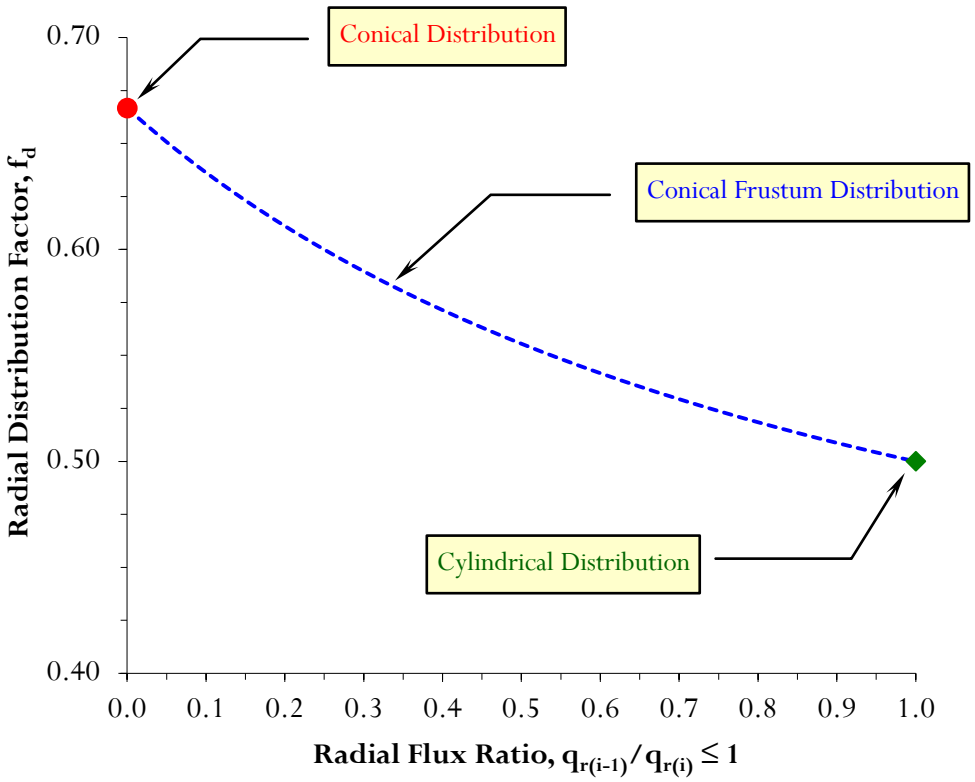

Figure 4.11: Various radial flux distributions along a wellbore element.

4.8 Wellbore Element Efficiency Model

Total axial head h is divided into two axial head losses which are; axial head loss, h_a and axial head loss associated with the existence of radial leakage flow along the element, h_{ar}. Substituting Equation (4.33) into Equation (4.8), then

$$\begin{aligned} h &= h_a + h_{ar} \\ &= h_a + f_d \, \Omega_r \, h_r \end{aligned} \tag{4.34}$$

Substituting Equation (4.15) and Equation (4.16) into Equation (4.34) gives:

$$\begin{aligned} h &= \frac{L}{KA} Q_a + f_d \frac{L}{KA} Q_r \\ &= \frac{L}{KA} \left(Q_a + f_d Q_r \right) \end{aligned} \tag{4.35}$$

Rearranging Equation (4.35):

$$Q_a + f_d Q_r = \frac{KA}{L} h \tag{4.36}$$

Recalling the relationship of wellbore leakage factor λ and leakage rate, Equation (4.3), then

$$Q_a = \lambda Q$$

and

$$Q_r = (1 - \lambda) Q$$

Substituting these relationships into Equation (4.36) then

$$\lambda Q + f_d (1 - \lambda) Q = \frac{KA}{L} h \tag{4.37}$$

Substituting the reference state equation, Equation (4.14), into Equation (4.37), then

$$\lambda Q + f_d(1-\lambda)Q = \frac{K}{K_F} Q_R \tag{4.38}$$

Rearranging Equation (4.38):

$$\frac{Q_R}{Q} = \left(\lambda + f_d(1-\lambda)\right) \times \frac{K_F}{K} \tag{4.39}$$

and similarly,

$$\frac{Q_R}{Q_a} = \left(\frac{\lambda + f_d(1-\lambda)}{\lambda}\right) \times \frac{K_F}{K} \tag{4.40}$$

The above two expressions, Equation (4.39) and Equation (4.40), can be simplified by defining a wellbore element permeability index, I_{ke} and two wellbore element storage indices, I_{0e} and I_{ne} as:

$$\begin{aligned} I_{ke} &= \frac{K}{K_F} \\ &= \frac{\left(\frac{\rho g}{\mu}\right)}{\left(\frac{\rho g}{\mu}\right)_F} \frac{k}{k_F} \\ &= \frac{k}{k_F} \end{aligned} \tag{4.41}$$

where the subscripts F is for formation, e is for element, and

- ρ: fluid density,
- g: gravity acceleration,
- μ: dynamic viscosity, and
- k: permeability.

while,

$$\begin{aligned} I_{0e} &= \lambda + f_d(1-\lambda) \\ &= (1-\eta) + f_d\eta \end{aligned} \tag{4.42}$$

and

$$\begin{aligned} I_{ne} &= \frac{\lambda}{\lambda + f_d(1-\lambda)} \\ &= \frac{(1-\eta)}{(1-\eta) + f_d\eta} \end{aligned} \tag{4.43}$$

This allows Equation (4.39) and Equation (4.40) to be expressed in terms of these indices:

$$\frac{Q_R}{Q} = \frac{I_{0e}}{I_{ke}} \tag{4.44}$$

and

$$\frac{Q_R}{Q_a} = \frac{1}{I_{ne}\, I_{ke}} \tag{4.45}$$

Equations (4.44) and (4.45) identify two types of parameters to assess leakage through wellbore element for storage purposes. The first type will be called wellbore element storage indices I_{0e}, I_{ne} and the other will be called wellbore element permeability index, I_{ke}. These parameters define the status of the wellbore condition in a given locality.

Wellbore storage indices are indices range from 0.0 to 1.0 and relate the theoretical one dimensional flow to actual flow in both directions around a

wellbore. Figure 4.12 indicates the change of wellbore storage index, I_{0e}, for calculation of Q that enters the control volume.

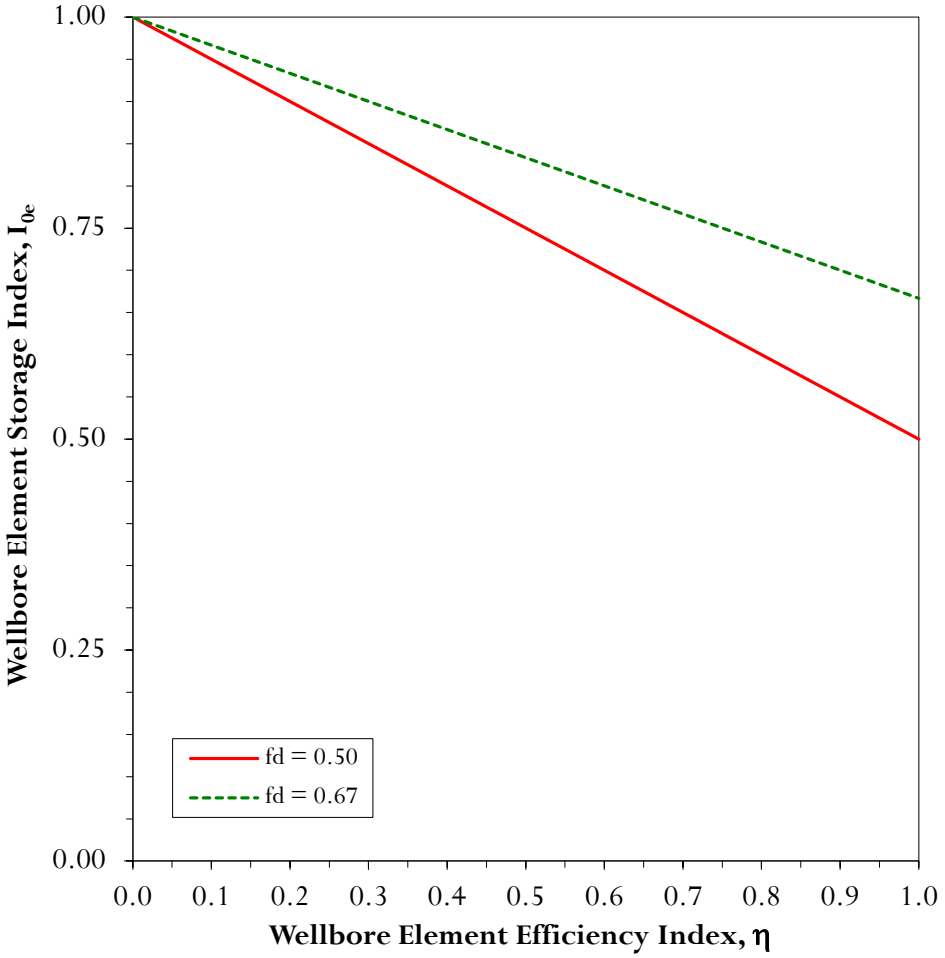

Figure 4.12: Wellbore element storage index I_{0e}.

The concern is the leakage Q_a that is related to wellbore element storage index, I_{ne}. Figure 4.13 indicates the change of wellbore efficiency index for calculation of Q_a that leaves the control volume to the subsequent one in the wellbore system and hence reduces the element efficiency. Figure 4.13

indicates that for the purpose of storage I_{ne} is not highly sensitive to the value of f_d. The conservative value is to take f_d equals to 0.50.

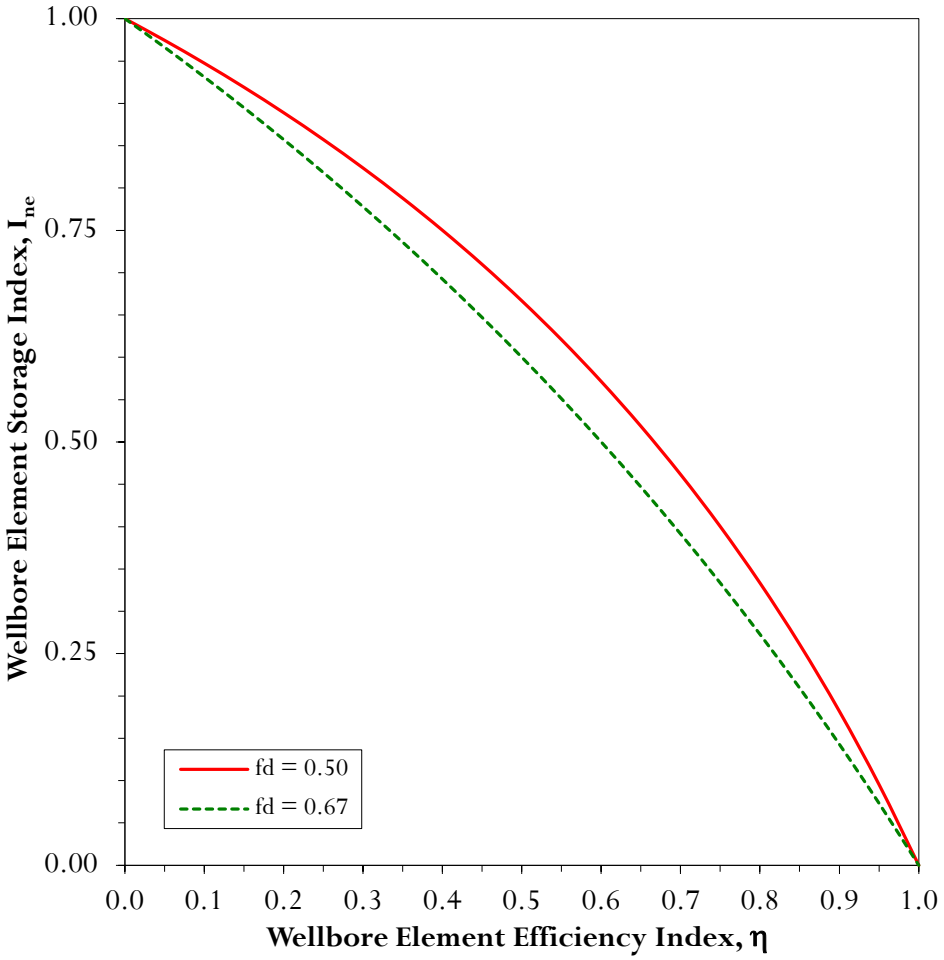

Figure 4.13: Wellbore element storage index I_{ne}.

The amount Q_R is the reference leakage state at wellbore location while Q_a is the leaked amount through a wellbore element. Ratio of these two amounts provides a measure for the performance of the wellbore element. Applying this concept, a factor of safety to assess the state of leakage for a given

wellbore element knowing the permeability index in specific locality can be obtained by the following equation:

$$FS_n = \frac{Q_R}{Q_n} = \frac{1}{I_{ne}\, I_{ke}} \tag{4.46}$$

Solution of Equation (4.46) is shown in Figure 4.14, which indicates that for any wellbore element if we have a permeability index more than 6 then the element efficiency for that element must be more than 0.90.

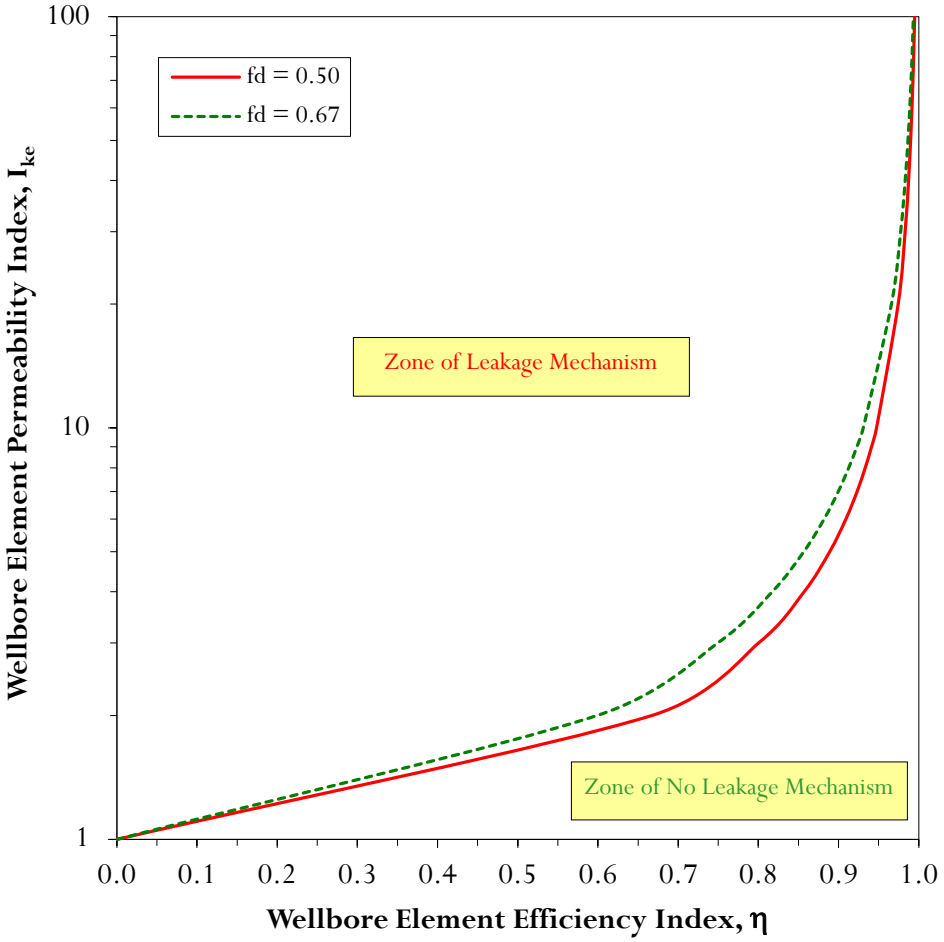

Figure 4.14: Safe performance chart for wellbore element.

Figure 4.14 illustrates that for the purpose of storage, wellbore element performance is not highly sensitive to the value of f_d. The conservative approach is to adopt a value of f_d equals to 0.50.

4.9 Summary

A new analytical model for modeling leakage through a wellbore element has been proposed. The model satisfies both the consideration of being a function of wellbore configuration "e.g. L, A" and being a function of head responsible for leakage. The assumptions of the analytical model can be summarized as;

1) Wellbore element has a constant circular cross sectional area.
2) The radial head pattern around the wellbore can be modeled as concentric cylinder.
3) Radial leakage is negligible beyond a specified radial distance or zone and is called radius of influence, R, or zone of influence respectively.
4) Formation is isotropic and homogenous with constant thickness within the radius of influence and infinitely extended in radial direction.
5) Vertical flow through wellbore element is considered as the source for any horizontal flow within the adjacent formation.
6) The model depends on the superposition method and takes into consideration the head loss in both axial and lateral direction.

The methodology to assess the wellbore leakage depends on the concept of sequence scenario of leakage, imports the concept of thermal efficiency, η_{th}, and considers the same analogy by concept of wellbore element efficiency, η, and finally postulates the concept of the reference state.

Modeling proposed an idealization of radial leakage through the wellbore element by a radial flux, q_r and represent this effect by radial leakage distribution factor, f_d. The idealization makes it possible to simplify the equations and hence to compare with the reference state.

Equation (4.46) results in obtaining the assessment (design) chart for the wellbore element performance. The assessment chart will be extended to include the entire wellbore system (Chapter 6).

4.10 References

Avci, C.B., (1992), Flow Occurrence between Confined Aquifers through Imperviously Plugged Boreholes, Journal of Hydrology, Vol. 139, pp. 97-114.

Avci, C.B., (1994), Evaluation of Flow Leakage through Abandoned Wells and Boreholes, Water Resources Research, Vol. 30, No. 9, pp. 2565-2578.

Brikowski, T., (1993), Flow between Aquifers through Filled Cylindrical Conduits: Analytical Solution and Application to Underground Nuclear Testing Sites, Journal of Hydrology, Vol. 146, pp. 115-130.

Celia, M.A., and Nordbotten, J.M, (2009), Practical Modeling Approaches for Geological Storage of Carbon Dioxide, Ground Water, Vol. 47, No. 5, pp. 627-638.

Celia, M.A., Nordbotten, J.M., Bachu, S., Dobossy, M. and Court, B., (2009), Risk of Leakage versus Depth of Injection in Geological Storage, Energy Procedia, 1, pp. 2573-2580.

Celia, M.A., Nordbotten, J.M., Court, B., Dobossy, M., and Bachu, S., (2011), Field-Scale Application of a Semi-Analytical Model for Estimation of CO2 and Brine Leakage along old Wells, International Journal of Greenhouse Gas Control, Vol. 5, pp. 257-269.

Chesnaux, R., and Chapuis, R.P., (2007), Detecting and Quantifying Leakage through Defective Borehole Seals: A New Methodology and Laboratory verification, Geotechnical Testing Journal, Vol. 30, No. 1, 8 p.

Chesnaux, R., Chapuis, R.P., and Molson, J.W., (2006), A New Method to Characterize Hydraulic Short-Circuit in Defective Borehole Seals, Ground Water, Vol. 44, No. 5, pp. 676-681.

Court, B., (2011), Safety and Water Challenges in CCS: Modeling Studies to Quantify CO2 and Brine Leakage Risk and Evaluate Promising Synergies for Active and Integrated Water Management, Ph.D. Thesis, Princeton University, USA, 244 p.

Dobossy, M.E., Celia, M.A., and Nordbotten, J.M., (2011), An Efficient Framework for performing Industrial Risk Assessment of Leakage for Geological Storage of CO2, Energy Procedia, 4, pp. 4207-4214.

Ebigbo, A., Class, H., and Helmig, R., (2007), CO2 Leakage through an Abandoned Well: Problem-Oriented Benchmarks, Computational Geosciences, Vol. 11, Issue 2, pp. 103-115.

Ellison, K.M., (2011), Risks Posed to Drinking Water Aquifers due to Leakage of Dissolved CO2 in Improperly Abandoned Wellbores, M.Sc. Thesis, Clemson University, USA, 73 p.

Gasda, S.A., (2008), Numerical Models for Evaluation CO2 Storgae in Deep, Saline Aquifers: Leaky Wells and Large-Scale Geological Features, Ph.D. Thesis, Princeton University, USA, 188 p.

Gasda, S.E., and Celia, M.A., (2005), Upscaling Relative Permeabilities in a Structured Porous Medium, Advances in Water Resources, Vol. 28, pp. 493-506.

Gasda, S.E., Bachu, S., and Celia, M.A., (2004), Spatial Characterization of the Location of Potentially Leaky Wells Penetrating a Deep Saline Aquifer in a Mature Sedimentary Basin, Environmental Geology, Vol. 46, Issue 6-7, pp. 707-720.

Hu, L., Pan, L., and Zhang, K., (2012), Modeling Brine Leakage to Shallow Aquifer through an Open Wellbore using T2WELL/ECO2N, International Journal of Greenhouse Gas Control, Vol. 9, pp. 393-401.

Humez, P., Audigane, P., Lions, J., Chiaberge, C., and Bellenfant, G., (2011), Modeling of CO2 Leakage Up Through an Abandoned Well from Deep Saline Aquifer to Shallow Fresh Groundwaters, Transport in Porous Media, Vol. 90, Issue 1, pp. 153-181.

Janzen, A.K., (2010), Development and Application of a Multi-Scale, Multi-Layer Numerical Model for CO2 Injection, M.Sc. Thesis, Princeton University, USA, 105 p.

Javandel, I., Tsang, C.F., and Witherspoon, P.A., (1988), Hydraulic Detection of Abandoned Wells Near Proposed Injection Wells for Hazardous Waste Disposal, Water Resources Research, Vol. 24, No. 2, pp. 261-270.

Lacombe, S., Sudicky, E.A., Frape, S.K., and Unger, A.J.A., (1995), Influence of Leaky Boreholes on Cross-Formational Groundwater Flow and Contaminant Transport, Water Resources Research, Vol. 31, No. 8, pp. 1871-1882.

LeNeveu, D.M., (2011), Analysis of Potential Acid Gas Leakage from Wellbore in Alberta – Canada, International Journal of Greenhouse Gas Control, Vol. 5, pp. 862-879.

LeNeveu, D.M., (2012), Potential for Environmental Impact due to Acid Gas Leakage from Welbores at EOR Injection Sites Near Zama Lake, Alberta, Greenhouse Gases: Science & Technology, Vol. 2, Issue 2, pp. 99-114.

Martinez-Landa, L., Rötting, T.S., Carrera, J., Russian, A., Dentz, M., and Cubilloc, B., (2013), Use of hydraulic tests to identify the residual CO2 saturation at a geological storage site, International Journal of Greenhouse Gas Control, Vol. 19, pp. 652-664.

Mishra, P.K., Vesselinov, V.V., and Neuman, S.P., (2012), Radial Flow to a Partially Penetrating Well with Storage in an Anisotropic Confined Aquifer, Journal of Hydrology, Vol. 448-449, pp. 255-259.

Nabih, A., and Chalaturnyk, R., (2013), Wellbore Efficiency Model for CO2 Geological Storage Part I: Theory and Wellbore Element, SPE Heavy Oil Conference-Canada, 11-13 June, Calgary, Alberta, Canada, SPE 165411, 14 p.

Nicot, J-P., Hosseini, S.A., and Solano, S.V., (2011), Are Single-Phase Flow Numerical Models Sufficient to Estimate Pressure Distribution in CO2 Sequestration Projects?, Energy Procedia, Vol. 4, pp. 3919-3926.

Nordbotten, J.M., and Celia, M.A., (2006), Similarity Solutions for Fluid Injection into Confined Aquifers, Journal of Fluid Mechanics, Vol. 561, 307-327.

Nordbotten, J.M., Celia, M.A., and Bachu, S., (2004), Analytical solutions for leakage rates through abandoned wells, Water Resources Research, Vol. 40, Issue 4, W04204, doi:10.1029/2003WR002997.

Nordbotten, J.M., Celia, M.A., and Bachu, S., (2005a), Injection and Storage of CO2 in Deep Saline Aquifers: Analytical Solution for CO2 Plume Evolution during Injection, Transport in Porous Media, Vol. 58, Issue 3, pp. 339-360.

Nordbotten, J.M., Celia, M.A., Bachu, S., and Dahle, H.K., (2005b), Semianalytical Solution for CO2 Leakage through an Abandoned Well, Environmental Science & Technology, Vol. 39, No. 2, pp. 602-611.

Nordbotten, J.M., Kavettski, D., Celia, M.A., and Bachu, S., (2009), Model for CO2 Leakage Including Multiple Geological Layers and Multiple Leaky Wells, Environmental Science & Technology, Vol. 43, No. 3, pp. 743-749.

Nogues, J.P., Court, B., Dobossy, M., Nordbotten, J.M., and Cleia, M.A., (2012), A Methodology to estimate Maximum Probable Leakage along Old Wells in a Geological Sequestration Operation, International Journal of Greenhouse Gas Control, Vol. 7, pp. 39-47.

Nogues, J.P., Nordbotten, J.M., and Cleia, M.A., (2011), Detecting Leakage of Brine or CO2 through abandoned Wells in a Geological Sequestration Operation using Pressure Monitoring Wells, Energy Procedia, 4, 3620-3627.

Oldenburg, C.M., Bryant, S.L., and Nicot, JP, (2009), Certification Framework based on Effective Trapping for Geologic Carbon Sequestration, International Journal of Greenhouse Gas Control, Vol. 3, pp. 444-457.

Shakya, S.K., and Singh, S.R., (1986), Steady Groundwater Flow from Constant Head Recharage Wells in Semi-Confined Aquifers, Journal of Hydrology, Vol. 84, pp. 323-332.

Shakya, S.K., Singh, S.R., and Anjaneyulu, B., (1986), Steady Flow from an Injection Well in Leaky Aquifers, Journal of Hydrology, Vol. 86, pp. 329-341.

Silliman, S. and Higgins, D., (1990), An Analytical Solution for Steady-State Flow between Aquifers through an Open Well, Ground Water, Vol. 28, No. 2, pp. 184-190.

Watson, T.L., and Bachu, S., (2008), Identification of Wells with High CO2-Leakage Potential in Mature Oil Fields Developed for CO2-Enhanced Oil Recovery, SPE Symposium on Improved Oil Recovery, 20-23 April, Tulsa, Oklahoma, USA, SPE 112924, 10 p.

Young, H.D. and Freedman, R.A., (2004), "University Physics with Modern Physics", 11th edition, PEARSON-Addison Wesley, 1714 p.

Zeidouni, M., (2011), Analytical and Inverse Models for Leakage Characterization of CO2 Storage, Ph.D. Thesis, University of Calgary, Canada, 227 p.

Zeidouni, M., Pooladi-Darvish, M., and Keith, D.W. (2011), Analytical Models for Determining Pressure Change in an Overlying Aquifer due to Leakage, Energy Procedia, 4, pp. 3833-3840.

Chapter 5: Wellbore Bulk Permeability[4]

5.1 Introduction

For wellbore leakage assessment, Nabih and Chalaturnyk (2013a) developed a new analytical approach for modeling leakage through a wellbore element. The wellbore element was defined as the length of each wellbore segment that crosses an individual formation (Celia et al., 2011).

Nabih and Chalaturnyk (2013b) used the wellbore element as a basic unit to model the whole wellbore system as serially connected units (sub-systems). This provides an advantage that each element can possess its own characteristics. Each wellbore element is a function of wellbore configuration and flow through each element is a function of pressure head responsible for leakage. Wellbore bulk "effective" permeability also can differ from element to element within a wellbore system and is used to estimate the permeability index required to assess the performance of wellbore element and the performance of the entire wellbore system.

This key property, which is assigned to each well segment in a wellbore system, is problematic as there have been no direct measurements of the bulk permeability along well segments (Nordbotten et al., 2009; Celia et al., 2011). Researchers deal with wellbore element bulk permeability by assuming either a deterministic value (Nordbotten et al., 2004, 2005, 2009; Gasda, 2008; Janzen, 2010; Celia et al., 2011; Nogues et al., 2011) or random

---

[4] A version of this chapter has been submitted for publication in the Proceedings of SPE Heavy Oil Conference Canada held in Calgary, Alberta, Canada, 10-12 June 2014.
Nabih, A., and Chalaturnyk, R., (2014), Stochastic Life Cycle Approach to Assess Wellbore Integrity for CO2 Geological Storage, SPE 170183.

variable value picked from an assumed probability distribution (Celia et al., 2009, 2011; Court, 2011; Dobossy et al., 2011; Nicot et al., 2012; Nogues et al., 2012).

Assurance of storage capacity of a storage site is a major concern. It is essential to identify and predict the wellbore performance under storage site conditions. For CO2 storage, the ultimate goal for well-leakage models is to serve as inputs for quantitative risk analysis (Gasda and Celia, 2005; Watson and Bachu, 2008; Celia and Nordbotten, 2009; Celia et al., 2009; Oldenburg et al., 2009; Dobossy et al., 2011; Humez et al., 2011; LeNeveu, 2012). In order to achieve this goal, there is a need for further study to investigate a more realistic representation of wellbore element bulk permeability that can differ from element to element in the wellbore system.

5.2 Wellbore Leakage Identification

The modeling approach adopts the following three concepts, as discussed in Chapter 4, to model the wellbore element:

4) sequence scenarios of possible leakage paths,
5) wellbore efficiency for storage purposes, and
6) reference state.

By adopting first concept, Figure 5.1, Nabih and Chalaturnyk (2013a) indicated that the highest possible occurrence of leakage is the flow through cement sheath and the interface of this cement with the formation and/or the casing. Leakage in axial direction represents flow through wellbore at cement-formation interface, outer cement-casing interface and the cement in the wellbore annulus.

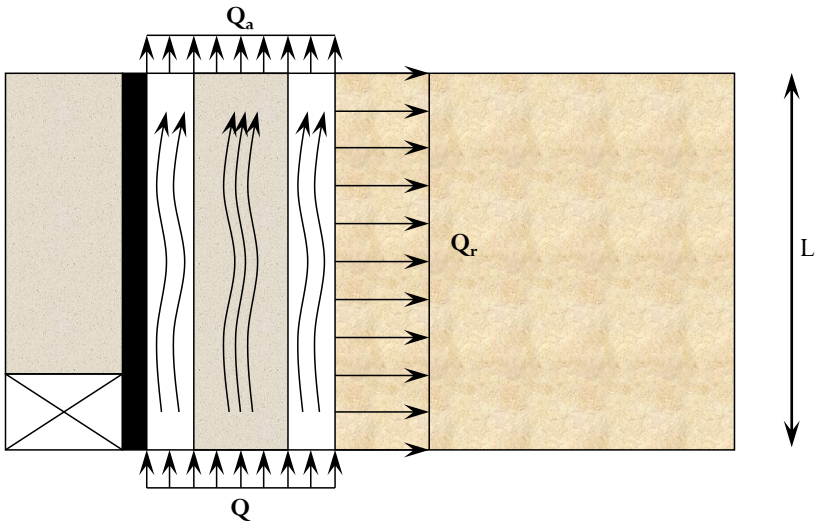

Figure 5.1: Basic wellbore element model.

Nabih and Chalaturnyk (2013a) proposed a super position model identifying that this leakage is characterized by the axial head loss h_a, which is a part of the total head loss h affecting the whole model element. Axial leakage rate, Q_a for an element is:

$$Q_a = \frac{KA}{L} h_a \tag{5.1}$$

where,

K: axial bulk wellbore hydraulic conductivity (i.e. vertical direction),

A: cross sectional area of the wellbore element, and

L: length of the wellbore element.

Axial bulk wellbore hydraulic conductivity, K, represents a "smeared" conductivity considering the effect of cement-formation interface, cement-casing interface and the cement sheath in the wellbore annulus characteristics.

Hydraulic conductivity, K, depends jointly on the attributes of the formation and of the pore fluid. The formation characteristics that affect the conductivity are the total porosity, the distribution of pore sizes, and tortuosity, which has an indirect relation to the formation's pore geometry. The pore fluid attributes that affect conductivity are density and viscosity (Hillel, 1998).

In theory, it is possible to separate K into two factors; the intrinsic permeability (i.e. simply permeability) of the formation, k and the fluidity of the pore fluid, f (Hillel, 1998):

$$K = f\ k \tag{5.2}$$

Fluidity can be defined as:

$$f = g\frac{\rho}{\mu} = g\frac{1}{\left(\frac{\mu}{\rho}\right)} = \frac{g}{\upsilon} \tag{5.3}$$

hence,

$$k = K\frac{\mu}{\rho g} \tag{5.4}$$

where,

μ: dynamic viscosity (simply viscosity),

g: Gravitational acceleration, and

υ: kinematic viscosity.

Nabih and Chalaturnyk (2013a) developed a one dimensional analytical leakage flow transfer model. Axial leakage through wellbore element, Q_a, can be expressed by:

$$Q_a = Q_{Icf} + Q_{cem} + Q_{Icc} \tag{5.5}$$

where,

Q_{Icf}: leakage through interface between cement and formation,

Q_{cem}: leakage through cement sheath, and

Q_{Icc}: leakage through interface between cement and casing.

From Equation (5.1) and applying Darcy's law:

$$\frac{KA}{L}h_a = \frac{K_{Icf}A_{Icf}}{L}h_a + \frac{K_{cem}A_{cem}}{L}h_a + \frac{K_{Icc}A_{Icc}}{L}h_a \tag{5.6}$$

Therefore,

$$K = \left(\frac{1}{A}\right)\left(K_{Icf}A_{Icf} + K_{cem}A_{cem} + K_{Icc}A_{Icc}\right) \tag{5.7}$$

where,

K_{Icf}: conductivity through interface between cement and formation,

A_{Icf}: area of interface between cement and formation,

K_{cem}: conductivity through cement sheath,

A_{cem}: area of cement sheath,

K_{Icc}: conductivity through interface between cement and casing, and

A_{Icc}: area of interface between cement and casing.

Substituting Equation (5.4) into Equation (5.7), hence:

$$k\frac{\rho g}{\mu} = \left(\frac{1}{A}\right)\left(k_{Icf}\frac{\rho g}{\mu}A_{Icf} + k_{cem}\frac{\rho g}{\mu}A_{cem} + k_{Icc}\frac{\rho g}{\mu}A_{Icc}\right) \tag{5.8}$$

Therefore,

$$k = k_{Icf}\left(\frac{A_{Icf}}{A}\right) + k_{cem}\left(\frac{A_{cem}}{A}\right) + k_{Icc}\left(\frac{A_{Icc}}{A}\right) \tag{5.9}$$

where,

k_{Icf}: permeability of interface between cement and formation,

k_{cem}: permeability of cement sheath, and

k_{lcc}: permeability of interface between cement and casing.

For the reference stage of a wellbore when the cement is fully set, the following conditions applies:

$A_{cem} = A = A_{ref}$, and

$A_{lcf} = A_{lcc} = 0.00$

5.3 Flow through Circular Discontinuities

Modeling itself is considered as an idealization of real problem. The lower the assumptions and simplification the higher optimization and sound results can be obtained. Loius (1969) summarized flow laws and flow rates for open joints and indicated that flow through a fracture depends on relative roughness and type of the flow (Lee et al., 1983; Wittke, 1990).

The simplest conceptual model of flow through discontinuity is based on the flow between two smooth, parallel walls separated by a uniform aperture. Hudson and Harrison (2000) expressed Darcy's law in a rewritten form as:

$$Q = C_H \, h_a \tag{5.10}$$

where,

C_H: hydraulic conductance, and

h_a: head loss.

The model's results in what is known as the cubic law (Jaeger et al, 2007). The volumetric flow rate in this case, $Q_{Fracture}$, with units of (m^3/s) can be written as:

$$Q_{Fracture} = \frac{b\,\omega_a^3}{12}\,\frac{\rho g}{\mu}\,\frac{h_a}{L} \qquad (5.11)$$

where,

b: width of the fracture, and

ω_a: aperture between the pair of plates.

Wellbore has a circular cross section and hence permeability modeling must consider an elementary thin cylindrical gap shown in Figure 5.2.

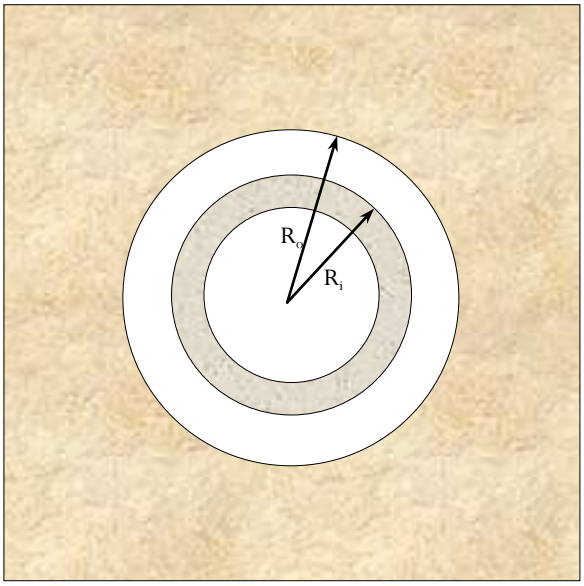

Figure 5.2: Wellbore cement-formation gap.

For a circular element "section", the velocity at any point is u and the dynamic viscosity is μ. The element has a length L with inside radius of r and a radial thickness of dr. The pressure difference, Δp, is over the element length, L. The shear stress on the surface increases by $d\tau$ from the inner to the outer surface. The procedure is important to investigate which part influences

wellbore bulk permeability. Basics for flow rate derivation can be found in any fluid mechanics textbook as Durst (2008) and White (2008). The derivation of an expression for flow velocity, as described in Appendix D, is based on equating the driving force due to pressure and the resisting force due to the shear stress by the walls. The general equation for flow velocity at any radius r within circular section is:

$$u_r = -\frac{r^2}{4\mu}\left(\frac{\Delta p}{L}\right) + A\ln(r) + B \tag{5.12}$$

where A and B are the constants of integration.

Equation (5.12) can be used to obtain volumetric flow rates through circular sections. The flow may be through the whole circular section (i.e. pipe) as in Appendix E or through micro-annulus as in Appendix F. Flow through a circular section of the pipe with radius R (Appendix E) is:

$$\begin{aligned} Q_{Pipe} &= \frac{1}{8\mu}\left(\frac{\Delta p}{L}\right) R^2 \times \pi R^2 \\ &= \frac{\pi}{8\mu}\left(\frac{\Delta p}{L}\right) R^4 \end{aligned} \tag{5.13}$$

Using head loss h_a, (i.e. $\Delta p = \rho g h_a$) instead of pressure loss allows Equation (5.13) to be rewritten as:

$$Q_{Pipe} = \frac{\rho g}{\mu}\frac{\pi R^4}{8}\frac{h_a}{L} \tag{5.14}$$

Rearranging Equation (5.14) to include pipe area $A_{Pipe} = \pi R^2$, then

$$\begin{aligned} Q_{Pipe} &= \frac{\rho g}{\mu}\frac{1}{8}R^2\frac{\pi R^2}{L}h_a \\ &= \frac{\rho g}{\mu}\frac{1}{8}R^2\frac{A_{Pipe}}{L}h_a \end{aligned} \tag{5.15}$$

For flow through wellbore micro-annulus gap with an outer radius, R_o and inner radius, R_i (Appendix F) is:

$$Q_{Annulus} = \frac{\pi}{8\mu}\left(R_o^2 - R_i^2\right)\left(\frac{\Delta p}{L}\right)\left(\left(R_o^2 + R_i^2\right) - \frac{\left(R_o^2 - R_i^2\right)}{\ln\left(R_o / R_i\right)}\right) \tag{5.16}$$

Using head loss h_a, (i.e. $\Delta p = \rho g h_a$) instead of pressure loss allows Equation (5.16) to be rewritten as:

$$Q_{Annulus} = \frac{\pi\rho g}{8\mu}\left(R_o^2 - R_i^2\right)\left(\left(R_o^2 + R_i^2\right) - \frac{\left(R_o^2 - R_i^2\right)}{\ln\left(R_o / R_i\right)}\right)\frac{h_a}{L} \tag{5.17}$$

Rearranging Equation (5.17) to include annulus area $A_{Annulus} = \pi\left(R_o^2 - R_i^2\right)$, then,

$$Q_{Annulus} = \frac{\rho g}{\mu}\frac{1}{8}\left(\left(R_o^2 + R_i^2\right) - \frac{\left(R_o^2 - R_i^2\right)}{\ln\left(R_o / R_i\right)}\right)\frac{A_{Annulus}}{L}h_a \tag{5.18}$$

5.4 Flow through Cement Sheath

Permeability is one of the most problematic properties because it varies over a wide range. It is important to derive the general relation for cement as a porous material.

The general relation needs to take into consideration the volumetric strain existing in the cement sheath at the same time as the reference stage for calculating the permeability of cement-formation interface and cement-casing interface. In the following sub-sections, the conclusion of cement sheath permeability followed the same procedure of Touhidi-Baghini (1998).

5.4.1 Porosity and Volumetric Strain Relationship

Volumetric strain, ε_v, is a mechanical parameter that can be related to the hydraulic parameter porosity, n, to calculate the changes in the conductivity and hence the permeability. The initial porosity, n_0 is defined as:

$$n_0 = \frac{V_0 - V_s}{V_0} \tag{5.19}$$

where,

V_0: total initial volume, and

V_s: volume of solids.

Current porosity, n_i, after a volume change of, ΔV_i, is defined as:

$$n_i = \frac{(V_0 + \Delta V_i) - V_s}{(V_0 + \Delta V_i)} \tag{5.20}$$

The current volumetric strain, ε_{vi}, is defined as:

$$\varepsilon_{vi} = \frac{\Delta V_i}{V_0} \tag{5.21}$$

which leads to:

$$\Delta V_i = \varepsilon_{vi} V_0 \tag{5.22}$$

By substituting Equation (5.22) into Equation (5.20), Touhidi-Baghini (1998) showed that the porosity-volumetric stain relationship is:

$$n_i = \frac{n_0 + \varepsilon_{vi}}{1 + \varepsilon_{vi}} \tag{5.23}$$

Equation (5.23) is a special case that shows that volumetric strain at n_0 is zero and the increase in volume (dilation) is assumed to be positive. When cement

is fully hydrated (i.e. reference stage of simulation), cement is pre-stressed and hence the volumetric strain, ε_v, at this stage of wellbore time frame is not zero. Therefore, considering a reference stage during the wellbore time frame is required in order to generalize porosity and permeability relations with any given reference stage of loading. From Equation (5.23), then

$$n_{Ref} = \frac{n_0 + \varepsilon_{vRef}}{1 + \varepsilon_{vRef}} \tag{5.24}$$

Solving for n_0 in Equations (5.23) and (5.24) then:

$$n_i (1 + \varepsilon_{vi}) - \varepsilon_{vi} = n_{Ref} (1 + \varepsilon_{vRef}) - \varepsilon_{vRef} \tag{5.25}$$

Rearranging Equation (5.25):

$$n_i (1 + \varepsilon_{vi}) = n_{Ref} (1 + \varepsilon_{vRef}) + (\varepsilon_{vi} - \varepsilon_{vRef}) \tag{5.26}$$

Therefore, the general relationship between porosity and volumetric strain at any reference value is as follows:

$$\begin{aligned} n_i &= \frac{n_{Ref} (1 + \varepsilon_{vRef}) + (\varepsilon_{vi} - \varepsilon_{vRef})}{(1 + \varepsilon_{vi})} \\ &= 1 - \frac{(1 - n_{Ref})(1 + \varepsilon_{Ref})}{(1 + \varepsilon_{vi})} \end{aligned} \tag{5.27}$$

As a check for this general relationship, substituting by $n_{Ref} = n_0$, and $\varepsilon_{vRef} = \varepsilon_{v0} = \text{Zero}$ in Equation (5.27) leads to Equation (5.23);

$$\begin{aligned} n_i &= \frac{n_{Ref} (1 + \varepsilon_{vRef}) + (\varepsilon_{vi} - \varepsilon_{vRef})}{(1 + \varepsilon_{vi})} = \frac{n_0 (1 + 0.00) + (\varepsilon_{vi} - 0.00)}{(1 + \varepsilon_{vi})} \\ &= \frac{n_0 + \varepsilon_{vi}}{1 + \varepsilon_{vi}} \end{aligned}$$

5.4.2 Permeability and Volumetric Strain Relationship

A theoretical solution for the hydraulic conductivity, K, exists in the literature (McCarthy, 2007; Das, 2007). The solution is generally referred to as the Kozeny-Carman equation, which is:

$$K = \frac{1}{C_s S_s^2 T^2} \frac{\rho g}{\mu} \frac{e^3}{1+e} \tag{5.28}$$

where,

C_s: shape factor,

S_s: wetted surface area per unit volume of soil solids,

T: tortuosity, and

e: Void ratio.

Void ratio is related to porosity as

$$e = \frac{n}{1-n}$$

Therefore;

$$K = \frac{1}{C_s S_s^2 T^2} \frac{\rho g}{\mu} \frac{n^3}{(1-n)^2} \tag{5.29}$$

From Equation (5.28) and Equation (5.29) and assuming that tortuosity is constant under the geomechanical processes, then

$$\begin{aligned} K &\propto \frac{e^3}{1+e} \\ &\propto \frac{n^3}{(1-n)^2} \end{aligned} \tag{5.30}$$

Assuming the reference and the current conductivity to be K_{Ref} and K_i respectively, then from Equation (5.30) permeability ratio is:

$$\frac{K_i}{K_{Ref}} = \frac{n_i^3}{(1-n_i)^2} \times \frac{(1-n_{Ref})^2}{n_{Ref}^3} \tag{5.31}$$

Assuming constant pore fluid properties (i.e. fluidity), the same equation will be considered for permeability that is:

$$\frac{k_i}{k_{Ref}} = \frac{n_i^3}{(1-n_i)^2} \times \frac{(1-n_{Ref})^2}{n_{Ref}^3} \tag{5.32}$$

Touhidi-Baghini (1998) cited that Rajani (1988) expressed any permeability as a function of different factors affecting it. Permeability can be expressed as:

$$k = f(n) \times g(s) \times D_s^2 \tag{5.33}$$

where,

f(n): porosity (packing characteristics) function,

g(s): particle and pore shape function, and

D_s: Mean size of solid particles.

Rajani (1988) suggested that Kozeny-Carman equation can be a generalized by changing the porosity function to be:

$$f(n) = \frac{n^a}{(1-n)^b} \tag{5.34}$$

Recalling Equation (5.31) and assuming the reference and current conductivities to be K_{Ref} and K_i respectively, the ratio is given by:

$$\begin{aligned} \frac{K_i}{K_{Ref}} &= \frac{n_i^a}{(1-n_i)^b} \times \frac{(1-n_{Ref})^b}{n_{Ref}^a} \\ &= \left(\frac{n_i}{n_{Ref}}\right)^a \times \left(\frac{1-n_{Ref}}{1-n_i}\right)^b \end{aligned} \tag{5.35}$$

From Equation (5.27), we get

$$\frac{1-n_{Ref}}{1-n_i}=\frac{1+\varepsilon_{vi}}{1+\varepsilon_{Ref}} \tag{5.36}$$

Substituting by Equations (5.27) and (5.36) into Equation (5.35), then:

$$\frac{K_i}{K_{Ref}}=\left(\frac{n_{Ref}\left(1+\varepsilon_{vRef}\right)+\left(\varepsilon_{vi}-\varepsilon_{vRef}\right)}{\left(1+\varepsilon_{vi}\right)}\right)^a\times\left(\frac{1+\varepsilon_{vi}}{1+\varepsilon_{vRef}}\right)^b \tag{5.37}$$

Multiplying right side by $\left(\frac{1+\varepsilon_{vRef}}{1+\varepsilon_{vRef}}\right)^a$ and rearrange the equation, then:

$$\frac{K_i}{K_{Ref}}=\left(\frac{n_{Ref}\left(1+\varepsilon_{vRef}\right)+\left(\varepsilon_{vi}-\varepsilon_{vRef}\right)}{n_{Ref}\left(1+\varepsilon_{vi}\right)}\right)^a\times\left(\frac{1+\varepsilon_{vi}}{1+\varepsilon_{vRef}}\right)^b\times\left(\frac{1+\varepsilon_{vRef}}{1+\varepsilon_{vRef}}\right)^a$$

$$=\left(\frac{n_{Ref}\left(1+\varepsilon_{vRef}\right)+\Delta\varepsilon_{vi}}{n_{Ref}\left(1+\varepsilon_{vRef}\right)}\right)^a\times\left(\frac{1+\varepsilon_{vi}}{1+\varepsilon_{vRef}}\right)^b\times\left(\frac{1+\varepsilon_{vRef}}{1+\varepsilon_{vi}}\right)^a$$

Therefore;

$$\frac{K_i}{K_{Ref}}=\left(1+\frac{\Delta\varepsilon_{vi}}{n_{Ref}\left(1+\varepsilon_{vRef}\right)}\right)^a\times\left(\frac{1+\varepsilon_{vi}}{1+\varepsilon_{vRef}}\right)^{b-a} \tag{5.38}$$

Inserting $\varepsilon_{vRef}-\varepsilon_{vRef}$ in the second term of right hand side, then:

$$\frac{K_i}{K_{Ref}}=\left(1+\frac{\Delta\varepsilon_{vi}}{n_{Ref}\left(1+\varepsilon_{vRef}\right)}\right)^a\times\left(\frac{1+\varepsilon_{vRef}-\varepsilon_{vRef}+\varepsilon_{vi}}{\left(1+\varepsilon_{vRef}\right)}\right)^{b-a}$$

$$=\left(1+\frac{\Delta\varepsilon_{vi}}{n_{Ref}\left(1+\varepsilon_{vRef}\right)}\right)^a\times\left(\frac{\left(1+\varepsilon_{vRef}\right)+\Delta\varepsilon_{vi}}{\left(1+\varepsilon_{vRef}\right)}\right)^{b-a} \tag{5.39}$$

$$=\left(1+\frac{\Delta\varepsilon_{vi}}{n_{Ref}\left(1+\varepsilon_{vRef}\right)}\right)^a\times\left(1+\frac{\Delta\varepsilon_{vi}}{\left(1+\varepsilon_{vRef}\right)}\right)^{b-a}$$

Taking natural logarithm of Equation (4.39) results in:

$$\ln\left(\frac{K_i}{K_{Ref}}\right) = a\ln\left(1+\frac{\Delta\varepsilon_{vi}}{n_{Ref}\left(1+\varepsilon_{vRef}\right)}\right) - (a-b)\ln\left(1+\frac{\Delta\varepsilon_{vi}}{\left(1+\varepsilon_{vRef}\right)}\right) \tag{5.40}$$

Taylor's series expansion for a logarithm is:

$$\ln(1+x) = x - \frac{x^2}{2} + \frac{x^3}{3} - \frac{x^4}{4} + \frac{x^5}{5} - \ldots\ldots \qquad \text{for } |x| < 1$$

Using Taylor's series expansion to express the logarithmic terms of Equation (5.40), then:

$$\begin{aligned}\ln\left(\frac{K_i}{K_{Ref}}\right) = a&\left(\left(\frac{\Delta\varepsilon_{vi}}{n_{Ref}\left(1+\varepsilon_{vRef}\right)}\right) - \frac{1}{2}\left(\frac{\Delta\varepsilon_{vi}}{n_{Ref}\left(1+\varepsilon_{vRef}\right)}\right)^2 + \ldots\ldots\right) \\ &-(a-b)\left(\left(\frac{\Delta\varepsilon_{vi}}{\left(1+\varepsilon_{vRef}\right)}\right) - \frac{1}{2}\left(\frac{\Delta\varepsilon_{vi}}{\left(1+\varepsilon_{vRef}\right)}\right)^2 + \ldots\ldots\right)\end{aligned} \tag{5.41}$$

Volumetric strain value is fairly small and thus the second and any higher orders terms of Taylor's expansion can be neglected (Touhidi-Baghini, 1998). Therefore,

$$\ln\left(\frac{K_i}{K_{Ref}}\right) = a\left(\frac{\Delta\varepsilon_{vi}}{n_{Ref}\left(1+\varepsilon_{vRef}\right)}\right) - (a-b)\left(\frac{\Delta\varepsilon_{vi}}{\left(1+\varepsilon_{vRef}\right)}\right) \tag{5.42}$$

And hence;

$$\ln\left(\frac{K_i}{K_{Ref}}\right) = \left(\frac{a}{n_{Ref}} - a + b\right)\left(\frac{\Delta\varepsilon_{vi}}{\left(1+\varepsilon_{vRef}\right)}\right) \tag{5.43}$$

Rearranging Equation (5.43):

$$\ln\left(\frac{K_i}{K_{Ref}}\right)=\left(\frac{a-(a-b)n_{Ref}}{n_{Ref}}\right)\left(\frac{\varepsilon_{vi}-\varepsilon_{vRef}}{1+\varepsilon_{vRef}}\right) \tag{5.44}$$

Substituting from Equation (5.4) into Equation (5.44) leads to:

$$\ln\left(\frac{k_i}{k_{Ref}}\right)=\left(\frac{a-(a-b)n_{Ref}}{n_{Ref}}\right)\left(\frac{\varepsilon_{vi}-\varepsilon_{vRef}}{1+\varepsilon_{vRef}}\right) \tag{5.45}$$

Equation (4.45) indicates a linear relationship between logarithm of permeability and volumetric strain (i.e. semi-logarithmic relationship). Substituting Kozeny-Carman values of $a=3$ and $b=2$ in Equation (5.44) and Equation (5.45):

$$\ln\left(\frac{K_i}{K_{Ref}}\right)=\left(\frac{3-n_{Ref}}{n_{Ref}}\right)\left(\frac{\varepsilon_{vi}-\varepsilon_{vRef}}{1+\varepsilon_{vRef}}\right) \tag{5.46}$$

and,

$$\ln\left(\frac{k_i}{k_{Ref}}\right)=\left(\frac{3-n_{Ref}}{n_{Ref}}\right)\left(\frac{\varepsilon_{vi}-\varepsilon_{vRef}}{1+\varepsilon_{vRef}}\right) \tag{5.47}$$

As a check for this general relationship, substituting by $n_{Ref}=n_0$, and $\varepsilon_{vRef}=\varepsilon_{v0}=$Zero in Equation (5.47), then same equation concluded by Touhidi-Baghini (1998) can be obtained:

$$\ln\left(\frac{k_i}{k_{Ref}}\right)=\left(\frac{3-n_0}{n_0}\right)\varepsilon_{vi}$$

5.5 Wellbore Permeability Modeling

Bulk wellbore permeability depends on possible sources of leakage through wellbore element, which were identified in Section 5.2. One can recognize

the parameters needed to model the bulk permeability by recalling Equation (5.9) which was:

$$k = k_{Icf}\left(\frac{A_{Icf}}{A}\right) + k_{cem}\left(\frac{A_{cem}}{A}\right) + k_{Icc}\left(\frac{A_{Icc}}{A}\right) \tag{5.48}$$

For the reference stage of a wellbore during its time frame:

$$A_{cem} = A = A_{ref}$$

$$A_{Icf} = A_{Icc} = 0.00$$

Table 5.1 summarizes flow parameters for circular cross section

Table 5.1: Summary of wellbore flow parameters.

Parameter	**Flow through**	
	Pipe	**Annulus**
Q	$\frac{\rho g}{\mu}\frac{1}{8}R^2\frac{A_{Pipe}}{L}h_a$	$\frac{\rho g}{\mu}\frac{1}{8}\left(\left(R_o^2+R_i^2\right)-\frac{\left(R_o^2-R_i^2\right)}{\ln\left(R_o/R_i\right)}\right)\frac{A_{Annulus}}{L}h_a$
Area	πR^2	$\pi\left(R_o^2-R_i^2\right)$
Conductance	$\frac{\rho g}{\mu}\frac{1}{8}R^2\frac{A_{Pipe}}{L}$	$\frac{\rho g}{\mu}\frac{1}{8}\left(\left(R_o^2+R_i^2\right)-\frac{\left(R_o^2-R_i^2\right)}{\ln\left(R_o/R_i\right)}\right)\frac{A_{Annulus}}{L}$
Conductivity	$\frac{\rho g}{\mu}\frac{1}{8}R^2$	$\frac{\rho g}{\mu}\frac{1}{8}\left(\left(R_o^2+R_i^2\right)-\frac{\left(R_o^2-R_i^2\right)}{\ln\left(R_o/R_i\right)}\right)$
Permeability	$\frac{1}{8}R^2$	$\frac{1}{8}\left(\left(R_o^2+R_i^2\right)-\frac{\left(R_o^2-R_i^2\right)}{\ln\left(R_o/R_i\right)}\right)$

5.5.1 Interface Permeability

Table 5.1 indicates that the permeability of the interface between inner formation face and outer cement face, k_{Icf}, that can be rewritten as:

$$k_{Icf} = \frac{1}{8}\left(\left(R_{iform}^2 + R_{ocem}^2\right) - \frac{\left(R_{iform}^2 - R_{ocem}^2\right)}{\ln\left(\frac{R_{iform}}{R_{ocem}}\right)} \right) \tag{5.49}$$

where,

R_{iform}: inner formation radius of the wellbore, and

R_{ocem}: outer cement sheath radius of the wellbore.

Similarly to cement-formation interface permeability, cement-casing interface permeability can be defined as:

$$k_{Icc} = \frac{1}{8}\left(\left(R_{icem}^2 + R_{oc}^2\right) - \frac{\left(R_{icem}^2 - R_{oc}^2\right)}{\ln\left(\frac{R_{icem}}{R_{oc}}\right)} \right) \tag{5.50}$$

where,

R_{icem}: inner cement sheath radius of the wellbore, and

R_{oc}: outer casing radius of the wellbore.

Inserting cement-formation interface gap, ω_{cf} into Equation (5.49), then:

$$k_{Icf} = \frac{1}{8}\left(\left(R_{iform}^2 + \left(R_{iform} - \omega_{cf}\right)^2\right) - \frac{\left(R_{iform}^2 - \left(R_{iform} - \omega_{cf}\right)^2\right)}{\ln\left(\frac{R_{iform}}{R_{iform} - \omega_{cf}}\right)} \right) \tag{5.51}$$

Rearranging Equation (5.51), then:

$$k_{Icf} = \frac{R_{iform}^2}{8}\left(\left(1+\left(1-\frac{\omega_{cf}}{R_{iform}}\right)^2\right) - \frac{\left(1-\left(1-\frac{\omega_{cf}}{R_{iform}}\right)^2\right)}{\ln\left(\frac{1}{\left(1-\frac{\omega_{cf}}{R_{iform}}\right)}\right)}\right) \tag{5.52}$$

Equation (5.52) can be further simplified by inserting cement-formation interface gap factor, f_{cf} that leads to:

$$k_{Icf} = \frac{R_{iform}^2}{8} f_{cf} \quad , \; k_{Icf} \geq 0.0 \tag{5.53}$$

In which cement-formation interface gap factor can be defined as:

$$f_{cf} = \left(1+\left(1-\frac{\omega_{cf}}{R_{iform}}\right)^2\right) - \frac{\left(1-\left(1-\frac{\omega_{cf}}{R_{iform}}\right)^2\right)}{\ln\left(\frac{1}{\left(1-\frac{\omega_{cf}}{R_{iform}}\right)}\right)} \tag{5.54}$$

Figure 5.3 shows the change of normalized interface gap factor for a wellbore. The normalization is at $\omega/R = 0.01$ %. Bulk wellbore permeability is very sensitive to the presence of interfaces gaps.

The factor is the same for both interfaces but the difference will be in the calculation of the interface permeability when multiplying by its corresponding wellbore formation or casing radius, respectively.

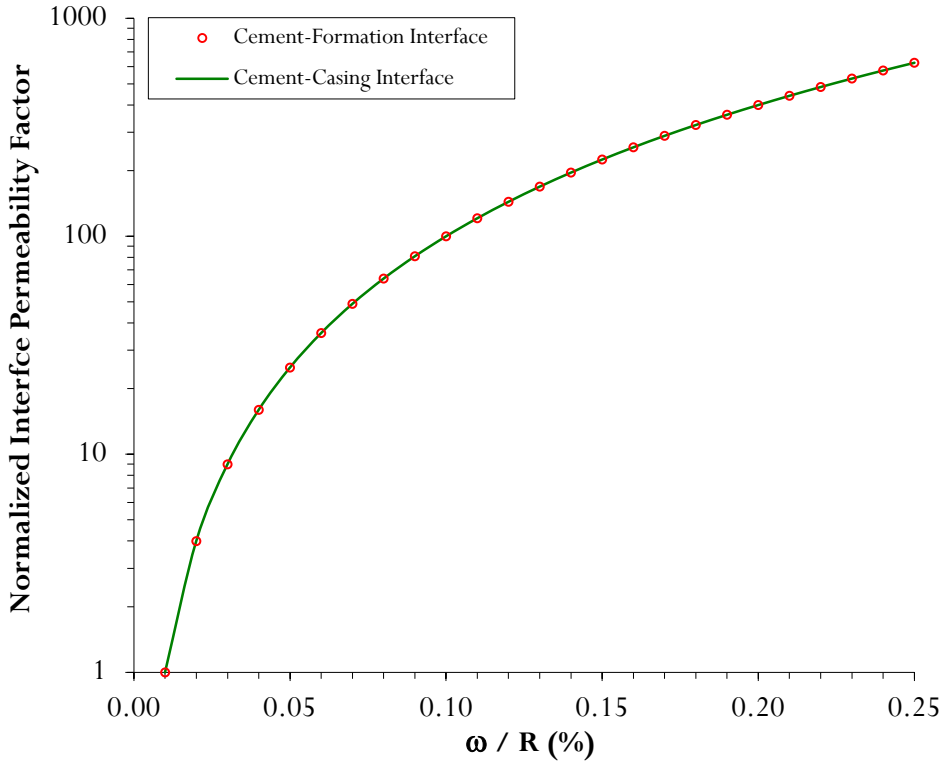

Figure 5.3: Wellbore interface permeability factor.

Following the same procedure, Equation (5.50) can be further simplified by inserting cement-casing interface gap factor, f_{cc} which leads to:

$$k_{Icc} = \frac{R_{oc}^2}{8} f_{cc} \qquad , \; k_{Icc} \geq 0.0 \tag{5.55}$$

In which cement-casing interface gap factor can be defined as:

$$f_{cc} = \left(\left(1+\frac{\omega_{cc}}{R_{oc}}\right)^2 + 1\right) - \frac{\left(\left(1+\frac{\omega_{cc}}{R_{oc}}\right)^2 + 1\right)}{\ln\left(1+\frac{\omega_{cc}}{R_{oc}}\right)} \tag{5.56}$$

5.5.2 Cement Sheath Permeability

Cement sheath permeability can be determined from Equation (5.47). Reference stage for cement properties is when the cement is fully hydrated and the time reference for this stage will be one month (i.e. 28 days). Therefore, logarithm of cement permeability, k_{cem}, can be rewritten as:

$$\ln\left(k_{cem}\right)=\left(\frac{3-n_{Ref}}{n_{Ref}}\right)\left(\frac{\varepsilon_{vi}-\varepsilon_{vRef}}{1+\varepsilon_{vRef}}\right)+\ln\left(k_{Ref}\right) \tag{5.57}$$

hence,

$$k_{cem}=e^{\left(\left(\frac{3-n_{Ref}}{n_{Ref}}\right)\left(\frac{\varepsilon_{vi}-\varepsilon_{vRef}}{1+\varepsilon_{vRef}}\right)+\ln\left(k_{Ref}\right)\right)} \quad , \; k_{cem}\geq k_{Ref} \tag{5.58}$$

The condition in Equation (5.58) is to assure a lower boundary limit for wellbore permeability. Cement paste porosity is around 18-21% (Hu and Stroeven, 2005). Cement sheath permeability factor, f_{cem}, can be obtained from Equation (5.32) as:

$$f_{cem}=\left(\frac{n_i}{n_{Ref}}\right)^3\times\left(\frac{1-n_{Ref}}{1-n_i}\right)^2 \tag{5.59}$$

where

$$k_{cem}=f_{cem}\,k_{Ref} \quad , \; k_{cem}\geq k_{Ref} \tag{5.60}$$

Figure 5.4 compares between the change of cement sheath permeability factor and interface permeability factor. The figure indicates that the change in cement permeability is fairly small while the effect of interfaces gap is predominant for calculating wellbore permeability hence volumetric strain has a weaker effect in determining wellbore bulk permeability.

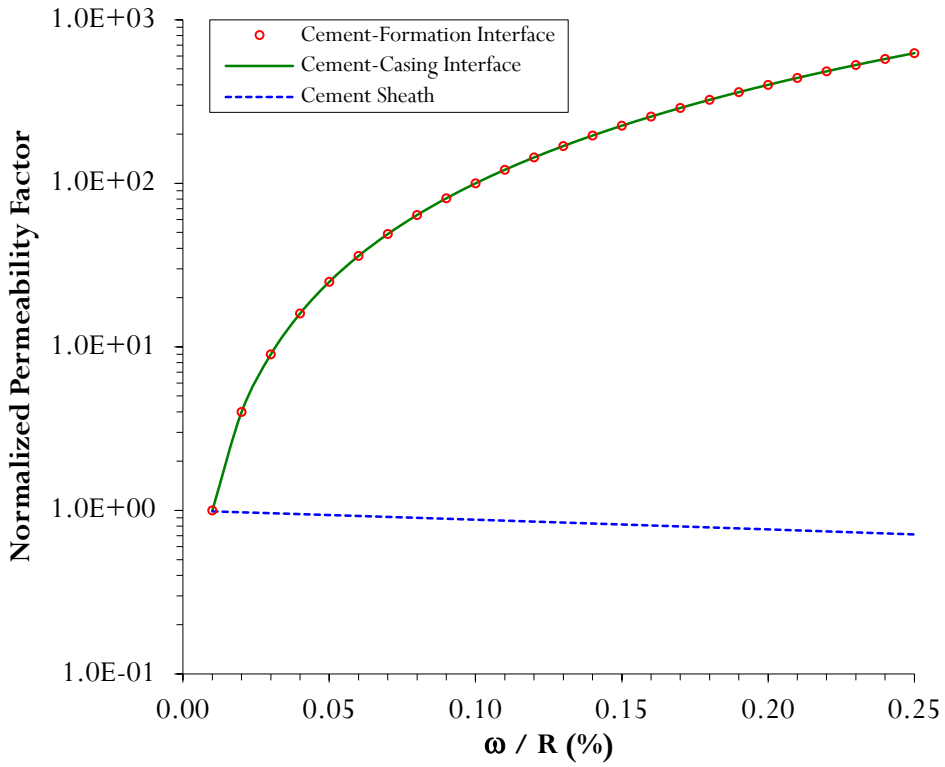

Figure 5.4: Theoretical wellbore permeability sensitivity.

5.5.3 Simulated Wellbore Permeability

Wellbore permeability can be obtained by applying the results of the numerical models that generated the gap width for both interfaces. Assessment of wellbore integrity, as discussed in Chapter 3, results in monitoring and expecting the cement-formation interfaces gap width, as in Figure 3.14, and cement-casing interfaces gap width, as in Figure 3.15.

These lifecycle expected gap widths under wellbore conditions can be used to estimate the interface gap factors, Equations (5.53) and (5.55), to estimate the permeability of wellbore interfaces. Figures 5.5 and 5.6 show box-and-

whiskers plots of the generated distribution of the formation-cement interface gap and casing-cement interface gap at selected years during wellbore lifecycle.

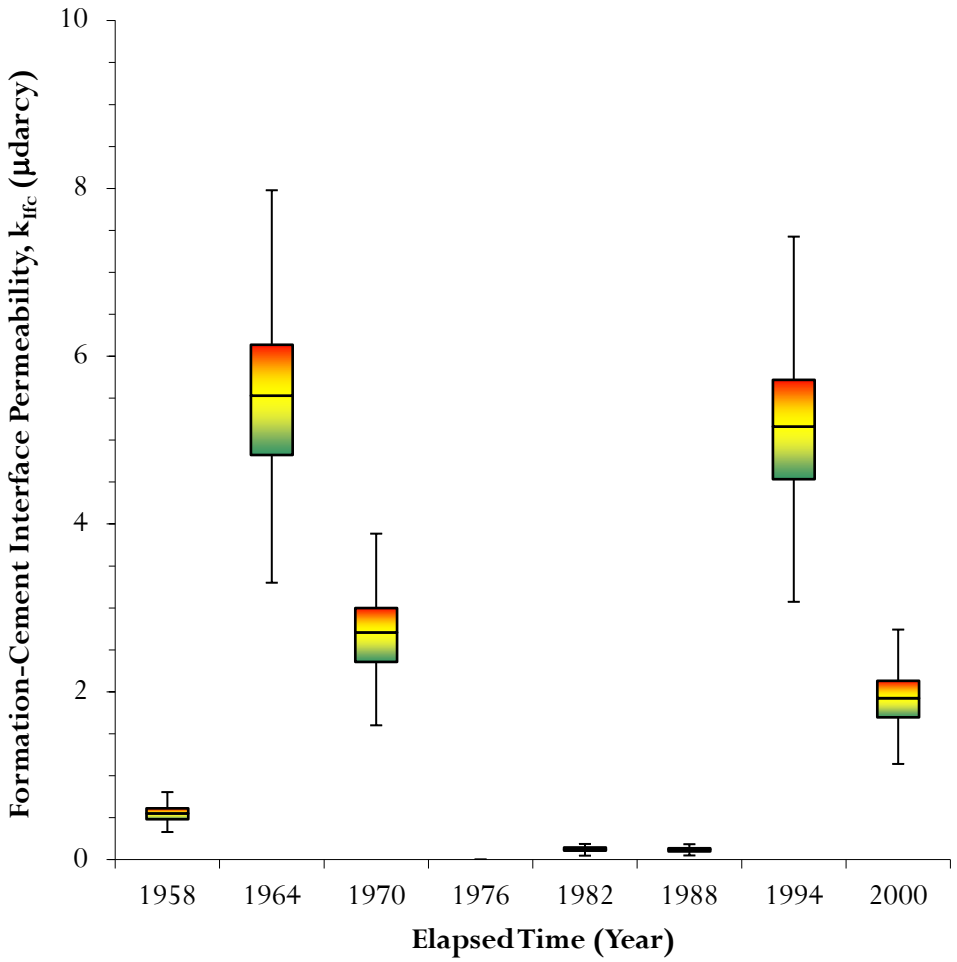

Figure 5.5: Simulated cement-formation interface permeability.

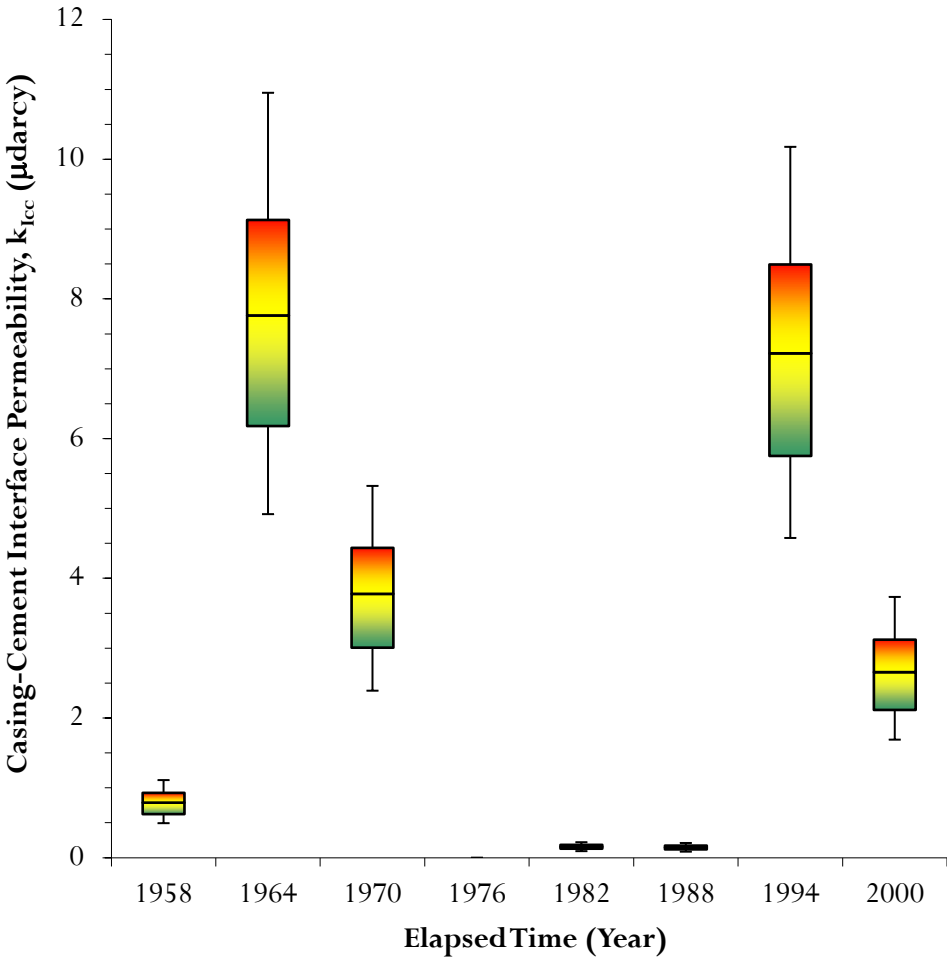

Figure 5.6: Simulated cement-casing interface permeability.

Furthermore, probability density functions (PDFs) for both cases correspond to these distributions are illustrated in Figure 5.7 and Figure 5.8 respectively. Stochastic approach may facilitate adopting of response surface methodology to optimize wellbore response and demonstrates the possibility to perform reliability based analysis for the wellbore.

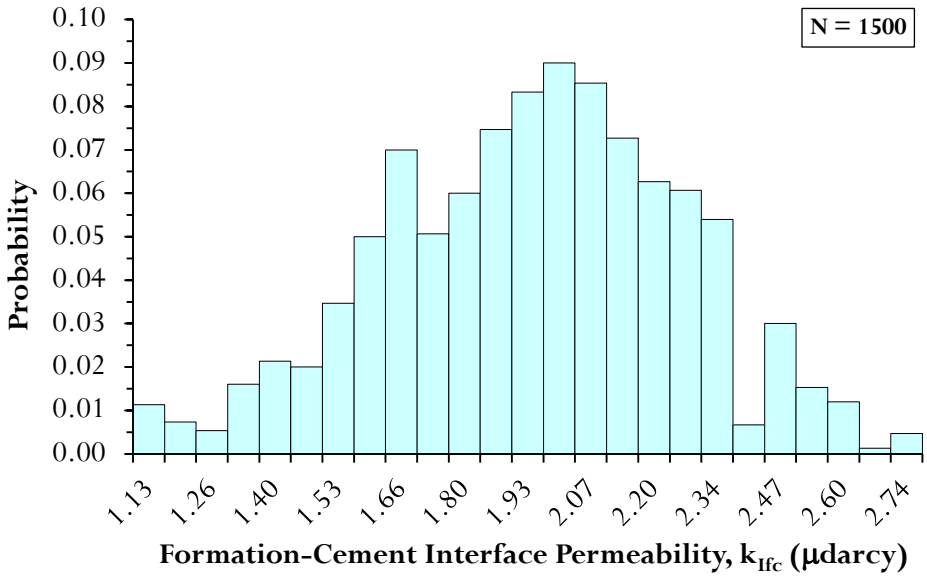

Figure 5.7: Generated cement-formation interface permeability at year 2000.

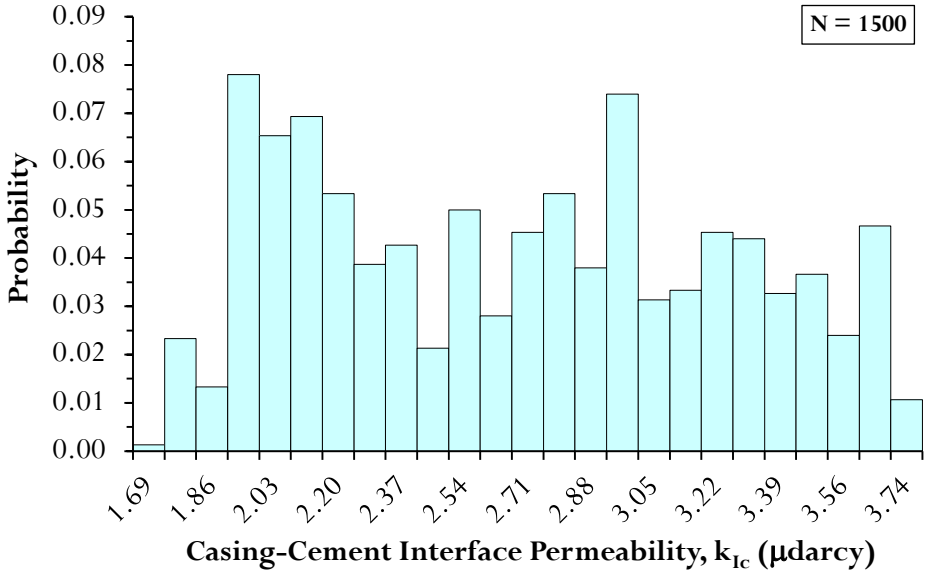

Figure 5.8: Generated cement-casing interface permeability at year 2000.

5.6 Summary

Rigorous modeling of all possible leakage pathways would be far too complex to simulate. However, leakage through cement sheath and through cement-formation and cement-casing interfaces were chosen as a possible pathway under different conditions that affects wellbore.

Wellbore bulk "effective" permeability can differ from element to another element in a wellbore system according to the cement sheath permeability and interfaces gap permeability if exist.

Bulk wellbore permeability is used to estimate the permeability index proposed by Nabih and Chalaturnyk (2013a) required to assess the performance of wellbore element and the performance of the wellbore system.

Bulk wellbore permeability depends mainly on the gap width at either cement-formation and/or cement-casing interfaces. Flow through micro annulus differs from flow through circular opening and characterized by interface permeability factor.

Cement at reference stage will be affected by the wellbore conditions and will influence the estimation of bulk wellbore permeability. In order to complete the frame work for wellbore assessment, it is important to investigate the behavior of the cement during hydration until reaching the reference stage. The reference stage is stage when cement is fully hydrated and will be taken after 1 month of wellbore lifecycle time frame.

5.7 References

Celia, M.A., and Nordbotten, J.M, (2009), Practical Modeling Approaches for Geological Storage of Carbon Dioxide, Ground Water, Vol. 47, No. 5, pp. 627-638.

Celia, M.A., Nordbotten, J.M., Bachu, S., Dobossy, M. and Court, B., (2009), Risk of Leakage versus Depth of Injection in Geological Storage, Energy Procedia, 1, pp. 2573-2580.

Celia, M.A., Nordbotten, J.M., Court, B., Dobossy, M., and Bachu, S., (2011), Field-Scale Application of a Semi-Analytical Model for Estimation of CO2 and Brine Leakage along old Wells, International Journal of Greenhouse Gas Control, Vol. 5, pp. 257-269.

Court, B., (2011), Safety and Water Challenges in CCS: Modeling Studies to Quantify CO2 and Brine Leakage Risk and Evaluate Promising Synergies for Active and Integrated Water Management, Ph.D. Thesis, Princeton University, USA, 244 p.

Das, B.M., (2007), Advanced Soil Mechanics, 3rd edition, Taylor & Francis Publications, 567 p.

Dobossy, M.E., Celia, M.A., and Nordbotten, J.M., (2011), An Efficient Framework for performing Industrial Risk Assessment of Leakage for Geological Storage of CO2, Energy Procedia, 4, pp. 4207-4214.

Durst, F., (2008), Fluid Mechanics: An Introduction to the theory of Fluid Flow, 1st edition, Springer-Verlag Berlin Heidelberg, 723 p.

Gasda, S.A., (2008), Numerical Models for Evalaution CO2 Storgae in Deep, Slaine Aquifers: Leaky Wells and Larga-Scale Geological Features, Ph.D. Thesis, Princeton University, USA, 188 p.

Gasda, S.E., and Celia, M.A., (2005), Upscaling Relative Permeabilities in a Structured Porous Medium, Advances in Water Resources, Vol. 28, pp. 493-506.

Guen, Y.L., Asamoto, S., Houdu, E., and Poupard, O., (2012), Well Integrity: Modeling of Thermo-Mechanical Behavior and Gas Migration along Wells - Application to Ketzin Injection Well, Energy Procedia, 23, pp. 462 – 471.

Hillel, D. (1998), Environmental Soil Physics, Academic Press, 2nd edition, 771 p.

Hu, J., and Stroeven, P, (2005), Local Porosity of Pore Structure in Cement Paste, Cement and Concrete Research, 35, pp. 233-242.

Hudson, J.A., and Harrison, J.P., (1997), Engineering Rock Mechanics: An Introduction to the principles, 1st edition, Pergamon Publications, 444 p.

Humez, P., Audigane, P., Lions, J., Chiaberge, C., and Bellenfant, G., (2011), Modeling of CO2 Leakage Up Through an Abandoned Well from Deep Saline Aquifer to Shallow Fresh Groundwaters, Transport in Porous Media, Vol. 90, Issue 1, pp. 153-181.

Jaeger, J.C., Cook, N.G.W., and Zimmerman, R.W. (2007), Fundamentals of Rock Mechanics, Blackwell Publishing, 4th edition, 500 p.

Janzen, A.K., (2010), Development and Application of a Multi-Scale, Multi-Layer Numerical Model for CO2 Injection, M.Sc. Thesis, Princeton University, USA, 105 p.

Lee, I.K., White, W., and Ingles O.G., (1983), Geotechnical Engineering, Pitman Publishing Pty Ltd., 1st edition, 508 p.

LeNeveu, D.M., (2012), Potential for Environmental Impact due to Acid Gas Leakage from Welbores at EOR Injection Sites Near Zama Lake, Alberta, Greenhouse Gases: Science & Technology, Vol. 2, Issue 2, pp. 99-114.

McCarthy, D.F., (2007), Essentials of Soil Mechanics and Foundations: Basic Geotechnics, 7th edition, 850 p.

Nabih, A., and Chalaturnyk, R., (2013a), Wellbore Efficiency Model for CO2 Geological Storage Part I: Theory and Wellbore Element, SPE Heavy Oil Conference-Canada, 11-13 June, Calgary, Alberta, Canada, SPE 165411, 14 p.

Nabih, A., and Chalaturnyk, R., (2013b), Wellbore Efficiency Model for CO2 Geological Storage Part II: Wellbore System, SPE Unconventional Resources Conference Canada, 5-7 November, Calgary, Alberta, Canada , SPE 167149, 14 p.

Nordbotten, J.M., Celia, M.A., and Bachu, S., (2004), Analytical solutions for leakage rates through abandoned wells, Water Resources Research, Vol. 40, Issue 4, W04204, doi:10.1029/2003WR002997.

Nordbotten, J.M., Celia, M.A., Bachu, S., and Dahle, H.K., (2005), Semianalytical Solution for CO2 Leakage through an Abandoned Well, Environmental Science & Technology, Vol. 39, No. 2, pp. 602-611.

Nordbotten, J.M., Kavettski, D., Celia, M.A., and Bachu, S., (2009), Model for CO2 Leakage Including Multiple Geological Layers and Multiple Leaky Wells, Environmental Science & Technology, Vol. 43, No. 3, pp. 743-749.

Nogues, J.P., Court, B., Dobossy, M., Nordbotten, J.M., and Cleia, M.A., (2012), A Methodology to estimate Maximum Probable Leakage along Old Wells in a Geological Sequestration Operation, International Journal of Greenhouse Gas Control, Vol. 7, pp. 39-47.

Oldenburg, C.M., Bryant, S.L., and Nicot, JP, (2009), Certification Framework based on Effective Trapping for Geologic Carbon Sequestration, International Journal of Greenhouse Gas Control, Vol. 3, pp. 444-457.

Touhidi-Baghini, A., (1998), Absolute Permeability of McMurry Formation Oil Sands at Low Confining Stresses, Ph.D. Thesis, University of Alberta, 339 p.

Watson, T.L., and Bachu, S., (2008), Identification of Wells with High CO2-Leakage Potential in Mature Oil Fields Developed for CO2-Enhanced Oil Recovery, SPE Symposium on Improved Oil Recovery, 20-23 April, Tulsa, Oklahoma, USA, SPE 112924, 10 p.

White, F.M., (2008), Fluid Mechanics, 6th edition, McGraw Hill, 864 p.

Wittke, W., (1990), Rock Mechanics: Theory and Applications with Case Histories, Springer-Verlag, 1st edition, 1075 p.

Chapter 6: Assessment of Wellbore Performance[5]

6.1 Introduction

Storing carbon dioxide (CO2) in deep geological formations is one part of the carbon capture and storage (CCS) process that is defined as geological CO2 sequestration or CO2 geo-sequestration. Injecting CO2 into a reservoir does not guarantee safe storage because CO2 could leak back to the surface and/or may contaminate specific strata where other energy, mineral and/or groundwater resources are present. Two mechanisms control assurance of storage integrity, which are geological leakage mechanism and wellbore leakage mechanism (Espie, 2005).

Leakage predictions through wellbores can be done by either analytical or numerical approaches. Analytical methods usually simplify the problems to solve the system analytically. They are more efficient computationally than numerical methods and are important for modeling if stochastic approaches, such as Monte Carlo simulations, are used. On the other hand, the numerical methods have the advantage to incorporate more complex geometry and heterogeneity in the large-scale system, which is not possible with an analytical method. Numerical methods prefer using a coarse grid to reduce the number of the nodes and hence be computationally faster. Many wellbores may penetrate a storage site each having a diameter of less than 0.5 meter, so to correctly capture leakage along the wellbore as a permeable pathway, grid refinement around each wellbore is required. This can result in total number of grid cells numbering in millions (Gasda, 2008; Court, 2011).

---

[5]A version of this chapter has been published in the Proceedings of SPE Unconventional Resources Conference Canada held in Calgary, Alberta, Canada, 5-7 November 2013.
Nabih, A., and Chalaturnyk, R., (2013), Wellbore Efficiency Model for CO2 Geological Storage Part II: Wellbore System, SPE 167149.

For multi-layers system, Nordbotten et al. (2004, 2009) demonstrated the importance of the application of multiple aquifers and aquitards to model the leakage through wellbores. Intervening aquifers help in mitigating leakage into upper layers. This is due to successive leakage from the wellbore into the overlying aquifers. The highest leakage occurs across the bottom aquitard while the lowest leakage occurs across the top aquitard.

Nordbotten et al. (2004) referred to the mechanism of leakage along a wellbore as an "elevator model". The elevator model process is similar to the analogy with an elevator (e.g. wellbore) full of people (e.g. leakage rate) on the main floor (e.g. storage reservoir), who then get off at various floors (e.g. overlying aquifers) such that only very few people ride all the way to the top floor (e.g. layer of concern).

The key property assigned to each well segment in a wellbore system is the equivalent wellbore bulk "effective" permeability. This property is problematic as there are no any measurements of the bulk permeability along well segments (Nordbotten et al., 2009; Celia et al., 2011). The wellbore segment was defined by the length of each wellbore that crosses an individual formation (Celia et al., 2011). The definition is the same for the wellbore element proposed by Nabih and Chalaturnyk (2013).

Researchers deal with wellbore element bulk permeability by assuming either a deterministic value (Nordbotten et al., 2004, 2005, 2009; Gasda, 2008; Janzen, 2010; Celia et al., 2011; Nogues et al., 2011) or random variable value picked from an assumed probability distribution (Celia et al., 2009, 2011; Court, 2011; Dobossy et al., 2011; Nogues et al., 2012; Nicot et al., 2013).

The models discussed above assume bulk permeability for the wellbore system and the model top layer is an aquitard that close the system at the top end of the wellbore system. As in Chapter five, the topsoil layer is added to the wellbore system to represent the shallow zone. Permeability of the formations in the vicinity of the wellbore is assumed to be equal (Nordbotten et al., 2004, 2005; Birkholzer et al., 2009; Janzen, 2010). However, there is a need for further study to represent a more realistic wellbore system in which not all aquifers have the same permeability (Janzen, 2010).

Janzen (2010) studied the impact of the number of layers modeled in the wellbore system using a model that consisted of 10 aquifers separated by 10 aquitards in addition to a topsoil layer for a total of 21 layers. He concluded that it is enough to model only 5 of the aquifers if assuming a 10 μDarcy permeability for aquitards. The 5 aquifers (10 layers) model produces a pressure profile in the lower aquifer that matches the pressure profile in that formation when all layers are modeled. Lowering the aquitard permeability decreases the number of the aquifers system required to match the full system profile. He suggested that an aquifer-aquitard boundary may be assumed impermeable if the ratio of the aquitard permeability to aquifer permeability is less than 10^6. For the impact of adjacent aquifer permeability, he concluded that the pressure response of layered system cannot be based on aquitard permeability alone.

6.2 Basic Wellbore Leakage Relations

In Chapter 4, the concept of a wellbore element was discussed as a method for developing a model of an entire wellbore system (Nabih and Chalaturnyk, 2013). Each wellbore element will be denoted by subscript i in the proposed model. Thus, flow enters each wellbore element with flow rate Q_{i-1}, formerly

Q, and leaves it axially with axial flow rate Q_i, formerly Q_a, and horizontally with radial flow rate Q_{ri}, formerly Q_r.

Recalling the basic equations governing the wellbore element and summarizing in new formats that are;

$$Q_{i-1} = Q_i + Q_{ri} \tag{6.1}$$

while for the axial head loss along wellbore element and adjacent formation,

$$h_i = h_{ai} + h_{ari} \tag{6.2}$$

and relation between the flow rates leaving the control volume and the axial head loss can be written as;

$$Q_i + f_{di} Q_{ri} = \frac{K_i A_i}{L_i} h_i \tag{6.3}$$

Adopting the efficiency concept we get:

$$\begin{aligned} Q_i &= (1-\eta_i)\, Q_{i-1} \\ &= \lambda_i\, Q_{i-1} \end{aligned} \tag{6.4}$$

and

$$\begin{aligned} Q_{ri} &= \eta_i\, Q_{i-1} \\ &= (1-\lambda_i)\, Q_{i-1} \end{aligned} \tag{6.5}$$

where,

η_i: wellbore element sealing efficiency for element i, and

λ_i: wellbore element leakage factor for element i.

Figure 6.1 shows a conceptual model for leakage through the whole wellbore system.

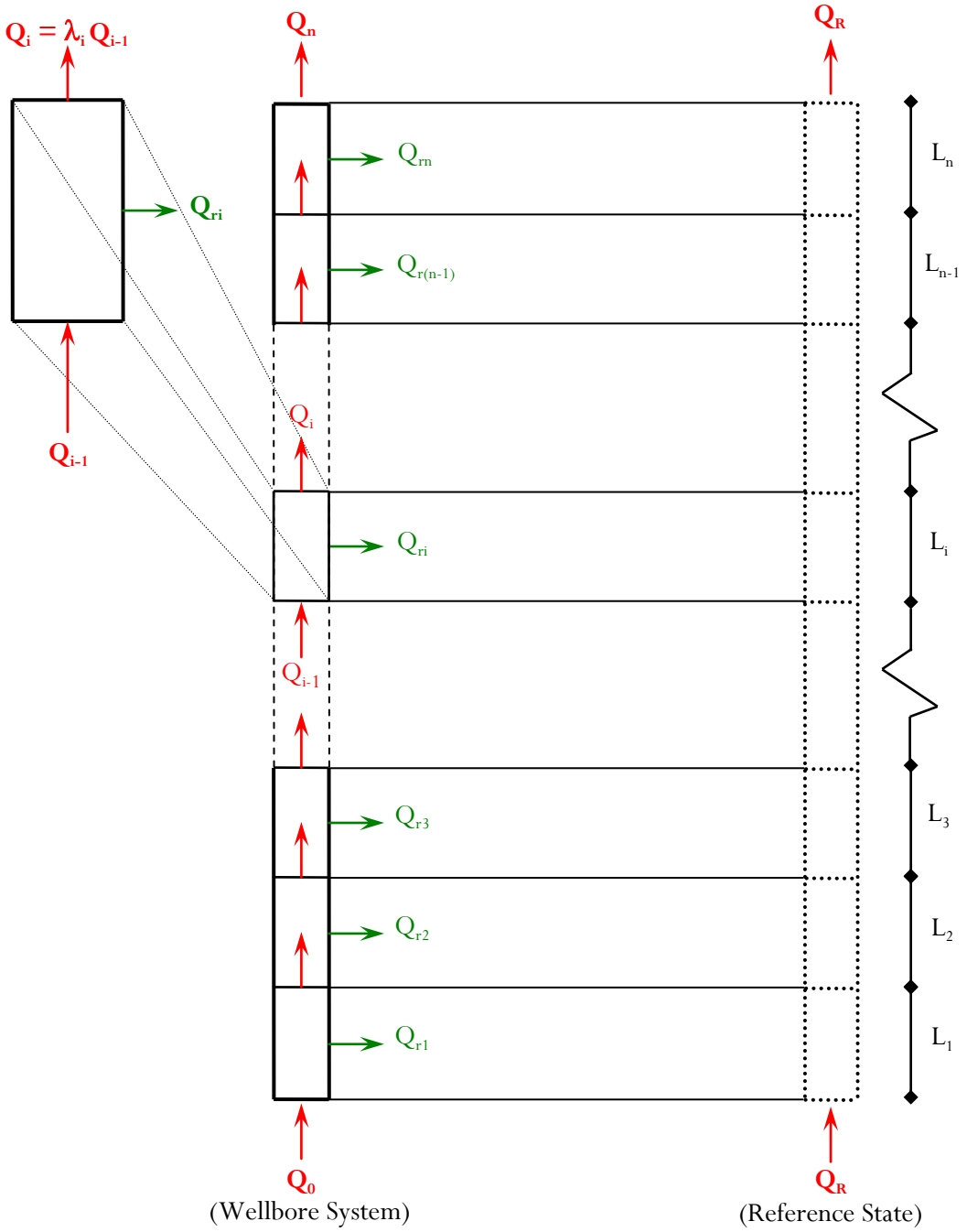

Figure 6.1: A schematic representation for a wellbore system model.

6.3 Wellbore Reference State

The concept of reference state for a wellbore element was illustrated in Chapter 4. Adopting this concept for the whole wellbore system, the reference state will be the state of the wellbore assuming it is represented by the properties of the formations along its length and flow is only in vertical direction. In electrical systems, this is analogous to the flow of current through resistors in series. This "imaginary" reference state is a representation of the resistance of leakage by any in-situ geological arrangement in the vicinity of the wellbore and before drilling in any given locality.

For flow normal to the different formation layers, the total head loss is the sum of the head losses in each layer:

$$h_L = h_1 + h_2 + \ldots\ldots + h_n \tag{6.6}$$

where h_L is the total head loss, and h_1 to h_n are the head losses in each of the n layers. The volumetric flow rate in each layer is the same and hence;

$$Q_R = Q_1 = Q_2 = \ldots\ldots = Q_n \tag{6.7}$$

From Darcy's law, we obtain:

$$K_F A \frac{h_L}{L} = K_{F1} A_1 \frac{h_1}{L_1} = K_{F2} A_2 \frac{h_2}{L_2} = \ldots\ldots = K_{Fn} A_n \frac{h_n}{L_n} \tag{6.8}$$

where K_F is the equivalent formation hydraulic conductivity in the vertical direction and K_{F1} to K_{Fn} are the vertical hydraulic conductivities of the first to the n^{th} layer. For constant flow area;

$$A = A_1 = A_2 = \ldots\ldots = A_n \tag{6.9}$$

solving Equations (6.6) and (6.8) leads to:

$$K_F = \frac{L}{\sum_{i=1}^{n} \frac{L_i}{K_{Fi}}} \tag{6.10}$$

and from Equations (6.8) and (6.9):

$$\frac{h_i}{L_i} = \frac{K_F}{K_{Fi}} \frac{h_L}{L} \tag{6.11}$$

Comparing the leakage through the wellbore system and leakage through this reference state, Figure 6.1, provides a measure of the wellbore condition. If the ratio between the two leakages (Q_R/Q_n) is > 1.0, then the wellbore hydraulic performance will exceed that of the formations. If the ratio is equal to 1.0 then the system behaviour is not affected by the presence of the well. If the ratio is < 1.0, then the wellbore performance is predicted to underperform relative to the formations alone and would potentially identify a well of concern for long-term leakage.

6.4 Wellbore System Model

A schematic representation for a proposed wellbore system model was illustrated in Figure 6.1. The wellbore model (system) is composed of wellbore elements (sub-systems) that are connected in serial manner. Equations for the wellbore system can be summarized as follows:

$$Q_0 = Q_n + \sum_{i=1}^{n} Q_{ri} \tag{6.12}$$

and

$$h_L = \sum_{i=1}^{n} h_i \tag{6.13}$$

where,

Q_0: leakage rate from a storage reservoir through a wellbore,

Q_n: axial leakage rate at layer n,

Q_{ri}: radial leakage rate at each wellbore element i,

h_L: total head loss, and

h_i: head losses in each wellbore element i.

6.5 Wellbore System Efficiency

Concept of wellbore efficiency identifies the similarity of a wellbore element as a system to the heat engine efficiency. Wellbore system sealing efficiency, η_W differs from wellbore element sealing efficiency, η_i.

According to the proposed model in Figure 6.1, wellbore system sealing efficiency, η_W can be defined as:

$$\eta_W = 1 - \lambda_W = \frac{Q_0 - Q_n}{Q_0} = \frac{\sum_{i=1}^{n} Q_{ri}}{Q_0} \tag{6.14}$$

in which wellbore system leakage factor λ_W is:

$$\lambda_W = \frac{Q_n}{Q_0} \tag{6.15}$$

6.6 Wellbore Leakage Modeling

For CO2 storage, the ultimate goal for well-leakage models is to serve as inputs for certification framework and risk analysis (Gasda and Celia, 2005; Barlet-Gouedard et al., 2006; Gerard et al., 2006; Watson and Bachu, 2008;

Celia and Nordbotten, 2009; Celia et al., 2009; Oldenburg et al., 2009; Dobossy et al., 2011; Humez et al., 2011; LeNeveu, 2012).

Basic equations for a wellbore element were detailed in Section 6.2, while wellbore system equations were listed in Section 6.4 and Section 6.5. From Equation (6.3) and summing over the whole model, therefore;

$$\sum_{i=1}^{n} Q_i + \sum_{i=1}^{n} f_{di} Q_{ri} = \sum_{i=1}^{n} \frac{K_i A_i}{L_i} h_i \tag{6.16}$$

Assuming that the radial leakage distribution along the wellbore elements are the same, then radial leakage factor is constant where $f_{di} = f_d$. Hence,

$$\sum_{i=1}^{n} Q_i + f_d \sum_{i=1}^{n} Q_{ri} = \sum_{i=1}^{n} \frac{K_i A_i}{L_i} h_i \tag{6.17}$$

From Equation (6.12) and Equation (6.17)

$$\sum_{i=1}^{n} Q_i + f_d (Q_0 - Q_n) = \sum_{i=1}^{n} \frac{K_i A_i}{L_i} h_i \tag{6.18}$$

Dealing with the first term on the left hand side of Equation (6.18), recall Equation (6.4) which defined the leakage factor of a wellbore element, therefore:

$$\begin{aligned}
Q_1 &= \lambda_1 Q_0 \quad &&= (\lambda_1) Q_0 \\
Q_2 &= \lambda_2 Q_1 \quad &&= (\lambda_2 \lambda_1) Q_0 \\
Q_3 &= \lambda_3 Q_2 \quad &&= (\lambda_3 \lambda_2 \lambda_1) Q_0 \\
\vdots &= \vdots \quad &&= \quad \vdots \\
Q_n &= \lambda_n Q_{n-1} &&= (\lambda_n \lambda_{n-1} \ldots\ldots \lambda_3 \lambda_2 \lambda_1) Q_0 \\
&---------- &&----------
\end{aligned} \tag{6.19}$$

Summing the above equations, we get:

$$\sum_{i=1}^{n} Q_i = \left(\lambda_1 + \lambda_1\lambda_2 + \lambda_1\lambda_2\lambda_3 + \ldots\ldots + \lambda_1\lambda_2\lambda_3 \ldots\ldots \lambda_{n-1}\lambda_n\right) Q_0 \tag{6.20}$$

Also,

$$Q_n = \left(\lambda_1\lambda_2\lambda_3 \ldots\ldots \lambda_{n-1}\lambda_n\right) Q_0 = \lambda_W\, Q_0 \tag{6.21}$$

where,

$$\lambda_W = \lambda_1\lambda_2\lambda_3 \ldots\ldots \lambda_{n-1}\lambda_n = \prod_{i=1}^{n} \lambda_i \tag{6.22}$$

Substituting Equation (6.20) and Equation (6.21) into Equation (6.18):

$$\left(\lambda_1 + \lambda_1\lambda_2 + \lambda_1\lambda_2\lambda_3 + \ldots\ldots + \lambda_1\lambda_2 \ldots\ldots \lambda_n\right) Q_0 + f_d(Q_0 - \lambda_W Q_0) = \sum_{i=1}^{n} \frac{K_i A_i}{L_i} h_i \tag{6.23}$$

Rearranging Equation (6.23) then,

$$Q_0\left(\left(\lambda_1 + \lambda_1\lambda_2 + \lambda_1\lambda_2\lambda_3 + \ldots\ldots + \lambda_1\lambda_2 \ldots\ldots \lambda_n\right) + f_d(1 - \lambda_W)\right) = \sum_{i=1}^{n} \frac{K_i A_i}{L_i} h_i \tag{6.24}$$

Introducing λ_{sys} to simplify left hand side of the equation

$$\lambda_{sys} = \left(\lambda_1 + \lambda_1\lambda_2 + \lambda_1\lambda_2\lambda_3 + \ldots\ldots + \lambda_1\lambda_2 \ldots\ldots \lambda_n\right) + f_d(1 - \lambda_W) \tag{6.25}$$

Therefore,

$$Q_0\, \lambda_{sys} = \sum_{i=1}^{n} \frac{K_i A_i}{L_i} h_i \tag{6.26}$$

Dealing with the right hand side of the Equation (6.26), Equation (6.11) can be substituting into Equation (6.26):

$$Q_0 \lambda_{sys} = \sum_{i=1}^{n} K_i A_i \frac{K_F}{K_{Fi}} \frac{h_L}{L} \tag{6.27}$$

Assuming that the wellbore cross section area is constant, Equation (6.27) can be rearranged as:

$$Q_0 \lambda_{sys} = \left(K_F A \frac{h_L}{L} \right) \times \sum_{i=1}^{n} \frac{K_i}{K_{Fi}} \tag{6.28}$$

Recalling Equation (6.7) and substituting into Equation (6.28);

$$Q_0 \lambda_{sys} = Q_R \sum_{i=1}^{n} \frac{K_i}{K_{Fi}} \tag{6.29}$$

In Chapter 4, wellbore element permeability index was introduced and the above expression can be simplified by introducing wellbore permeability index, I_{ki}, for element i defined as the ratio between wellbore permeability to formation permeability, hence,

$$I_{ki} = \frac{K_i}{K_{Fi}} = \frac{k_i}{k_{Fi}} \tag{6.30}$$

Therefore, Equation (6.29) can be rewritten as:

$$Q_0 \lambda_{sys} = Q_R \sum_{i=1}^{n} I_{ki} \tag{6.31}$$

Dividing both sides by number of wellbore elements (sub-systems), then

$$Q_0 \frac{\lambda_{sys}}{n} = Q_R \frac{\sum_{i=1}^{n} I_{ki}}{n} \tag{6.32}$$

Therefore,

$$Q_0 \frac{\lambda_{sys}}{n} = Q_R \, I_k \tag{6.33}$$

where I_k is the average permeability index of the wellbore system. And since λ_{sys} represents an aggregate leakage factor for the wellbore system, Equation (6.25), a storage index, I_0, can be defined for Q_0 calculations and is defined as;

$$I_0 = \frac{\lambda_{sys}}{n} \tag{6.34}$$

Therefore,

$$\frac{Q_R}{Q_0} = \frac{I_0}{I_k} \tag{6.35}$$

Substituting Equation (6.21) in Equation (6.35) then,

$$\frac{Q_R}{Q_n} = \frac{I_0}{\lambda_W \, I_k} \tag{6.36}$$

A second storage index I_n can also be adopted for Q_n calculations where;

$$\begin{aligned} I_n &= \frac{\lambda_W}{I_0} \\ &= \frac{n \, \lambda_W}{\lambda_{sys}} \end{aligned} \tag{6.37}$$

Therefore,

$$\frac{Q_R}{Q_n} = \frac{1}{I_n \, I_k} \tag{6.38}$$

Equations (6.35) and (6.38) are similar to Equations (4.44) and (4.45) respectively. They represent the general solution for the performance of a wellbore system where a wellbore element, described in Chapter 4, is the special case when number of elements equals to one. Wellbore system storage indices I_0 and I_n depend on the nature of the formation arrangement, Figure 6.2, in the storage site.

6.7 Wellbore Storage Indices

Wellbore system storage indices, I_0 and I_n, depend on the value of wellbore leakage factor, λ, and hence wellbore sealing efficiency, η. In addition, these indices depend on the number of wellbore elements (sub-systems) which are defined according to the change of permeability in a given locality. The arrangement of formation layers (strata) can be modeled to calculate storage indices that correspond to a specific wellbore location.

Figure 6.2 defines two systems for the wellbore system model with respect to the arrangement of the geological formations. These two systems are the case of the general system, G-System, and the case of repeated configuration of aquitard-aquifer system, R-System. Different arrangement cases lead to different storage indices values.

Theoretically, the efficiency may have any value between 0 and 1 but for practical purposes, this value may take a recommended range to become an industrial standard measure for accepting and/or rejecting wellbore condition (i.e. system and subsystem failure criteria).

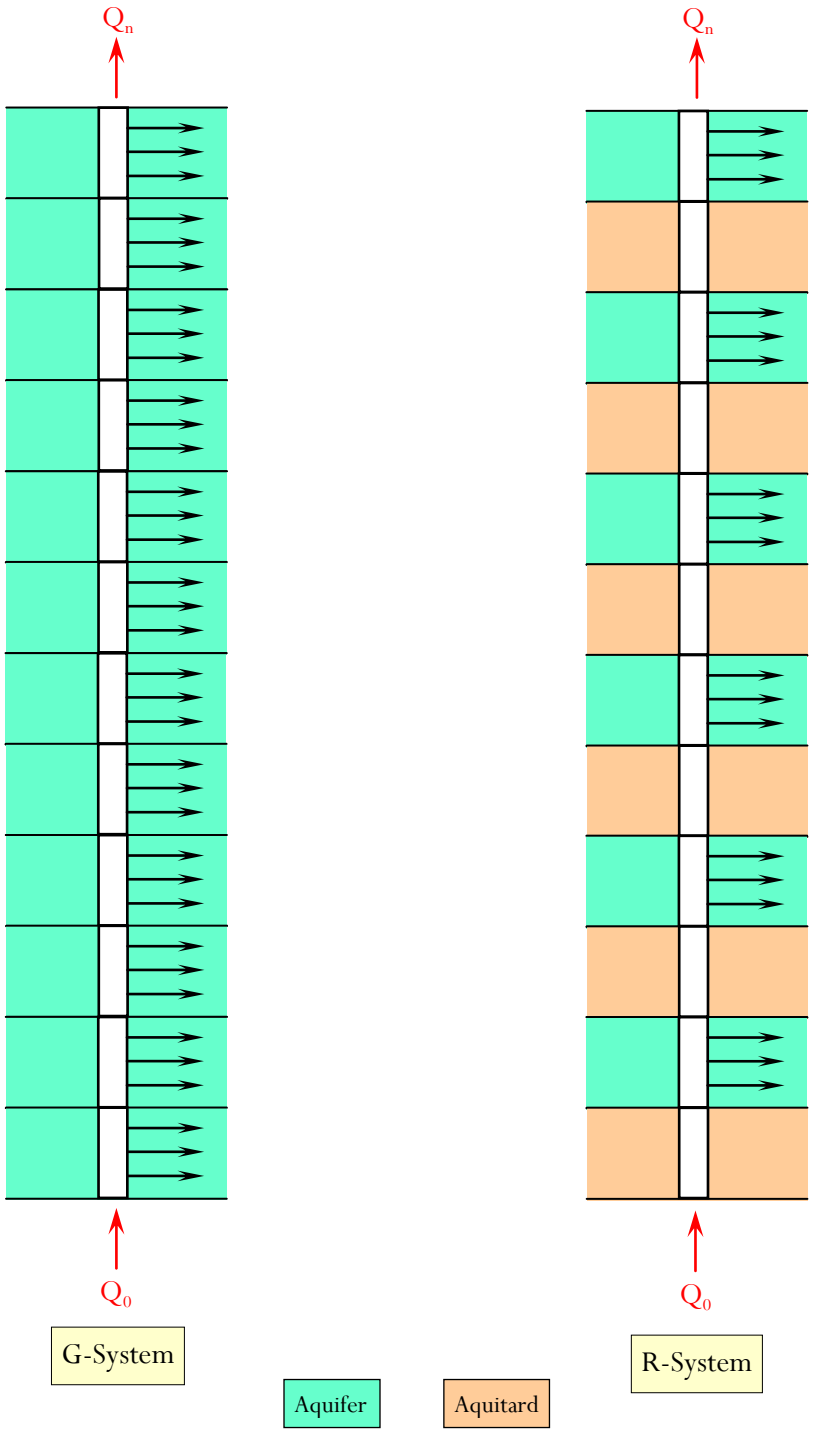

Figure 6.2: Wellbore system leakage according to formation arrangement.

6.7.1 Case of General Formation System

The general system of formation arrangement, G-System, represents a normal system allowing the flow in both directions for any wellbore element and has a constant leakage factor λ. Recalling Equation (6.25) which is:

$$\lambda_{sys} = \left(\lambda_1 + \lambda_1\lambda_2 + \lambda_1\lambda_2\lambda_3 + \ldots\ldots + \lambda_1\lambda_2 \ldots\ldots \lambda_n\right) + f_d\left(1 - \lambda_W\right)$$

with constant $\lambda_i = \lambda$ then,

$$\lambda_{(G\text{-}sys)} = \left(\lambda + \lambda^2 + \lambda^3 + \ldots\ldots + \lambda^n\right) + f_d\left(1 - \lambda^n\right) \tag{6.39}$$

The first term in Equation (6.39) is a geometric series. Therefore,

$$\begin{aligned} \lambda_{(G\text{-}sys)} &= \frac{\lambda\left(1-\lambda^n\right)}{(1-\lambda)} + f_d\left(1-\lambda^n\right) \\ &= \left(1-\lambda^n\right)\left(\frac{\lambda}{(1-\lambda)} + f_d\right) \end{aligned} \tag{6.40}$$

Hence,

$$\begin{aligned} I_{0(G\text{-}sys)} = \frac{\lambda_{(G\text{-}sys)}}{n} &= \frac{1-\lambda^n}{n}\left(\frac{\lambda}{(1-\lambda)} + f_d\right) \\ &= \frac{1-(1-\eta)^n}{n}\left(\frac{(1-\eta)}{\eta} + f_d\right) \end{aligned} \tag{6.41}$$

and

$$I_{n(G\text{-}sys)} = \frac{\lambda_W}{I_{0(G\text{-}sys)}} = \frac{\lambda^n}{I_{0(G\text{-}sys)}} = \frac{(1-\eta)^n}{I_{0(G\text{-}sys)}} \tag{6.42}$$

Figure 6.3 shows the relation between wellbore element sealing efficiency, η, and wellbore system sealing efficiency, η_W, in case of different numbers of elements composing the whole system. It indicates that increasing the number

of the elements enhances the overall system efficiency for all values of element efficiency.

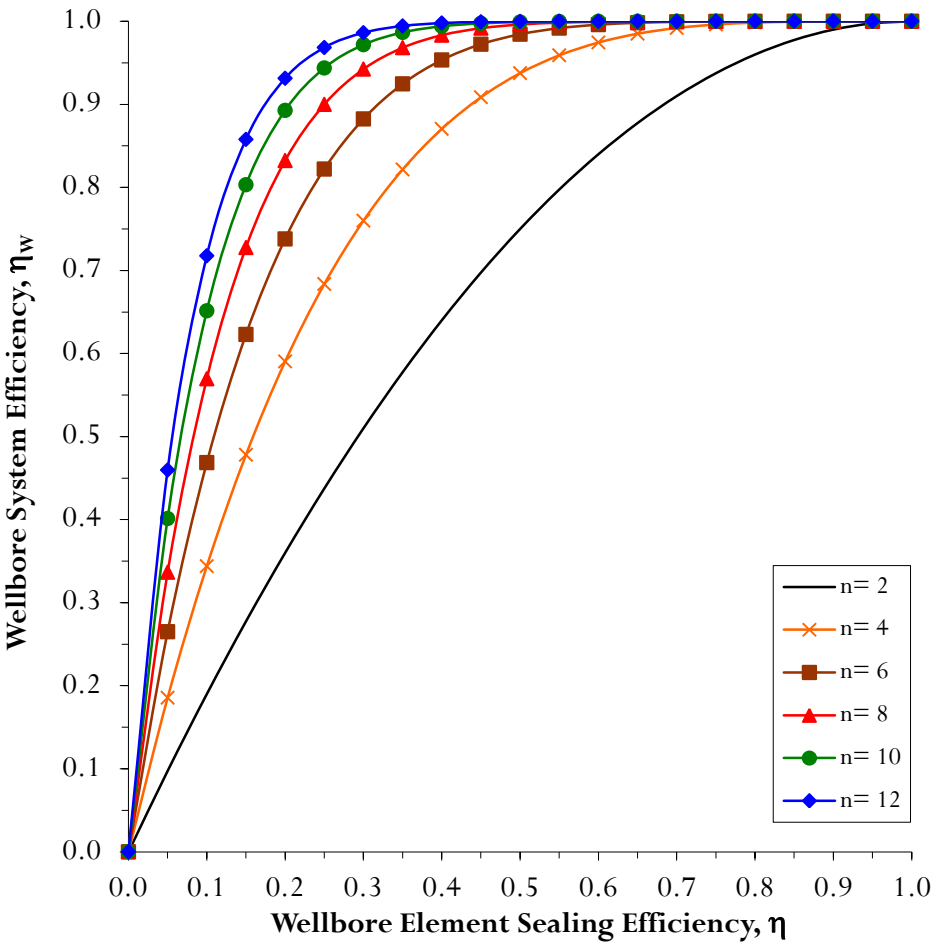

Figure 6.3: Wellbore efficiency for G-System arrangement.

Figure 6.4 and Figure 6.5 illustrate a graphical representation of wellbore system storage indices I_0 and I_n respectively for general case arrangement. Both indices have the advantage of ranging between 0 and unity.

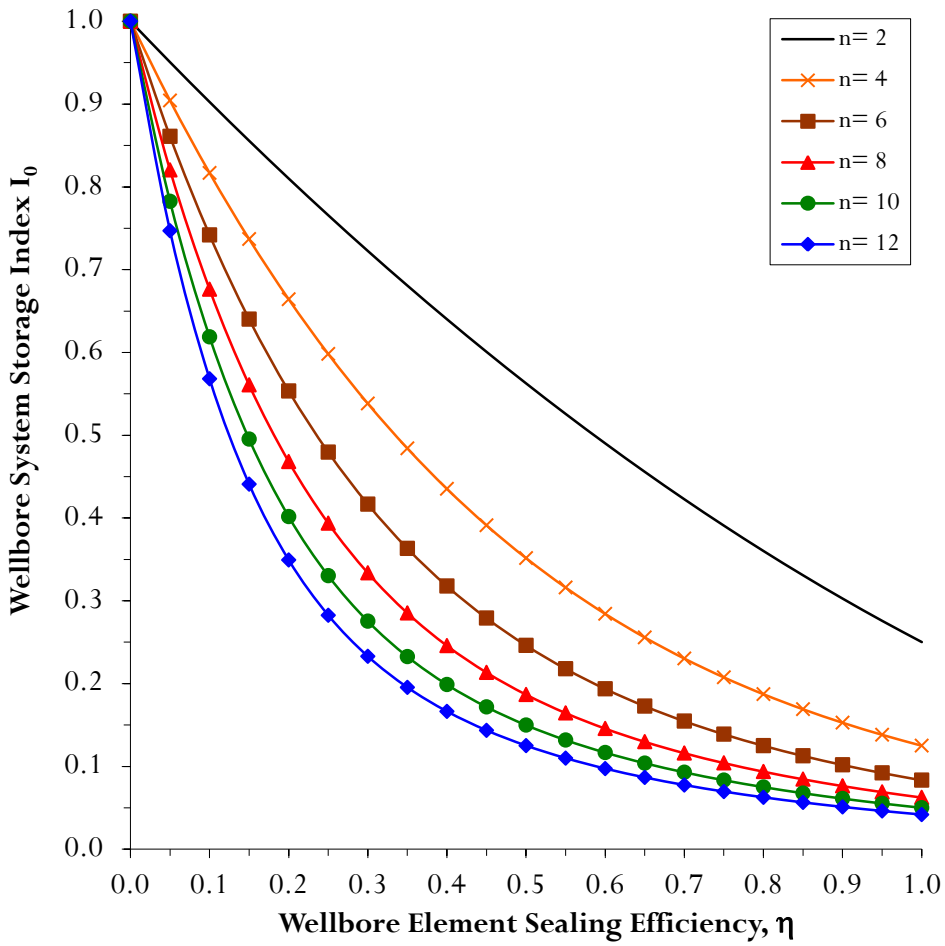

Figure 6.4: Wellbore storage index I_0 for G-System arrangement.

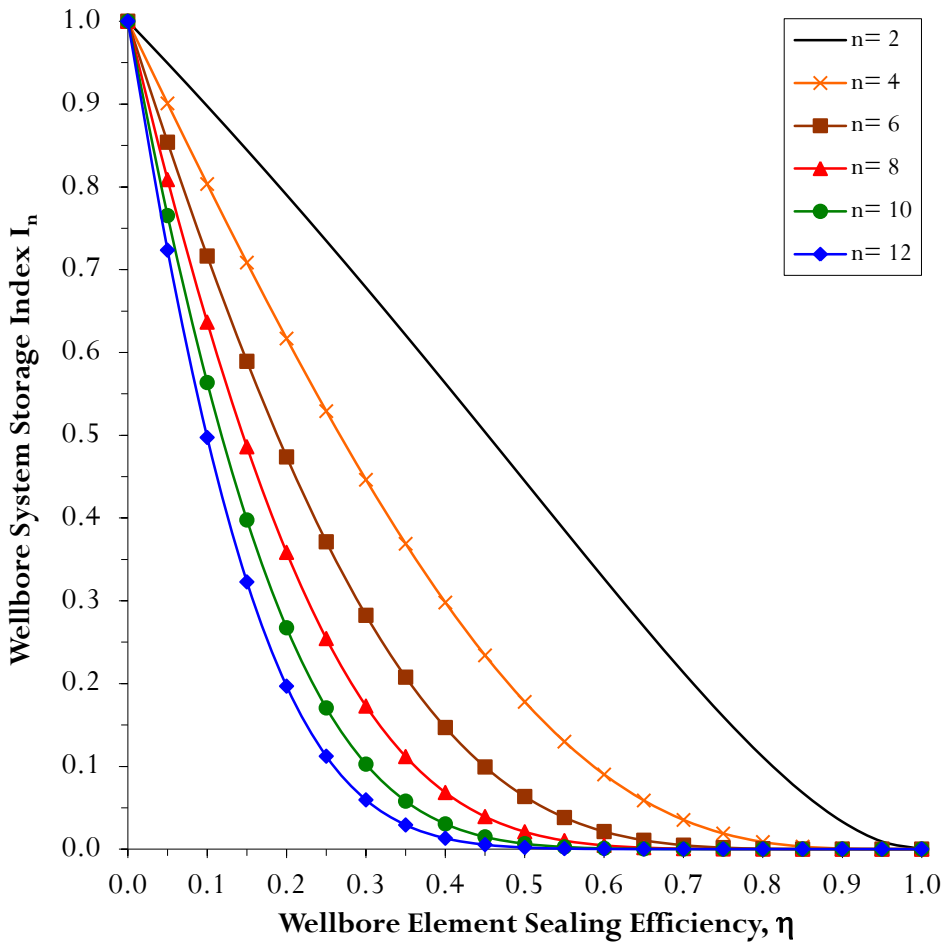

Figure 6.5: Wellbore storage index I_n for G-System arrangement.

6.7.2 Case of Aquitard-Aquifer Formation System

The aquitard-aquifer system of formation arrangement, R-System, represents a system of a repeated configuration of aquitards and aquifers. Due to this arrangement, the system has the following characteristics:

1) Repeated units of aquitard-aquifer system, therefore n is even integer,
2) $\lambda = 1.0$ when n = odd number, and
3) Constant leakage factor at aquifer formations where $\lambda_{even} = \lambda$

From condition 1, then,

$$N = \text{number of auitards} = \text{number of aquifers} = \frac{n}{2}$$

Again, by recalling Equation (6.25) that is:

$$\lambda_{sys} = \left(\lambda_1 + \lambda_1\lambda_2 + \lambda_1\lambda_2\lambda_3 + \ldots\ldots + \lambda_1\lambda_2\ldots\ldots\lambda_n\right) + f_d\left(1 - \lambda_W\right)$$

From condition 2, then,

$$\lambda_{(R\text{-}sys)} = \begin{pmatrix} 1 + 1\lambda_2 + 1\lambda_2 1 + 1\lambda_2 1\lambda_4 + 1\lambda_2 1\lambda_4 1 + \ldots\ldots \\ + 1\lambda_2 1\lambda_4\ldots\ldots\lambda_{n-2} + 1\lambda_2 1\lambda_4\ldots\ldots\lambda_{n-2}1 + 1\lambda_2 1\lambda_4\ldots\ldots\lambda_{n-2}1\lambda_n \end{pmatrix} + f_d\left(1 - 1\lambda_2 1\lambda_4\ldots\ldots\lambda_{n-2}1\lambda_n\right) \quad (6.43)$$

Simplifying $\lambda_{(R\text{-}sys)}$ from condition 2, therefore:

$$\lambda_{(R\text{-}sys)} = \left(1 + 2\lambda_2 + 2\lambda_2\lambda_4 + \ldots\ldots + 2\lambda_2\lambda_4\ldots\ldots\lambda_{n-2} + \lambda_2\lambda_4\ldots\ldots\lambda_n\right) + f_d\left(1 - \lambda_2\lambda_4\ldots\ldots\lambda_n\right) \quad (6.44)$$

Applying condition 1 and condition 3 into Equation (6.44), therefore,

$$\lambda_{(R\text{-}sys)} = \left(1 + 2\lambda + 2\lambda^2 + \ldots\ldots + 2\lambda^{N-1} + \lambda^N\right) + f_d\left(1 - \lambda^N\right) \quad (6.45)$$

Adding $\left(\lambda^N - \lambda^N\right)$ to the first term,

$$\begin{aligned}\lambda_{(\text{R-sys})} &= \left(\left(1-\lambda^{N}\right)+2\lambda+2\lambda^{2}+\ldots..+2\lambda^{N-1}+2\lambda^{N}\right)+f_{d}\left(1-\lambda^{N}\right)\\ &= \left(1-\lambda^{N}\right)+2\left(\lambda+\lambda^{2}+\ldots..+\lambda^{N-1}+\lambda^{N}\right)+f_{d}\left(1-\lambda^{N}\right)\end{aligned} \tag{6.46}$$

Again, the second term is a geometrical series, therefore,

$$\lambda_{(\text{R-sys})} = \left(1-\lambda^{\frac{n}{2}}\right)\left(\frac{2\lambda}{1-\lambda}+\left(1+f_{d}\right)\right) \tag{6.47}$$

Hence,

$$\begin{aligned}I_{0(\text{R-sys})} = \frac{\lambda_{(\text{R-sys})}}{n} &= \frac{1-\lambda^{\frac{n}{2}}}{n}\left(\frac{2\lambda}{1-\lambda}+\left(1+f_{d}\right)\right)\\ &= \frac{1-(1-\eta)^{\frac{n}{2}}}{n}\left(\frac{2(1-\eta)}{\eta}+\left(1+f_{d}\right)\right)\end{aligned} \tag{6.48}$$

and

$$I_{n(\text{R-sys})} = \frac{\lambda_{W}}{I_{0(\text{R-sys})}} = \frac{\lambda^{\frac{n}{2}}}{I_{0(\text{R-sys})}} = \frac{(1-\eta)^{\frac{n}{2}}}{I_{0(\text{R-sys})}} \tag{6.49}$$

Figure 6.6 shows the relation between wellbore element sealing efficiency, η, and wellbore system sealing efficiency, η_W, in case of different numbers of elements composing the whole system. It indicates that increasing of the number of the elements enhances the overall system efficiency for all values of element efficiency.

Figure 6.7 and Figure 6.8 show a graphical representation of wellbore system storage indices I_0 and I_n respectively for repeated system case arrangement. Both of these indices have the advantage of having a limited range between 0 and unity.

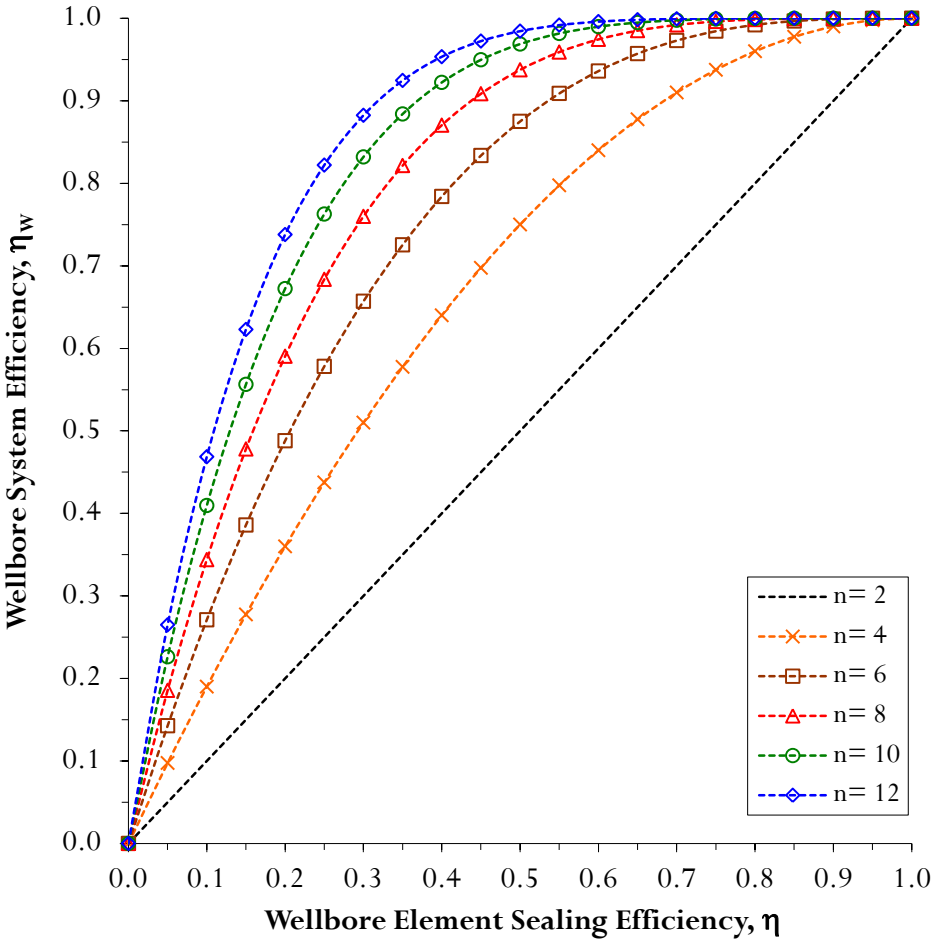

Figure 6.6: Wellbore efficiency for R-System arrangement.

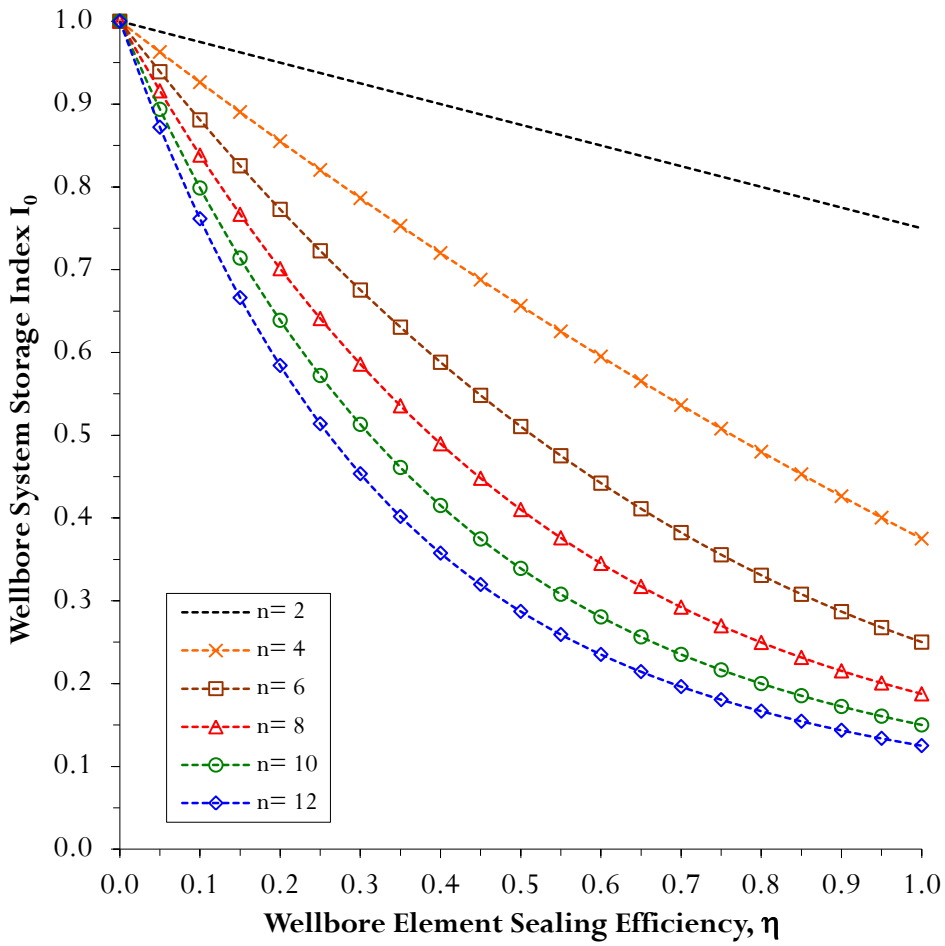

Figure 6.7: Wellbore storage index I_0 for R-System arrangement.

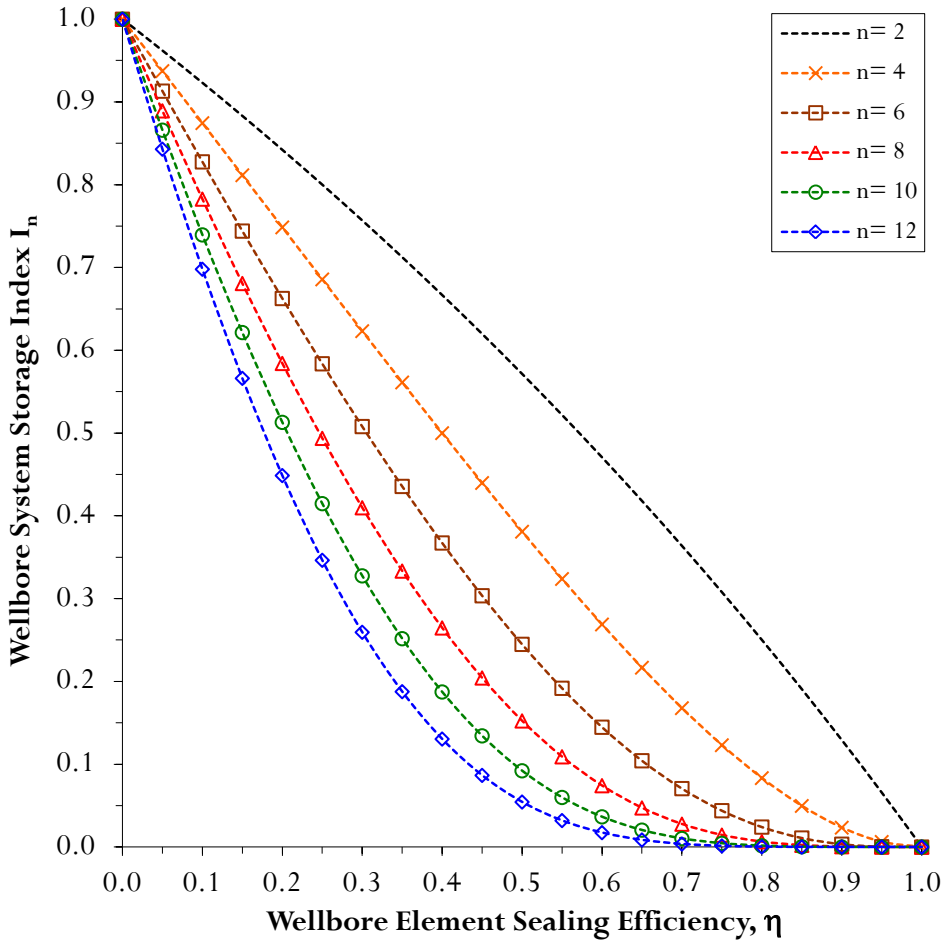

Figure 6.8: Wellbore storage index I_n for R-System arrangement.

Analyzing these curves and comparing them to the general case shows that wellbore efficiency indices have the same trend for both cases. Consequently, assessing the leakage through the entire repeated system will require higher efficiency values due to a decrease in the number of the formations available for radial storage.

6.8 Wellbore Model Verification

In our analytical approach, the wellbore element is the smallest unit of the whole system. Flow through this element considers variation of flow in both the vertical direction and horizontal (radial) direction into adjacent formations. The model has the advantage to allow the change of both wellbore bulk permeability and formation permeability from one element to another. Wellbore sealing efficiency concept is introduced to mimic the elevator concept of Nordbotten et al. (2004). The efficiency concept transfers the descriptive elevator model to a model with engineering rigor. The efficiency model can be used as a quantification index and as a sound tool to demonstrate and to assess wellbore leakage failure mechanism.

To verify the concept of wellbore sealing efficiency, a comparison to the example given by Nordbotten et al. (2004) is presented. They used a multiple aquifers model, as shown in Table 6.1, which has 11 aquitard and 11 aquifers for a passive well. The results of their approach were shown for the bottom, middle, and top aquitards respectively. In one example, Nordbotten et al. (2004) analyzed two different scenarios for injection process:

7) injection is continuous over a period of 200 years, and
8) injection takes place over the first 30 years, followed by 170 years of no injection.

The results are for normalized cumulative leakage for both the continuous injection and the 30 year injection cases. Also, they show the normalized leakage rates, as a fraction of the injection rate. Figure 6.9 and Figure 6.10 represent their prediction for normalized leakage rates and normalized cumulative leakage rates at three levels, in a well, that was located above the bottom, middle, and top aquitard respectively.

Table 6.1: Formation arrangement for model example.

Element ID		Formation Arrangement	k_F (m^2)	depth (m)	Note(s)
Present Study	Nordbotten et al. (2004)				
22		Aquifer	2.0E-14	40	Biosphere
21	11	Aquitard	2.0E-15	60	Top Aquitard
20		Aquifer	2.0E-14	40	
19	10	Aquitard	2.0E-15	60	
18		Aquifer	2.0E-14	40	
17	9	Aquitard	2.0E-15	60	
16		Aquifer	2.0E-14	40	
15	8	Aquitard	2.0E-15	60	
14		Aquifer	2.0E-14	40	
13	7	Aquitard	2.0E-15	60	
12		Aquifer	2.0E-14	40	
11	6	Aquitard	2.0E-15	60	Middle Aquitard
10		Aquifer	2.0E-14	40	
9	5	Aquitard	2.0E-15	60	
8		Aquifer	2.0E-14	40	
7	4	Aquitard	2.0E-15	60	
6		Aquifer	2.0E-14	40	
5	3	Aquitard	2.0E-15	60	
4		Aquifer	2.0E-14	40	
3	2	Aquitard	2.0E-15	35	
2		Aquifer	2.0E-14	30	
1	1	Aquitard	2.0E-15	15	Bottom Aquitard
0		Aquifer	2.0E-14	20	Storage Reservoir

Wellbore bulk permeability k was 2.00E-11 m^2 and aquifers' permeability was 2.00E-14 m^2. It is assumed that the aquitards' permeability is one tenth of the aquifers' permeability.

Table 6.2 represents the results of the example for the first scenarios at the bottom, middle, and top aquitards respectively.

Table 6.2: Normalized leakage for scenario 1, (Nordbotten et al. 2004).

Elapsed Time (Year)	Cumulative at Aquitard			Rates at Aquitard		
	Bottom	Middle	Top	Bottom	Middle	Top
	$\Sigma Q_0/Q_{inj}$	$\Sigma Q_{10}/Q_{inj}$	$\Sigma Q_{20}/Q_{inj}$	Q_0/Q_{inj}	Q_{10}/Q_{inj}	Q_{20}/Q_{inj}
2.5	6.81E-02	2.15E-08	4.64E-15	6.81E-02	2.15E-08	4.64E-15
5	2.45E-01	1.00E-07	2.45E-14	1.77E-01	7.85E-08	1.98E-14
10	5.99E-01	2.78E-07	8.80E-14	3.55E-01	1.78E-07	6.35E-14
20	1.47E+00	7.74E-07	2.45E-13	8.68E-01	4.96E-07	1.57E-13
30	2.15E+00	1.47E-06	4.64E-13	6.87E-01	6.94E-07	2.19E-13
40	3.16E+00	2.15E-06	7.74E-13	1.01E+00	6.87E-07	3.10E-13
50	3.59E+00	2.78E-06	1.00E-12	4.32E-01	6.28E-07	2.26E-13
60	4.64E+00	3.59E-06	1.47E-12	1.05E+00	8.11E-07	4.68E-13
70	5.27E+00	4.08E-06	1.90E-12	6.33E-01	4.90E-07	4.28E-13
80	5.99E+00	5.27E-06	2.15E-12	7.20E-01	1.19E-06	2.59E-13
90	6.81E+00	5.99E-06	2.45E-12	8.18E-01	7.20E-07	2.94E-13
100	7.74E+00	6.81E-06	2.78E-12	9.30E-01	8.18E-07	3.34E-13
110	8.80E+00	7.74E-06	3.16E-12	1.06E+00	9.30E-07	3.80E-13
120	1.00E+01	8.80E-06	4.08E-12	1.20E+00	1.06E-06	9.22E-13
130	1.14E+01	1.00E-05	4.35E-12	1.36E+00	1.20E-06	2.70E-13
140	1.21E+01	1.07E-05	4.64E-12	7.51E-01	6.61E-07	2.88E-13
150	1.29E+01	1.14E-05	5.27E-12	8.00E-01	7.04E-07	6.33E-13
160	1.38E+01	1.29E-05	5.99E-12	8.53E-01	1.55E-06	7.20E-13
170	1.47E+01	1.38E-05	6.39E-12	9.09E-01	8.53E-07	3.96E-13
180	1.56E+01	1.47E-05	6.81E-12	9.69E-01	9.09E-07	4.22E-13
190	1.67E+01	1.67E-05	7.26E-12	1.03E+00	2.00E-06	4.50E-13
200	1.90E+01	1.90E-05	7.74E-12	2.28E+00	2.28E-06	4.80E-13

According to the present study, Table 6.3 shows equivalent wellbore element efficiency, η, for the same scenario above the bottom, the middle, and the top aquitards respectively.

Table 6.3: Wellbore element sealing efficiency, η.

Elapsed Time (Year)	λ_{w10} = Q_{10}/Q_0 n = 10	λ_{w20} = Q_{20}/Q_0 n = 20	Wellbore Sealing Efficiency η_i if n = 10	n = 20	$\eta_{i\ Avg.}$
2.5	3.16E-07	6.81E-14	0.9499	0.9518	0.9509
5	4.44E-07	1.12E-13	0.9464	0.9493	0.9479
10	5.03E-07	1.79E-13	0.9450	0.9469	0.9460
20	5.71E-07	1.81E-13	0.9436	0.9468	0.9452
30	1.01E-06	3.19E-13	0.9368	0.9437	0.9403
40	6.81E-07	3.08E-13	0.9416	0.9439	0.9428
50	1.46E-06	5.23E-13	0.9320	0.9409	0.9365
60	7.74E-07	4.46E-13	0.9401	0.9418	0.9410
70	7.74E-07	6.76E-13	0.9401	0.9393	0.9397
80	1.65E-06	3.59E-13	0.9302	0.9430	0.9366
90	8.80E-07	3.59E-13	0.9385	0.9430	0.9408
100	8.80E-07	3.59E-13	0.9385	0.9430	0.9408
110	8.80E-07	3.59E-13	0.9385	0.9430	0.9408
120	8.80E-07	7.68E-13	0.9385	0.9385	0.9385
130	8.80E-07	1.98E-13	0.9385	0.9463	0.9424
140	8.80E-07	3.83E-13	0.9385	0.9427	0.9406
150	8.80E-07	7.92E-13	0.9385	0.9384	0.9385
160	1.82E-06	8.44E-13	0.9289	0.9380	0.9335
170	9.38E-07	4.35E-13	0.9377	0.9419	0.9398
180	9.38E-07	4.35E-13	0.9377	0.9419	0.9398
190	1.94E-06	4.35E-13	0.9280	0.9419	0.9350
200	1.00E-06	2.11E-13	0.9369	0.9460	0.9415
		Average	0.9384	0.9433	0.9408
			0.9408		0.9408

Cross verification, Table 6.4, shows the predicted normalized leakage rates and predicted normalized cumulative for the middle and top aquitards for Scenario 1 according to the proposed model.

Table 6.4: Cross validation of wellbore leakage.

Elapsed Time (Year)	Predicted Leakage Rates				Cumulative Leakage	
	λ_{w10}	λ_{w20}	Q_{10}/Q_{inj}	Q_{20}/Q_{inj}	Q_{10}/Q_{inj}	Q_{20}/Q_{inj}
	n = 10	n = 20	n = 10	n = 20	n = 10	n = 20
2.5	2.60E-07	9.96E-14	1.77E-08	6.79E-15	1.77E-08	6.79E-15
5	3.35E-07	1.96E-13	5.92E-08	3.46E-14	7.69E-08	4.14E-14
10	4.22E-07	2.53E-13	1.50E-07	8.98E-14	2.27E-07	1.31E-13
20	4.26E-07	3.26E-13	3.70E-07	2.83E-13	5.97E-07	4.14E-13
30	5.66E-07	1.02E-12	3.88E-07	6.98E-13	9.85E-07	1.11E-12
40	5.56E-07	4.61E-13	5.60E-07	4.65E-13	1.55E-06	1.58E-12
50	7.21E-07	2.11E-12	3.11E-07	9.12E-13	1.86E-06	2.49E-12
60	6.68E-07	5.95E-13	7.00E-07	6.23E-13	2.56E-06	3.11E-12
70	8.24E-07	5.95E-13	5.22E-07	3.77E-13	3.08E-06	3.49E-12
80	6.02E-07	2.75E-12	4.33E-07	1.98E-12	3.51E-06	5.47E-12
90	6.02E-07	7.74E-13	4.92E-07	6.33E-13	4.00E-06	6.10E-12
100	6.02E-07	7.74E-13	5.59E-07	7.20E-13	4.56E-06	6.82E-12
110	6.02E-07	7.74E-13	6.36E-07	8.18E-13	5.20E-06	7.64E-12
120	8.80E-07	7.74E-13	1.06E-06	9.29E-13	6.25E-06	8.57E-12
130	4.47E-07	7.74E-13	6.09E-07	1.06E-12	6.86E-06	9.62E-12
140	6.18E-07	7.74E-13	4.64E-07	5.81E-13	7.33E-06	1.02E-11
150	8.87E-07	7.74E-13	7.10E-07	6.19E-13	8.04E-06	1.08E-11
160	9.16E-07	3.30E-12	7.82E-07	2.82E-12	8.82E-06	1.36E-11
170	6.62E-07	8.81E-13	6.02E-07	8.01E-13	9.42E-06	1.44E-11
180	6.62E-07	8.81E-13	6.42E-07	8.54E-13	1.01E-05	1.53E-11
190	6.62E-07	3.74E-12	6.84E-07	3.87E-12	1.07E-05	1.92E-11
200	4.59E-07	1.00E-12	1.05E-06	2.28E-12	1.18E-05	2.14E-11

For Scenario 1, Figure 6.9 depicts the results of Nordbotten et al. (2004) and the predicted normalized cumulative leakage using the respective sealing efficiency of wellbore elements.

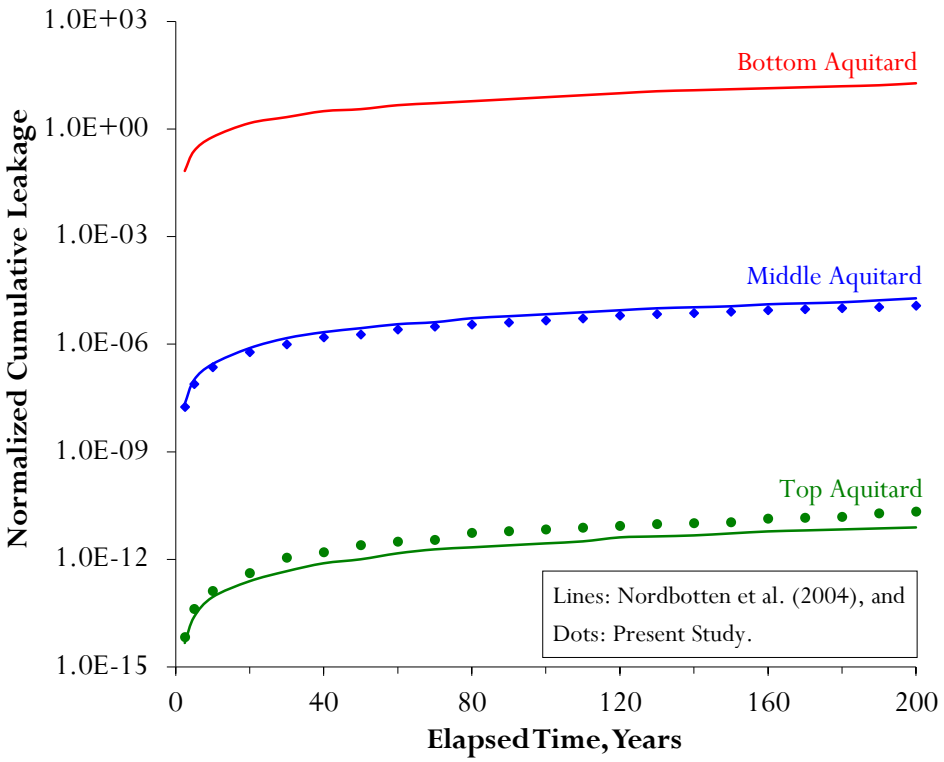

Figure 6.9: Cross verification of normalized cumulative leakage scenario 1.

Similarly, for Scenario 2, Figure 6.10 depicts the results of Nordbotten et al. (2004) and the predicted normalized cumulative leakage. Figure 6.11 shows the comparison of both scenarios by cross validation approach. The figure indicates a close match with the change of η from one element to another along the wellbore according to Nordbotten et al. (2004) results.

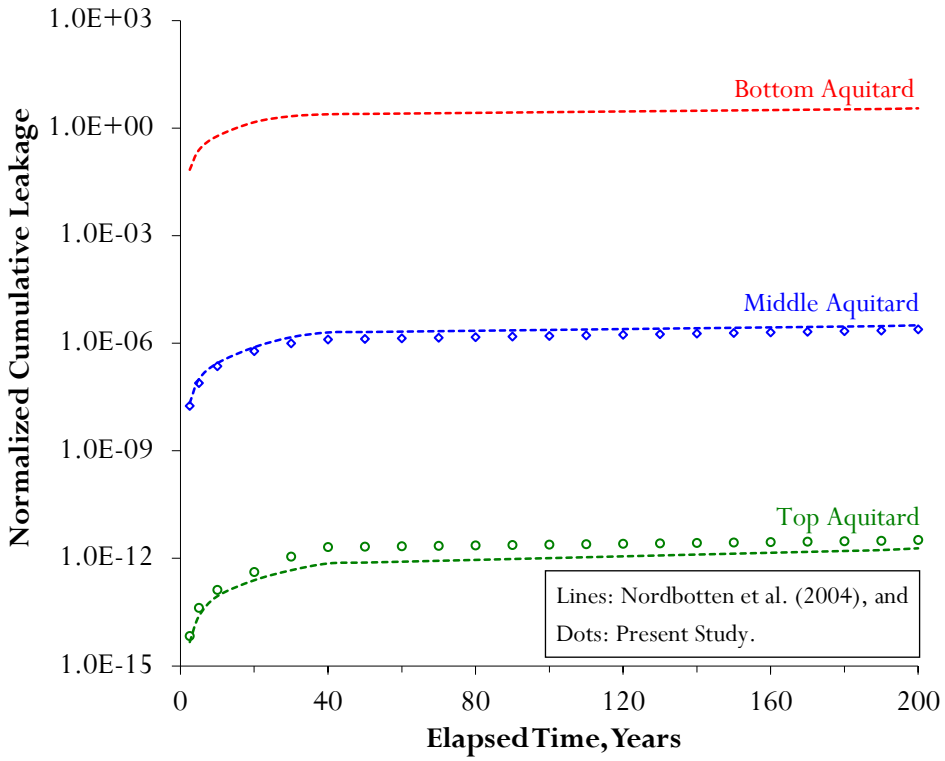

Figure 6.10: Cross verification of normalized cumulative leakage scenario 2.

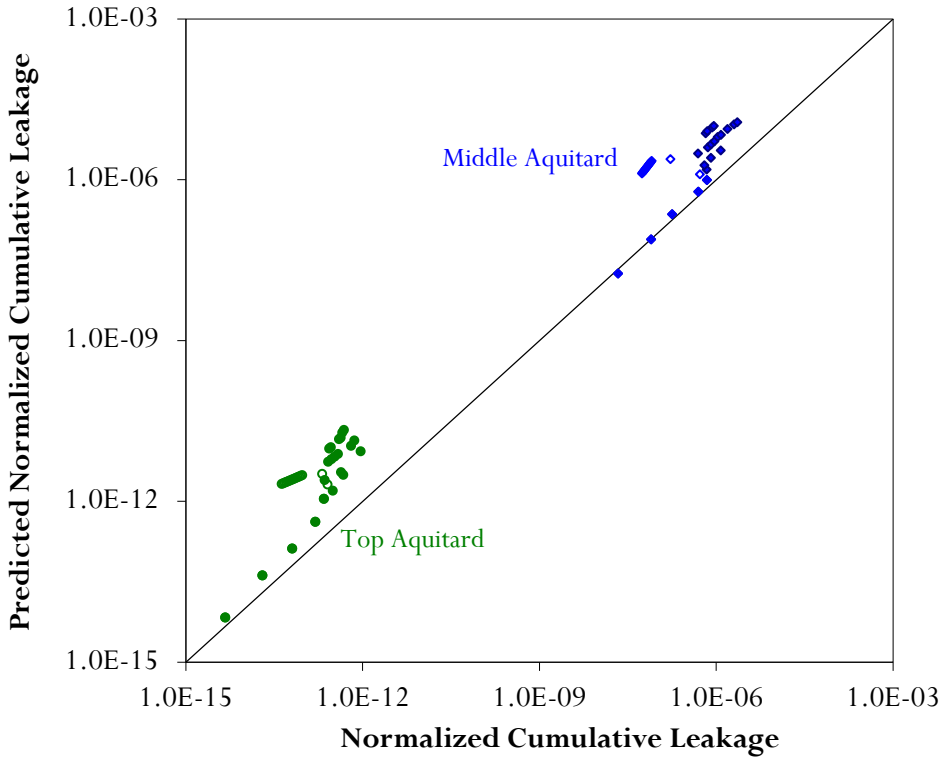

Figure 6.11: Cross verification of normalized cumulative leakage.

In the present study and similarly another verification, shown in Table 6.5, can be done by using the average value of the wellbore efficiency $\eta_{Avg.}$. Table 6.5, shows the predicted normalized leakage rates and predicted normalized cumulative for the middle and top aquitards for Scenario 1.

Table 6.5: Prediction of wellbore leakage based on average efficiency, $\eta_{Avg.}$

Elapsed Time (Year)	Predicted Leakage Rates				Cumulative Leakage		
	$\eta_{i\ Avg.}$	Q_0/Q_{inj}	Q_{10}/Q_{inj}	Q_{20}/Q_{inj}	Q_0/Q_{inj}	Q_{10}/Q_{inj}	Q_{20}/Q_{inj}
2.5	0.9509	6.58E-02	1.95E-08	5.60E-15	6.58E-02	1.95E-08	5.60E-15
5	0.9479	1.68E-01	6.82E-08	2.63E-14	2.34E-01	8.77E-08	3.19E-14
10	0.9460	3.42E-01	1.64E-07	7.55E-14	5.77E-01	2.51E-07	1.07E-13
20	0.9452	8.23E-01	4.29E-07	2.12E-13	1.40E+00	6.80E-07	3.19E-13
30	0.9403	6.44E-01	5.23E-07	3.98E-13	2.04E+00	1.20E-06	7.18E-13
40	0.9428	9.68E-01	6.20E-07	3.81E-13	3.01E+00	1.82E-06	1.10E-12
50	0.9365	4.08E-01	4.47E-07	4.64E-13	3.42E+00	2.27E-06	1.56E-12
60	0.9410	1.02E+00	7.52E-07	5.40E-13	4.44E+00	3.02E-06	2.10E-12
70	0.9397	6.44E-01	5.05E-07	4.03E-13	5.08E+00	3.53E-06	2.51E-12
80	0.9366	7.05E-01	7.37E-07	7.55E-13	5.79E+00	4.27E-06	3.26E-12
90	0.9408	7.69E-01	5.97E-07	4.36E-13	6.56E+00	4.86E-06	3.70E-12
100	0.9408	8.73E-01	6.79E-07	4.96E-13	7.43E+00	5.54E-06	4.19E-12
110	0.9408	9.93E-01	7.72E-07	5.63E-13	8.42E+00	6.31E-06	4.76E-12
120	0.9385	1.20E+00	1.06E-06	9.29E-13	9.62E+00	7.37E-06	5.69E-12
130	0.9424	1.28E+00	8.65E-07	5.49E-13	1.09E+01	8.23E-06	6.23E-12
140	0.9406	7.10E-01	5.55E-07	4.10E-13	1.16E+01	8.79E-06	6.64E-12
150	0.9385	8.04E-01	7.07E-07	6.24E-13	1.24E+01	9.50E-06	7.27E-12
160	0.9335	8.05E-01	1.11E-06	1.45E-12	1.32E+01	1.06E-05	8.72E-12
170	0.9398	8.56E-01	7.19E-07	5.68E-13	1.41E+01	1.13E-05	9.29E-12
180	0.9398	9.13E-01	7.67E-07	6.06E-13	1.50E+01	1.21E-05	9.90E-12
190	0.9350	1.03E+00	1.20E-06	1.40E-12	1.60E+01	1.33E-05	1.13E-11
200	0.9415	2.16E+00	1.57E-06	1.08E-12	1.82E+01	1.49E-05	1.24E-11

For both scenarios, Figure 6.12 depicts the results of Nordbotten et al. (2004) and the predicted normalized cumulative leakage. Figure 6.13 shows the comparison of both scenarios by average validation approach. The figure indicates a close match with an average value of $\eta_{avg.} = 0.9408$ according to Nordbotten et al. (2004) results.

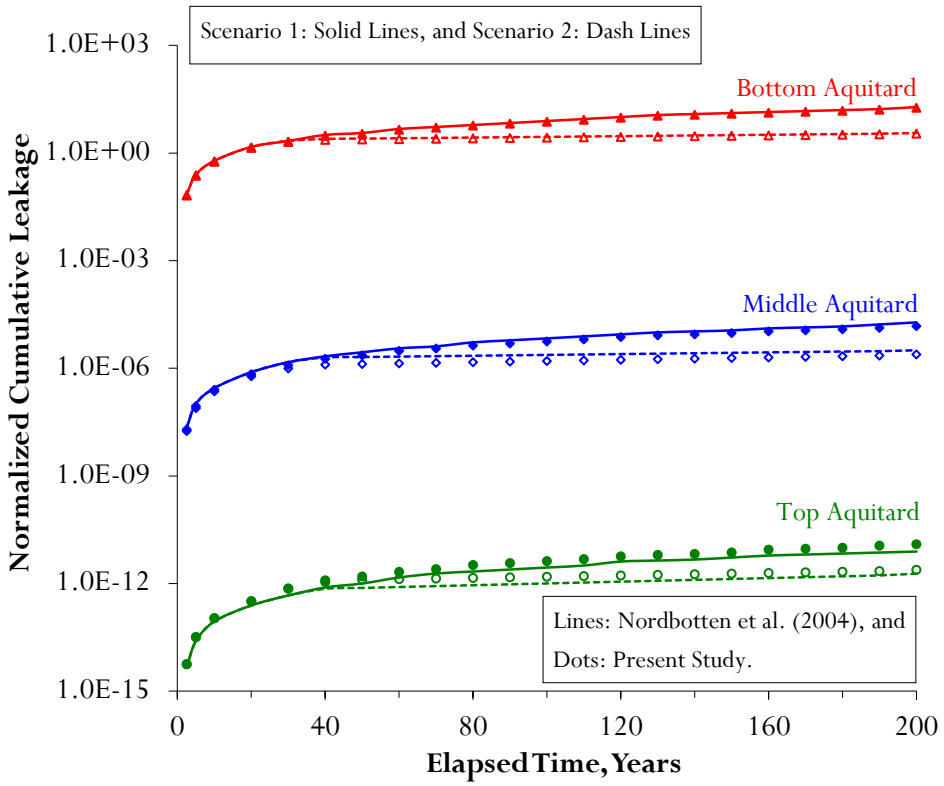

Figure 6.12: Verification of normalized cumulative leakage by Avg. η_i.

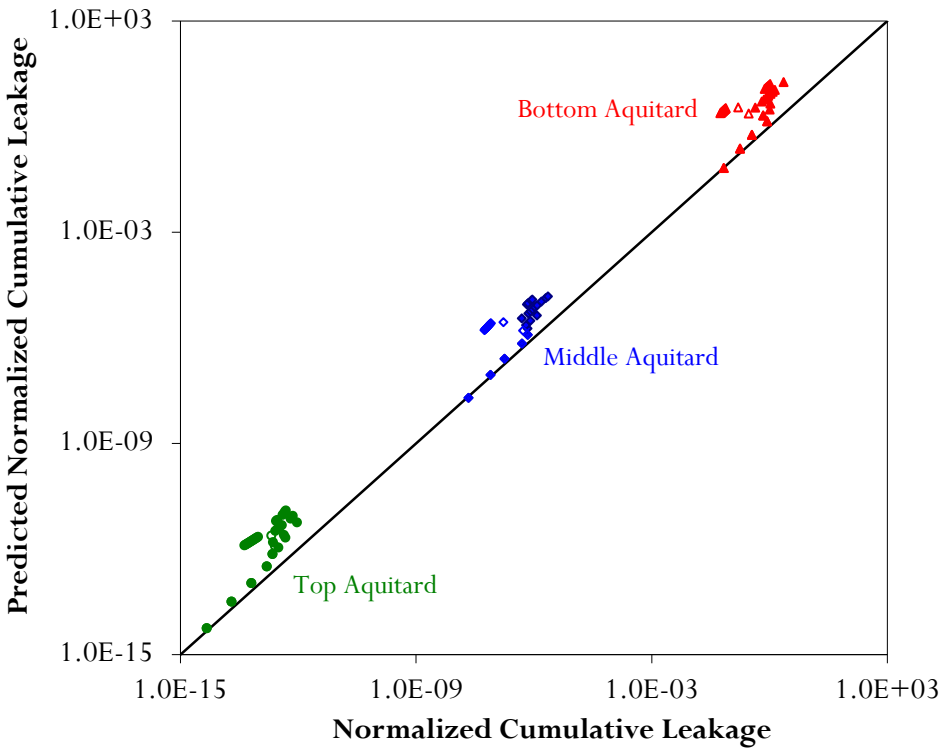

Figure 6.13: Verification of normalized cumulative leakage by Avg. η_i.

6.9 Wellbore Leakage Assessment

Equations (6.35) and (6.38) identify two types of parameters in order to assess leakage through wellbore system for storage purposes. The first type is wellbore system storage indices, I_0 and I_n, and the other is the average permeability integrity index, I_k. These parameters provide a measure of the wellbore performance in a certain locality.

The amount Q_R is the maximum leakage for a given site while Q_0 and Q_n are the flow rates into the wellbore from the storage reservoir and out of the wellbore system, respectively. With respect to flow rates within a wellbore, the ratios of these rates provide an analog measure of the factor of safety within a wellbore. Regardless of the formation arrangement at site storage, the application of this concept allows for an assessment of the state of leakage for a given wellbore at a specific location and can be represented by the following equations:

$$FS_0 = \frac{Q_R}{Q_0} = \frac{I_0}{I_k} \tag{6.50}$$

and,

$$FS_n = \frac{Q_R}{Q_n} = \frac{1}{I_n I_k} \tag{6.51}$$

Based on the model formation presented previously, Figure 6.14 and Figure 6.15 represent design charts for both the general and repeated system configurations respectively. These charts can be used to determine the rank of the wellbore in a given site and the state of acceptance and/or rejection of wellbore leakage integrity. These charts show that the repeated system arrangement requires a higher efficiency value than general system arrangement.

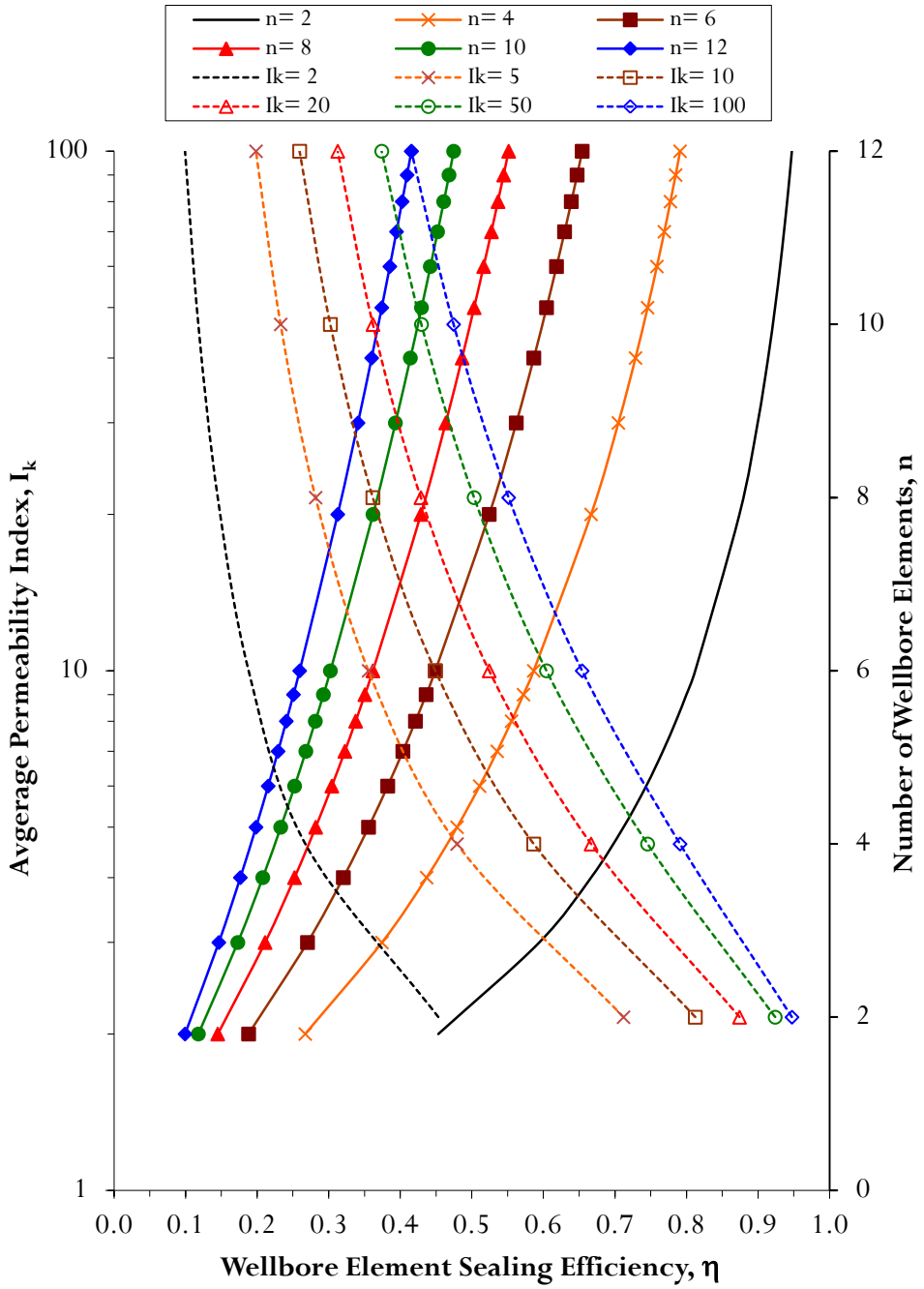

Figure 6.14: Wellbore leakage assessment for general system.

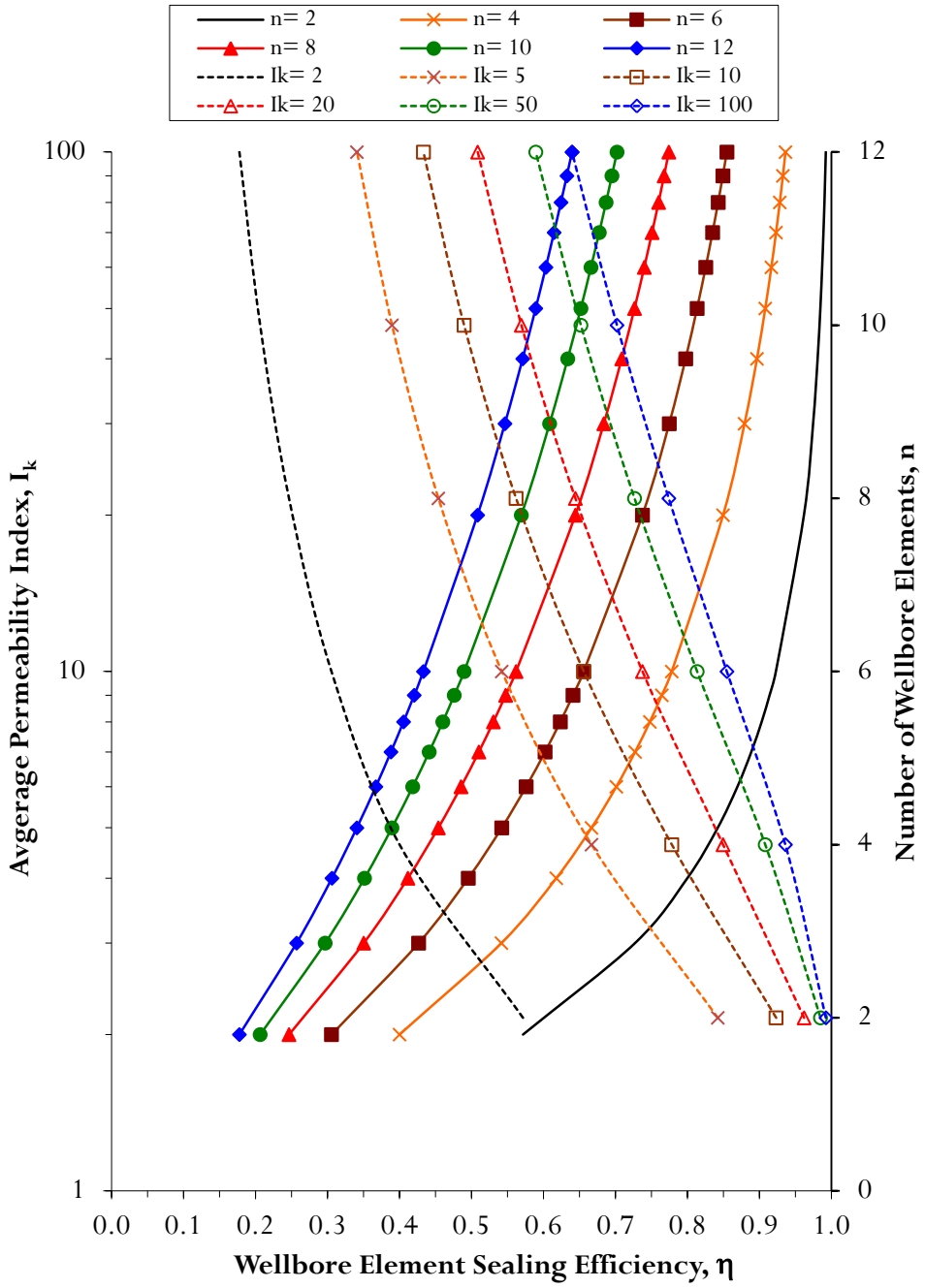

Figure 6.15: Wellbore leakage assessment for repeated system.

It is worth to mention that Figure 6.16 indicates the state of the wellbore in Nordbotten et al (2004) example according to the given permeabilities, I_k, is 5304.35, with the aid of the performance chart.

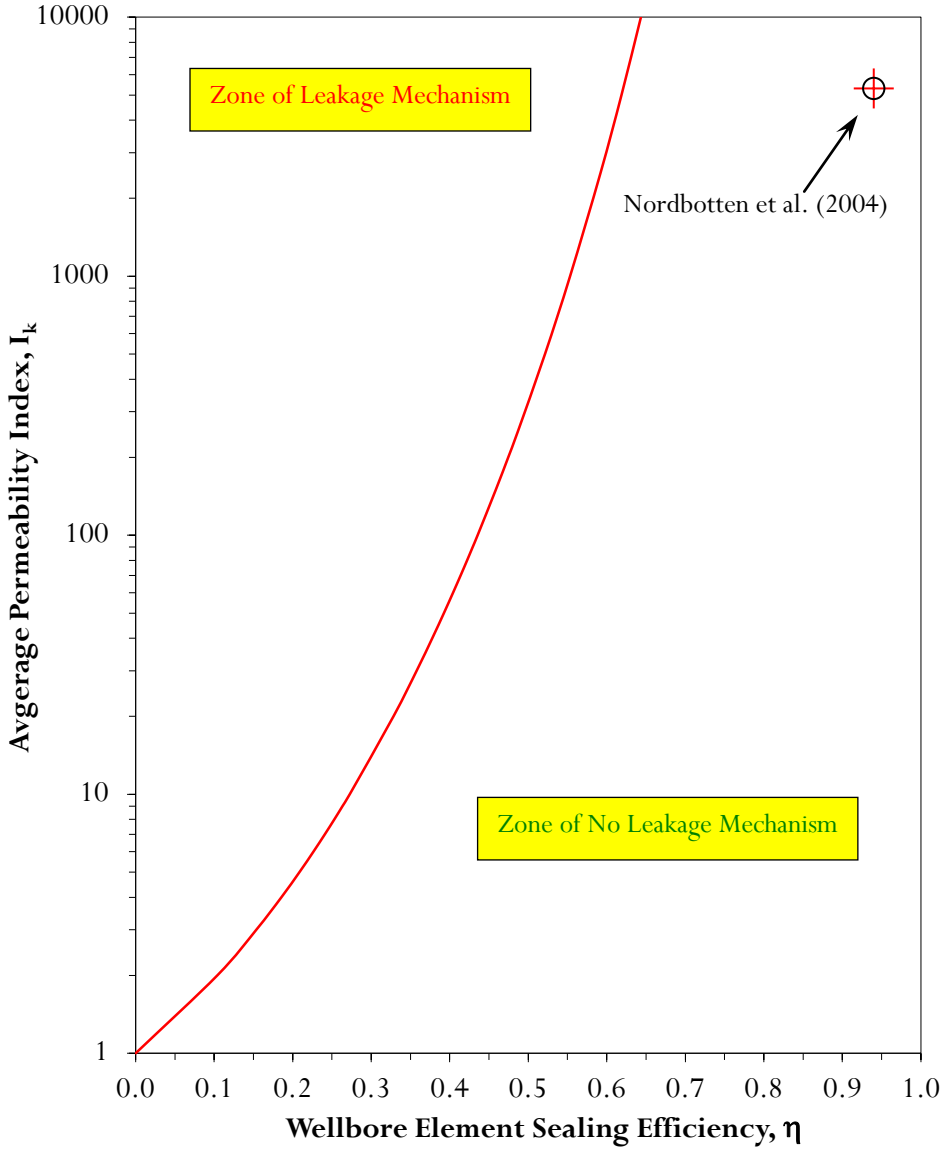

Figure 6.16: Wellbore performance chart for verification case.

6.10 Effect of Radial Distribution Pattern

Figures 6.3 through 6.16 were created assuming the radial leakage distribution has a cylindrical pattern and hence f_d= 0.50 if considered. The same assumption for f_d was adopted in the charts in Figure 6.14 and Figure 6.15. Based on these results, the cylindrical distribution provides the most conservative solution, and the distribution has a small effect on the wellbore element storage index I_{ne}.

Figure 6.17 depicts the effect of the choice of the distribution pattern for both general system (G-System) and aquitard-aquifer system (R-System) on wellbore system storage index I_0. It indicates that a very slight difference in both distribution for both cases of arrangement.

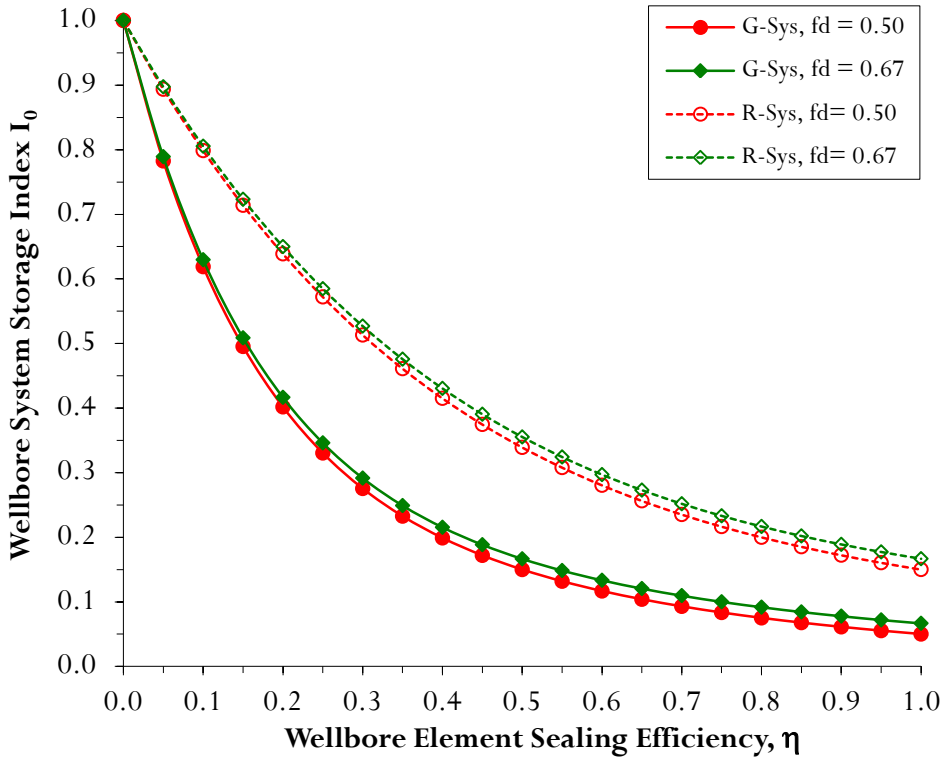

Figure 6.17: Effect of radial distribution pattern on storage index I_0.

In addition, Figure 6.18 illustrates the same effect of the choice of the distribution pattern for both general system (G-System) and aquitard-aquifer system (R-System) on wellbore system storage index I_n. Index I_n is important because it is related directly to the prediction of the leakage at the desired depth.

Figure 6.18 indicates a very slight difference in both distributions for both cases of arrangement. In addition, it clearly shows that effect of site arrangement decreases significantly until no effect of the wellbore sealing efficiency is observed for $\eta \geq 0.70$.

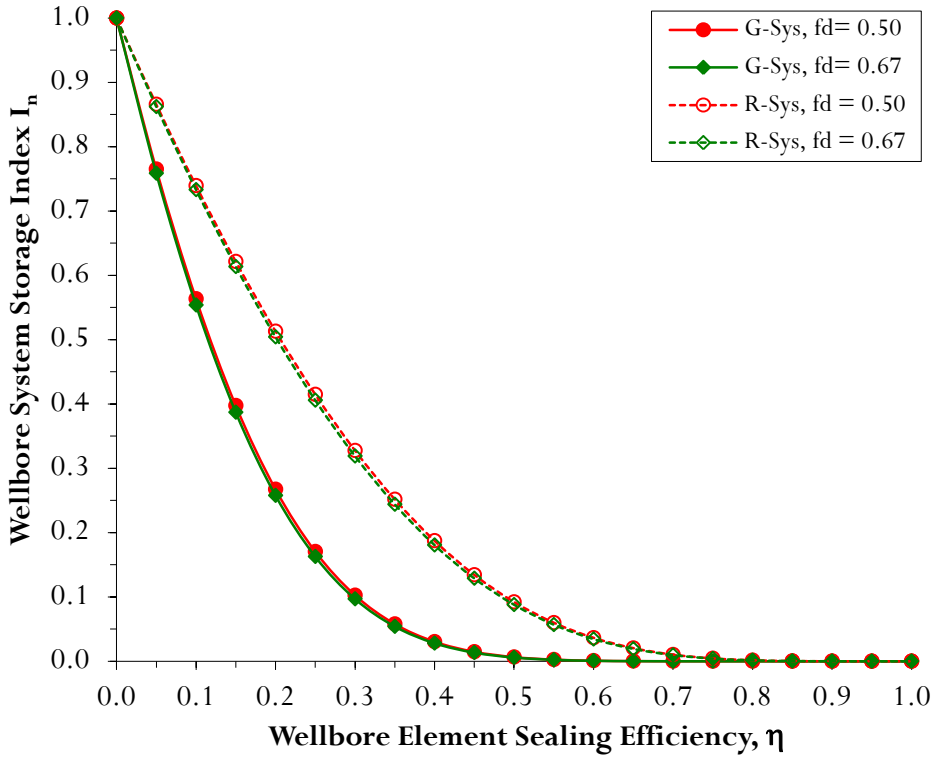

Figure 6.18: Effect of radial distribution pattern on storage index I_n.

6.11 Summary

A new analytical model for modeling leakage through a wellbore system has been proposed to assess the leakage through wellbore system. The analytical model represents the wellbore system as serially connected wellbore elements. This provides an advantage that each element can differ from the subsequent one and will have its own characteristics. Each wellbore element is a function of wellbore configuration "e.g. L, A" and are a function of pressure head responsible for leakage. Bulk "effective" wellbore permeability also can differ from element to another.

Using assessment charts is very simple. The steps can be summarized as follows;

1) Assuming that we have the value of wellbore effective bulk permeability, k and vertical permeability of adjacent formation, k_F.
2) Get permeability index for each element by I_{ki}.
3) Get the average permeability index of the whole wellbore system I_k.
4) From the site arrangement, determine if the site is more suitable to be idealized to general or repeated formation arrangement system.
5) Determine wellbore sealing efficiency, η, from charts represented in Figure 6.14 and Figure 6.15 depending on site arrangement.
6) Determine wellbore system sealing efficiency, η_W, from Figure 6.3 and Figure 6.6.
7) Wellbore efficiency index can be used as a ranking indicator between different wells in the same site and/or a base to accept and/or reject the status of a wellbore performance.

6.12 References

Barlet-Gouedard, V., Rimmele, G., Goffe, B., and Porcherie, O., (2006), Mitigation Strategies for the Risk of CO2 Migration through Wellbores, IADC/SPE Drilling Conference, 21-23 February, Miami, Florida, USA, SPE 98924, 17 p.

Birkholzer, J.T., Zhou, Q., and Tsang, C.F. (2009). Large-scale impact of CO2 storage in deep saline aquifers: A sensitivity study on pressure response in stratified systems. International Journal of Greenhouse Gas Control, Vol. 3, pp. 181-194.

Celia, M.A., and Nordbotten, J.M, (2009), Practical Modeling Approaches for Geological Storage of Carbon Dioxide, Ground Water, Vol. 47, No. 5, pp. 627-638.

Celia, M.A., Nordbotten, J.M., Bachu, S., Dobossy, M. and Court, B., (2009), Risk of Leakage versus Depth of Injection in Geological Storage, Energy Procedia, Vol. 1, pp. 2573-2580.

Celia, M.A., Nordbotten, J.M., Court, B., Dobossy, M., and Bachu, S., (2011), Field-Scale Application of a Semi-Analytical Model for Estimation of CO2 and Brine Leakage along old Wells, International Journal of Greenhouse Gas Control, Vol. 5, pp. 257-269.

Court, B., (2011), Safety and Water Challenges in CCS: Modeling Studies to Quantify CO2 and Brine Leakage Risk and Evaluate Promising Synergies for Active and Integrated Water Management, Ph.D. Thesis, Princeton University, USA, 244 p.

Dobossy, M.E., Celia, M.A., and Nordbotten, J.M., (2011), An Efficient Framework for performing Industrial Risk Assessment of Leakage for Geological Storage of CO2, Energy Procedia, Vol. 4, pp. 4207-4214.

Gasda, S.A., (2008), Numerical Models for Evalaution CO2 Storgae in Deep, Slaine Aquifers: Leaky Wells and Larga-Scale Geological Features, Ph.D. Thesis, Princeton University, USA, 188 p.

Gasda, S.E., and Celia, M.A., (2005), Upscaling Relative Permeabilities in a Structured Porous Medium, Advances in Water Resources, Vol. 28, pp. 493-506.

Gerard, B., Frenette, R., Auge, L., Barlet-Gouedard, V., Desroches, J., and Jammes, L., (2006), Well Integrity in CO2 Environment: Performance Risk, and Technologies, Proceeding of CO2SC Symposium, March 20-22, Berkeley, California, USA, 4 p.

Humez, P., Audigane, P., Lions, J., Chiaberge, C., and Bellenfant, G., (2011), Modeling of CO2 Leakage Up Through an Abandoned Well from Deep Saline Aquifer to Shallow Fresh Groundwaters, Journal of Transport in Porous Media, Vol. 90, pp. 153-181.

Janzen, A.K., (2010), Development and Application of a Multi-Scale, Multi-Layer Numerical Model for CO2 Injection, M.Sc. Thesis, Princeton University, USA, 105 p.

LeNeveu, D.M., (2012), Potential for Environmental Impact due to Acid Gas Leakage from Welbores at EOR Injection Sites Near Zama Lake, Alberta, Greenhouse Gases: Science & Technology, Vol. 2, Issue 2, pp. 99-114.

Nabih, A., and Chalaturnyk, R., (2013), Wellbore Efficiency Model for CO2 Geological Storage Part I: Theory and Wellbore Element, SPE Heavy Oil Conference-Canada, 11-13 June, Calgary, Alberta, Canada , SPE 165411, 14 p.

Nicot, J-P., Oldenburg, C.M., Houseworth, J.E., and Choi, J-W., (2013), Analysis of Potential Leakage Pathways at the Cranfield, MS, USA, CO2 Sequestration Site, International Journal of Greenhouse Gas Control, Vol. 18, pp. 388-400.

Nogues, J.P., Nordbotten, J.M., and Cleia, M.A., (2011), Detecting Leakage of Brine or CO2 through abandoned Wells in a Geological Sequestration Operation using Pressure Monitoring Wells, Energy Procedia, Vol. 4, pp. 3620-3627.

Nogues, J.P., Court, B., Dobossy, M., Nordbotten, J.M., and Cleia, M.A., (2012), A Methodology to estimate Maximum Probable Leakage along Old Wells in a Geological Sequestration Operation, International Journal of Greenhouse Gas Control, Vol. 7, pp. 39-47.

Nordbotten, J.M., Celia, M.A., and Bachu, S., (2004), Analytical solutions for leakage rates through abandoned wells, Water Resources Research, Vol. 40, Issue 4, W04204, doi:10.1029/2003WR002997.

Nordbotten, J.M., Celia, M.A., and Bachu, S., (2005), Semianalytical Solution for CO2 Leakage through an Abandoned Well, Environ. Sci. Technol., Vol. 39, pp. 602-611.

Nordbotten, J.M., Kavettski, D., Celia, M.A., and Bachu, S., (2009), Model for CO2 Leakage Including Multiple Geological Layers and Multiple Leaky Wells, Environ. Sci. Technol., Vol. 43, pp. 743-749.

Oldenburg, C.M., Bryant, S.L., and Nicot, JP, (2009), Certification Framework based on Effective Trapping for Geologic Carbon Sequestration, International Journal of Greenhouse Gas Control, Vol. 3, pp. 444-457.

Watson, T.L., and Bachu, S., (2008), Identification of Wells with High CO2-Leakage Potential in Mature Oil Fields Developed for CO2-Enhanced Oil Recovery, SPE Symposium on Improved Oil Recovery, 20-23 April, Tulsa, Oklahoma, USA, SPE 112924, 10 p.

Chapter 7: Conclusions and Recommendations[6]

7.1 General

Carbon capture and storage (CCS) is an approach to reduce carbon dioxide (CO2) emissions. The approach involves three main steps, which are capturing, transporting, and storing of CO2. The primary storage option is the geological storage of CO2 in saline aquifers or depleted oil and gas reservoirs. These geological formations are normally secured by an overlying seal or caprock formation that provides a physical barrier against leakage. For geological storage projects, assurance is governed by two mechanisms; geological leakage mechanism and wellbore leakage mechanism.

There is a need for a methodology to standardize the assessment of wellbore integrity to check wellbore leakage mechanism in a more regulatory procedure. To be a standard code of practice, key elements of the methodology must be gathered, recognized, classified, and systematically ordered.

In this research, such considerations necessitate an appropriate procedure that can be standardized and considered as a sound and practical tool to check the safety evaluation of wellbores with respect to wellbore leakage mechanism.

In this chapter, the conclusions and the recommendations of this research are outlined and discussed.

---

[6]A report of invention (ROI) patent application related to this study was submitted to TEC-Edmonton, ROI 2011089. A US provisional patent application numbered 61/897,617 has been filed and is titled by Full Life Cycle Assessment of Wellbore Integrity.

7.2 Conclusions

Assessment of wellbore integrity for CO2 geological storage purposes involved three aspects. These aspects were; prediction of cement properties, detailed near-wellbore modeling, and safety evaluation of wellbore leakage mechanism.

Understanding how wellbore cement properties evolve during its hydration stage is important in detailed wellbore modeling. There is a need to obtain an improved understanding about the initial state of wellbore when the objective for wellbore integrity assessment is long-term behavior.

The maturity rule serves as a base to check the structural integrity in many applications and to recommend a success of concrete job. Importing this method to the oil and gas industry may help in the evaluation quality of the cementing job, change of "waiting on cement" (WOC) time and determination of suitability for certain additives to cement slurries.

Cement properties are the response of chemical reactions occurring within the cement. The evolution of cement properties can be modeled macroscopically by means of population dynamic modeling rather than depending on empirical relations. The fundamental relation and understanding between empiricism and old existing models was clarified.

A mathematical model was proposed and validated based on well-documented data. The model has an advantage of being based on a minimum number of coefficients that can be characterized under wellbore condition.

One more benefit of the maturity method is its reliability in the cementing job evaluation and can be a criterion for specifying appropriate WOC times. In

addition, a unified mathematical model for cement properties estimation during hydration was attained.

The hydration mathematical model was adopted in a detailed near-wellbore modeling code. Assessment of wellbore integrity depends on zonal isolation provided by cement sheath. An interface gap may develop between different components of the wellbore and is considered as a preferential path for leakage. The creation of gaps or micro-annuli is a response of the wellbore under the effect of conditions parameters and controlled by different state parameters. Wellbore interface gaps directly affect the estimation of wellbore bulk permeability.

An extensive numerical workflow based on the FLAC modeling environment was developed in this research that allows a detailed full lifecycle near-wellbore model to be simulated. Each major stage in the history of ta well is sequentially processed based on stochastic input data parameters from predefined statistical distributions. The model includes conceptual, generic, and organized procedures and details to optimize any desired output. The aim of the workflow is to perform a sufficient number of simulations to generate a statistical distribution of the gap width over lifecycle duration of a wellbore.

Once the development of cement property evolution and estimation of micro-annulus are completed, the next step in the well integrity assessment is the estimation of the permeability of the interfaces that will be used in the safety assessment of wellbore leakage.

A case study of the main caprock in the Weyburn field illustrated that it is highly suitable for geological storage of CO2. It agrees with the results of Chalaturnyk et al. (2005) that primary seals that including Midale Evaporite

formation is observed to be highly competent. However, for another case investigated by Guen et al. (2012), observations match in that no interface micro-annulus is observed or gap width is in very small order of magnitude.

The permeability of the well system can now serve as an input parameter to rank and check the safety of leakage through wellbores. Therefore, a new analytic model to characterize leakage through wellbore element was developed that utilizes the well permeability estimates.

The model depends on the superposition method and takes into consideration the head loss in both axial and radial direction. The model idealizes radial flux by standard distribution patterns that have a universal pattern (shape) factor ranging from 0.50 to 0.67 rather than absolute values. Choosing a shape factor of 0.50 was shown to produce conservative results. Idealization of radial flow flux to take a standard distribution pattern has a significant advantage by transforming the problem into a simple 1-D problem.

A wellbore element sealing efficiency index has been proposed to be a criterion to rank different wellbore elements in the same formation, to compare with different elements within the same wellbore, and/or to check the safety condition of wellbore element if accepted as a standard code of practice tool. Wellbore leakage is governed by two parameters affecting the performance. These two parameters are recognized to be storage index and permeability index. This lead to the creation of a wellbore element performance chart indicating that any wellbore element will remain in a safe condition even if the permeability index is doubled as long as sealing efficiency is $\geq$ 67% and if permeability index $\geq$ 6 then the element sealing efficiency must be $\geq$ 90%.

The efficiency index provides a base to analytically model the wellbore system as a serially connected element and hence obtain another wellbore system efficiency index.

Wellbore system storage indices are not affected by the choice of the radial leakage distribution pattern. Formation arrangement in a storage site affects these indices. However, the arrangement will has no effect if wellbore element sealing efficiency $\eta \geq 0.70$.

Taking efficiency concept into consideration, wellbore system sealing efficiency was not enhanced significantly if a system is composed of a number of elements more than 8. Thus, a good reliable storage site should have a barrier of number of formations $\geq$ 8. Any increase of the number of formations will have less effect on the performance of the wellbore due to geometric reduction of leakage along a wellbore system. It mathematically proofs that wellbore hydraulic integrity represented by permeability index is the main issue for the assessment of wellbore leakage mechanism.

The model also showed that wellbore permeability index, I_k, was a suitable parameter to define the state of the wellbore. It is not the permeability of the wellbore that governs the performance but its contrast with the adjacent formation permeability.

Performance charts were developed that allowed the assessment of wellbore leakage for general system and aquitard-aquifer system respectively.

Failure at any wellbore subsystem is not necessarily an indication of overall failure of the whole system. However, it points to a severe condition of

integrity and an alert for requiring a remedial action at a certain location and/or depth.

7.3 Recommendations

Although a methodology has been established and a new procedure has been implemented to assess the wellbore leakage mechanism, the following points are recommended:

- With the aid of more cement data, the hydration model approach should be used to construct tables and/or design charts for hydration model coefficients. These tables and charts can be expanded to include several cement slurry mixtures and with different additives. Therefore, this will lead to a mix design approach for wellbore cements, design procedure can be established, and cement properties can be pre-expected.

- Reaching a mix design will enhance certain modification and/or recommendation of both cement types and cement additives specifications under given conditions.

- Detailed near-wellbore modeling requires a more realistic deterioration model that can be implemented in the numerical model.

- Detailed near-wellbore modeling needs interface properties of the wellbore to be further investigated with different formations and under downhole conditions.

- Detailed near-wellbore modeling requires an additional work on the explicit treatment of the cracks and to be linked to the estimated expected calculations of wellbore bulk permeability.

- Using stochastic approach facilitates adopting of response surface methodology to investigate wellbore response. If succeeded, it will ease system optimization process and hence have a more realistic course of actions for suspected wellbores.

- Sealing efficiency index is proposed as a criterion for acceptance and/or rejection of a wellbore in a given locality. If the index is accepted, it will pave a path for reliability based analysis for any wellbore and will fulfill a requirement to reach a standard code of practice for leakage.

7.4 Summary

A summary representation for the methodology to check wellbore leakage mechanism is illustrated in Figure 7.1.

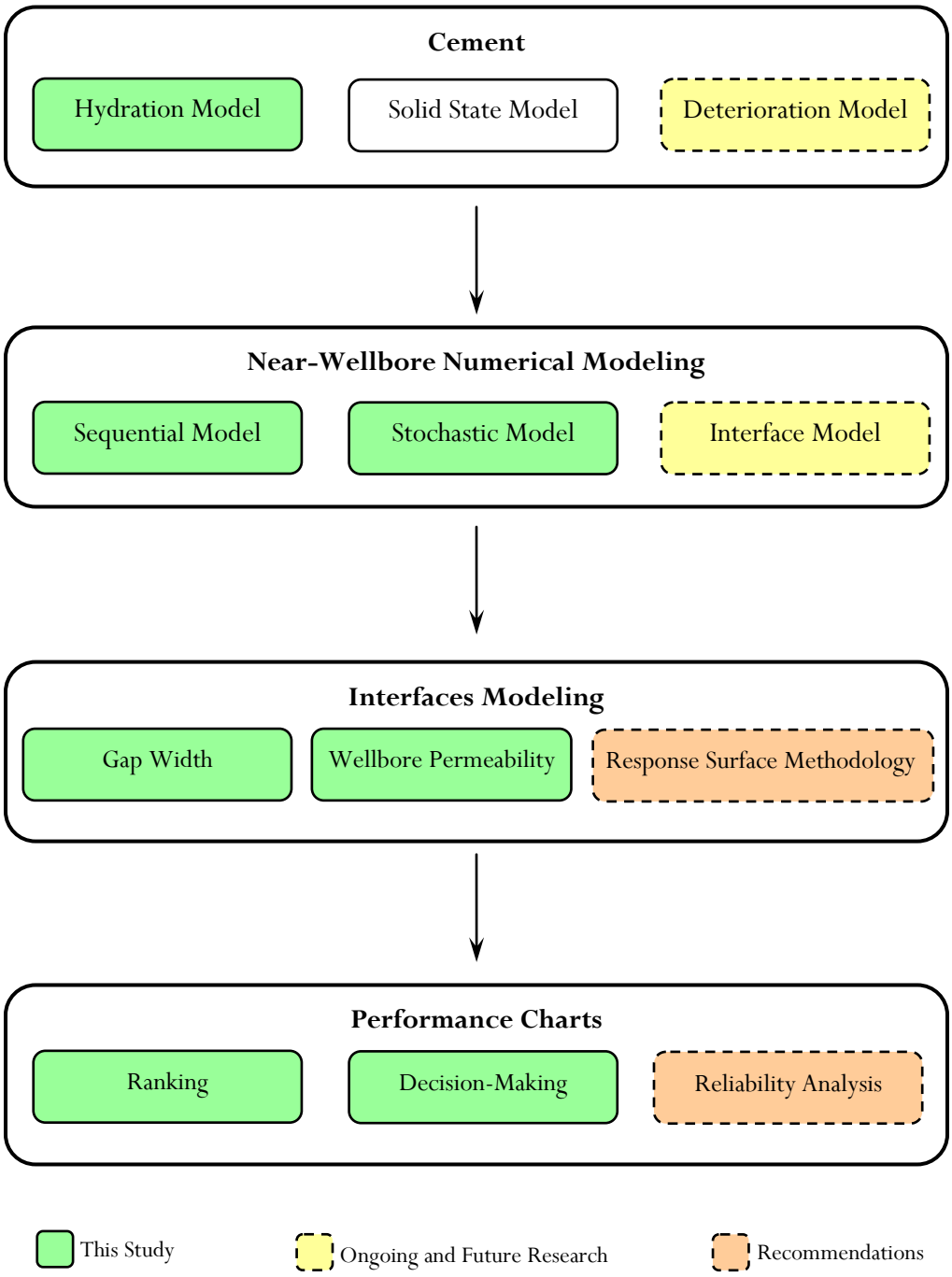

Figure 7.1: A schematic representation of framework for leakage assessment.

Appendix A: Weyburn Mechanical Earth Model

Table A.1: General stratigraphy of Weyburn area (Whittaker et al., 2004).

Formation	Main Rock and Hydrostratigraphy		Aquifer Group	
Intertill / Surface Till	Sandstone	Aquifer	Shallow	Biosphere
Bearpaw	Shale	Aquitard	Mesozoic	Geosphere
Belly River	Sandstone	Aquifer		
Colorado	Shale	Aquitard		
Newcastle	Sandstone	Aquifer		
Joli Fou	Shale	Aquitard		
Manville	Sandstone	Aquifer		
Vanguard	Shale	Aquitard		
Jurassic	Carbonate	Aquifer		
Waterous	Lower Red Beds / Upper Evaporite	Aquitard		
Ratcliffe	Carbonate	Aquifer		
Midale Evaporite	Anhydrite	Aquitard		

Table A.2: Average depth arrangement for Weyburn.

Formation[1]	Main Rock[1]	Depth to Top[2] (m)	Average Thickness[2] (m)
Intertill / Surface Till	Sandstone	0.00	30.00
Bearpaw	Shale	30.00	426.20
Belly River	Sandstone	456.20	45.40
Colorado	Shale	501.60	415.40
Newcastle	Sandstone	917.00	20.80
Joli Fou	Shale	937.80	39.90
Manville	Sandstone	977.70	134.40
Vanguard	Shale	1112.10	93.30
Jurassic	Carbonate	1205.40	124.90
Waterous	Lower Red Beds / Upper Evaporite	1330.30	92.10
Ratcliffe	Carbonate	1422.40	17.80
Midale Evaporite	Anhydrite	1440.20	6.80

[2]Temperature at depth 1447 (°C) = 63.00

[2]Average Temperature Gradient (°C/m) = 0.035

Sources for data values:

1) Whittaker et al. (2004)
2) Walton et al. (2004)

Stress gradients values are from Gomez (2006).

Table A.3: Static mechanical properties for different rocks.

Rock	Mechanical Properties				
	Density	**Elastic Modulus**	**Poisson's Ratio**	**Cohesion**	**Internal Friction**
	ρ (kg/m^3)	**E (GPa)**	**ν (-----)**	**C (MPa)**	**ϕ (degree)**
Sandstone	(2000 - 2650)[1] (2000 - 2400)[3]	(0.1 - 30)[1]	(0.0 - 0.45)[1]	30[2]	(20 – 40)[1] 35[2]
Shale	(2300 - 2800)[1]	(0.4 – 70)[1]	(0.0 - 0.30)[1]		
Carbonate	(2400 - 2700)[1] 2700[3]	(2 - 100)[1]	(0.0 - 0.30)[1]	30[2]	35[2]
Anhydrite	2800[2]	Eq. (6.11)[2]	(0.20 - 0.40)[2]	(13 - 20)[2]	(30 - 45)[2]

Sources for data values:

1) Fjær et al. (2008)
2) Gomez (2006)
3) Kutasov (1999)

Casing data values is from Gabolde and Nguyen (1999).

Appendix B: Input Data

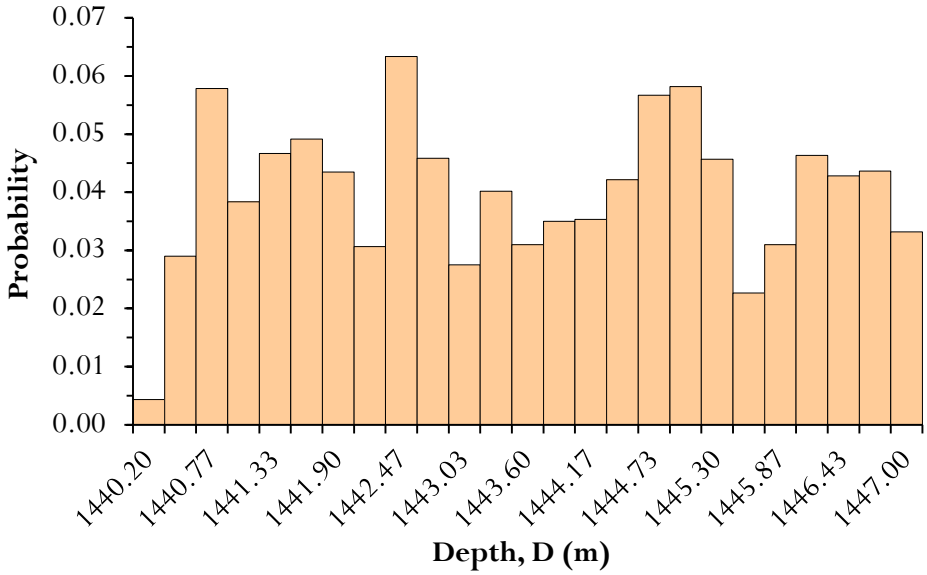

Figure B.1: Generated depth of caprock formation.

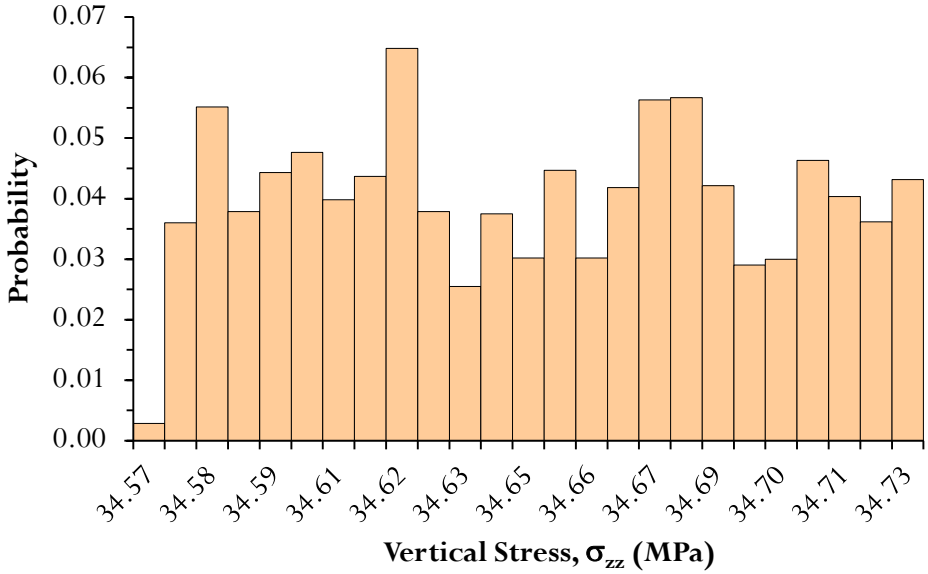

Figure B.2: Generated vertical stress in caprock formation.

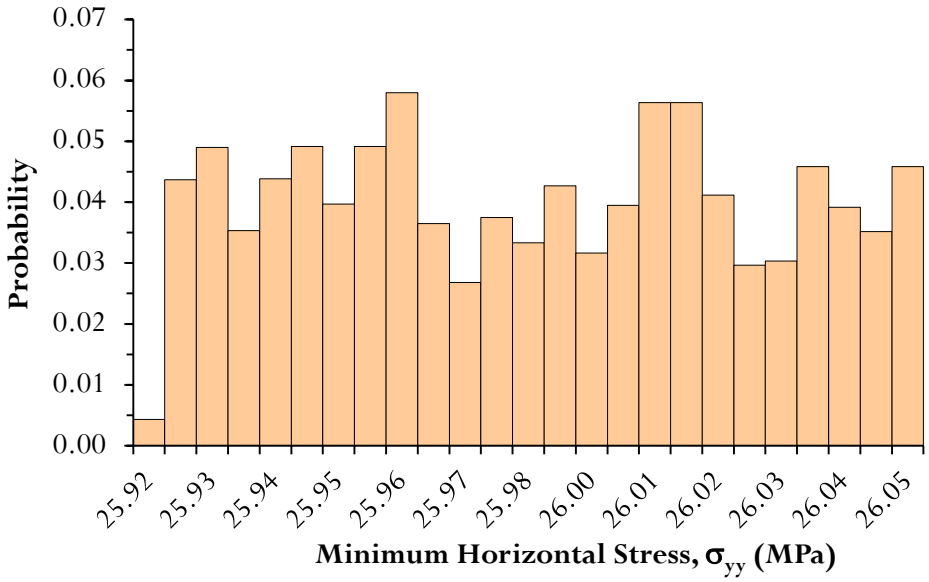

Figure B.3: Generated minimum horizontal stress in caprock formation.

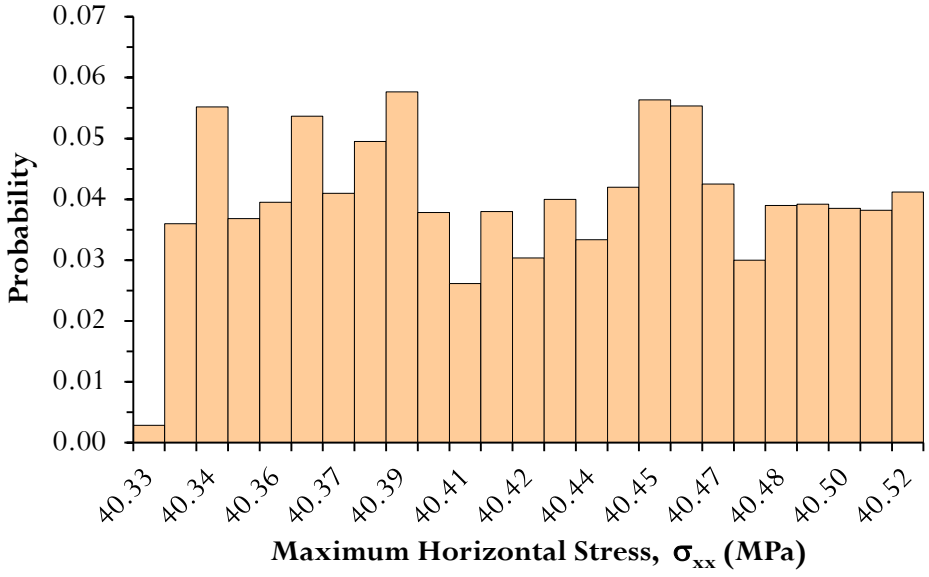

Figure B.4: Generated maximum horizontal stress in caprock formation.

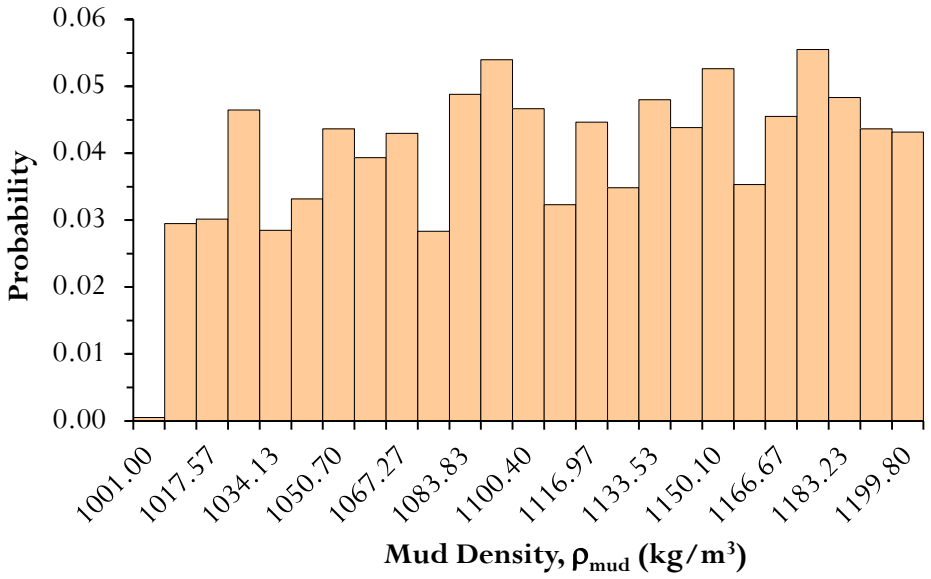

Figure B.5: Generated mud density at caprock formation.

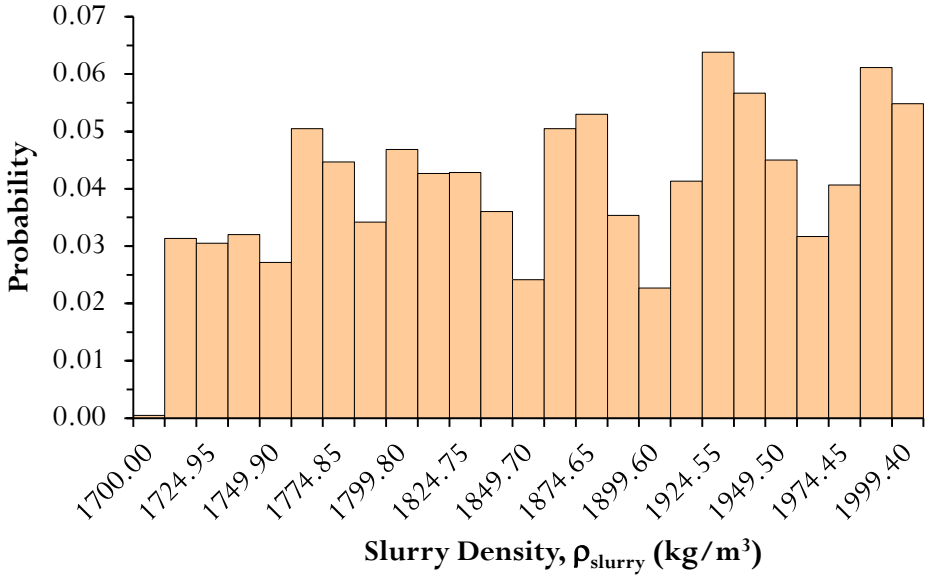

Figure B.6: Generated slurry density at caprock formation.

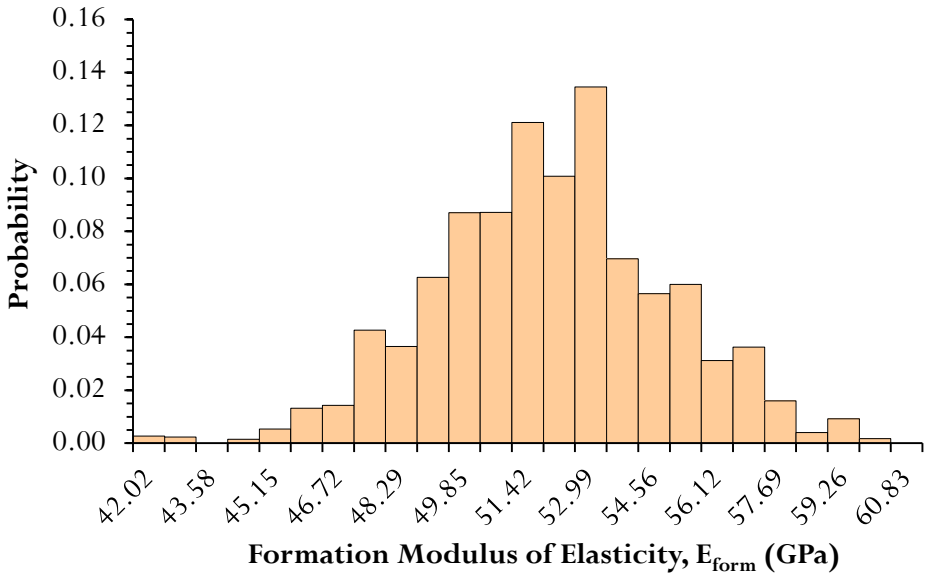

Figure B.7: Generated modulus of elasticity for caprock formation.

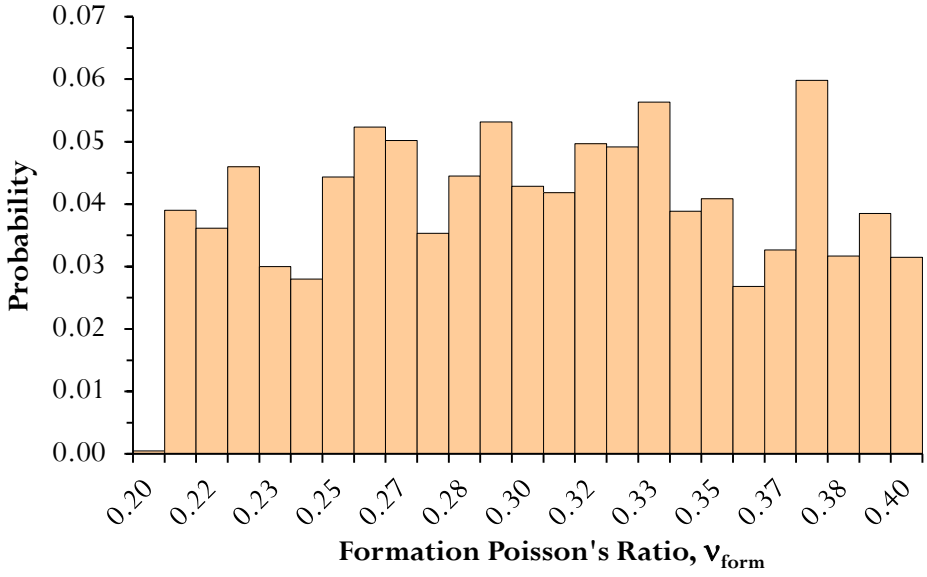

Figure B.8: Generated Poisson's ratio for caprock formation.

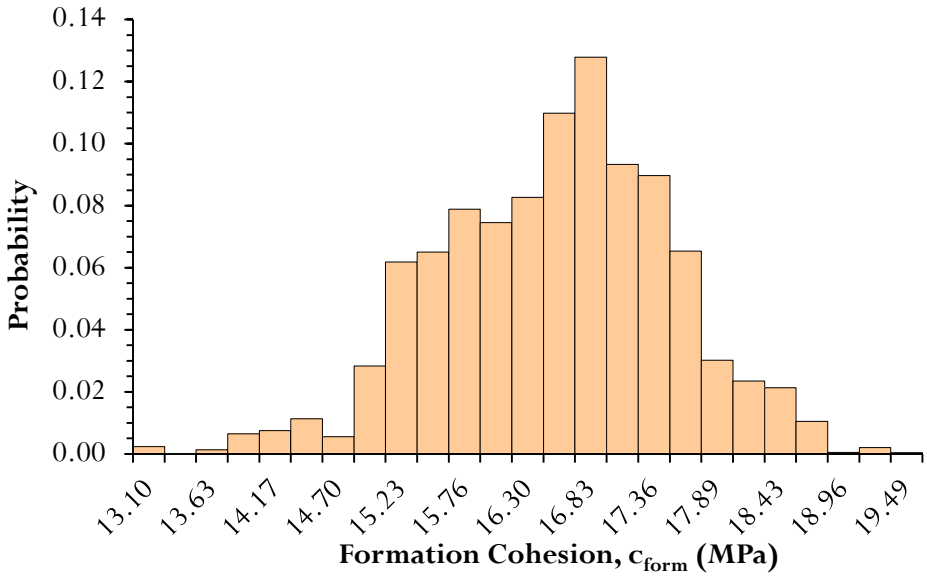

Figure B.9: Generated cohesion for caprock formation.

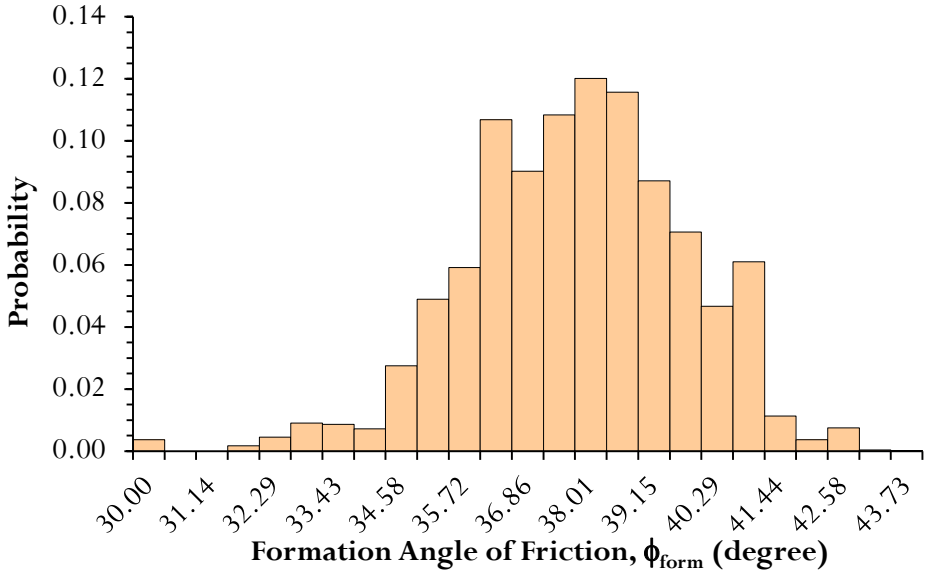

Figure B.10: Generated friction angle for caprock formation.

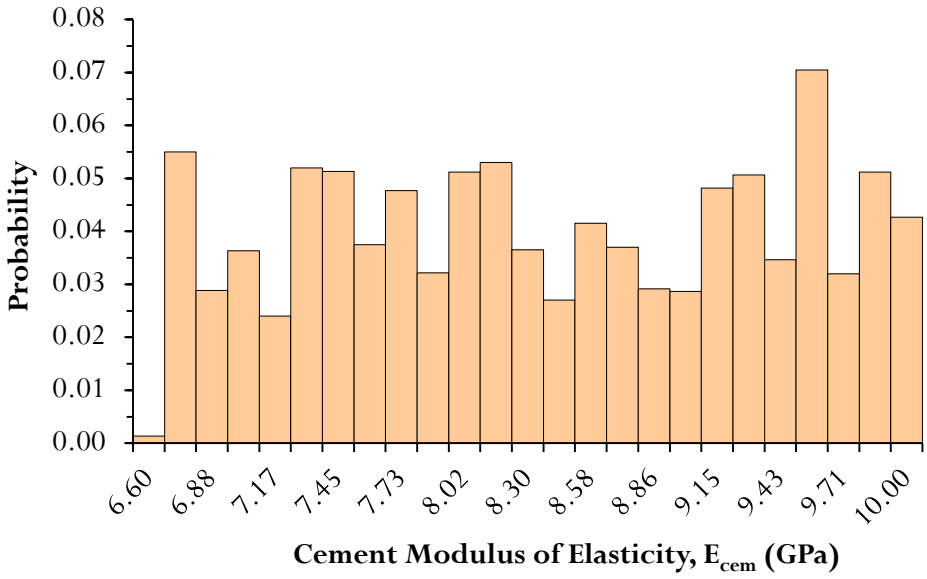

Figure B.11: Generated modulus of elasticity for cement.

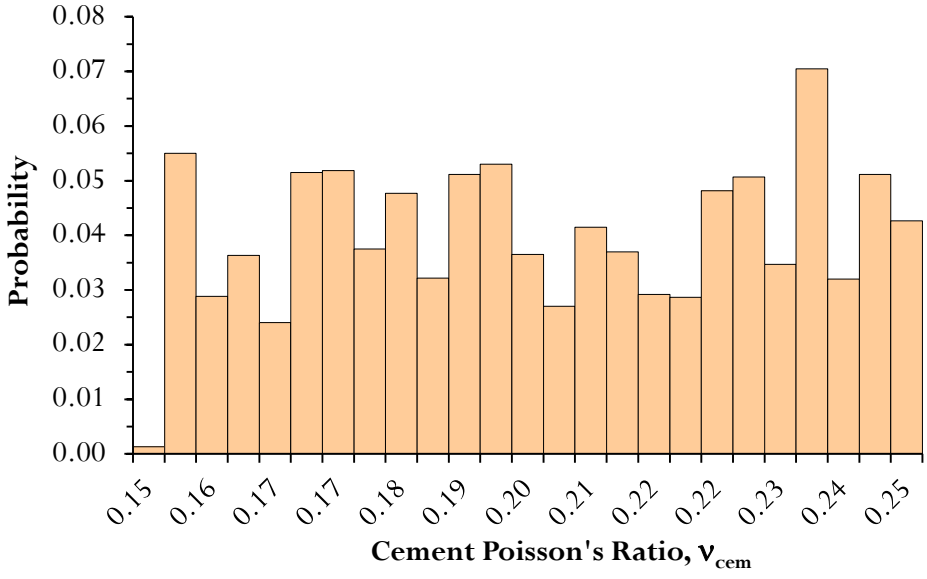

Figure B.12: Generated Poisson's ratio for cement.

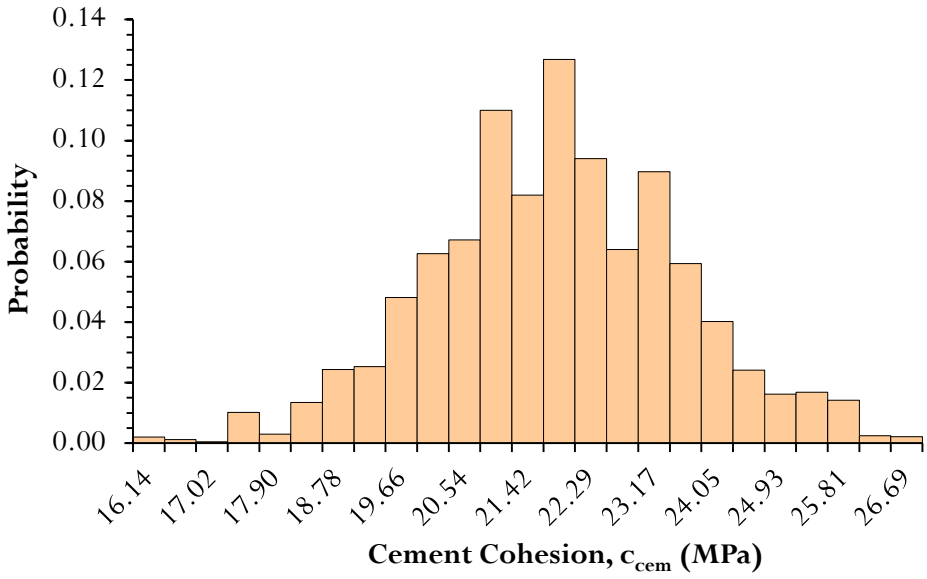

Figure B.13: Generated cohesion for cement.

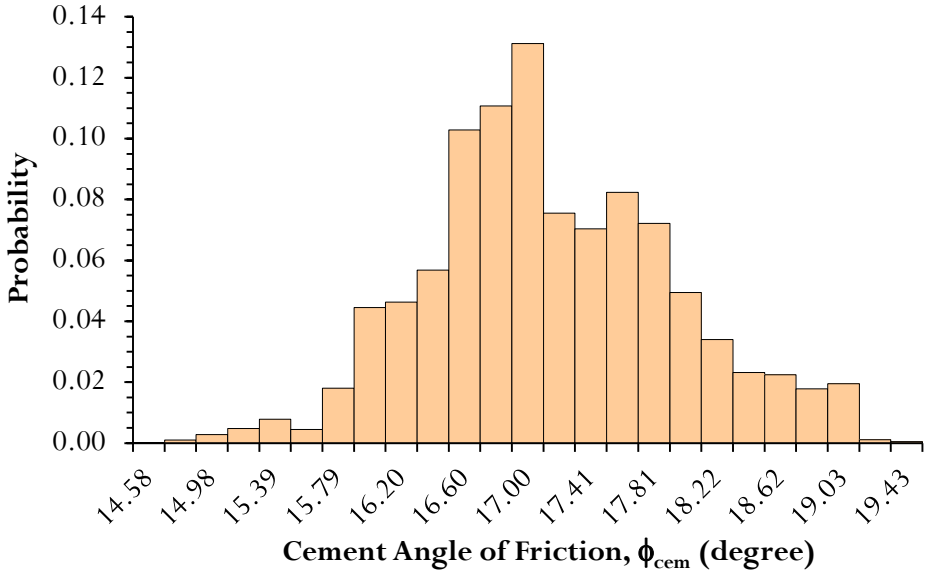

Figure B.14: Generated friction angle for cement.

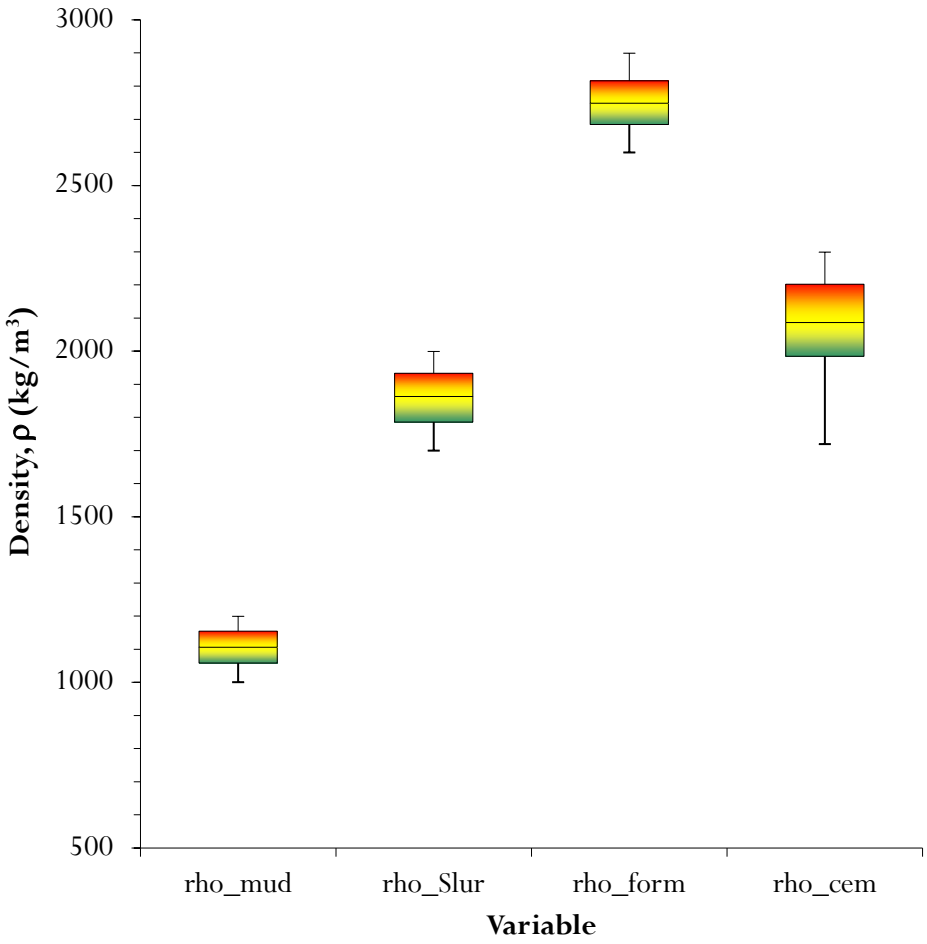

Figure B.15: Box and whiskers plot for model density data.

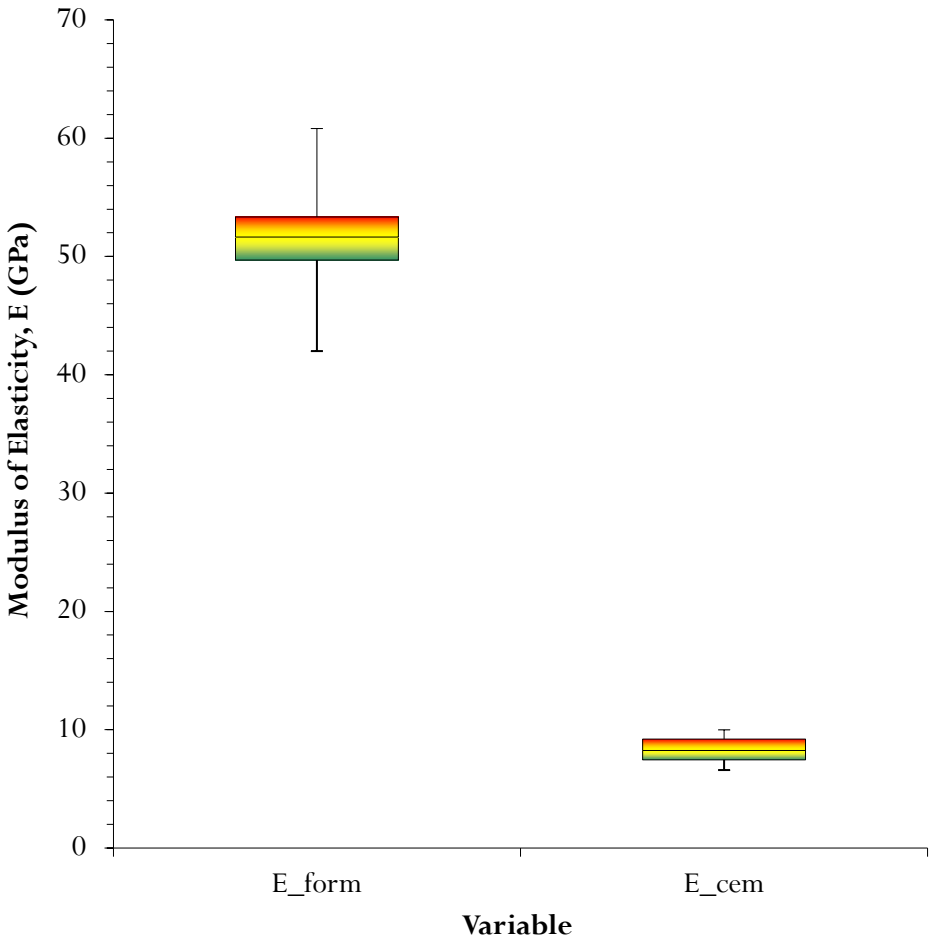

Figure B.16: Box and whiskers plot for model modulus of elasticity data.

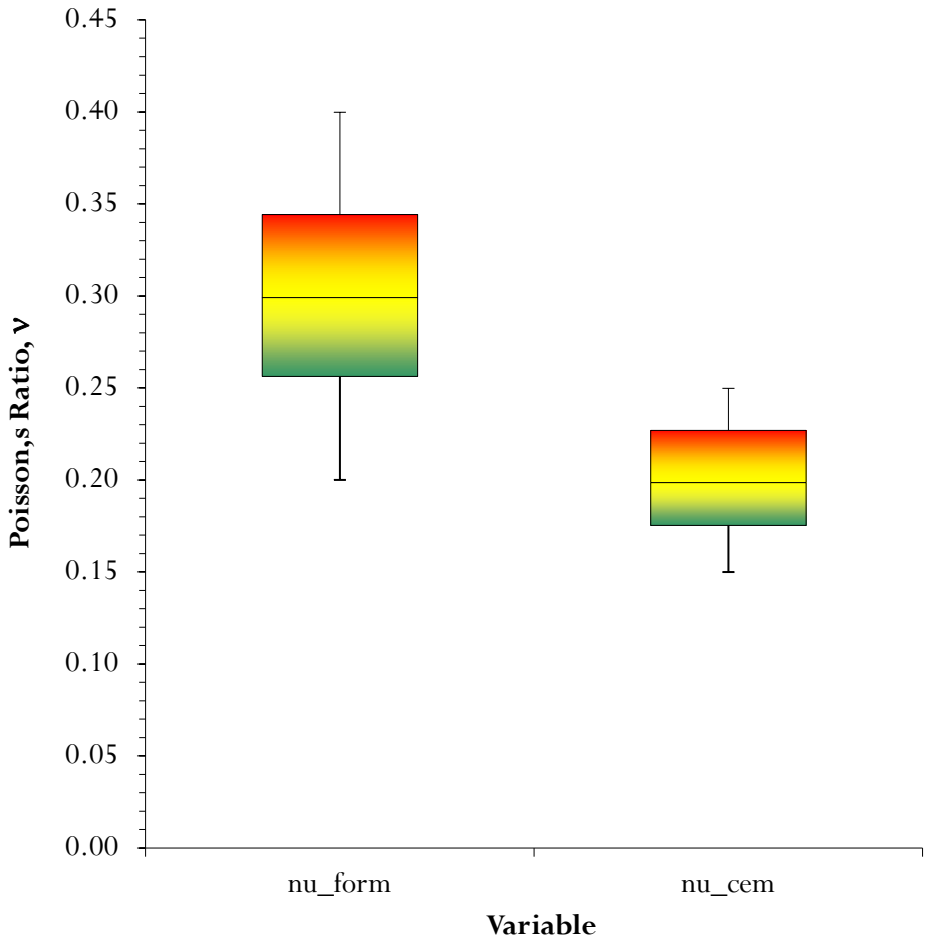

Figure B.17: Box and whiskers plot for model Poisson's ratio data.

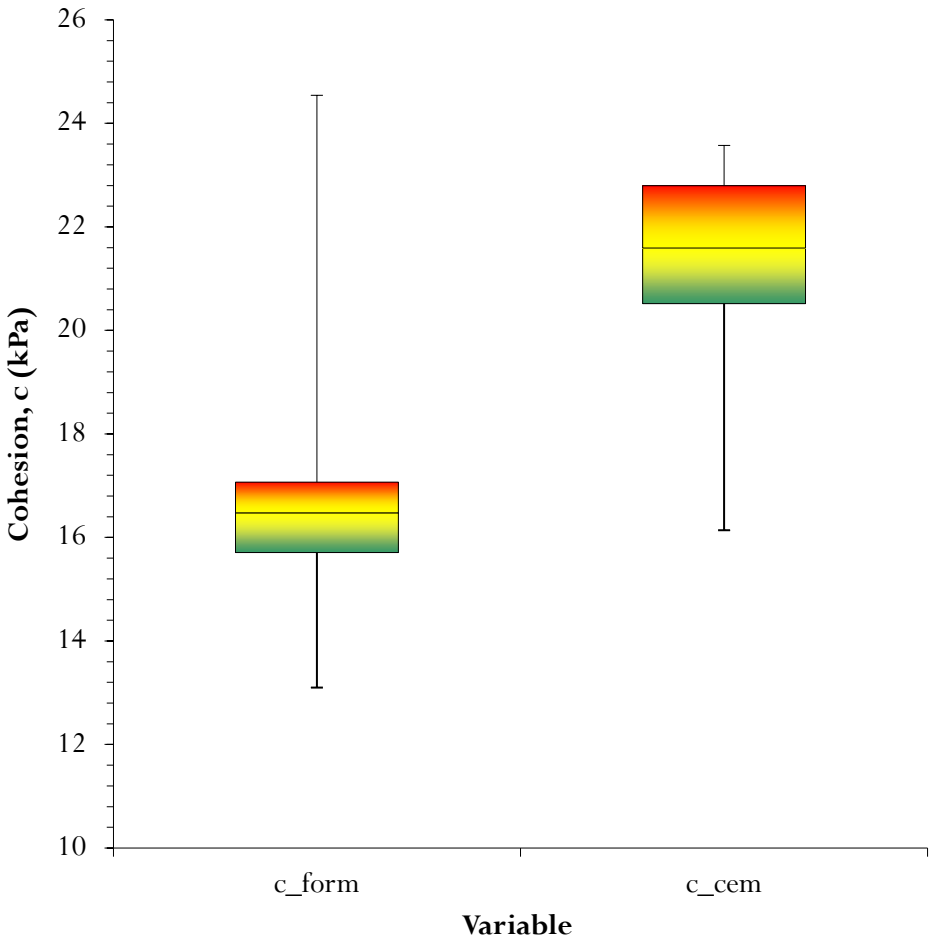

Figure B.18: Box and whiskers plot for model cohesion data.

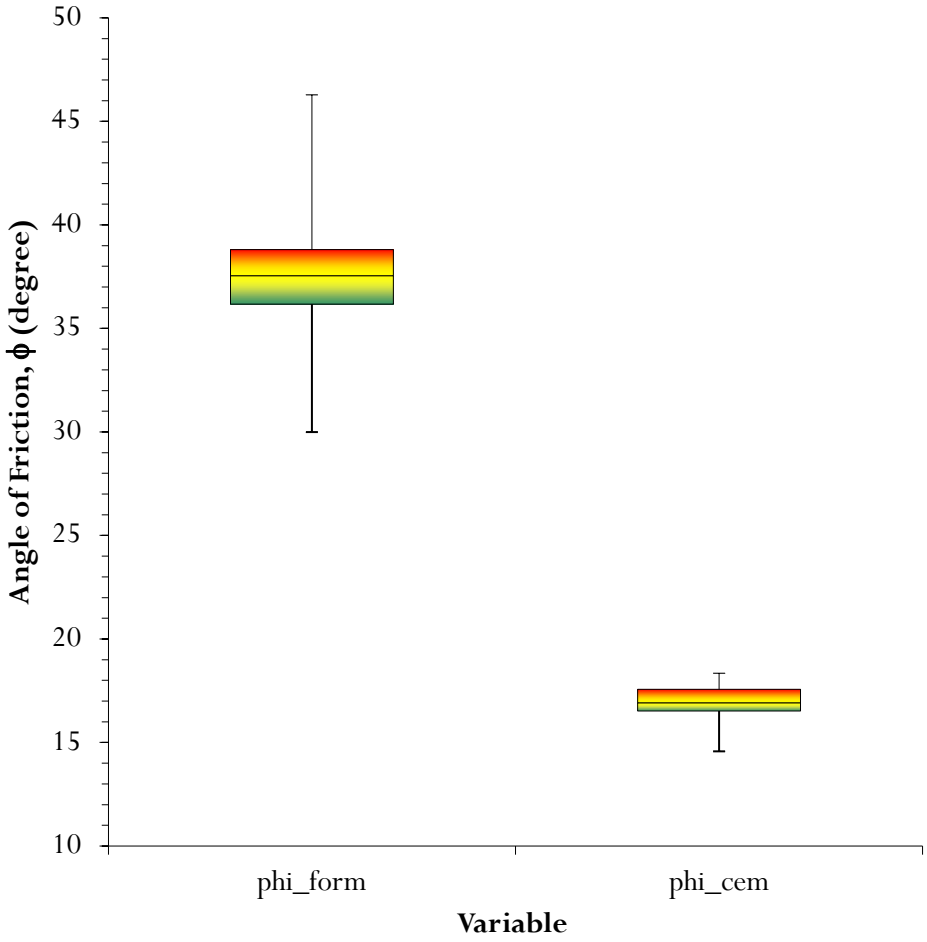

Figure B.19: Box and whiskers plot for model friction angle data.

Appendix C: Output Data

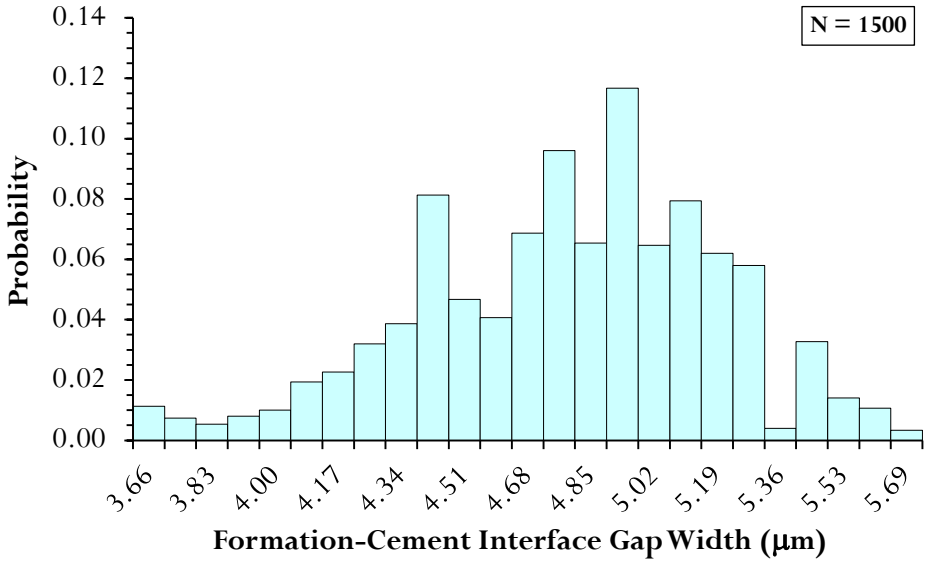

Figure C.1: Generated cement-formation gap width at year 2000.

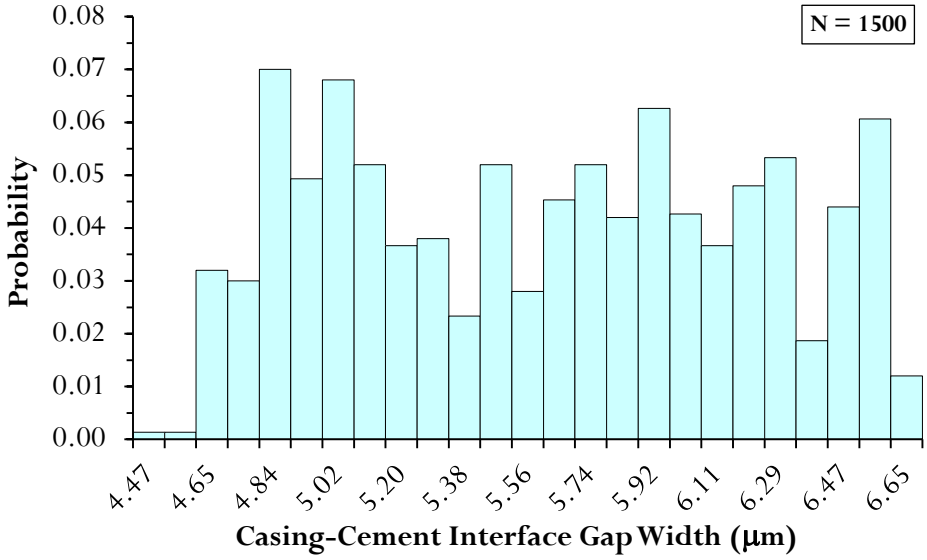

Figure C.2: Generated cement-casing gap width at year 2000.

Appendix D: Velocity Profile in Circular Sections

For a circular element "section", Figure D.1, the velocity at any point, of a radius r, is u and the dynamic viscosity is μ. The element has a length L with inside radius of r and a radial thickness of dr. The pressure difference, Δp, is over the element length, L. The shear stress on the surface increases by $d\tau$ from the inner to the outer surface.

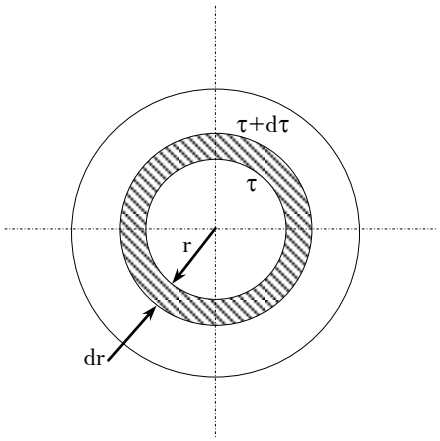

Figure D.1: Flow through circular element "pipe".

The driving force due to pressure, $F = \text{Pressure} \times \text{Area}$ can be written as:

$$\begin{aligned} \text{driving force} &= \text{pressure force at inlet} - \text{pressure force at outlet} \\ &= \left(\pi(r+dr)^2 - \pi r^2\right)\Delta p \end{aligned} \qquad (D.1)$$

The resisting (retarding) force, shear force, is that due to the shear stress by the walls, which is:

$$\begin{aligned} \text{shear force} &= \text{shear stress} \times \text{area over which it acts} \\ &= \tau \times \text{area of pipe wall} \\ &= \left((\tau+d\tau)(2\pi)(r+dr) - \tau 2\pi r\right)L \end{aligned} \qquad (D.2)$$

By equating Equations (D.1) and (D.2),

$$\left(2r\,dr + dr^2\right)\Delta p = \left(\tau\,dr + r\,d\tau + d\tau\,dr\right)2L$$

ignoring the product of the small quantities, then

$$\frac{\Delta p}{L} = \frac{\tau}{r} + \frac{d\tau}{dr} \tag{D.3}$$

where for Newtonian fluids.

$$\tau = \mu\frac{du}{dy}$$

where $y = R - r$ and $dy = -dr$, and hence,

$$\tau = -\mu\frac{du}{dr}$$

Substituting into Equation (D.3), then

$$\frac{\Delta p}{L} = -\frac{\mu}{r}\frac{du}{dr} - \mu\frac{d^2u}{dr^2} \tag{D.4}$$

Hence,

$$\frac{du}{dr} + r\frac{d^2u}{dr^2} = -\frac{r}{\mu}\left(\frac{\Delta p}{L}\right) \tag{D.5}$$

but

$$\frac{d}{dr}\left(r\frac{du}{dr}\right) = \frac{du}{dr} + r\frac{d^2u}{dr^2} \tag{D.6}$$

Equating Equation (D.5) and Equation (D.6):

$$\frac{d}{dr}\left(r\frac{du}{dr}\right) = -\frac{r}{\mu}\left(\frac{\Delta p}{L}\right) \tag{D.7}$$

Integrating Equation (D.7), then

$$r\frac{du}{dr} = -\frac{r^2}{2\mu}\left(\frac{\Delta p}{L}\right) + A \tag{D.8}$$

where A is the first constant of integration. Therefore,

$$\frac{du}{dr} = -\frac{r}{2\mu}\left(\frac{\Delta p}{L}\right) + \frac{A}{r} \tag{D.9}$$

Integrating Equation (D.9), then:

$$u_r = -\frac{r^2}{4\mu}\left(\frac{\Delta p}{L}\right) + A\ln(r) + B \tag{D.10}$$

where B is the second constant of integration.

Change of volumetric flow rate is:

$$\begin{aligned} dQ &= u_r \,.\, dA \\ &= u_r \, 2\pi r \,.\, dr \end{aligned} \tag{D.11}$$

Appendix E: Flow through Pipes

Flow through circular section of the pipe can be obtained by applying boundary conditions. Recalling Equation (D.8), then when $r = 0$ then the first constant of integration, A = 0. Therefore, Equation (D.10) can be written as:

$$u_r = -\frac{r^2}{4\mu}\left(\frac{\Delta p}{L}\right) + B \tag{E.1}$$

At the pipe wall, $u = 0$ and $r = R$. Therefore, the second constant of integration, B is:

$$B = \frac{R^2}{4\mu}\left(\frac{\Delta p}{L}\right) \tag{E.2}$$

Therefore, the velocity profile at radius r is:

$$\begin{aligned} u_r &= -\frac{r^2}{4\mu}\left(\frac{\Delta p}{L}\right) + \frac{R^2}{4\mu}\left(\frac{\Delta p}{L}\right) \\ &= \frac{1}{4\mu}\left(\frac{\Delta p}{L}\right)\left(R^2 - r^2\right) \end{aligned} \tag{E.3}$$

Volumetric flow rate through pipe, Q_{Pipe}, is obtained by integration of the Equation (D.11) that is:

$$\begin{aligned} Q_{Pipe} &= \int_0^R \frac{1}{4\mu}\left(\frac{\Delta p}{L}\right)\left(R^2 - r^2\right) 2\pi r \,.dr \\ &= \frac{\pi}{2\mu}\left(\frac{\Delta p}{L}\right)\int_0^R \left(R^2 - r^2\right) r \,.dr \\ &= \frac{\pi R^4}{8\mu}\left(\frac{\Delta p}{L}\right) \end{aligned} \tag{E.4}$$

Using head loss h_a, (i.e. $\Delta p = \rho g h_a$) instead of pressure loss yields that Equation (E.4) can be written as:

$$Q_{Pipe} = \frac{\rho g}{\mu} \frac{\pi R^4}{8} \frac{h_a}{L} \tag{E.5}$$

Rearranging Equation (E.5) to include pipe area, $A_{Pipe} = \pi R^2$, then

$$\begin{aligned} Q_{Pipe} &= \frac{\rho g}{\mu} \frac{1}{8} R^2 \frac{\pi R^2}{L} h_a \\ &= \frac{\rho g}{\mu} \frac{1}{8} R^2 \frac{A_{Pipe}}{L} h_a \end{aligned} \tag{E.6}$$

Appendix F: Flow through Micro-Annulus

For flow through wellbore micro-annulus gap, the boundary conditions, Figure F.1, are $u=0$ at $r=R_i$ and $r=R_o$ where R_i and R_o is the inner and outer radius respectively. Putting this into Equation (D.10) yields

$$0=-\frac{R_o^2}{4\mu}\left(\frac{\Delta p}{L}\right)+A\ln(R_o)+B \tag{F.1}$$

and

$$0=-\frac{R_i^2}{4\mu}\left(\frac{\Delta p}{L}\right)+A\ln(R_i)+B \tag{F.2}$$

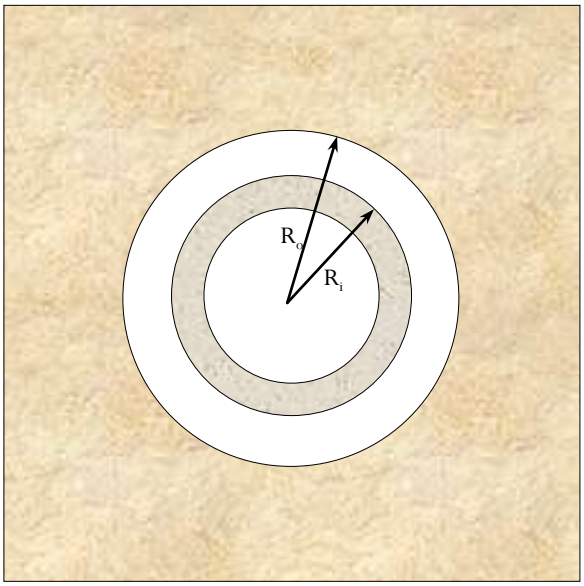

Figure F.1: Flow through wellbore annulus.

Subtracting Equation (F.2) from Equation (F.1) yields to

$$0=\frac{1}{4\mu}\left(\frac{\Delta p}{L}\right)\left(R_i^2-R_o^2\right)+A\ln\left(\frac{R_o}{R_i}\right) \tag{F.3}$$

Therefore,

$$A = \frac{1}{4\mu}\left(\frac{\Delta p}{L}\right)\left(\frac{\left(R_o^2 - R_i^2\right)}{\ln\left(\frac{R_o}{R_i}\right)}\right) \tag{F.4}$$

Substituting by Equation (F.4) into Equation (F.2), then

$$0 = -\frac{R_i^2}{4\mu}\left(\frac{\Delta p}{L}\right) + \frac{1}{4\mu}\left(\frac{\Delta p}{L}\right)\left(\frac{\left(R_o^2 - R_i^2\right)}{\ln\left(\frac{R_o}{R_i}\right)}\right)\left(\ln(R_i)\right) + B \tag{F.5}$$

Therefore,

$$B = \frac{1}{4\mu}\left(\frac{\Delta p}{L}\right)\left(R_i^2 - \left(\frac{\left(R_o^2 - R_i^2\right)}{\ln\left(\frac{R_o}{R_i}\right)}\right)\left(\ln(R_i)\right)\right) \tag{F.6}$$

Similarly, to pipe flow, velocity at a point r from the pipe center can be obtained by substituting by constants A and B into Equation (D.10) that is:

$$\begin{aligned} u_r = & -\frac{r^2}{4\mu}\left(\frac{\Delta p}{L}\right) + \frac{1}{4\mu}\left(\frac{\Delta p}{L}\right)\left(\frac{\left(R_o^2 - R_i^2\right)}{\ln\left(\frac{R_o}{R_i}\right)}\right)\left(\ln(r)\right) \\ & + \frac{1}{4\mu}\left(\frac{\Delta p}{L}\right)\left(R_i^2 - \left(\frac{\left(R_o^2 - R_i^2\right)}{\ln\left(\frac{R_o}{R_i}\right)}\right)\left(\ln(R_i)\right)\right) \end{aligned} \tag{F.7}$$

Rearranging Equation (F.7), then

$$u_r = \frac{1}{4\mu}\left(\frac{\Delta p}{L}\right)\left(-r^2 + \left(\frac{\left(R_o^2 - R_i^2\right)}{\ln\left(\frac{R_o}{R_i}\right)}\right)\left(\ln(r)\right) + \left(R_i^2 - \left(\frac{\left(R_o^2 - R_i^2\right)}{\ln\left(\frac{R_o}{R_i}\right)}\right)\left(\ln(R_i)\right)\right)\right)$$

Therefore,

$$u_r = \frac{1}{4\mu}\left(\frac{\Delta p}{L}\right)\left(\left(\frac{\left(R_o^2 - R_i^2\right)}{\ln\left(\frac{R_o}{R_i}\right)}\right)\ln\left(\frac{r}{R_i}\right) - \left(r^2 - R_i^2\right)\right) \qquad \text{(F.8)}$$

Volumetric flow rate through annulus, $Q_{Annulus}$, is obtained by integration of the Equation (D.11) which yields:

$$Q_{Annulus} = \int_{R_i}^{R_o} \frac{1}{4\mu}\left(\frac{\Delta p}{L}\right)\left(\left(\frac{\left(R_o^2 - R_i^2\right)}{\ln\left(\frac{R_o}{R_i}\right)}\right)\ln\left(\frac{r}{R_i}\right) - \left(r^2 - R_i^2\right)\right) 2\pi r\,.dr \qquad \text{(F.9)}$$

Therefore,

$$Q_{Annulus} = \frac{\pi}{2\mu}\left(\frac{\Delta p}{L}\right)\frac{\left(R_o^2 - R_i^2\right)}{\ln\left(\frac{R_o}{R_i}\right)}\int_{R_i}^{R_o}\left(\ln(r) - \ln(R_i)\right) r\,.dr - \frac{\pi}{2\mu}\left(\frac{\Delta p}{L}\right)\int_{R_i}^{R_o}\left(r^2 - R_i^2\right) r\,.dr \qquad \text{(F.10)}$$

Further rearrangement of Equation (F.10) leads to:

$$Q_{Annulus} = \frac{\pi}{2\mu}\left(\frac{\Delta p}{L}\right)\frac{\left(R_o^2 - R_i^2\right)}{\ln\left(\frac{R_o}{R_i}\right)}\int_{R_i}^{R_o} \ln(r)\, r\, .dr$$

$$- \frac{\pi}{2\mu}\left(\frac{\Delta p}{L}\right)\frac{\left(R_o^2 - R_i^2\right)}{\ln\left(\frac{R_o}{R_i}\right)}\int_{R_i}^{R_o} \ln(R_i)\, r\, .dr \qquad \text{(F.11)}$$

$$- \frac{\pi}{2\mu}\left(\frac{\Delta p}{L}\right)\int_{R_i}^{R_o} \left(r^2 - R_i^2\right) r\, .dr$$

Product of $r\ln(r)$ is involved in the expression, thus the following integral is needed:

$$\int r\ln(r).dr = \frac{r^2}{2}\ln(r) - \frac{r^2}{4} \qquad \text{(integration by parts)}$$

Integrating Equation (F.11) gives:

$$Q_{Annulus} = \frac{\pi}{8\mu}\left(R_o^2 - R_i^2\right)\left(\frac{\Delta p}{L}\right)\left(\left(R_o^2 + R_i^2\right) - \frac{\left(R_o^2 - R_i^2\right)}{\ln\left(R_o / R_i\right)}\right) \qquad \text{(F.12)}$$

Using head loss h_a, (i.e. $\Delta p = \rho g h_a$) instead of pressure loss yields that Equation (F.12) can be written as:

$$Q_{Annulus} = \frac{\pi\rho g}{8\mu}\left(R_o^2 - R_i^2\right)\left(\left(R_o^2 + R_i^2\right) - \frac{\left(R_o^2 - R_i^2\right)}{\ln\left(R_o / R_i\right)}\right)\frac{h_a}{L} \qquad \text{(F.13)}$$

Rearranging Equation (F.13) to include annulus area $A_{Annulus} = \pi\left(R_o^2 - R_i^2\right)$, then,

$$Q_{Annulus} = \frac{\rho g}{\mu}\frac{1}{8}\left(\left(R_o^2 + R_i^2\right) - \frac{\left(R_o^2 - R_i^2\right)}{\ln\left(R_o / R_i\right)}\right)\frac{A_{Annulus}}{L}h_a \qquad \text{(F.14)}$$

Appendix G: Model Coding

FLAC, Fast Lagrangian Analysis of Continua program, has an embedded programming language called FISH. FISH facilities the user to define variables and functions that are not available with existing FLAC program structure. FISH will be used to control and modify the wellbore simulation modeling process. FISH functions can be created in a file and then called when required to be executed in their order. Each FISH function has a unique name that starts with command “define” and terminates by command “end”.

G.1 Input Parameters

Preparing a global input data function is important to serve any part in the simulation. An example for material model parameters function is as follows:

```
def Model_Material_Parameters                          ; Example of material input data function
 ; 1) Materials Interfaces
 ; -------------------------
 ; 1.1) Deterministic Data
 ; N/A  =====> All parameters will be randomly generated

 ; 1.2) Random Variables Data
 ; Cement-Formation Interface 01
 Int01_RF1 = 1.00                                      ; Min. mechanical strength reduction factor
 Int01_RF2 = 1.00                                      ; Max. mechanical strength reduction factor
 ; Cement-Casing Interface 02
 Int02_RF1 = 1.00                                      ; Min. mechanical strength reduction factor
 Int02_RF2 = 1.00                                      ; Max. mechanical strength reduction factor

 ; 2) Casing (c)
 ; ---------------
 ; 2.1) Deterministic Data
 ; During Installation
 SurForce_c = 0.00                                     ; Force holding casing at surface (N)
 ; Mechanical Model Parameters "Elastic"
 rho_c = 7850.0                                        ; Dry density (kg/m^3)
 E_c = 200.0e9                                         ; Elastic modulus (Pa)
 nu_c = 0.33                                           ; Poisson's ratio (Dimensionless)
 ; Thermal Model Parameters "Isotropic Heat Conduction"
 Therm_Cond_c = 50.0                                   ; Thermal conductivity (W/(m.K))
 Spec_Heat_c = 500.0                                   ; Specific heat (J/(kg.K))
 LinTherm_Exp_c = 1.11e-5                              ; Linear thermal expansion (1/K)

 ; 2.2) Random Variables Data
 ; N/A  =====> All parameters are deterministic


 ; 3) Formation (form)
```

```
; ------------------------
; 3.1) Deterministic Data
; N/A  =====> All parameters will be randomly generated

; 3.2) Random Variables Data
; Mechanical Model Parameters (MMP) "Mohr-Coulomb"
rho1_form = 2600.0                                  ; Min. density (kg/m^3)
;E1_form = 50.0e9                                   ;  "   elastic modulus (Pa)
nu1_form = 0.20                                     ;  "   Poisson's ratio (Dimensionless)
c1_form = 13.0e6                                    ;  "   cohesion (Pa)
phi1_form = 30.0                                    ;  "   friction angle (Degree)
d1_form = 0.0                                       ;  "   dilation (Degree)

rho2_form = 2900.0                                  ; Max. density (kg/m^3)
;E2_form = 50.0e9                                   ;  "   elastic modulus (Pa)
nu2_form = 0.40                                     ;  "   Poisson's ratio (Dimensionless)
c2_form = 20.0e6                                    ;  "   cohesion (Pa)
phi2_form = 45.0                                    ;  "   friction angle (Degree)
d2_form = 0.0                                       ;  "   dilation (Degree)
; Thermal Model Parameters (TMP) "Isotropic Heat Conduction"
TC1_form = 1.60                                     ; Min. thermal conductivity (W/(m.K))
SH1_form = 0.92e3                                   ;  "   specific heat (J/(kg.K))
LTE1_form = 1.0e-5                                  ;  "   linear thermal expansion (1/K)

TC2_form = 1.60                                     ; Max. thermal conductivity (W/(m.K))
SH2_form = 0.92e3                                   ;  "   specific heat (J/(kg.K))
LTE2_form = 1.0e-5                                  ;  "   linear thermal expansion (1/K)


; 4) Drilling Mud (mud)
; --------------------------
; 4.1) Deterministic Data
Sur_Press_mud = 0.00                                ; Applied pressure @ G.S. (Pa) (= ZERO)

; 4.2) Random Variables Data
rho1_mud = 1000.0                                   ; Min. mud density (kg/m^3)
rho2_mud = 1200.0                                   ; Max. mud density (kg/m^3)


; 5) Water (w)
; ----------------
; 5.1) Deterministic Data
Sur_Press_w = 0.0                                   ; Applied pressure @ G.S. (Pa)

; 5.2) Random Variables Data
rho1_w = 1000.0                                     ; Min. water density (kg/m^3)
rho2_w = 1000.0                                     ; Max. water density (kg/m^3)


; 6) Cement Slurry (cemSlur)
; ---------------------------------
; 6.1) Deterministic Data
Sur_Press_cemSlur = 0.0                             ; Applied pressure @ G.S. (Pa)
Cement_Top_Depth = 0.0                              ; Depth to cement top in the Annulus (m)
Delta_Hyd_Temp = 9.0                                ; Temp. increase during hydration (K or C)

; 6.2) Random Variables Data
; Stage_0210
rho1_01cemSlur = 1700.0                             ; Min. initial density (kg/m^3)
rho2_01cemSlur = 2000.0                             ; Max. initial density (kg/m^3)
```

```
; Stage_0220
rho1_02cemSlur = 1700.0                    ; Min. density @ max. heat (kg/m^3)
rho2_02cemSlur = 2000.0                    ; Max. density @ max. heat (kg/m^3)


; 7) Completion Fluid (compF)
; ----------------------------------
; 7.1) Deterministic Data
Sur_Press_compF = 0.0                      ; Applied pressure @ G.S. (Pa) (= ZERO)

; 7.2) Random Variables Data
rho1_compF = 1000.0                        ; Min. completion fluid density (kg/m^3)
rho2_compF = 1000.0                        ; Max. completion fluid density (kg/m^3)


; 8) Cement during Constant Parameters (cem)   ; Used in Stage_0300 and Stage_0500
; ----------------------------------------------------
; 8.1) Deterministic Data
; N/A  =====> All parameters will be randomly generated

; 8.2) Random Variables Data
; Mechanical Model Parameters (MMP) "Mohr-Coulomb"
;rho1_cem = 1700.0                         ; Min. density (kg/m^3) (In Input Functions)
E1_cem = 6.6e9                             ;  "   elastic modulus (Pa)
nu1_cem = 0.15                             ;  "   Poisson's ratio (Dimensionless)
c1_cem = 15.0e6                            ;  "   cohesion (Pa)
phi1_cem = 14.0                            ;  "   friction angle (Degree)

rho2_cem = 2300.0                          ; Max. density (kg/m^3)
E2_cem = 10.0e9                            ;  "   elastic modulus (Pa)
nu2_cem = 0.25                             ;  "   Poisson's ratio (Dimensionless)
c2_cem = 28.2e6                            ;  "   cohesion (Pa)
phi2_cem = 20.0                            ;  "   friction angle (Degree)
; Thermal Model Parameters (TMP) "Isotropic Heat Conduction"
TC1_cem = 1.0                              ; Min. thermal conductivity (W/(m.K))
SH1_cem = 2100.0                           ;  "   specific heat (J/(kg.K))
LTE1_cem = 10.0e-6                         ;  "   linear thermal expansion (1/K)

TC2_cem = 1.0                              ; Max. thermal conductivity (W/(m.K))
SH2_cem = 2100.0                           ;  "   specific heat (J/(kg.K))
LTE2_cem = 10.0e-6                         ;  "   linear thermal expansion (1/K)


; 9) Cement during 1st Day Hydration (Hydcem)   ; Stage_0300
; 9.1) Deterministic Data
; Temperature Change during Hydration
Temp_MathModel_Hydcem = 4                  ; Temperature math. model = Int[1,4]
                                           ; Linear Model = 1, Power Model = 2,
                                           ; Exponential Model = 3,
                                           ; Hyperbolic Model = 4, and else no change.


; 9.2) Random Variables Data
; Variables are calculated according to their proposed equations.
end
```

G.2 Mesh Generation

Three steps are needed to make an automatic meshing of the problem. The first step is to prepare the mesh variables to be suitable for any geometric configuration. The second step is to calculate number of meshing in both i and j direction that satisfies FLAC zones' limitations. Finally, to relocate this generated mesh into its location with the corresponding dimensions defined in the first step. For casing as an example, each of these steps are defined by the following three FISH functions; Grid_Preparation, Grid_Generation, and Casing_Donut function. First and the second steps have the same approach as presented here, while the third step slightly differs according to the zonez' limitation presented in FLAC manual. The following codes are to create casing mesh for the problem.

```
; Notes:
; ------
; It will be the same through all stages of simulation
; The Codes aim to:
;     1) Avoid bad aspect ratio message by calculating # of elements to achieve the accepted FLAC aspect ratio.


def Grid_Preparation
  r_maximum = Model_Width / 2
  rwo = dwo/2                                                    ; dwo <= 5*dco
  rco = dco/2
  dci = dco - 2*tc                                               ; dco <= 5*dci
  rci = dci/2
  r_minimum = rci / Model_Extent_Factor

  if e = 0.0 then                                                ; Adjust reference for grid relocation
   Theta = 90.0                                                  ; Azimuth angle of eccentricity, Degree
  else
   Theta = Angle_Step * int(Azimuth_EccentricityAngle_factor)
  endif

  alpha_o = (90 - Theta) * (pi/180)                              ; Radian from x direction
  e_east = (e/100.0) * (rwo-rco) * cos(alpha_o)
  e_north = (e/100.0) * (rwo-rco) * sin(alpha_o)
end


;   Function is to determine:
;       1- The Number of elements in i direction
;       2- The Number of elements in j direction
;
def Grid_Generation
```

```
  F_j_zone_all = 1
  L_j_zone_all = int(360.0/Angle_Step)

  F_j_gp_all = F_j_zone_all
  L_j_gp_all = L_j_zone_all + 1

  Number_j_elements = L_j_zone_all

  F_i_zone_c = 1
  t_c = tc
  F_AspectRatio_c = 1.0
  AspectRatio_factor_c = rco / rci
  L_AspectRatio_c = AspectRatio_factor_c / F_AspectRatio_c
  L_jLength_c = rco * (Angle_Step * (pi/180))                    ; Thickness of casing donut
  L_iLength_c = L_jLength_c / L_AspectRatio_c                    ; Assumed first casing zone aspect ratio
  Number_i_elements_c = t_c / L_iLength_c                        ; rco = ]rci,5*rci]
  if Number_i_elements_c <= 1.0 then
    No_i_elements_c = 1
  else
    No_i_elements_c = int(Number_i_elements_c)
  endif
  Actual_iLength_c = t_c / No_i_elements_c
  L_i_zone_c = F_i_zone_c + (No_i_elements_c-1)
end


def Casing_Donut
  rmin_c = rci
  rmax_c = rco

  F_igp_c = F_i_zone_c
  L_igp_c = F_igp_c + No_i_elements_c
  F_jgp_c = F_j_gp_all
  L_jgp_c = L_j_gp_all

  FF_jgp_c = float(F_jgp_c)

  loop j (F_jgp_c,L_jgp_c)
    alpha_i = ((j-FF_jgp_c)/(L_jgp_c-FF_jgp_c)) * (2.0*pi)
    alpha = alpha_o + alpha_i
    loop i (F_igp_c,L_igp_c)
      increasing_ratio_c = float((i-F_igp_c)/(L_igp_c-F_igp_c))
      ro_c = rmin_c + (rmax_c-rmin_c)*increasing_ratio_c
      if j = L_jgp_c then
        x(i,j) = x(i,F_jgp_c)
        y(i,j) = y(i,F_jgp_c)
      else
        x(i,j) = e_east + (ro_c * cos(alpha))                    ; Avoid error accumulation in i-direction
        y(i,j) = e_north + (ro_c * sin(alpha))                   ; Avoid error accumulation in j-direction
      endif
    end_loop
  end_loop
end
```

G.3 Generating of Normally Distributed Variable

The normal distribution is an unbounded statistical distribution. A common method is to generate two independent uniform random numbers U_1 and U_2. Based on these uniform numbers, another two independent standard normal numbers Z_1 and Z_2 can be generated. For strength parameters as an example, two steps were performed to sample a random variable that should avoid resulting in negative (non-physical) sampled values at the lower tail. The steps involved generating Z1 and Z1 and then picked the minimum and maximum values to conclude the corresponding mean and standard deviation for the current iteration.

```
def Global_Inputs_Variables
  ; 3.2.4) Normally Distributed Variables                    ; If variables are normally distributed
  ; -----------------------------------------
  loop n_Numbers_form(1,10000)
    U01_form = urand
    U02_form = urand

    Z01_form = sqrt(-2*ln(U01_form)) * cos(2*pi*U02_form)    ; Taken for formation cohesion
    Z02_form = sqrt(-2*ln(U01_form)) * sin(2*pi*U02_form)    ; Taken for formation friction

    ; Random number for cohesion
    c_Zmin_form = min(Z01_form,Z01min_tmp_form)
    c_Zmax_form = max(Z01_form,Z01max_tmp_form)
    ;
    Z01min_tmp_form = c_Zmin_form
    Z01max_tmp_form = c_Zmax_form

    ; Random number for friction
    phi_Zmin_form = min(Z02_form,Z02min_tmp_form)
    phi_Zmax_form = max(Z02_form,Z02max_tmp_form)
    ;
    Z02min_tmp_form = phi_Zmin_form
    Z02max_tmp_form = phi_Zmax_form
  endloop

  ; Formation cohesion as Normal Random Variable
  b_c_form = (c2_form-c1_form) / (c_Zmax_form-c_Zmin_form)
  a_c_form = c2_form - (b_c_form*c_Zmax_form)

  c_ND_form = a_c_form + (b_c_form*Z01_form)
  if c_ND_form <= c1_form then
    c_ND_form = c1_form
  else
    if c_ND_form >= c2_form then
      c_ND_form = c2_form
```

```
    else
      c_ND_form = c_ND_form
    endif
  endif

  ; Formation friction as Normal Random Variable
  b_phi_form = (phi2_form-phi1_form) / (phi_Zmax_form-phi_Zmin_form)
  a_phi_form = phi2_form - (b_phi_form*phi_Zmax_form)

  phi_ND_form = a_phi_form + (b_phi_form*Z02_form)
  if phi_ND_form <= phi1_form then
    phi_ND_form = phi1_form
  else
    if phi_ND_form >= phi2_form then
      phi_ND_form = phi2_form
    else
      phi_ND_form = phi_ND_form
    endif
  endif
end
```

G.4 Cement during Hydration

For cement properties during hydration, the procedure follows the methodology presented in Chapter 2. After defining a variable hour for the Stage_0300, wellbore temperature at the corresponding depth was calculated. The temperature was used to estimate coefficients for each cement property. Finally, the coefficients were used to predict the corresponding cement property value that will be used to define cement as a material during this stage of simulation.

```
def cement_hydration
 initial_tempC = Avg_Surface_Temp + (Temp_Gradient * Depth)          ; Formation temperature (°C)

 ; 1) Hyd Cement Temperature Coefficients
 ; ------------------------------------------------
 ; Mechanical Model Parameters (MMP) "Mohr-Coulomb"
  ; Density Calculations
 a_rho_Hydcem = (-0.02757 * initial_tempC) + 4.33876                 ; Density time "induction" constant
 r_rho_Hydcem = (-0.01238 * initial_tempC) + 1.23421                 ; Density growth rate

  ; Compression Wave Velocity Calculations
 a_VpSQ_Hydcem = (-0.01648 * initial_tempC) - 0.44729                ; Wave vel. time "induction" constant
 r_VpSQ_Hydcem = (0.01598 * initial_tempC) + 0.17140                 ;     "    "    "    growth rate

  ; c, phi Calculations
 a_UCS_Hydcem = (-0.01516 * initial_tempC) - 1.49275                 ; UCS time "induction" constant
 r_UCS_Hydcem = (0.01198 * initial_tempC) + 0.36078                  ; UCS growth rate


 ; 2) Hyd. Cement Dynamic Mechanical Properties
 ; ------------------------------------------------------------
 ; Density
 Line_rho = - a_rho_Hydcem -(r_rho_Hydcem*ln(Hour))
 rho_Hydcem = Ult_rho_Hydcem * NC^(-NC^Line_rho)                     ; Density (kg/m3)

 ; Compression Wave Velocity, Vp
 Line_VpSQ = - a_VpSQ_Hydcem -(r_VpSQ_Hydcem*ln(Hour))
 VpSQ_Hydcem = Ult_VpSQ_Hydcem * NC^(-NC^Line_VpSQ)                  ; Primary wave velocity (m/sec)2
 Vp_Hydcem = VpSQ_Hydcem^0.50                                        ; Primary wave velocity (m/sec)

 ; Dynamic Poisson's Ratio
 Dnu_Hydcem = Dnu_cem

 ; Dynamic Elastic Modulus, Ed
 F_Dnu_Hydcem = ((1+Dnu_Hydcem) * (1-2*Dnu_Hydcem)) / (1-
                    Dnu_Hydcem)
 DE_Hydcem_rod = rho_Hydcem * VpSQ_Hydcem                            ; (Pa)
 DE_Hydcem = DE_Hydcem_rod * F_Dnu_Hydcem                            ; (Pa)
 DE_Hydcem_pfsi = DE_Hydcem * (1/6894.757)                           ; (pfsi)
```

```
 ; 3) Hyd. Cement Static Mechanical Properties
 ; ----------------------------------------------------
 ; Unconfined Compressive Strength, UCS
 Cnst_01 = 2.0e-14                                          ; Paper SPE36476: Fig.1
 Cnst_02 = 2.71                                             ; Paper SPE36476: Fig.1
 UCS_Hydcem_pfsi = Cnst_01*(DE_Hydcem_pfsi^Cnst_02)         ; Paper SPE36476: (pfsi)
 UCS_Hydcem = UCS_Hydcem_pfsi * (6894.757)                  ; (Pa)

 ; Elastic Modulus, E
 SE_Hydcem_pfsi = (1/2.8227)*DE_Hydcem_pfsi - (384646/2.8227)   ; Paper SPE95921: Fig.3 (pfsi)
 E_Hydcem = SE_Hydcem_pfsi * (6894.757)                     ; Static elastic modulus (Pa)

 ; Poisson's Ratio
 Snu_Hydcem = nu_cem                                        ; Paper SPE95921: Table.1
 nu_Hydcem = Snu_Hydcem                                     ; Static Poisson's ratio (Dimensionless)

 ; UCS, c, phi
 Line_UCS = - a_UCS_Hydcem -(r_UCS_Hydcem*ln(Hour))
 cohesion_Hydcem = Ult_c_Hydcem * NC^(-NC^Line_UCS)         ; Predicted cohesion (Pa)
 friction_Hydcem = Ult_phi_Hydcem * NC^(-NC^Line_UCS)       ;       "       friction angle (Degree)
end
```